PB88-166822

Fundamental Combustion Research Applied to Pollution Formation. Volume 2B
Physics and Chemistry of Two-Phase Systems
Devolatilization and Volatile Reactions

Energy and Environmental Research Corp.
Irvine, CA

Prepared for

Environmental Protection Agency
Research Triangle Park, NC

Jan 88

U.S. Department of Commerce
National Technical Information Service
NTIS

PB88-166822

EPA/600/7-88/001b
January 1988

FUNDAMENTAL COMBUSTION RESEARCH APPLIED TO POLLUTION FORMATION

Volume IIb. Physics and Chemistry of Two-Phase Systems: Devolatilization and Volatile Reactions

by

W. R. Seeker and M. P. Heap
Energy and Environmental Research Corporation
18 Mason
Irvine, California 92714

EPA Contract No. 68-02-2631
EPA Project Officer: W. Steven Lanier
Air and Energy Engineering Research Laboratory
Research Triangle Park, North Carolina 27711

AIR AND ENERGY ENGINEERING RESEARCH LABORATORY
OFFICE OF RESEARCH AND DEVELOPMENT
U.S. ENVIRONMENTAL PROTECTION AGENCY
RESEARCH TRIANGLE PARK, NC 27711

REPRODUCED BY
U.S. DEPARTMENT OF COMMERCE
NATIONAL TECHNICAL
INFORMATION SERVICE
SPRINGFIELD, VA. 22161

TECHNICAL REPORT DATA

(Please read Instructions on the reverse before completing)

1. REPORT NO. EPA/600/7-88/001b	2.	3. RECIPIENT'S ACCESSION NO. PB88 166822/AS
4. TITLE AND SUBTITLE Fundamental Combustion Research Applied to Pollution Formation, Volume IIb. Physics and Chemistry of Two-Phase Systems: Devolatilization and Volatile Reactions		5. REPORT DATE January 1988
		6. PERFORMING ORGANIZATION CODE
7. AUTHOR(S) W. R. Seeker and M. P. Heap		8. PERFORMING ORGANIZATION REPORT NO.
9. PERFORMING ORGANIZATION NAME AND ADDRESS Energy and Environmental Research Corporation 18 Mason Irvine, California 92714		10. PROGRAM ELEMENT NO.
		11. CONTRACT/GRANT NO. 68-02-2631
12. SPONSORING AGENCY NAME AND ADDRESS EPA, Office of Research and Development Air and Energy Engineering Research Laboratory Research Triangle Park, NC 27711		13. TYPE OF REPORT AND PERIOD COVERED Final; 1/77 - 9/80
		14. SPONSORING AGENCY CODE EPA/600/13

15. SUPPLEMENTARY NOTES Project officer W. S. Lanier is no longer with the Agency. For details, contact William P. Linak, Mail Drop 65, 919/541-5792.

16. ABSTRACT The reports included in this three-part volume describe eight studies by various investigators, to better understand the physics and chemistry of two-phase combustion with respect to pollution formation. Volume IIb gives information on the influence of various combustion parameters (i.e., fuel type, stoichiometry, residence time, temperature, and mixing) on the fate of volatile fuel nitrogen, in four parts: (1) method for characterization of coal during thermal decomposition (United Technologies Research Center), (2) the volatility of fuel nitrogen species (Rockwell), (3) stirred reactor study of pollutant formation from combusting pulverized coal clouds (Acurex), and (4) pollutant formation from combustion of fuel oils in a well-mixed combustor (Battelle).

17. KEY WORDS AND DOCUMENT ANALYSIS

a. DESCRIPTORS		b. IDENTIFIERS/OPEN ENDED TERMS	c. COSATI Field/Group	
Pollution	Nitrogen	Pollution Control	13B	07B
Combustion	Nitrogen Oxide (NO)	Stationary Sources	21B	
Research	Pulverized Fuels	Fundamental Research	14F	21D
Physics	Fuel Oil		20A	
Chemistry	Measurement		07A	14G
Flames				
Volatility			20M	

18. DISTRIBUTION STATEMENT Release to Public	19. SECURITY CLASS *(This Report)* Unclassified	21. NO. OF PAGES 378
	20. SECURITY CLASS *(This page)* Unclassified	22. PRICE

EPA Form 2220-1 (9-73)

NOTICE

This document has been reviewed in accordance with U.S. Environmental Protection Agency policy and approved for publication. Mention of trade names or commercial products does not constitute endorsement or recommendation for use.

ABSTRACT

This document is one of the series of reports describing work performed under the Fundamental Combustion Research Applied to Pollution Formation Program (EPA contract 68-02-2631). The FCR program was structured under a master contract concept with Energy and Environmental Research (EER) as the prime contractor and with individual studies generally performed under subcontract. Volume IIb of the final report series provides subcontractor reports from four studies on devolatilization and volatile reactions for coal and heavy fuel oil. Sections I and II document studies by United Technologies Research Center and Rockwell International on the devolatilization kinetics and volatile nitrogen yield from thermal decomposition of fuel. Sections III and IV present results from studies by Acurex Corporation and Battelle Columbus Laboratories. Each of these studies were directed toward development and testing of two-phase, stirred reactor systems to simulate the near field of high intensity flames. The Acurex study addressed pulverized coal fired systems while the Battelle effort was directed toward oil.

TABLE OF CONTENTS

Page

Abstract ii

Table of Contents iii

Introduction 1

SECTION I "Method for Characterization of Coal During Thermal Decomposition" by J.D. Freihaut and D.J. Seery I-1

SECTION II "Volatility of Fuel Nitrogen" by A.E. Axworthy, H.L. Recht, Y.H. Dayan, R.L. Gay, and C.L. Nealy II-1

SECTION III "Stirred Reactor Study of Pollutant Formation From Combusting Pulverized Coal Clouds" by P.M. Goldberg, P.A. Cawley, J.T. Kelly, H. Tong, and R.M. Kendall III-1

SECTION IV "Pollutant Formation From Combustion of Fuel Oils in a Well-Mixed Combustor" by M.J. Murphy, A.A. Putnam, A. Levy, and J.R. Overley IV-1

NOTE: Sections I through IV contain separate, more detailed tables of contents.

INTRODUCTION

The Fundamental Combustion Research Applied to Pollution Formation (FCR) program was a 77,000 man-hour, level-of-effort contract with Energy and Environmental Research Corporation (EER) as the prime contractor. The focus of the program was to perform fundamental research studies to better understand the chemistry and physics of combustion phenomena controlling formation of nitrogen oxide (NO_x) emissions. The outputs from the program were designed to assist the EPA s Combustion Research Branch (CRB) in developing NO_x control technologies for stationary combustion sources.

The FCR program was structured into three main research areas plus program support functions. The three main research areas included:

-- Gas Phase Chemistry
-- Physics and Chemistry of Two Phase Systems, and
-- Transport Processes in Reacting Systems.

The program support functions included development of numerical analysis tools and evaluation of required measurement systems. The final report for this program is divided into four volumes (or volume series) reflecting the technical structuring of the program. Thus, Volume I provides both an introduction to the report series and documentation of work performed in the Gas Phase Chemistry Program area. Volume II documents program efforts in the Physics and Chemistry of Two-Phase Systems. Volume III covers activities in the measurement support area while Volume IV covers Engineering Analysis and Transport Processes.

The largest fraction of the FCR program resources was devoted to the Physics and Chemistry of Two-Phase Systems Area. In total there were eight individual research efforts pursued under this portion of the program. Because of the size of this effort, it was necessary that Volume II be produced as a report series with designations IIa, IIb, and IIc. Volume IIa documents the research performed under three separate investigations directed toward better defining "Flame Combustion Processes". The current volume, Volume IIb, includes final reports from four subcontracted activities which have been loosely grouped under the heading "Devolatilization and Volatile Reactions". The final binding for the Volume II series (Volume IIc) documents an extensive investigation of gas/solid reactions which reduce NO to molecular nitrogen. Volume IIc is subtitled "Heterogeneous NO Reduction" and the reported effort was performed under a subcontract between EER and Institute Francais du Petrole (IFP). As mentioned above, Volume IIb consists of final reports from four FCR subcontracts. Each report is provided as a separate section to the volume and contains its own abstract, Table of Contents, List of Figures and List of References. EER and the EPA project Officer have reviewed each of these reports for technical content and certain revisions have been made by either the subcontractor or by EER. It must be noted, however, that in several areas the subcontractor Principal Investigators and EER hold different technical opinions on the interpretation of data. EER has not imposed its views upon the section authors allowing the Principal Investigators to state their technical opinions. It is felt that honest technical disagreement stimulates thought, leads to enhanced understanding of phenomena, and improves the quality of future research.

The remainder of this introductory section will briefly describe the contents of the four attached reports and will identify key issues of technical concern. We emphasize that the concerns are those of EER and do not represent the views of the subcontractors. It is up to the individual reader to evaluate each section, draw his own conclusions and to use the reported results appropriately. By listing our concerns, EER does not mean to criticize but rather is attempting to focus the reader's technical evaluation.

SECTION I

Section I of the Volume IIb reports on a study entitled "Method for Characterization of Coal During Thermal Decomposition" which was performed under subcontract to United Technology Research Center. The report authors are J.D. Freihaut and D.J. Seery. This study was initiated as a continuation of a Department of Energy sponsored effort with Peter Solomon as Principal Investigator. The basic thrust of the effort was to evaluate the evolution of volatile products from coals undergoing thermal decomposition. Coal samples were thermally decomposed by controlled rate electrical heating of a wire mesh grid under both vacuum and one-atmosphere (inert) environments. Through a combination of elemental analysis of the parent coal and char coupled with

Fourier Transform Infrared Analysis (FTIR) of gaseous and tar products, it was possible to monitor the devolatilization process as a function of time and final reaction temperature. Particular attention was given to the fate of fuel nitrogen species during thermal decomposition. An additional portion of the study involved further development of a model to describe the devolatilization process as a function of the chemical/physical properties of the parent fuel. As part of this study, eight coals were subjected to initial characterization tests. From that group four coals were subjected to detailed thermal decomposition investigations. The eight coals were selected from among the list of coals being used in other EPA sponsored programs to develop low-NO_x coal burner technology.

The results from this study provide valuable insights into the chemistry of coal decomposition. The vacuum experiments indicate that product distribution is reflective of the intrinsic chemical characteristics of the parent coal. The results also confirm earlier data that the dominant gaseous nitrogenous species from coal devolatilization is HCN. The one-atmosphere experiments revealed that observed behavior is influehced by physical parameters such as particle size and thermal drive.

EER provides the following observations which should be considered by the reader in reviewing this section of the report. First, we are concerned that the significant tar yields observed in the vacuum experiments may not be representative of events occurring in pulverized coal fired boiler flames. Our second observation is a bit more subtle but, perhaps, of greater significance. Specially, we are concerned that the slow heating rate of the coal samples in the heated grid experiments may have biased the results, particularly the extracted kinetic rate data at higher temperatures. With a slow heating rate significant devolatilization can occur on the temperature ramp and the results will not be characteristic of the final temperature as assumed in the data analysis. It should be noted that the experimental particle heating rates are one to three orders of magnitude less than that expected in a pulverized coal fired boiler. Moreover, there is a significant discrepancy between the high temperature rate data extracted from the heated grid experiments and the atmospheric pressure trials where the coal particles were injected into a near isothermal environment. Only at lower temperature (near 500°C) do the rate data from the two-experiments converge. EER suggests that the reader consider these factors in evaluating and using the result from this study.

SECTION II

Section II of Volume IIb provides the final report from a subcontract to Rockwell International dealing with the Volatility of Fuel Nitrogen. The report authors are A.E. Axworthy, H.L. Recht, V.H. Dayan, R.L. Gay and C.C. Nealy. The thrust of this effort was continuation of an earlier EPA contract (68-02-1886) with Rockwell International concerning the fate of fuel nitrogen. Under this earlier EPA study a two stage inert pyrolysis reactor was developed whereby the fuel sample was thermally decomposed in the first stage and the gaseous products flowed into a second state. The thermal conditions in the second stage were such that volatile nitrogen species were converted to HCN. The purpose of the FCR task was to screen a variety of coal and liquid fuel samples using this experimental technique and to compare the HCN yield results with bench/pilot scale combustion experiments using the same fuels.

In the program, nine fuel oils, three alternate fuels (coal and shale liquids) and eight coals were evaluated. (Six of these coals were also evaluated under the UTRC subcontract). The combustion trials had been performed by EER under other EPA funded contracts (68-02-1488 and 68-02-2624).

Perhaps the most startling outcome is the comparison of combustion experimental results with results from these rather simple pyrolysis tests. An excellent correlation was found between the percent conversion of fuel nitrogen to exhaust NO in the combustion tests and the percentage conversion of the fuel nitrogen to HCN in the pyrolysis experiments (first stage operated at 1100°C). A least squares fit to the data produced the correlation:

$$\%\text{FBN to NO} = -0.013 + 1.99\ (\%\text{FBN to HCN})$$

Though the correlation looks statistically excellent, it lacks in fundamental justification. First, the negative leading term is difficult to fundamentally rationalize. More important, however, the 1.99 slope term indicates that the NO production is essentially double the HCN yield. These factors would suggest that either the correlation is fortuitous or that the pyrolysis experiments are in error. EER suggests a significantly broader data base should be developed before such a correlation is applied to practical problem. The correlation is, however, sufficiently interesting to justify that additional research.

SECTION III

Section III of the Volume IIb documents research performed by Acurex Corporation investigating chemical and physical impacts on NO_x formation under conditions similar to those found in the near burner region of high-intensity pulverized coal burner flames. It was the intent that experimental data produced under this program would be used in developing and evaluating critical components of a coal combustion numerical model.

EER made a decision that the simplest chemical reactor simulating the near field environment of a pulverized coal flame was a stirred reactor. For a perfectly stirred reactor, the devolatilization, heat release, gas phase reactions and heterogeneous reactions occur simultaneously under spatially uniform thermal and chemical conditions. It can.also be argued that this environment is a good analogue to the early portion of a high-intensity coal flame, particularly the recirculation zone. It is necessary, however, that the characteristic residence time of such a reactor be in the range of 20 to 200 msec if conditions in a practical flame are to be simulated. Such residence times are 1 to 2 orders of magnitude greater than employed in classical, gas-phase stirred reactors (see reference 1 in Section III).

The primary thrust of the initial portion of this program was to develop the required experimental hardware. It was fully expected that the reactor would not be perfectly stirred and, in fact, it was likely that the gas phase and solid phase material would have different characteristic residence times. A significant portion of this section of Volume IIb deals with the development and characterization of the experimental hardware. As will be noted, there were numerous problems encountered in this hardware development effort. In general, the gas phase exhibited nominally well-stirred behavior but the solid phase did not. Specifically, the solid phase characteristics were more akin to a plug flow reactor and the injectors exhibited a hysteresis effect.

One of the techniques used to quantify the gas phase residence time was to add an inert impulse tracer to the air input and to monitor the exhaust as a function of time with a hot wire anemometer. Results indicate that the hardware design achieved a high degree of mixing on a microscale but that mixing was deficient on a macroscale. That is to say, the exhaust products consisted of many well-mixed pockets but that each pocket had experienced different chemical (and possibly thermal) environments.

Having noted the shortcomings of the experimental hardware, several experimental test series were performed. The report documents a cursory evaluation of the results. The noted uncertainties in unit operations cast doubt on interpretation of the results and it is EER's opinion that further development of the experimental hardware is required before additional testing programs should be pursued.

SECTION IV

Section IV of Volume IIb documents results from a subcontractual study performed by Battelle Columbus Laboratories (BCL). The thrust of this BCL study was almost identical to the forementioned Acurex study, except that it focused on heavy fuel oil combustion as opposed to coal. The requirement for atomization of the liquid fuel resulted in a significantly different reactor configuration for the BCL study than for the Acurex study. The major portion of Section IV deals with development and characterization of the hardware.

It is EER's opinion that the hardware characterizations are far from complete and that there are numerous questions concerning acceptability of unit operations. In general, however, it appears that the unit approaches a well mixed state on the macroscale, at least for the gas phase in cold flow experiments. Significant questions exists relative to dispersion of the liquid phase and impingement of droplets on the reactor walls.

Limited testing was performed using natural gas, distillate oil and residual oil as the fuel and the results are documented in the report. An initial evaluation of the results is presented but all conclusions must be considered preliminary in view of the experimental uncertainties.

I. METHOD FOR CHARACTERIZATION OF COAL DURING THERMAL DECOMPOSITION

Prepared by:

J.D. Freihaut and D.J. Seery

United Technologies Research Center
East Hartford, Connecticut 06108

Prepared for:

Energy and Environmental Research Corporation
EER Subcontract No. R80-954430-13

ACKNOWLEDGMENTS

The authors wish to acknowledge the contributions of P. R. Solomon who was the principal investigator during much of this program and is responsible for the devolatization model in this report. The technical assistance of D. Santos and G. Wagner is also acknowledged.

TABLE OF CONTENTS

PAGE

ABSTRACT . . . . I-iv

I. INTRODUCTION I-1

II. FUEL SELECTION I-2

III. FUEL CHARACTERIZATION RESULTS I-4

- A. ELEMENTAL ANALYSIS RESULTS I-4
- B. INFRARED ANALYSIS I-8
- C. THERMAL DECOMPOSITION PRODUCT DISTRIBUTION AND CHARACTERISTICS I-14

IV. COAL THERMAL DECOMPOSITION MODEL I-56

- A. EXPERIMENTAL BASES OF THE MODEL I-56
- B. VACUUM DEVOLATILIZATION MODEL - WORKING HYPOTHESES FROM VACUUM DEVOLATILIZATION STUDIES . . . I-60
- C. MODEL RESULTS AND DISCUSSION I-64
- D. ISOTHERMAL FURNACE STUDIES: AN EXPERIMENTAL CHECK OF MODEL HYPOTHESES AND KINETIC PARAMETERS . . . I-64

V. SUMMARY I-82

VI. SUGGESTIONS FOR FUTURE WORK I-84

REFERENCES I-86

Method of Characterization of Coal During Thermal Decompostion

ABSTRACT

This report contains results and interpretations of investigations performed to establish a method for characterization of coal during thermal decomposition. The report discusses in detail transformations which occur in various coals during their thermal decomposition. Both vacuum and one-atmosphere experiments were performed. Final temperatures achieved in the vacuum devolatilization experiments were ranged from 500°C to 1700°C. The one-atmosphere decompostion studies ranged from elemental analysis and infrared analysis. Elemental and infrared analysis of the tars were also performed. Light gas evolution areas were monitored by use of the rapid scan feature of the FTIR while quantitative determinations were made high resolution FTIR. Particular attention was given to the fate of the fuel nitrogen during the decomposition process. An attempt to model the devoliatilization process by a chemical kinetic scheme was made for both the vacuum and one-atmosphere environments.

I. INTRODUCTION

The purpose of the research program has been twofold:

1. To characterize by the use of infrared analysis, elemental analysis and thermal decomposition products, coals and their behavior during thermal decomposition;
2. To assemble a coal thermal decomposition model which would form one component of a coal combustion model capable of predicting nitric oxide formation in pulverized coal flames.

Ultimately it is believed that such a program would generate the ability to predict thermal decomposition behavior of a given parent coal on the basis of a specific, standardized characterization of a coal. The work performed under this program demonstrates the infrared analysis of the parent coal can play an essential role in this characterization.

In order to achieve the goal noted above the Contractor has utilized existing Contractor-owned facilities in performing the following related tasks:

I. Fuel Selection
II. Coal, Char and Tar Characterization
III. Development and Integration of a Coal Decomposition Model
IV. Reporting and Documentation

The final report includes a discussion of accomplishments achieved with respect to each task, general insights into the nature of the thermal decomposition process that have been generated by performing the individual tasks, a discussion of the overall model of the thermal decomposition process formulated during the investigation, recommendations as to the nature of further research investigations needed to improve understanding of coal thermal decomposition, especially with respect to the combustion process.

II. FUEL SELECTION

Four coals were selected for extensive structural and decomposition characterization. Information exchange and discussions between UTRC and EER formed the framework for the selection process. Within the framework the following criteria formed the basis for fuel selection:

1. A coal selected should not be a coal already investigated in other laboratories or in a previous work performed at UTRC.
2. The coals selected should be from a reserve which is of potential commercial interest or is already being commercially developed.
3. A coal selected may be a coal which has particular aspects of combustion behavior that need to be more thoroughly characterized in order that the coal be utilized in an efficient and environmentally acceptable manner.

Within the content of these criteria, UTRC performed initial characterization tests on fourteen coals provided by EER. Table I lists the coals received and the initial characterization tests performed. The four coals in Table I selected for complete investigation are marked by an asterisk. Discussions with EER personnel led to the final selection.

TABLE I

INITIAL CHARACTERIZATION TESTS

COAL	Elemental Analysis	FTIR H-Distrib.	FTIR-Mineral Det.	Thermal Decomp.
Rosa, Alabama*	X	X	X	X
Upper Cliff, Alabama	X	X	X	X
Black Cliff, Alabama	X	X	X	X
TRW Coal #2	X	X	X	X
Utah*	X	X	X	X
Beulah, N. D.*	X	X	X	X
Scranton, N. D.	X	X	X	X
Savage, Montana*	X	X	X	X

* Selected for further thermal decomposition investigation.

III. FUEL CHARACTERIZATION RESULTS

Characterization of the four selected coals consisted of elemental analysis, infrared analysis of the parent coal and analysis of the products of the controlled, thermal decomposition of coals in vacuo by use of the heated grid apparatus. The elemental analysis of the coals consisted of a Perkin Elmer 240 elemental analysis for carbon, hydrogen, nitrogen and oxygen (by difference). When possible the electron microprobe was used to determine the levels of inorganic and organic sulfur present in the coal. The infrared analysis led to the determination of the major minerals present in the parent coal as well as an estimate of the hydroxyl, aliphatic and aromatic hydrogen present in the coal. The aromaticity of the coal can then be estimated from the hydrogen distribution.

The controlled thermal decomposition was performed using a heated grid apparatus operated in vacuo. The Fourier Transform Infrared Spectrometer (FTIR) system was used to observe the light gas products of the devolatilization process as well as to detect structural changes in the char and tar products of the devolatilization process as various final temperatures are achieved.

A. Elemental Analysis Results

Table II lists the elemental composition of the four coals extensively examined. When determinations were feasible, the organic and inorganic sulfur contents are given. The elemental analysis system converts the organic carbon, hydrogen and nitrogen in the sample to CO_2, H_2O and NO_x. The NO_x compounds are then reduced to free nitrogen. Using He as the carrier gas, the H_2O, CO_2 and N_2 are then passed through a series of thermal conductivity cells for measurement. Organic oxygen in the sample is measured by difference. Table II also lists the as-received moisture content of the samples. Coals are dried in vacuo at 105°C overnight.

Elemental analysis performed on the same coals by a commerical laboratory at times varied significantly from the UTRC results. Since the results from samples of the same coal sent to a laboratory varied as much as results from the same coal analyzed at two different laboratories, it is difficult to attribute variations in results to a specific set of factors. However, it is believed that the nitrogen determinations made by the Pregal-Dumas method on the Perkin-Elmer 240 are more reliable than the Kjeldahl method used at most commercial laboratories. The sulfur forms reported in Table III were determined by the scanning microprobe method (MASC). When concentrations of mineral sulfur proved to be too low for reliable results from the microprobe technique, a dashed line is inserted in the Table.

TABLE II

ELEMENTAL ANALYSIS (DRY)

COAL	Moisture	N	C	H	ASH	S + O
Rosa, Alabama		1.51	76.26	4.16	9.59	8.48
		1.55	75.31	4.30	9.72	9.11
		1.58	75.07	4.24	10.17	8.94
		1.52	76.18	4.40	7.22	10.61
	8.02					
Avg.		1.54	75.71	4.28	9.18	9.30
EER		1.74	81.24	4.74	7.38	4.90
	0.88	1.53	72.86	5.31	11.53	8.77
Upper Cliff, Alabama		1.57	80.01	4.36	8.35	5.71
		1.54	79.76	4.32	7.55	6.84
		1.58	79.91	4.56	8.16	5.79
Avg.	3.00	1.56	79.89	4.41	8.02	6.11
EER		1.46	79.32	4.50	9.78	4.96
Black Creek, Alabama		1.87	82.82	5.09	2.84	7.58
		1.91	83.67	5.25	3.22	5.93
		1.88	82.80	5.11	3.41	6.81
Avg.	2.25	1.89	83.16	5.15	3.16	6.71
EER		1.79	82.12	5.21	4.55	6.37
TRW Coal #2		1.42	75.18	4.97	8.43	10.00
		1.33	72.45	4.71	11.37	10.14
		1.39	72.82	4.80	12.24	8.74
Avg.	1.87	1.38	73.48	4.83	10.68	9.63
EER		1.35	72.93	5.03	11.88	8.79
Utah	6.39	1.49	71.01	5.10	6.85	15.56
		1.54	71.49	5.13	8.60	13.23
		1.51	71.65	5.22	6.36	15.26
		1.62	71.39	5.28	8.11	13.59
Avg.		1.54	7.139	5.18	7.48	14.40
EER		1.33	73.17	5.56	7.91	12.05
		1.42	70.98	5.32	8.77	13.51

TABLE II (Cont'd)

ELEMENTAL ANALYSIS (DRY)

Coal	Moisture	N	C	H	ASH	S + O
Beulah, N. Dakota (#9)		1.00	65.75	4.24	2.30	26.71
		0.97	62.51	3.95	7.58	24.99
		.91	62.91	4.38	8.45	27.48
Avg.		.96	63.72	4.19	6.11	26.39
EER	34.63	1.10	66.15	4.19	7.60	20.97
Scranton, N. Dakota		1.04	61.41	4.25	7.09	26.20
		0.85	63.79	4.22	4.93	26.21
		0.87	61.61	4.13	9.07	24.31
Avg.	34.96	.92	62.27	4.20	7.03	25.57
EER		.83	64.60	4.17	11.53	18.86
Savage, Montana		0.99	64.87	4.21	5.24	24.69
		1.04	64.10	3.97	4.76	26.13
		0.97	62.72	3.91	5.28	27.05
Avg.	36.36	1.00	63.90	4.03	5.09	25.96
EER		1.13	64.99	4.04	7.24	22.59

TABLE III

SULFUR ANALYSIS (%DRY)

COAL	S(O) MASC	S(O) EER	S(M) MASC	S(T) EER	S(T) MASC	EER
Rosa, Alabama	.49	.51	---	.46	---	1.04
Upper Cliff, Alabama	.54	.63	<1.08	.51	---	1.31
Black Creek, Alabama	.65	.68	< .30	.07	---	.76
TRW Coal #2	.88	---	< .36	---	---	1.11
Utah	.69	---	< .33	---	---	.68
Beulah, N. Dakota(#9)	.17	.32	2.27	.05	2.44	.37
Scranton, N. Dakota	1.25	1.00	< .84	.49	---	1.52
Savage, Montana	.43	.41	< .12	.02	---	.42

B. Infrared Analysis

Infrared spectra of coals, tars and chars were obtained on a Nicolet FTIR. KBr pellets of coals and chars are prepared by mixing 1 mg of dry, finely ground (20 min in a "Wig-L-Bug") sample with 300 mg of KBr. Thirteen mm diameter pellets are pressed in an evacuated die under 20,000 lb pressure for one minute and dried at 110°C overnight to remove water. Since the heating process was observed to destroy tar pellets the water correction was obtained by subtracting the spectrum of a blank disk prepared under the same conditions. The H_2O corrected spectra matched those from samples prepared by allowing the tar produced in thermal decomposition to fall directly onto a water free, blank KBr disk.

The FTIR obtains spectra in digital form and corrections for particle scattering, mineral content and water may be easily made. A typical correction sequence is illustrated in Fig. 1. The lower curve is the uncorrected spectrum of a dried coal. It has a slope due to particle scattering and peaks from the mineral components in the 1000 to 450 cm^{-1} region.

In the middle figure a mixture of kaolin and illite has been subtracted and the spectrum scaled to give the absorbance for 1 mg of coal dmmf. The top curve is corrected for particle scattering by subtraction of a straight-line scattering spectrum. The corrected spectra obtained for the coals of interest in this study are shown in Figs. 2a and 2b.

Much previous work has been done to identify the functional groups responsible for the observed peaks. Extensive references may be found in Lowry[1] and van Krevelen[2]. For a quantitative measure of the functional group concentrations, a curve analysis program (CAP) available in the Nicolet library was used to synthesize the IR spectra. The synthesis is accomplished by adding 26 absorption peaks with Gaussian shapes and variable position, width, and height as shown in Fig. 3. The peaks are separated according to the identified functional group. It has been determined that all the coals, chars, and tars which were studied could be synthesized by varying only the magnitudes of a set of Gaussians whose widths and positions were held constant. These samples could therefore be analyzed in terms of a fixed mix of functional groups.

The calibration of the aliphatic peaks near 2900^{-1} (lines A-E) and the aromatic peaks near 800 cm^{-1} (lines I-K) is shown in Fig. 4. The objective is to determine the values of the constants a and b, which relate peak areas to the corresponding hydrogen concentration, i.e.,

$$H_{ali} = a\ A_{ABCDE} \quad \text{and} \quad H_{aro} = b\ A_{IJK}$$

where A_{ABCDE} is the area under the aliphatic peaks A-E, A_{IJK} is the area under the aromatic peaks I-K, and H_{ali} and H_{aro} the aliphatic (or alicyclic) and aromatic

FIG. 1

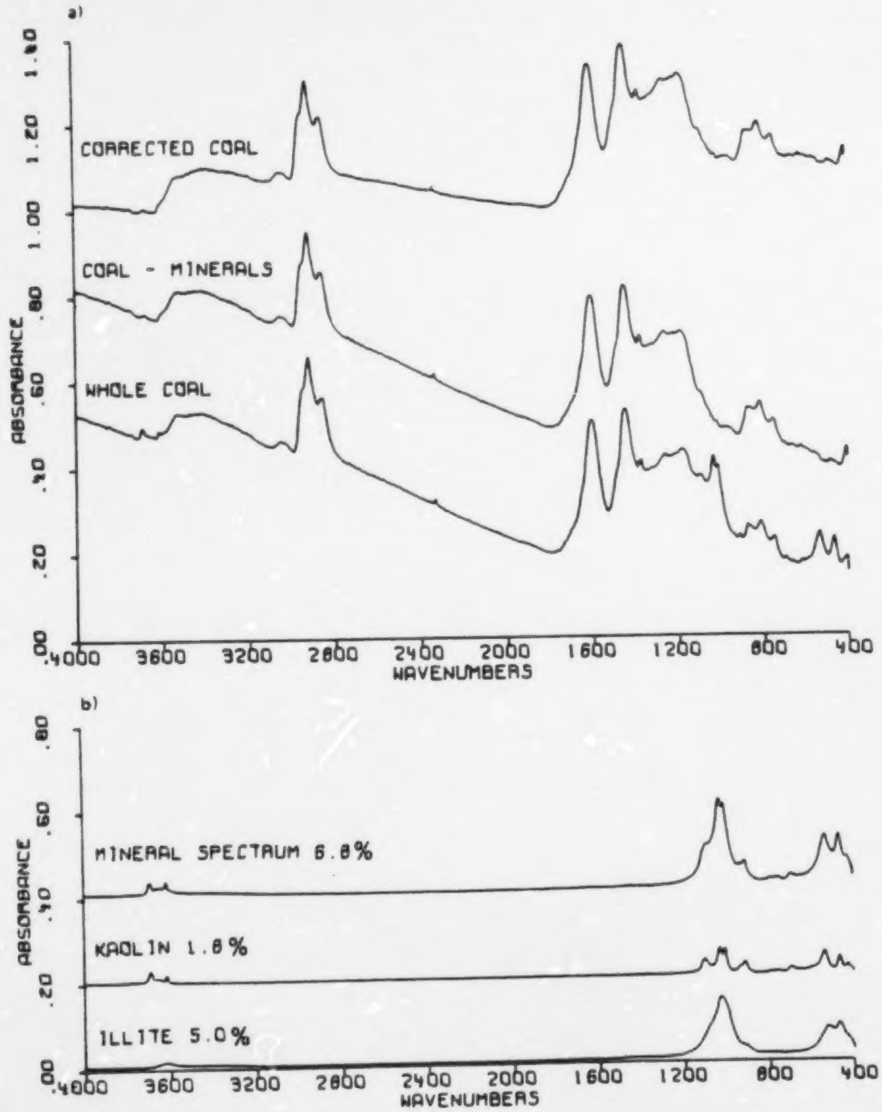

Correction of Coal Spectrum for Scattering and Minerals a) Correction of Coal Spectrum, b) Determination of Mineral Spectrum by Addition of Reference Spectra. The Absorbance is Normalized to a Sample Size of 1mg/cm^2 in the KBr Disc

79-05-130-15

FIG. 2a

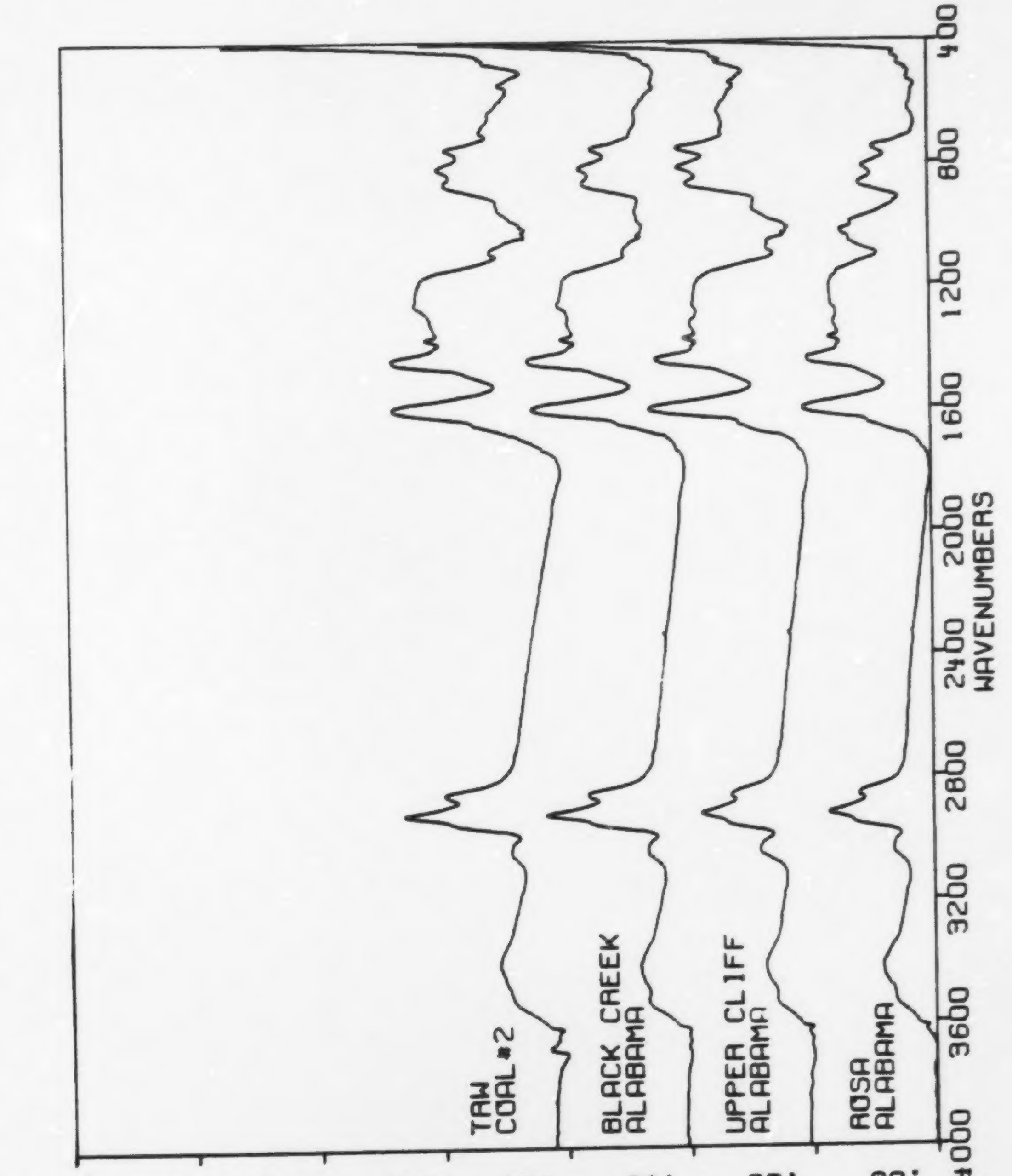

79–07–7–2

FIG. 2b

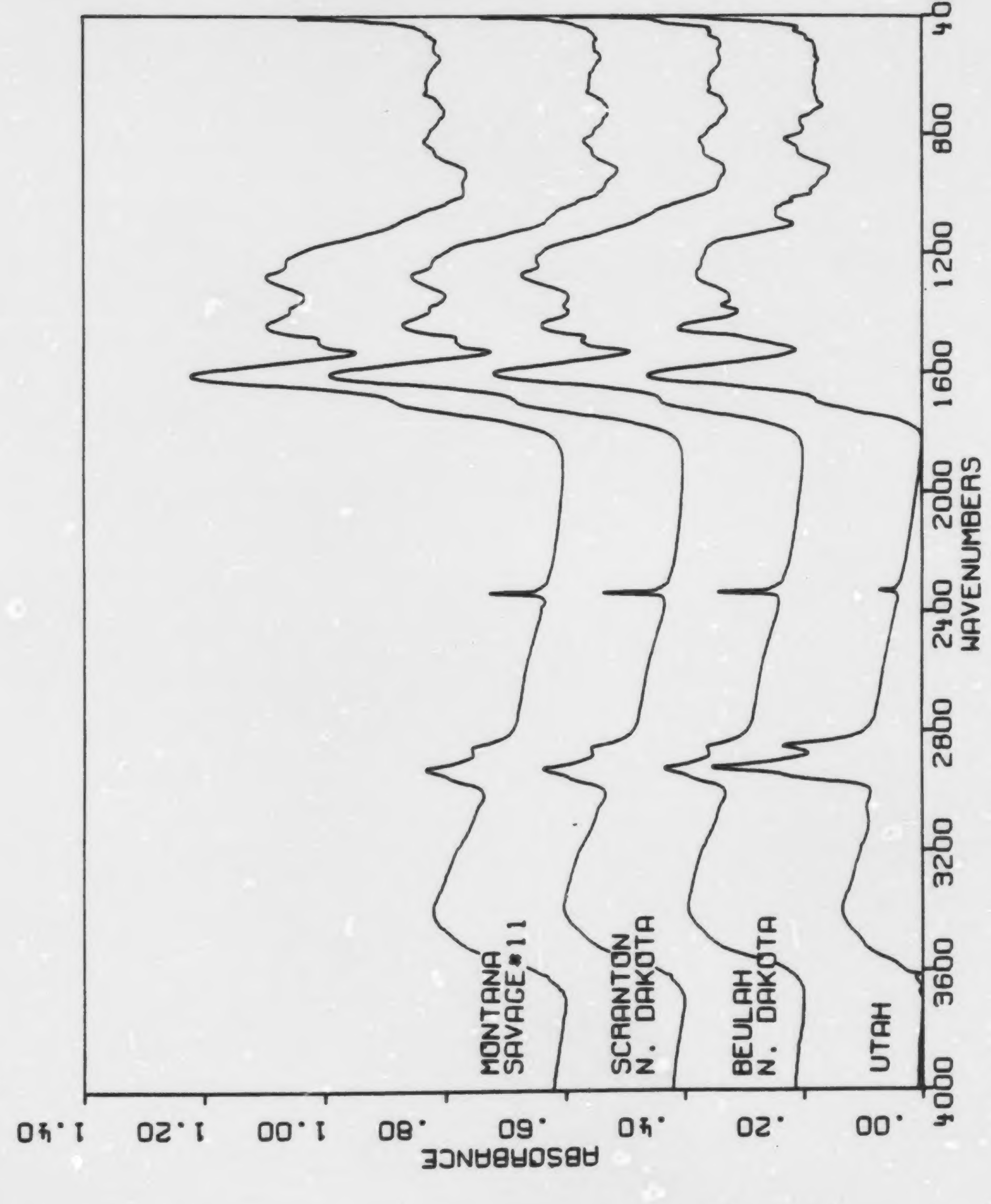

79-07-7-1

FIG. 3

SYNTHESIS OF INFRARED SPECTRUM

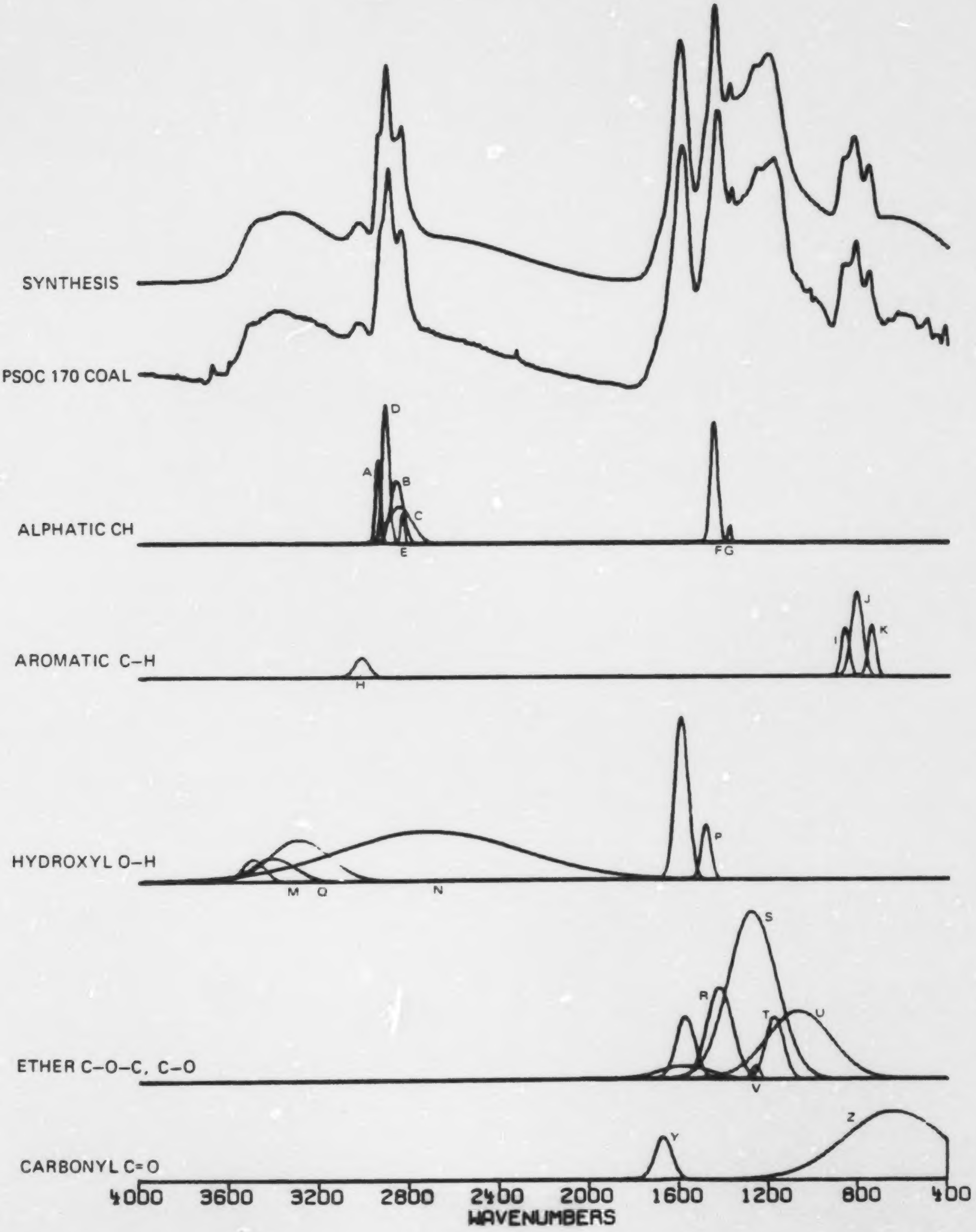

FIG. 4

CALIBRATION OF INFRARED INTENSITIES

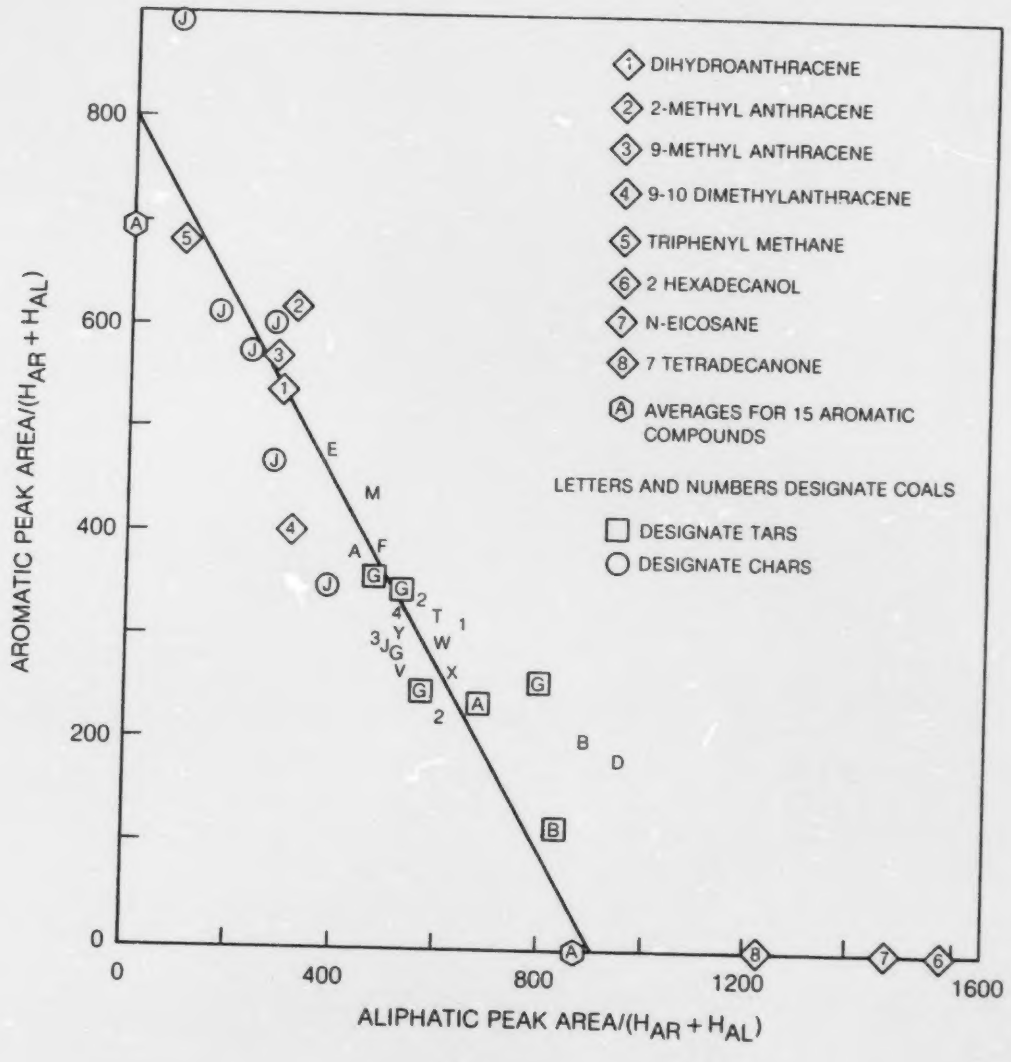

hydrogen concentrations, respectively. The equation for total hydrogen concentration $H_{total} = H_{ali} + H_{ar} + H_{hydroxyl}$ may be combined with the above equations to yield

$$a\left[\frac{A_{ABCDE}}{H_{total} - H_{hydroxyl}}\right] = 1 - b\left[\frac{A_{IJK}}{H_{total} - H_{hydroxyl}}\right]$$

where $H_{hydroxyl}$ is the hydrogen content in hydroxyl groups obtained from

$$H_{hydroxyl} = c\ A_{LMNQ}$$

where c has been determined using the relation between hydroxyl content and specific extinction coefficient at 3450 cm^{-1} derived by Ōsawa and Shih[3]. The hydrogen distribution determined in this manner for the coals of interest in this study are given in Table IV. The mineral contents of the coals are determined by the subtraction outlined are also given in Table IV.

The aromatic hydrogen values determined by this procedure are in agreement with those determined by Dormans[4] and by Mazumdar[5], et al., from pyrolysis measurements but are larger (by about a factor of 2) than those determined by Brown[6] using IR techniques.

C. Thermal Decomposition Product Distributions and Characteristics

1. Initial Characterization

In order to characterize the coals by identification and measurement of the thermal decomposition products, pyrolysis experiments were performed using the heated grid apparatus shown schematically in Fig. 5. About 50 mg of the coal -100 +324 mesh is evenly distributed between the folds of a screen and a current passed through the screen heats the coal. The Nicolet Fourier Tranform Infrared Spectrometer (FTIR) permits on-line identification of the evolved gases. The eight coals selected for initial thermal decomposition were heated to temperatures between 705°C and 830°C. The results for each coal and final temperature are shown in Tables V through XXIII.

The observed variation in product distributions obtained from the coals formed the basis of an attempt to relate the thermal decomposition product distribution to the functional group characteristics of a coal as revealed by infrared analysis (see Figs. 2a and 2b). These experiments provided the initial information supporting the hypothesis that the thermal decomposition behavior of a coal as revealed by its evolved products is a reflection of its functional group characteristics.

FIG. 5

80-7-79-5

HEATED GRID PYROLYSIS APPARATUS

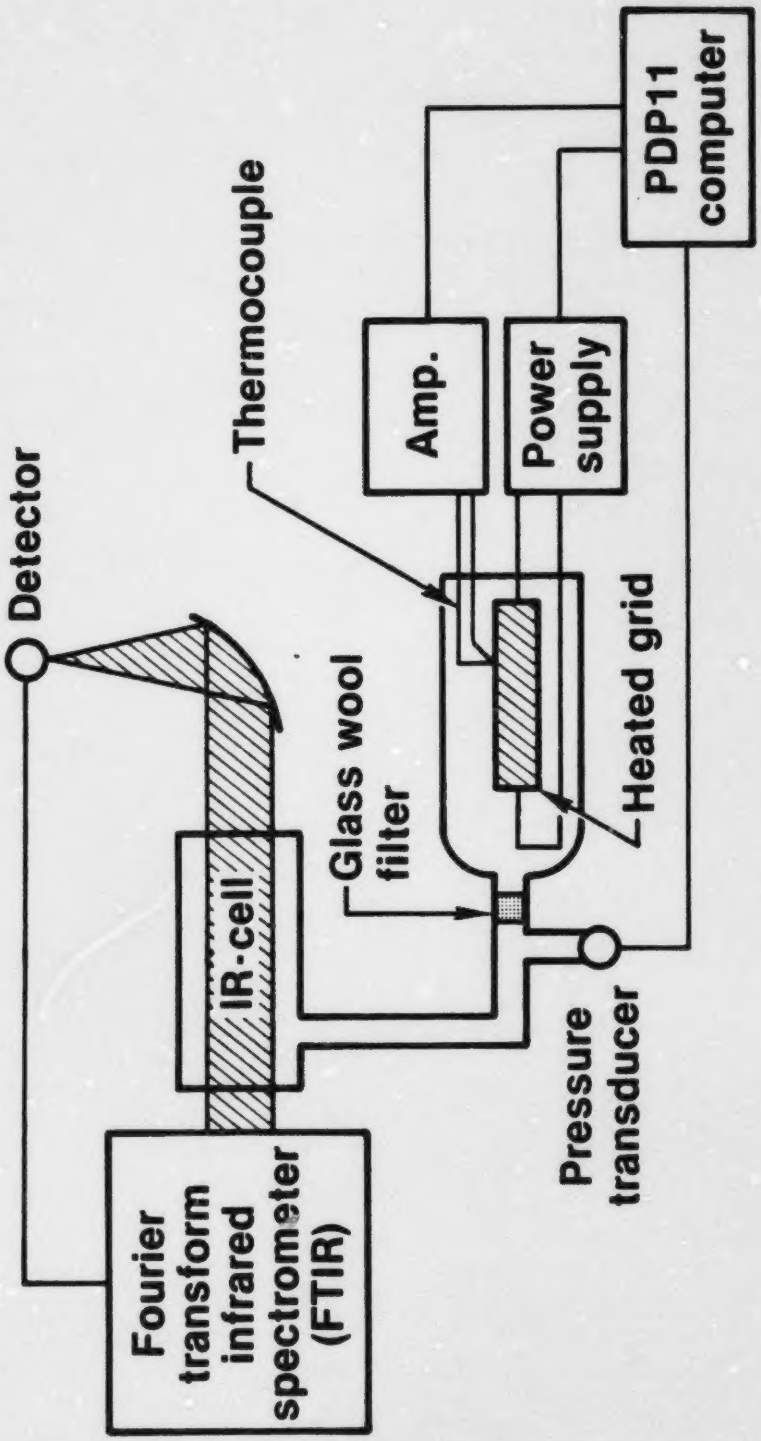
Detector
Thermocouple
Amp.
Power supply
PDP11 computer
Heated grid
Glass wool filter
IR-cell
Pressure transducer
Fourier transform infrared spectrometer (FTIR)

TABLE IV

HYDROGEN AND MINERAL COMPOSITION FROM INFRARED SPECTRA (DRY)

Coal	H(Hydr)	H(Ali)	H(Aro)	H(T)	H(ASTM)	Kaolin	Quartz	Illite	Total Clay	High Temp Ash
Rosa, Alabama	.14	2.0	1.9	4.0	4.28	2.0	1.5	0	3.5	9.2
Upper Cliff, Alabama	.16	1.8	2.0	4.0	4.41	3.5	.7	9.0	13.2	9.78
Black Creek, Alabama	.18	2.8	2.3	5.3	5.15	2.6	0	3.0	5.6	3.16
TRW Coal #2	.26	2.6	1.8	4.6	4.83	5.0	0	7.5	12.5	10.68
Utah	.36	3.7	1.5	5.6	5.18	5.0	2.5	1.5	9.0	7.48
Beulah, N. Dakota (#9)	.61	2.0	1.0	3.6	4.19	0	0	2.5	2.5	6.11
Scranton, N. Dakota	.64	1.9	1.0	3.5	4.20	1.6	1.0	1.5	4.1	7.03
Savage, Montana	.71	1.9	1.0	3.6	4.03	1.0	0	2.5	3.5	5.09

ROSA, ALABAMA

TABLE V

```
130777324  06-SEP-79     COMPOSITION OF DEVOLATILIZATION PRODUCTS  (MMF)
PRODUCT DISTRIB.  CARBON HYDROGEN OXYGEN NITROGEN  S(O)    S(M)    S(T)
 COAL       100.0 84.91     4.63    8.18    1.73    0.55    0.52    1.07

 CH(75.2)    72.7 88.45     1.96    7.17    1.94    0.49    0.37    0.86
 TAR         13.4 85.50     5.67    6.69    1.60    0.55    0.00    0.55
 GAS          8.0 66.88    20.87   12.03    0.74    1.09    3.10    4.59
 MISSING      5.9 64.82    12.94   18.70    0.82    0.55    0.00    0.55

   CONDITIONS                COMPONENT  VOL%     DIST    WT%   WT% MMF
TEMP          830.C          HYDROGEN   43.57            0.48    0.54
AMBIENT  VACUUM              METHANE    19.47            1.72    1.92
INIT PRESS -0.0MM            CO          2.82            0.43    0.49
MESH SIZE 100.               SUBTOTAL   65.86   65.86
AMOUNT        218.MG         CO2         1.06            0.26    0.29
HEAT RATE 600.C/S            C2H2        0.00            0.00    0.00
                             C2H4        1.38            0.21    0.24
   COAL                      C2H6        2.15            0.36    0.40
ROSA                         C3H6        0.88            0.20    0.23
SEAM        ERA#4            C3H8        1.49            0.36    0.41
ASTM RANK HVA#               C4H8        0.27            0.08    0.09
SS SCREEN DRIED IN           C6H6        0.06            0.03    0.03
 VAC, PELLET                 C6HX        0.00            0.00    0.00
ASH (DRY)        7.38        PARAFFIN    0.79            0.37    0.41
VOLATILES       23.71        OLEFINS     0.92            0.42    0.48
FIXED CARBON    68.91        HCN         0.61            0.09    0.10
                             NH3         0.08            0.01    0.01
                             H2S         0.00            0.00   -0.28
                             COS         0.00            0.00    0.00
P-END 16.9                   CS2         0.03            0.01    0.01
                             SO2         1.04            0.37    0.41
INIT  0.2 25.0    0.0        OTHER       3.99            1.84    2.07
SUST 30.0 24.0    0.0        SUBTOTAL   14.74   14.74
AV MOLECULAR WT    0.00      H2O        17.05   19.40    1.69    0.33
COMPUTED MOL WT   16.22      TOTAL      97.65            8.93    8.17
```

Reproduced from
best available copy.

TABLE VI

```
110740320  09-JUL-79     COMPOSITION OF DEVOLATILIZATION PRODUCTS   (MMF)
PRODUCT DISTRIB.   CARBON HYDROGEN OXYGEN NITROGEN  S(O)     S(M)     S(T)
 COAL       100.0  84.91     4.63    8.18     1.73   0.55     0.52     1.07

 CH(75.2)   77.2   86.10     2.75    8.85     1.81   0.49     0.37     0.86
 TAR        14.1   85.92     5.87    5.98     1.68   0.55    -0.05     0.50
 GAS         5.8   70.71    20.17   10.49     0.48   1.35     4.20     5.81
 MISSING     3.0   77.03    17.20   -3.11     2.19   0.55    -0.05     0.50

    CONDITIONS                COMPONENT   VOL%      DIST      WT%     WT% MMF
TEMP         705.C            HYDROGEN   38.59                0.24     0.27
AMBIENT  VACUUM               METHANE    25.25                1.26     1.41
INIT PRESS  0.1MM             CO          1.15                0.10     0.11
MESH SIZE 100.                SUBTOTAL   64.99     64.99
AMOUNT        158.MG          CO2         1.11                0.15     0.17
HEAT RATE 600.C/S             C2H2        0.00                0.00     0.00
                              C2H4        1.55                0.13     0.15
    COAL                      C2H6        3.90                0.36     0.41
ROSA                          C3H6        0.99                0.13     0.14
SEAM        ERA#4             C3H8        0.79                0.11     0.12
ASTM RANK HVA#                C4H8        0.20                0.04     0.04
SS SCREEN DRIED IN            C6H6        0.05                0.01     0.01
  VAC                         C6HX        0.00                0.00     0.00
ASH (DRY)        7.38         PARAFFIN    1.13                0.30     0.33
VOLATILES       23.71         OLEFINS     0.94                0.25     0.28
FIXED CARBON    68.91         HCN         0.51                0.04     0.05
                              NH3         0.06                0.00     0.00
                              H2S         0.00                0.00    -0.27
                              COS         0.00                0.00     0.00
P-END  7.0                    CS2         0.02                0.00     0.01
                              SO2         1.27                0.25     0.28
INIT  0.2  7.5     0.0        OTHER       6.47                1.69     1.90
SUST 10.0 20.0     0.0        SUBTOTAL   18.98     18.98
AV MOLECULAR WT    20.96      H2O        23.89     16.04      1.34     0.31
COMPUTED MOL WT    20.59      TOTAL     107.86                6.41     5.73
```

UPPER CLIFF, ALABAMA

TABLE VII

```
130782724  08-OCT-79      COMPOSITION OF DEVOLATILIZATION PRODUCTS  (MMF)
PRODUCT DISTRIB.  CARBON HYDROGEN OXYGEN NITROGEN  S(O)    S(M)    S(T)
 COAL      100.0   88.30    4.73    4.66     1.72   0.60    0.56    1.16

 CH(78.3)   74.8   90.09    1.97    5.54     1.86   0.54    0.38    0.92
 TAR        15.1   88.00    5.68    4.16     1.57   0.60   -0.05    0.54
 GAS         7.9   60.72   21.95   17.16     0.85   1.13    3.63    4.91
 MISSING     2.1  129.81   30.43  -68.82     1.27   0.60   -0.05    0.54

   CONDITIONS                  COMPONENT  VOL%     DIST      WT%    WT% MMF
TEMP        830.C              HYDROGEN   44.08             0.58    0.64
AMBIENT  VACUUM                METHANE    18.02             1.91    2.11
INIT PRESS -0.0MM              CO          2.86             0.53    0.59
MESH SIZE 100.                 SUBTOTAL   64.96    64.96
AMOUNT       209.MG            CO2         0.99             0.29    0.32
HEAT RATE 600.C/S              C2H2        0.00             0.00    0.00
                               C2H4        1.07             0.20    0.22
    COAL                       C2H6        2.09             0.42    0.46
UPPER CL                       C3H6        0.61             0.17    0.19
SEAM       PITTSBURG#          C3H8        1.15             0.33    0.37
ASTM RANK HVA#                 C4H8        0.17             0.07    0.07
SS SCREEN DRIED IN             C6H6        0.06             0.03    0.04
 VAC, PELLET                   C6HX        0.00             0.00    0.00
ASH (DRY)       9.78           PARAFFIN    0.53             0.29    0.32
VOLATILES      21.07           OLEFINS     0.88             0.49    0.54
FIXED CARBON   69.11           HCN         0.60             0.11    0.12
                               NH3         0.07             0.01    0.01
                               H2S         0.00             0.00   -0.30
                               COS         0.00             0.00    0.00
P-END 19.4                     CS2         0.01             0.01    0.01
                               SO2         0.94             0.40    0.44
INIT  0.2 25.0    0.0          OTHER       2.03             1.13    1.25
SUST 30.0 24.0    0.0          SUBTOTAL   11.20    11.20
AV MOLECULAR WT     0.00       H2O        15.20    23.84    1.81    0.67
COMPUTED MOL WT    13.24       TOTAL      91.36             8.75    8.05
```

TABLE VIII

```
110738720  09-JUL-79     COMPOSITION OF DEVOLATILIZATION PRODUCTS  (MMF)
PRODUCT DISTRIB.  CARBON HYDROGEN OXYGEN NITROGEN  S(O)     S(M)     S(T)
 COAL      100.0   88.30     4.73    4.66    1.72    0.60     0.56     1.16

 CH(78.3)  87.7    87.77     3.53    6.48    1.68    0.54     0.32     0.86
 TAR        8.7    87.14     5.50    5.29    1.47    0.60    -0.05     0.55
 GAS        2.8    81.53    20.99    3.84    0.33    2.41    10.41    13.00
 MISSING    0.9   172.39    64.78 -179.38   13.37    0.60    -0.05     0.55

   CONDITIONS              COMPONENT  VOL%      DIST      WT%   WT% MMF
TEMP        705.C          HYDROGEN   35.83               0.12    0.13
AMBIENT  VACUUM            METHANE    26.08               0.69    0.76
INIT PRESS  0.1MM          CO          1.56               0.07    0.08
MESH SIZE 100.             SUBTOTAL   63.46     63.46
AMOUNT      220 MG         CO2         1.50               0.11    0.12
HEAT RATE 600.C/S          C2H2        0.00               0.00    0.00
                           C2H4        1.24               0.06    0.06
    COAL                   C2H6        4.17               0.21    0.23
UPPER CL                   C3H6        0.67               0.05    0.05
SEAM       PITTSBURG#      C3H8        0.82               0.06    0.07
ASTM RANK HVA#             C4H8        0.00               0.00    0.00
SS SCREEN DRIED IN         C6H6        0.04               0.01    0.01
  VAC                      C6HX        0.00               0.00    0.00
ASH (DRY)       9.78       PARAFFIN    1.01               0.14    0.15
VOLATILES      21.07       OLEFINS     0.69               0.10    0.11
FIXED CARBON   69.11       HCN         0.35               0.02    0.02
                           NH3         0.00               0.00    0.00
                           H2S         0.00               0.00   -0.29
                           COS         0.00               0.00    0.00
P-END  5.2                 CS2         0.01               0.00    0.00
                           SO2         1.51               0.16    0.18
INIT  0.2  7.5     0.0     OTHER       7.59               1.05    1.16
SUST 10.0 20.0     0.0     SUBTOTAL   19.60     19.60
AV MOLECULAR WT   22.51    H2O        26.83     16.94     0.80   -0.13
COMPUTED MOL WT   21.96    TOTAL     109.89               3.62    2.70
```

TABLE IX

```
110739720  09-JUL-79     COMPOSITION OF DEVOLATILIZATION PRODUCTS  (MMF)
PRODUCT DISTRIB.   CARBON HYDROGEN OXYGEN NITROGEN  S(O)     S(M)     S(T)
 COAL      100.0   88.30     4.73    4.66     1.72   0.60     0.56     1.16

 CH(78.3)   78.5   88.88     2.89    5.99     1.69   0.54     0.36     0.90
 TAR        14.6   87.76     5.50    4.57     1.57   0.60    -0.05     0.55
 GAS         5.9   66.96    21.11   13.49     0.40   1.36     4.90     6.35
 MISSING     1.0  176.04    41.61 -152.29    14.32   0.60    -0.05     0.55

    CONDITIONS                COMPONENT  VOL%     DIST     WT%    WT% MMF
TEMP         705.C            HYDROGEN   40.35             0.28    0.30
AMBIENT  VACUUM               METHANE    26.59             1.45    1.61
INIT PRESS  0.1MM             CO          1.77             0.17    0.19
MESH SIZE 100.                SUBTOTAL   68.70    68.70
AMOUNT       186.MG           CO2         1.21             0.18    0.20
HEAT RATE 600.C/S             C2H2        0.00             0.00    0.00
                              C2H4        1.41             0.13    0.15
    COAL                      C2H6        3.82             0.39    0.43
UPPER CL                      C3H6        0.81             0.12    0.13
SEAM       PITTSBURG#         C3H8        0.94             0.14    0.16
ASTM RANK HVA#                C4H8        0.16             0.03    0.03
SS SCREEN DRIED IN            C6H6        0.07             0.02    0.02
  VAC                         C6HX        0.00             0.00    0.00
ASH (DRY)        9.78         PARAFFIN    1.01             0.29    0.32
VOLATILES       21.07         OLEFINS     0.78             0.22    0.25
FIXED CARBON    69.11         HCN         0.37             0.03    0.04
                              NH3         0.04             0.00    0.00
                              H2S         0.00             0.00   -0.29
                              COS         0.00             0.00    0.00
P-END  9.0                    CS2         0.02             0.00    0.00
                              SO2         1.35             0.30    0.33
INIT  0.2  7.5     0.0        OTHER       3.79             1.09    1.20
SUST 10.0 20.0     0.0        SUBTOTAL   15.77    15.77
AV MOLECULAR WT    19.26      H2O        20.11    15.53    1.24    0.35
COMPUTED MOL WT    17.81      TOTAL     104.58             6.09    5.42
```

BLACK CREEK, ALABAMA

TABLE X

```
130776F24  04-OCT-79     COMPOSITION OF DEVOLATILIZATION PRODUCTS  (MMF)
PRODUCT DISTRIB.  CARBON HYDROGEN OXYGEN NITROGEN   S(O)    S(M)    S(T)
 COAL       100.0  86.35     5.29   5.73     1.96   0.67    0.07    0.75

 CH(70.5)   59.5   91.01     1.52   4.78     2.04   0.65    0.06    0.71
 TAR        25.5   86.34     6.06   4.99     1.93   0.67   -0.02    0.66
 GAS        12.1   60.21    20.31  18.02     1.14   0.80    0.34    1.30
 MISSING     3.0   99.44    13.05 -19.14     4.04   0.67   -0.02    0.66

   CONDITIONS                COMPONENT  VOL%    DIST      WT%   WT% MMF
TEMP         830.C           HYDROGEN   50.23             0.82    0.85
AMBIENT  VACUUM              METHANE    16.81             2.19    2.27
INIT PRESS -0.0MM            CO          4.66             1.06    1.10
MESH SIZE 100.               SUBTOTAL   71.70   71.70
AMOUNT        164.MG         CO2         0.72             0.26    0.27
HEAT RATE 600.C/S            C2H2        0.00             0.00    0.00
                             C2H4        1.65             0.38    0.39
    COAL                     C2H6        1.92             0.47    0.49
BLACK CR                     C3H6        1.10             0.37    0.39
SEAM       PITTSBURG#        C3H8        1.46             0.52    0.54
ASTM RANK HVA#               C4H8        0.33             0.16    0.16
SS SCREEN DRIED IN           C6H6        0.07             0.04    0.04
  VAC   ,  PELLET            C6HX        0.00             0.00    0.00
ASH (DRY)        4.56        PARAFFIN    0.60             0.41    0.43
VOLATILES       28.92        OLEFINS     1.55             1.06    1.10
FIXED CARBON    66.52        HCN         0.96             0.21    0.22
                             NH3         0.21             0.03    0.03
                             H2S         0.00             0.00   -0.05
                             COS         0.00             0.00    0.00
P-END 18.7                   CS2         0.01             0.00    0.00
                             SO2         0.29             0.15    0.16
INIT  0.2 25.0     0.0       OTHER       3.37             2.30    2.39
SUST 30.0 24.0     0.0       SUBTOTAL   14.23   14.23
AV MOLECULAR WT     0.00     H2O        13.06   14.07     1.91    1.47
COMPUTED MOL WT    15.17     TOTAL      98.99            12.34   12.25
```

TABLE XI

```
110742F20  11-JUL-79     COMPOSITION OF DEVOLATILIZATION PRODUCTS  (MMF)
PRODUCT DISTRIB.  CARBON HYDROGEN OXYGEN NITROGEN  S(O)     S(M)     S(T)
 COAL      100.0   86.35     5.29    5.73     1.96   0.67     0.07     0.75

 CH(70.5)   82.9   85.72     4.56    7.10     1.97   0.65     0.04     0.69
 TAR        12.3   85.73     6.29    5.49     1.82   0.67    -0.02     0.66
 GAS         3.9   69.03    20.15   10.56     0.73   1.20     0.98     2.33
 MISSING     0.9  233.95    -5.74 -145.52     9.05   0.67    -0.02     0.66

    CONDITIONS                COMPONENT  VOL%     DIST      WT%    WT% MMF
TEMP        705.C             HYDROGEN   34.16              0.08     0.08
AMBIENT  VACUUM               METHANE    26.34              0.50     0.52
INIT PRESS  0.1MM             CO          2.49              0.08     0.09
MESH SIZE 100.                SUBTOTAL   62.99    62.99
AMOUNT       191.MG           CO2         0.80              0.04     0.04
HEAT RATE 600.C/S             C2H2        0.00              0.00     0.00
                              C2H4        1.58              0.05     0.05
    COAL                      C2H6        5.31              0.19     0.20
BLACK CR                      C3H6        1.43              0.07     0.07
SEAM        PITTSBURG#        C3H8        1.19              0.06     0.06
ASTM RANK HVA#                C4H8        0.00              0.00     0.00
SS SCREEN DRIED IN            C6H6        0.00              0.00     0.00
  VAC                         C6HX        0.00              0.00     0.00
ASH (DRY)        4.56         PARAFFIN    1.53              0.15     0.16
VOLATILES       28.92         OLEFINS     1.88              0.19     0.20
FIXED CARBON    66.52         HCN         0.69              0.02     0.02
                              NH3         0.13              0.00     0.00
                              H2S         0.00              0.00    -0.04
                              COS         0.00              0.00     0.00
P-END  3.3                    CS2         0.01              0.00     0.00
                              SO2         0.69              0.05     0.05
INIT  0.2  7.5     0.0        OTHER       2.89              0.29     0.30
SUST 10.0 20.0     0.0        SUBTOTAL   18.12    18.12
AV MOLECULAR WT   35.66       H2O        22.58    18.89     0.48     0.11
COMPUTED MOL WT   19.12       TOTAL     103.69              2.27     1.93
```

TABLE XII

```
110743F20  12-JUL-79      COMPOSITION OF DEVOLATILIZATION PRODUCTS   (MMF)
PRODUCT DISTRIB.   CARBON HYDROGEN OXYGEN NITROGEN   S(O)     S(M)     S(T)
 COAL      100.0   86.35     5.29    5.73     1.96   0.67     0.07     0.75

 CH(70.5)  68.7    87.73     4.02    5.60     2.00   0.65     0.05     0.70
 TAR       20.5    85.81     6.19    5.47     1.85   0.67    -0.02     0.65
 GAS        5.7    64.88    19.21   15.14     0.55   0.98     0.74     2.30
 MISSING    5.1    93.74     3.29   -2.06     3.52   0.67    -0.02     0.65

                            COMPONENT   VOL%     DIST      WT%    WT% MMF
    CONDITIONS              HYDROGEN    34.39              0.17    0.18
TEMP         725.C          METHANE     27.71              1.11    1.15
AMBIENT  VACUUM             CO           2.09              0.15    0.15
INIT PRESS  0.1MM           SUBTOTAL    64.20    64.20
MESH SIZE 100.              CO2          1.01              0.11    0.12
AMOUNT       216.MG         C2H2         0.00              0.00    0.00
HEAT RATE 600.C/S           C2H4         1.58              0.11    0.11
                            C2H6         4.70              0.35    0.37
     COAL                   C3H6         1.35              0.14    0.15
BLACK CR                    C3H8         1.11              0.12    0.13
SEAM        PITTSBURG#      C4H8         0.22              0.03    0.03
ASTM RANK HVA#              C6H6         0.06              0.01    0.01
SS SCREEN DRIED IN          C6HX         0.00              0.00    0.00
    VAC                     PARAFFIN     1.48              0.31    0.32
ASH (DRY)         4.56      OLEFINS      1.52              0.32    0.33
VOLATILES        28.92      HCN          0.55              0.04    0.04
FIXED CARBON     66.52      NH3          0.16              0.01    0.01
                            H2S          0.00              0.00   -0.04
                            COS          0.00              0.00    0.00
                            CS2          0.01              0.00    0.00
P-END  7.7                  SO2          0.58              0.09    0.10
                            OTHER        4.60              0.97    1.00
INIT  0.2  7.5     0.0      SUBTOTAL    18.94    18.94
SUST 10.0 20.0     0.0      H2O         20.90    16.86     0.94    0.56
AV MOLECULAR WT   24.03     TOTAL      104.05              4.99    4.71
COMPUTED MOL WT   19.94
```

TRW COAL #2

TABLE XIII

```
130781624  07-SEP-79     COMPOSITION OF DEVOLATILIZATION PRODUCTS  (MMF)
PRODUCT DISTRIB.   CARBON HYDROGEN OXYGEN NITROGEN   S(O)    S(M)    S(T)
 COAL      100.0   83.87     5.29    8.26    1.58    1.00    0.00    1.00

 CH(66.0)   59.2   89.36     1.52    6.51    1.73    0.88    0.00    0.88
 TAR        27.8   83.25     6.05    8.20    1.49    1.00   -0.13    0.88
 GAS        11.4   60.99    18.36   18.80    0.88    1.65    0.33    2.11
 MISSING     1.6   55.03    37.86   -1.04    2.28    1.00   -0.13    0.88

    CONDITIONS              COMPONENT   VOL%     DIST      WT%    WT% MMF
TEMP          830.C         HYDROGEN    35.64              0.54    0.61
AMBIENT  VACUUM             METHANE     17.03              2.05    2.34
INIT PRESS -0.0MM           CO           5.57              1.17    1.34
MESH SIZE 100.              SUBTOTAL    58.24     58.24
AMOUNT        202.MG        CO2          1.35              0.45    0.51
HEAT RATE 600.C/S           C2H2         0.00              0.00    0.00
                            C2H4         1.56              0.33    0.38
    COAL                    C2H6         1.89              0.43    0.49
TRW                         C3H6         0.94              0.30    0.34
SEAM       PITTSBURG#       C3H8         1.47              0.49    0.56
ASTM RANK HVA#              C4H8         0.26              0.11    0.13
SS SCREEN DRIED IN          C6H6         0.06              0.04    0.04
 VAC, PELLET                C6HX         0.00              0.00    0.00
ASH (DRY)       13.04       PARAFFIN     0.67              0.42    0.48
VOLATILES       31.51       OLEFINS      1.36              0.86    0.98
FIXED CARBON    55.45       HCN          0.79              0.16    0.18
                            NH3          0.06              0.01    0.01
                            H2S          0.00              0.00   -0.05
                            COS          0.00              0.00    0.00
P-END 21.4                  CS2          0.01              0.01    0.01
                            SO2          0.57              0.27    0.31
INIT  0.2 20.0     0.0      OTHER        2.64              1.67    1.91
SUST 30.0 24.0     0.0      SUBTOTAL    13.63     13.63
AV MOLECULAR WT     0.00    H2O         19.20     28.13    2.60    0.99
-COMPUTED MOL WT   15.81    TOTAL       91.07             11.90   11.55
```

TABLE XIV

```
110736620  09-JUL-79      COMPOSITION OF DEVOLATILIZATION PRODUCTS  (MMF)
PRODUCT DISTRIB.   CARBON HYDROGEN OXYGEN NITROGEN  S(O)     S(M)     S(T)
 COAL      100.0   83.87      5.29    8.26     1.58  1.00     0.00     1.00

 CH(66.0)   78.9   85.32      3.82    8.33     1.64  0.88     0.00     0.88
 TAR        14.8   83.56      6.39    7.57     1.47  1.00    -0.12     0.88
 GAS         3.4   78.18     16.43    3.66     0.25  3.90     0.63     5.29
 MISSING     2.9   52.59     26.65   15.12     1.80  1.00    -0.12     0.88

   CONDITIONS                 COMPONENT   VOL%    DIST     WT%    WT% MMF
TEMP         705.C            HYDROGEN   20.73             0.08    0.09
AMBIENT  VACUUM               METHANE    19.09             0.60    0.68
INIT PRESS  0.1MM             CO          2.70             0.15    0.17
MESH SIZE 100.                SUBTOTAL   42.52   42.52
AMOUNT        213.MG          CO2         1.96             0.17    0.19
HEAT RATE 600.C/S             C2H2        0.00             0.00    0.00
                              C2H4        1.40             0.08    0.09
    COAL                      C2H6        3.86             0.23    0.26
TRW                           C3H6        1.04             0.09    0.10
SEAM        PITTSBURG#        C3H8        0.79             0.07    0.08
ASTM RANK HVA#                C4H8        0.24             0.03    0.03
SS SCREEN DRIED IN            C6H6        0.00             0.00    0.00
  VAC                         C6HX        0.00             0.00    0.00
ASH (DRY)       13.04         PARAFFIN    1.52             0.25    0.29
VOLATILES       31.51         OLEFINS     0.94             0.15    0.18
FIXED CARBON    55.45         HCN         0.37             0.02    0.02
                              NH3         0.00             0.00    0.00
                              H2S         0.00             0.00   -0.02
                              COS         0.00             0.00    0.00
P-END  6.0                    CS2         0.00             0.00    0.00
                              SO2         1.24             0.16    0.18
INIT  0.2  7.5      0.0       OTHER      13.20             2.17    2.48
SUST 10.0 20.0      0.0       SUBTOTAL   26.56   26.56
AV MOLECULAR WT    22.28      H2O        33.13   30.92     1.17   -0.18
COMPUTED MOL WT    27.57      TOTAL     102.21             5.41    4.64
```

TABLE XV

```
110737620  09-JUL-79     COMPOSITION OF DEVOLATILIZATION PRODUCTS  (MMF)
PRODUCT DISTRIB.  CARBON HYDROGEN OXYGEN NITROGEN   S(O)     S(M)     S(T)
 COAL      100.0   83.87     5.29    8.26     1.58   1.00     0.00     1.00

 CH(66.0)  70.9    86.24     3.08    8.18     1.63   0.88     0.00     0.88
 TAR       19.6    85.02     6.53    5.88     1.57   1.00    -0.11     0.89
 GAS        5.4    69.29    17.26   11.48     0.29   2.63     0.48     3.79
 MISSING    4.1    56.59    21.89   16.83     2.42   1.00    -0.11     0.89

    CONDITIONS                 COMPONENT   VOL%     DIST     WT%    WT% MMF
TEMP        705.C              HYDROGEN   24.52              0.13     0.14
AMBIENT  VACUUM                METHANE    19.53              0.80     0.91
INIT PRESS  0.1MM              CO          2.11              0.15     0.17
MESH SIZE 100.                 SUBTOTAL   46.15    46.15
AMOUNT      209.MG             CO2         1.95              0.22     0.25
HEAT RATE 600.C/S              C2H2        0.00              0.00     0.00
                               C2H4        1.59              0.11     0.13
    COAL                       C2H6        3.87              0.30     0.34
TRW                            C3H6        1.11              0.12     0.14
SEAM        PITTSBURG0         C3H8        1.12              0.13     0.14
ASTM RANK HVA0                 C4H8        0.19              0.03     0.03
SS SCREEN DRIED IN             C6H6        0.00              0.00     0.00
   VAC                         C6HX        0.00              0.00     0.00
ASH (DRY)       13.04          PARAFFIN    1.55              0.33     0.38
VOLATILES       31.51          OLEFINS     1.39              0.30     0.34
FIXED CARBON    55.45          HCN         0.35              0.02     0.03
                               NH3         0.00              0.00     0.00
                               H2S         0.00              0.00    -0.03
                               COS         0.00              0.00     0.00
P-END  7.6                     CS2         0.01              0.00     0.00
                               SO2         1.17              0.19     0.22
INIT  0.2  7.5     0.0         OTHER       6.37              1.37     1.56
SUST 10.0 20.0     0.0         SUBTOTAL   20.67    20.67
AV MOLECULAR WT    24.07       H2O        32.52    33.17     1.50     0.20
COMPUTED MOL WT    22.27       TOTAL      99.35              5.71     4.97
```

UTAH

TABLE XVI

```
130754224  08-OCT-79     COMPOSITION OF DEVOLATILIZATION PRODUCTS  (MMF)
PRODUCT DISTRIB.   CARBON HYDROGEN OXYGEN NITROGEN   S(O)     S(M)     S(T)
 COAL      100.0    78.18     5.52   13.86     1.69   0.76     0.00     0.76

 CN(55.3)  49.8    84.64     2.23   10.51     1.93   0.69     0.00     0.69
 TAR       28.2    79.96     6.95   10.76     1.58   0.76    -0.04     0.71
 GAS       20.5    56.89    14.73   26.84     1.06   0.92     0.06     1.03
 MISSING    1.6   118.86   -35.51    6.32     3.95   0.76    -0.04     0.71

   CONDITIONS                  COMPONENT  VOL%      DIST      WT%    WT% MMF
TEMP        815.C              HYDROGEN   37.85               0.70    0.77
AMBIENT  VACUUM                METHANE    10.54               1.56    1.71
INIT PRESS -0.0MM              CO         10.70               2.77    3.03
MESH SIZE 100.                 SUBTOTAL   59.09     59.09
AMOUNT       194.MG            CO2         2.86               1.16    1.27
HEAT RATE 600.C/S              C2H2        0.09               0.02    0.02
                               C2H4        1.55               0.40    0.44
    COAL                       C2H6        1.23               0.34    0.37
UTAH                           C3H6        1.10               0.43    0.47
SEAM       ERA#4               C3H8        1.08               0.44    0.48
ASTM RANK HVA#                 C4H8        0.28               0.15    0.16
SS SCREEN PELLETS              C6H6        0.03               0.03    0.03
  DRIED IN VAC                 C6HX        0.00               0.00    0.00
ASH (DRY)        7.91          PARAFFIN    0.36               0.28    0.30
VOLATILES       41.54          OLEFINS     1.76               1.37    1.50
FIXED CARBON    50.06          HCN         1.43               0.36    0.39
                               NH3         0.13               0.02    0.02
                               H2S         0.00               0.00   -0.03
                               COS         0.00               0.00    0.00
P-END 25.2                     CS2         0.01               0.01    0.01
                               SO2         0.39               0.23    0.25
INIT  0.2 25.0     0.0         OTHER       7.58               5.88    6.44
SUST 30.0 24.0     0.0         SUBTOTAL   19.88     19.88
AV MOLECULAR WT     0.00       H2O        24.54     21.03     4.08    3.14
COMPUTED MOL WT    21.88       TOTAL     103.51              20.21   20.76
```

BEULAH, N. DAKOTA (#9)

TABLE XVII

```
130779124  08-OCT-79     COMPOSITION OF DEVOLATILIZATION PRODUCTS  (MMF)
PRODUCT DISTRIB.  CARBON HYDROGEN OXYGEN NITROGEN  S(O)     S(M)     S(T)
 COAL      100.0   68.60     4.39  25.79     1.03  0.18     0.05     0.24

 CH(56.6)   55.6   80.52     1.42  16.81     1.09  0.17     0.05     0.22
 TAR        14.7   72.07     5.90  20.61     1.24  0.18    -0.01     0.18
 GAS        42.6   55.05    10.38  34.09     0.33  0.20     0.06     0.21
 MISSING   -12.9   79.24    13.03   8.54    -0.81  0.18    -0.01     0.18

    CONDITIONS               COMPONENT  VOL%      DIST     WT%    WT% MMF
TEMP          830.C          HYDROGEN   25.49              0.70    0.76
AMBIENT  VACUUM              METHANE     3.99              0.88    0.95
INIT PRESS  0.0MM            CO         27.80             10.71   11.53
MESH SIZE 100.               SUBTOTAL   57.28     57.28
AMOUNT       190.MG          CO2         6.14              3.72    4.00
HEAT RATE 600.C/S            C2H2        0.00              0.00    0.00
                             C2H4        0.50              0.19    0.21
     COAL                    C2H6        0.42              0.17    0.19
BEULAH                       C3H6        0.26              0.15    0.16
SEAM       ERA#4             C3H8        0.25              0.15    0.16
ASTM RANK HVA#               C4H8        0.08              0.06    0.07
SS SCREEN DRIED IN           C6H6        0.00              0.00    0.00
 VAC, PELLET                 C6HX        0.00              0.00    0.00
ASH (DRY)       7.60         PARAFFIN    0.07              0.08    0.09
VOLATILES      41.34         OLEFINS     0.54              0.63    0.68
FIXED CARBON   51.06         HCN         0.69              0.26    0.27
                             NH3         0.00              0.00   -0.03
                             H2S         0.00              0.00    0.00
                             COS         0.00              0.00    0.00
P-END 36.9                   CS2         0.01              0.01    0.01
                             SO2         0.18              0.16    0.17
INIT  0.2 20.0     0.0       OTHER      14.62             16.90   18.20
SUST 30.0 24.0     0.0       SUBTOTAL   23.75     23.75
AV MOLECULAR WT     0.00     H2O        25.61     18.97    6.35    5.77
COMPUTED MOL WT    29.87     TOTAL     106.64             41.12   43.18
```

TABLE XVIII

```
110744120  12-JUL-79     COMPOSITION OF DEVOLATILIZATION PRODUCTS  (MMF)
PRODUCT DISTRIB.   CARBON HYDROGEN OXYGEN NITROGEN   S(O)     S(M)     S(T)
 COAL      100.0    68.60    4.39   25.79    1.03    0.18     0.05     0.24

 CH(56.6)   63.3    79.15    2.51   16.98    1.19    0.17     0.04     0.21
 TAR        13.0    73.18    6.43   19.23    0.98    0.18    -0.01     0.17
 GAS        23.1    56.24   12.58   30.60    0.23    0.22     0.12     0.35
 MISSING     0.6  -637.56 -149.59  875.41   16.20    0.18    -0.01     0.17

   CONDITIONS                  COMPONENT   VOL%     DIST      WT%    WT% MMF
TEMP         705.C             HYDROGEN   27.06              0.51     0.55
AMBIENT  VACUUM                METHANE     4.61              0.70     0.75
INIT PRESS  0.1MM              CO         10.46              2.77     2.99
MESH SIZE 100.                 SUBTOTAL   42.13    42.13
AMOUNT       182.MG            CO2         6.45              2.69     2.89
HEAT RATE 600.C/S              C2H2        0.00              0.00     0.00
                               C2H4        0.39              0.10     0.11
    COAL                       C2H6        0.64              0.18     0.20
BEULAH                         C3H6        0.23              0.09     0.10
SEAM        ERA#4              C3HS        0.26              0.11     0.12
ASTM RANK  HVA#                C4H8        0.00              0.00     0.00
SS SCREEN DRIED IN             C6H6        0.00              0.00     0.00
  VAC                          C6HX        0.00              0.00     0.00
ASH (DRY)       7.60           PARAFFIN    0.18              0.15     0.16
VOLATILES      41.34           OLEFINS     0.31              0.25     0.26
FIXED CARBON   51.06           HCN         0.47              0.12     0.13
                               NH3         0.00              0.00    -0.03
                               H2S         0.00              0.00     0.00
P-END 24.4                     COS         0.00              0.00     0.00
                               CS2         0.01              0.01     0.01
INIT  0.2  7.5      0.0        SO2         0.36              0.22     0.24
SUST 10.0 20.0      0.0        OTHER      17.22             13.71    14.76
AV MOLECULAR WT    23.77       SUBTOTAL   26.53    26.53
COMPUTED MOL WT    28.94       H2O        34.10    31.34     5.82     5.45
                               TOTAL     102.76             27.42    28.69
```

TABLE XIX

```
120745120  12-JUL-79     COMPOSITION OF DEVOLATILIZATION PRODUCTS  (MMF)
PRODUCT DISTRIB.  CARBON HYDROGEN OXYGEN NITROGEN  S(O)    S(M)    S(T)
 COAL      100.0   68.60     4.39  25.79     1.03  0.18    0.05    0.24

 CH(56.6)   67.4   73.56     2.42  22.84     1.01  0.17    0.04    0.21
 TAR         8.6   73.78     5.95  19.09     0.99  0.18   -0.00    0.18
 GAS        20.1   52.10    12.05  35.18     0.34  0.23    0.13    0.40
 MISSING     3.9   56.69    -4.37  42.92     5.13  0.18   -0.00    0.18

   CONDITIONS                COMPONENT   VOL%      DIST      WT%    WT% MMF
TEMP          725.C          HYDROGEN   29.37               0.53    0.57
AMBIENT  VACUUM              METHANE     4.72               0.68    0.73
INIT PRESS  0.1MM            CO         14.51               3.67    3.95
MESH SIZE 100.               SUBTOTAL   48.60     48.60
AMOUNT       164.MG          CO2         5.78               2.30    2.47
HEAT RATE 600.C/S            C2H2        0.00               0.00    0.00
                             C2H4        0.42               0.11    0.12
    COAL                     C2H6        0.59               0.16    0.17
BEULAH                       C3H6        0.26               0.10    0.10
SEAM        ERA#4            C3H8        0.20               0.08    0.09
ASTM RANK HVA#               C4H8        0.04               0.02    0.02
SS SCREEN DRIED IN           C6H6        0.00               0.00    0.00
  VAC                        C6HX        0.00               0.00    0.00
ASH (DRY)        7.60        PARAFFIN    0.13               0.10    0.11
VOLATILES       41.34        OLEFINS     0.41               0.31    0.33
FIXED CARBON    51.06        HCN         0.55               0.13    0.14
                             NH3         0.03               0.00    0.00
                             H2S         0.00               0.00   -0.03
                             COS         0.00               0.00    0.00
P-END 20.9                   CS2         0.01               0.01    0.01
                             SO2         0.32               0.18    0.20
INIT  0.2 15.0     0.0       OTHER      12.04               9.13    9.83
SUST 20.0 20.0     0.0       SUBTOTAL   20.78     20.78
AV MOLECULAR WT   21.91      H2O        31.18     30.62     5.07    4.60
COMPUTED MOL WT   25.01      TOTAL     100.56              22.58   23.42
```

SCRANTON, N. DAKOTA

TABLE XX

```
130784E24  05-OCT-79     COMPOSITION OF DEVOLATILIZATION PRODUCTS  (MMF)
PRODUCT DISTRIB.  CARBON HYDROGEN OXYGEN NITROGEN  S(O)     S(M)     S(T)
 COAL      100.0   67.95    4.46   25.22    1.00    1.36     0.53     1.90

 CHK53.0)   57.9   80.81    1.33   15.57    1.04    1.25     0.45     1.70
 TAR         9.8   75.63    6.68   15.15    1.18    1.36    -0.05     1.32
 GAS        46.7   56.04   10.03   34.04    0.39    1.51     0.58     1.68
 MISSING   -14.4   86.28   11.49    8.11   -0.73    1.36    -0.05     1.32

    CONDITIONS             COMPONENT  VOL%     DIST      WT%   WT% MMF
TEMP          850.C        HYDROGEN   21.29              0.67    0.73
AMBIENT   VACUUM           METHANE     5.21              1.32    1.44
INIT PRESS -0.1MM          CO         29.56             13.08   14.28
MESH SIZE 100.             SUBTOTAL   56.06    56.06
AMOUNT        199.MG       CO2         5.41              3.76    4.11
HEAT RATE 600.C/S          C2H2        0.00              0.00    0.00
                           C2H4        0.78              0.35    0.38
    COAL                   C2H6        0.50              0.24    0.26
SCRANTON                   C3H6        0.39              0.26    0.28
SEAM       PITTSBURG#      C3H8        0.33              0.23    0.25
ASTM RANK HVA#             C4H8        0.14              0.13    0.14
SS SCREEN PELLETS          C6H6        0.00              0.00    0.00
  DRIED IN VAC             C6HX        0.00              0.00    0.00
ASH (DRY)        11.53     PARAFFIN    0.03              0.04    0.05
VOLATILES        44.36     OLEFINS     0.78              1.03    1.13
FIXED CARBON     44.11     HCN         0.72              0.31    0.33
                           NH3         0.05              0.01    0.01
                           H2S         0.00              0.00   -0.32
                           COS         0.00              0.00    0.00
P-END 44.2                 CS2         0.01              0.01    0.01
                           SO2         0.10              0.10    0.11
INIT  0.2 25.0    0.0      OTHER      12.84             17.05   18.61
SUST 30.0 24.0    0.0      SUBTOTAL   22.06    22.06
AV MOLECULAR WT    0.00    H2O        21.45    21.87     6.10    5.52
COMPUTED MOL WT   28.27    TOTAL      99.58             44.70   47.32
```

TABLE XXI

```
120746E20  12-JUL-79     COMPOSITION OF DEVOLATILIZATION PRODUCTS  (MMF)
PRODUCT DISTRIB.   CARBON HYDROGEN OXYGEN NITROGEN  S(O)      S(M)      S(T)
 COAL       100.0   67.95     4.46   25.22     1.00   1.36      0.53      1.90

 CH(53.0)    70.8   73.89     2.37   21.71     0.78   1.25      0.37      1.62
 TAR          6.4   78.63     7.11   13.64    -0.74   1.36     -0.07      1.29
 GAS         22.3   57.45    12.33   30.56     0.25   1.73      1.24      3.00
 MISSING      0.6 -379.16   -73.58  383.01    78.12   1.36     -0.07      1.29

   CONDITIONS                COMPONENT   VOL%      DIST        WT%     WT% MMF
TEMP         725.C           HYDROGEN   24.85                 0.46      0.50
AMBIENT  VACUUM              METHANE     4.92                 0.72      0.79
INIT PRESS  0.1MM            CO         12.64                 3.24      3.54
MESH SIZE 100.               SUBTOTAL   42.41     42.41
AMOUNT       166.MG          CO2         6.23                 2.51      2.74
HEAT RATE 600.C/S            C2H2        0.00                 0.00      0.00
                             C2H4        0.35                 0.09      0.10
    COAL                     C2H6        0.73                 0.20      0.22
SCRANTON                     C3H6        0.27                 0.10      0.11
SEAM       PITTSBURG#        C3H8        0.20                 0.08      0.09
ASTM RANK HVA#               C4H8        0.00                 0.00      0.00
SS SCREEN DRIED IN           C6H6        0.00                 0.00      0.00
  VAC                        C6HX        0.00                 0.00      0.00
ASH (DRY)       11.53        PARAFFIN    0.14                 0.11      0.11
VOLATILES       44.36        OLEFINS     0.49                 0.38      0.41
FIXED CARBON    44.11        HCN         0.47                 0.12      0.13
                             NH3         0.02                 0.00      0.00
                             H2S         0.00                 0.00     -0.28
                             COS         0.00                 0.00      0.00
P-END 21.4                   CS2         0.01                 0.00      0.00
                             SO2         0.29                 0.17      0.18
INIT  0.2 15.0      0.0      OTHER      16.98                13.07     14.26
SUST 20.0 20.0      0.0      SUBTOTAL   26.17     26.17
AV MOLECULAR WT    23.80     H2O        32.72     31.42       5.40      4.96
COMPUTED MOL WT    29.08     TOTAL     101.29                26.65     27.88
```

SAVAGE, MONTANA

TABLE XXII

```
130786524  05-OCT-79     COMPOSITION OF DEVOLATILIZATION PRODUCTS   (MMF)
PRODUCT DISTRIB.   CARBON HYDROGEN OXYGEN NITROGEN   S(O)     S(M)     S(T)
 COAL      100.0   67.91     4.19   26.38     1.06   0.46     0.02     0.48

 CH(53.3)   50.2   80.23     1.75   16.34     1.25   0.43     0.02     0.45
 TAR        11.7   74.64     5.65   18.18     1.08   0.46    -0.01     0.44
 GAS        36.5   54.15    10.08   35.16     0.46   0.49     0.03     0.55
 MISSING     1.6  -54.90   -65.41  203.00     8.89   0.46    -0.01     0.44

    CONDITIONS                 COMPONENT  VOL%     DIST      WT%     WT% MMF
TEMP        815.C              HYDROGEN   17.74              0.45     0.48
AMBIENT  VACUUM                METHANE     4.92              1.00     1.07
INIT PRESS -0.0MM              CO         25.22              9.01     9.57
MESH SIZE 100.                 SUBTOTAL   47.88    47.88
AMOUNT      183.MG             CO2         6.07              3.41     3.62
HEAT RATE 600.C/S              C2H2        0.00              0.00     0.00
                               C2H4        0.69              0.25     0.26
    COAL                       C2H6        0.56              0.21     0.23
SAVAGE                         C3H6        0.42              0.22     0.24
SEAM       PITTSBURG#          C3H8        0.32              0.18     0.19
ASTM RANK HVA#                 C4H8        0.13              0.09     0.10
SS SCREEN PELLETS              C6H6        0.00              0.00     0.00
  DRIED IN VAC                 C6HX        0.00              0.00     0.00
ASH (DRY)        7.25          PARAFFIN    0.08              0.08     0.09
VOLATILES       44.76          OLEFINS     0.72              0.77     0.82
FIXED CARBON    47.99          HCN         0.84              0.29     0.31
                               NH3         0.06              0.01     0.01
                               H2S         0.00              0.00    -0.02
                               COS         0.00              0.00     0.00
P-END 32.7                     CS2         0.01              0.01     0.01
                               SO2         0.17              0.14     0.15
INIT  0.2 25.0     0.0         OTHER      12.72             13.62    14.48
SUST 30.0 24.0     0.0         SUBTOTAL   22.78    22.78
AV MOLECULAR WT     0.00       H2O        25.96    29.34     5.96     5.46
COMPUTED MOL WT    28.00       TOTAL      96.62             35.71    37.05
```

TABLE XXIII

```
130785524  07-SEP-79     COMPOSITION OF DEVOLATILIZATION PRODUCTS   (MMF)
PRODUCT DISTRIB.   CARBON HYDROGEN OXYGEN NITROGEN  S(O)    S(M)     S(T)
 COAL      100.0   67.91     4.19   26.38     1.06   0.46    0.02     0.48

 CH(53.3)  52.0    76.20     1.59   20.63     1.15   0.43    0.02     0.45
 TAR       12.4    74.64     5.65   18.18     1.08   0.46   -0.01     0.44
 GAS       37.1    51.80     9.45   38.06     0.55   0.49    0.03     0.51
 MISSING   -1.4     9.23    59.34   49.38    -9.04   0.46   -0.01     0.44

    CONDITIONS                COMPONENT  VOL%      DIST      WT%     WT% MMF
TEMP         850.C            HYDROGEN   22.37               0.63     0.67
AMBIENT  VACUUM               METHANE     4.75               1.07     1.14
INIT PRESS -0.0MM             CO         29.85              11.75    12.49
MESH SIZE 100.                SUBTOTAL   56.98     56.98
AMOUNT      194.MG            CO2         5.78               3.57     3.80
HEAT RATE 600.C/S             C2H2        0.00               0.00     0.00
                              C2H4        0.76               0.30     0.32
    COAL                      C2H6        0.50               0.21     0.22
SAVAGE                        C3H6        0.40               0.23     0.25
SEAM       PITTSBURG#         C3H8        0.33               0.20     0.22
ASTM RANK HVA#                C4H8        0.12               0.10     0.11
SS SCREEN PELLETS             C6H6        0.00               0.00     0.00
DRIED IN VAC                  C6HX        0.00               0.00     0.00
ASH (DRY)       7.25          PARAFFIN    0.06               0.08     0.08
VOLATILES      44.76          OLEFINS     0.65               0.77     0.82
FIXED CARBON   47.99          HCN         0.92               0.35     0.37
                              NH3         0.07               0.02     0.02
                              H2S         0.00               0.00    -0.02
                              COS         0.00               0.00     0.00
P-END 38.2                    CS2         0.01               0.01     0.01
                              SO2         0.14               0.13     0.14
INIT  0.2 25.0      0.0       OTHER       9.65              11.39    12.10
SUST 30.0 24.0      0.0       SUBTOTAL   19.38     19.38
AV MOLECULAR WT     0.00      H2O        21.44     23.64     5.42     4.89
COMPUTED MOL WT    25.77      TOTAL      97.80              36.23    37.61
```

FIG. 6

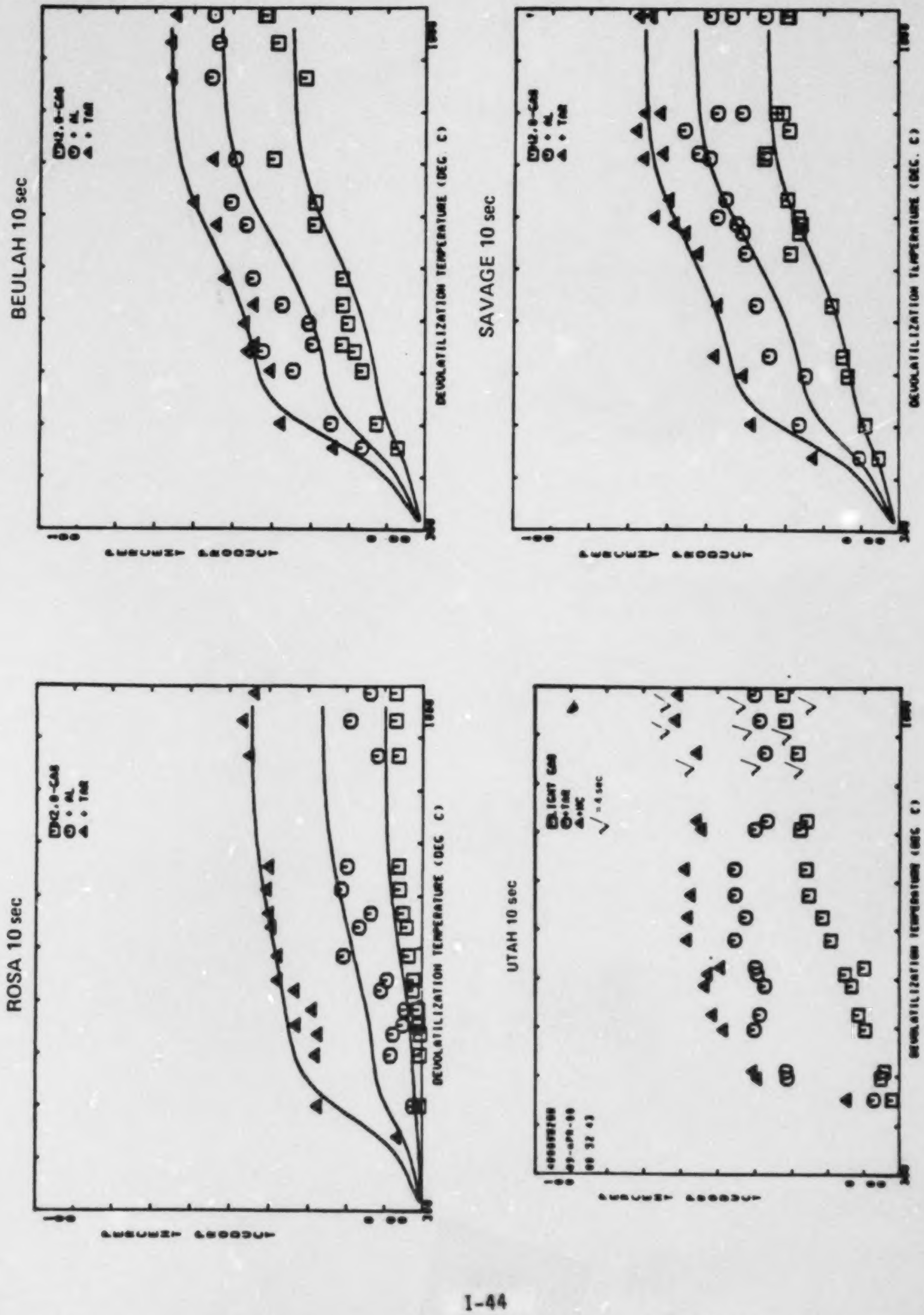
BEULAH 10 sec
SAVAGE 10 sec
ROSA 10 sec
UTAH 10 sec
DEVOLATILIZATION TEMPERATURE (DEG. C)
300
1000
0.00
100
GAS
AL
TAR
LIGHT GAS
TAR
HC
= 4 sec

FIG. 7

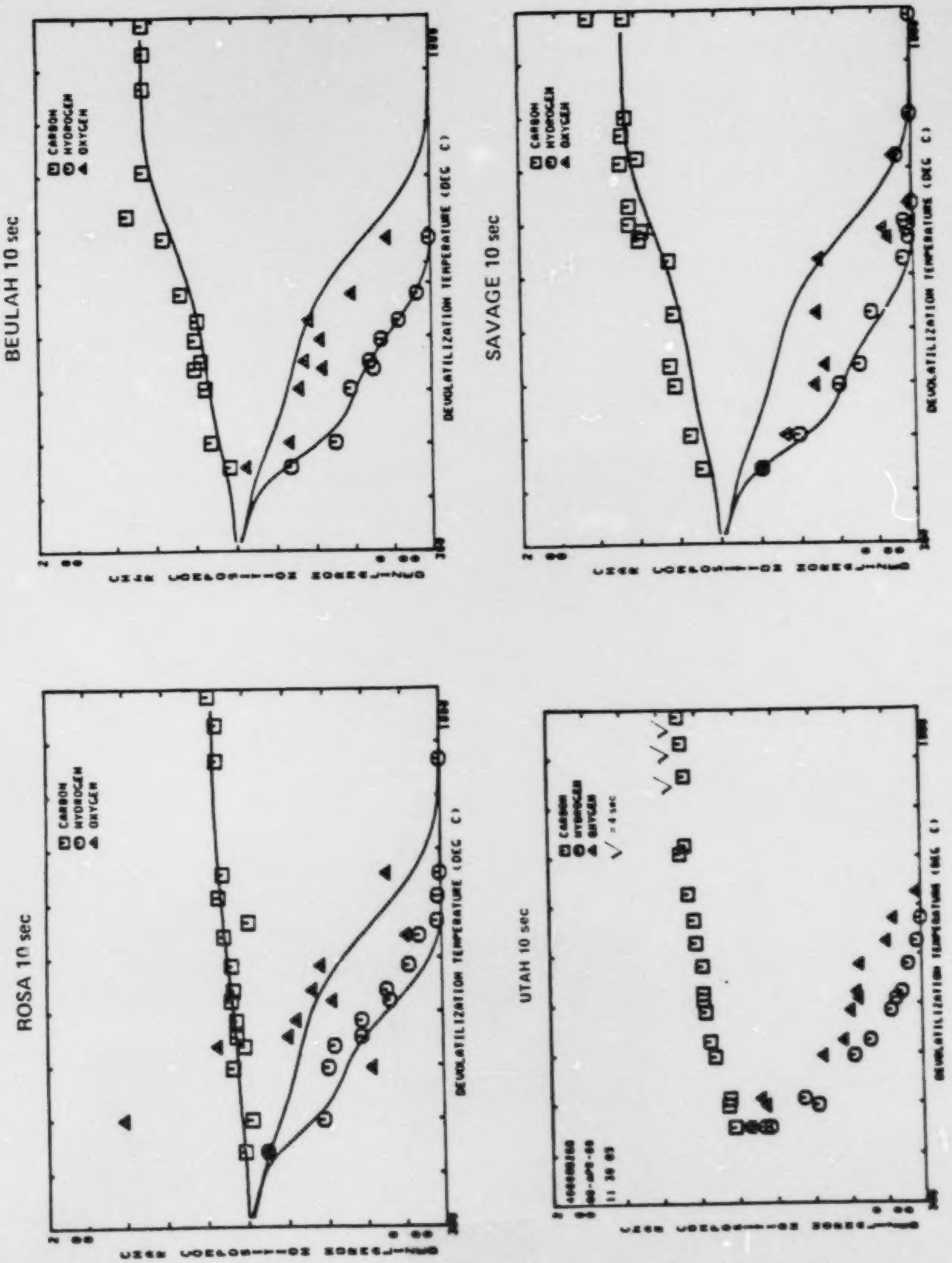
BEULAH 10 sec
SAVAGE 10 sec
ROSA 10 sec
UTAH 10 sec
CARBON
HYDROGEN
OXYGEN
√ = 4 sec
DEVOLATILIZATION TEMPERATURE (DEG C)
2.00
0.00
300
1000

FIG. 8

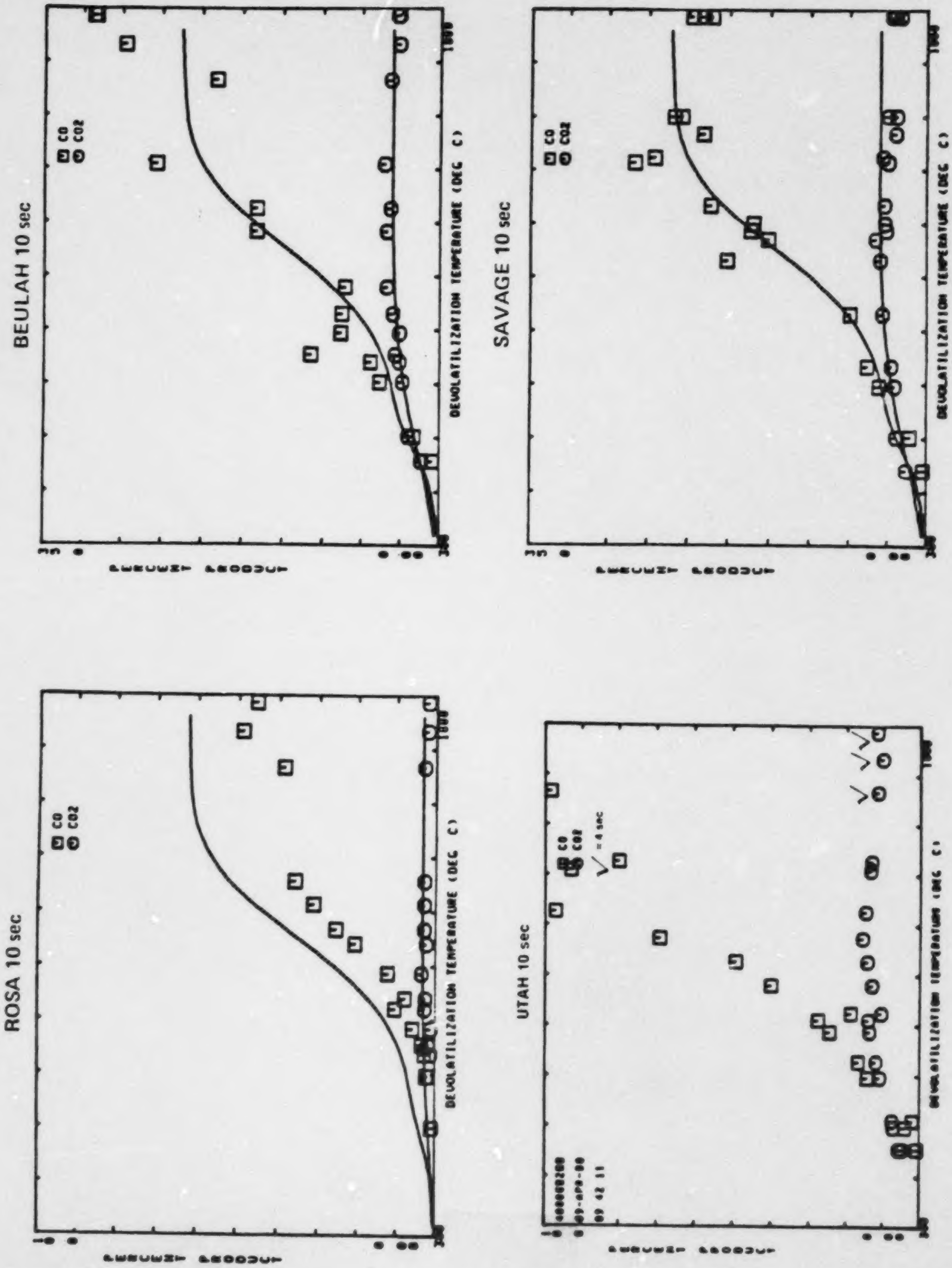
BEULAH 10 sec
SAVAGE 10 sec
ROSA 10 sec
UTAH 10 sec
CO
CO2
V = 4 sec
DEVOLATILIZATION TEMPERATURE (DEG C)
1000

FIG. 9

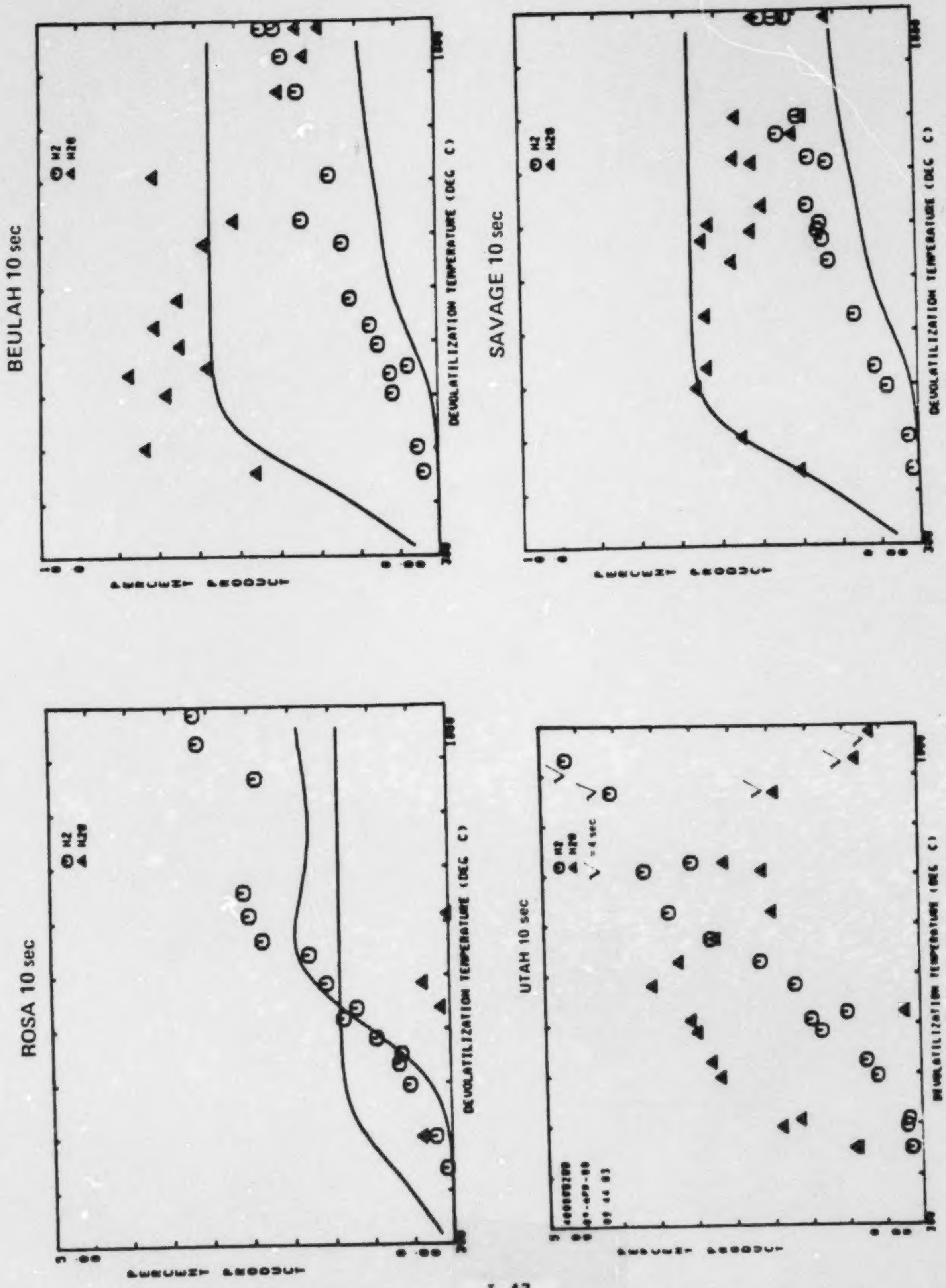

BEULAH 10 sec

SAVAGE 10 sec

ROSA 10 sec

UTAH 10 sec

FIG. 10

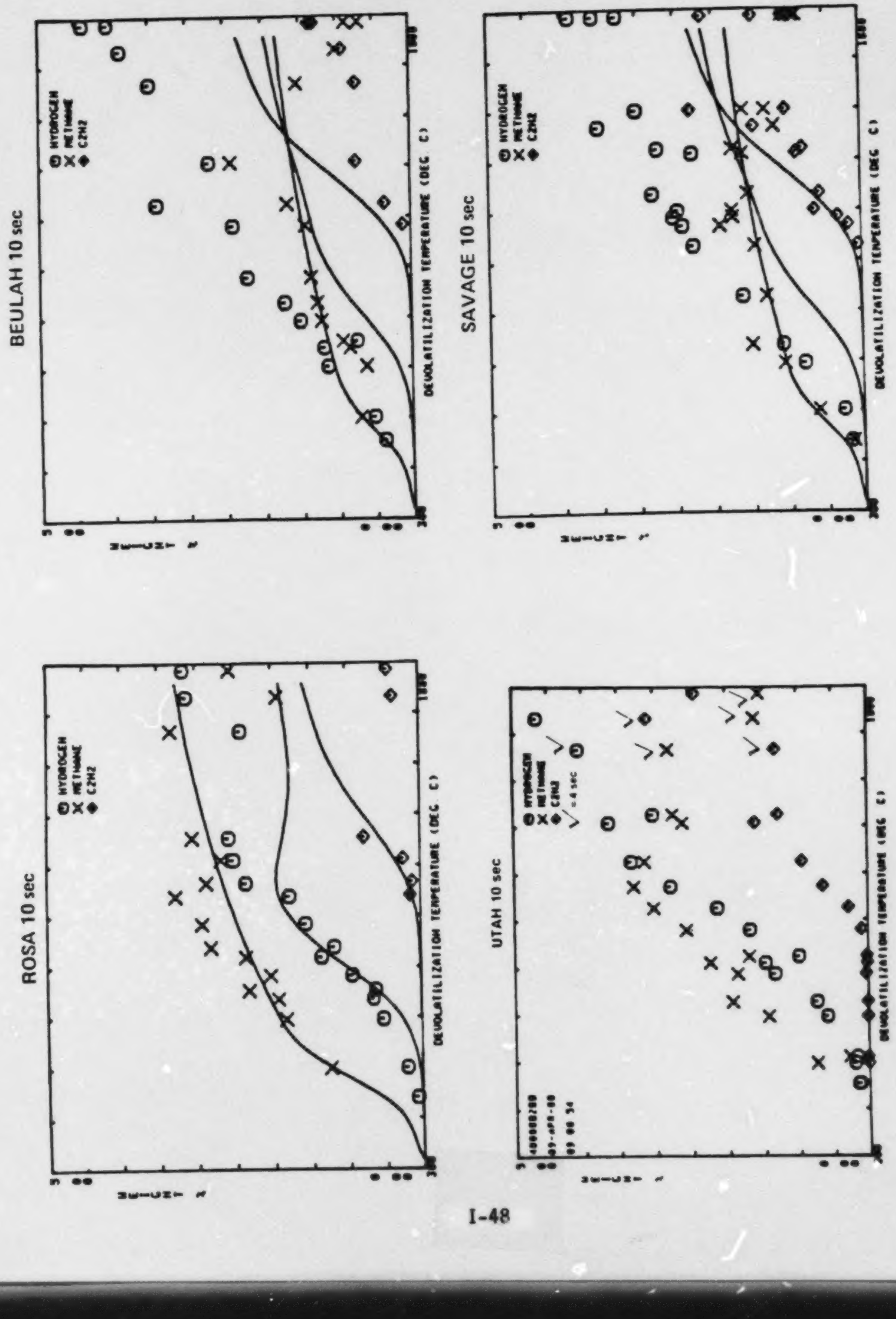
BEULAH 10 sec
SAVAGE 10 sec
ROSA 10 sec
UTAH 10 sec
HYDROGEN
METHANE
C2H2
√ = 4 sec
DEVOLATILIZATION TEMPERATURE (DEG C)
300
1000

FIG. 11

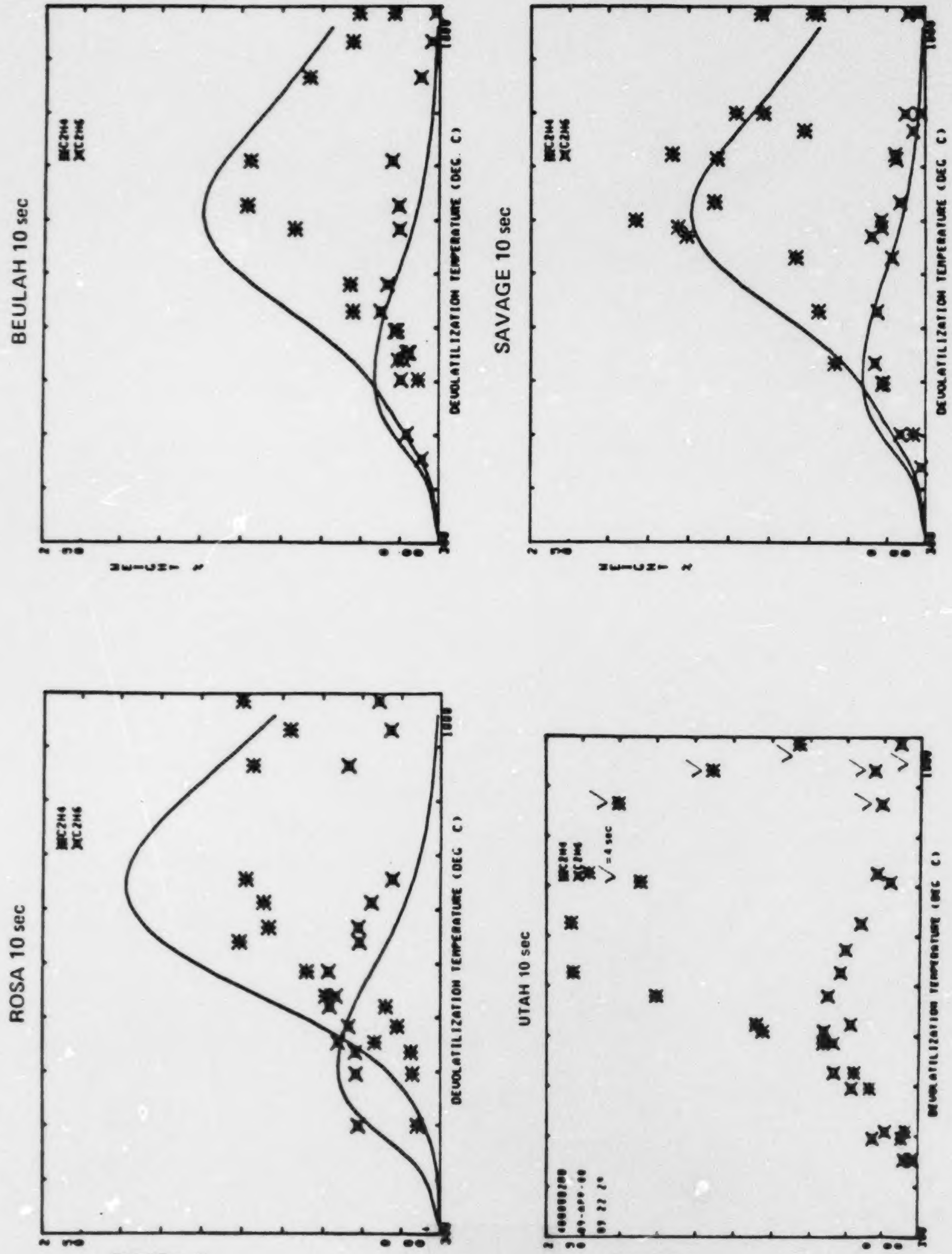
BEULAH 10 sec
SAVAGE 10 sec
ROSA 10 sec
UTAH 10 sec
C2H4
C2H6
√ = 4 sec
% YIELD
0.00
2.50
1000
DEVOLATILIZATION TEMPERATURE (DEG. C)

FIG. 12

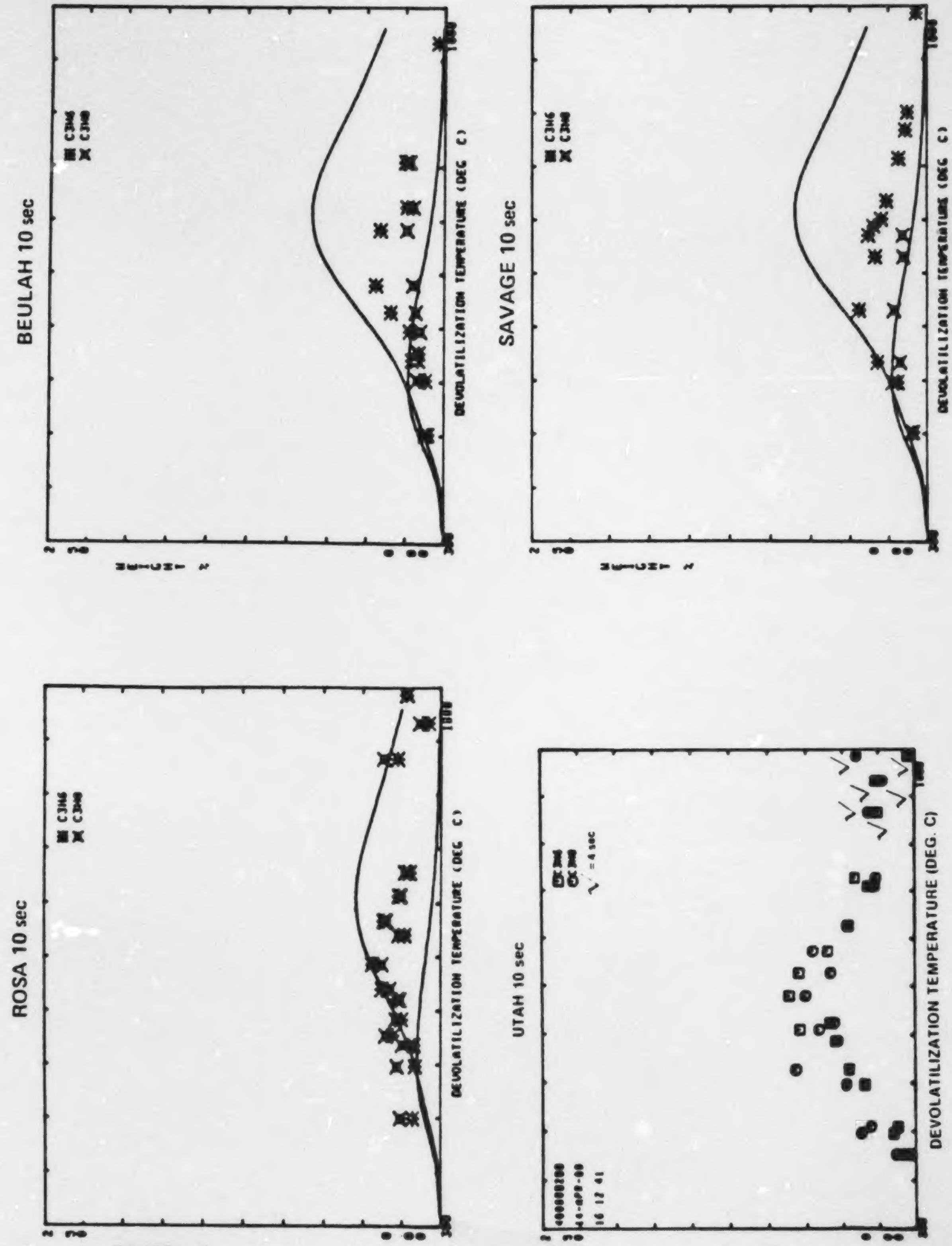

BEULAH 10 sec

SAVAGE 10 sec

ROSA 10 sec

UTAH 10 sec

FIG. 13

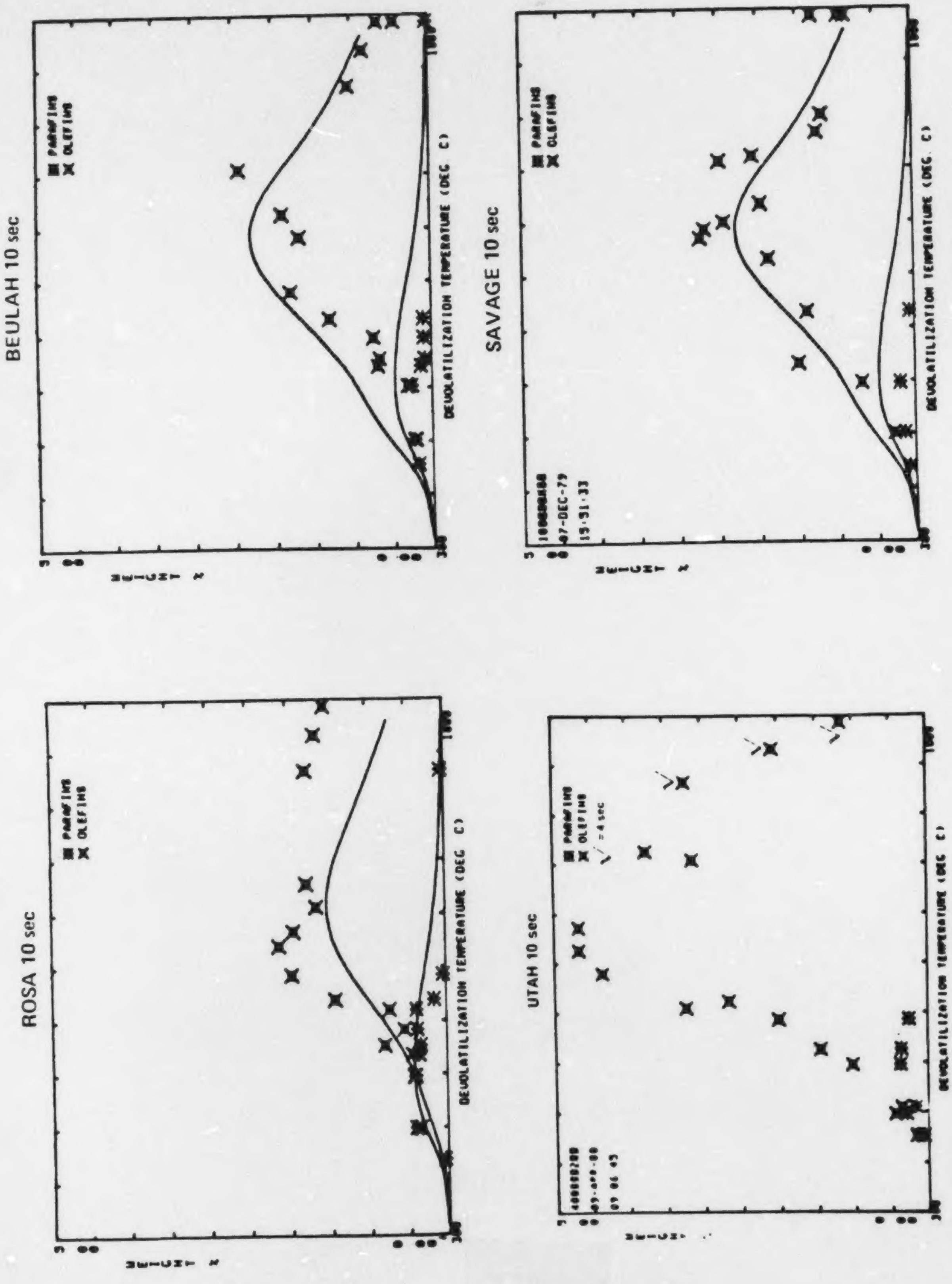
BEULAH 10 sec
PARAFINS
OLEFINS
DEVOLATILIZATION TEMPERATURE (DEG C)
SAVAGE 10 sec
PARAFINS
OLEFINS
07-DEC-79
15:51:33
DEVOLATILIZATION TEMPERATURE (DEG C)
ROSA 10 sec
PARAFINS
OLEFINS
DEVOLATILIZATION TEMPERATURE (DEG C)
UTAH 10 sec
PARAFINS
OLEFINS
√ = 4 sec
05-APR-80
07:06:43
DEVOLATILIZATION TEMPERATURE (DEG C)
1000
300

FIG. 14

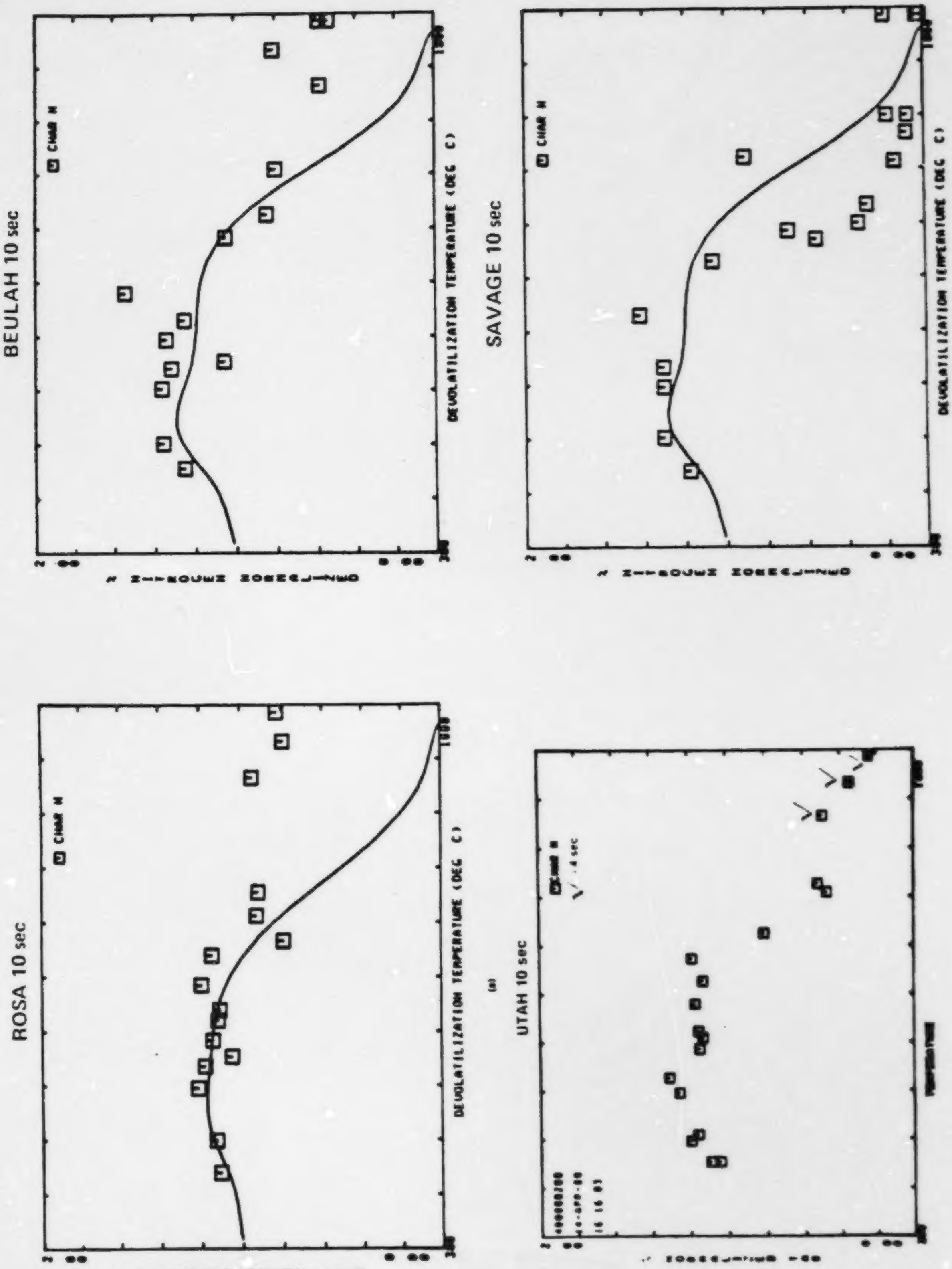
BEULAH 10 sec
CHAR N
DEVOLATILIZATION TEMPERATURE (DEG C)
1000
SAVAGE 10 sec
CHAR N
DEVOLATILIZATION TEMPERATURE (DEG C)
ROSA 10 sec
CHAR N
DEVOLATILIZATION TEMPERATURE (DEG C)
1000
UTAH 10 sec
CHAR N
.4 sec
TEMPERATURE

2. Product Distributions and Final Temperature

To test the structure-behavior hypothesis the four coals selected for complete characterization were devolatilized using the heated grid in a set of 10 second, in vacuo runs at final temperatures ranging from 500°C to 1800°C. Results for major product yields and light gases are displayed in Figs. 6 through 14.

Observations of relevance with respect to these plots are:

a. The char accounts for 40% to 90% by mass of the decomposition products, depending on coal type and final temperature achieved.

b. The combined char and tar products account for 50% or more of the initial coal mass for all coals and for all final temperatures achieved.

c. The most significant changes in mass loss occur at final temperatures from 500°C to 800°C. After 800°C the increase in mass loss with further increase in temperature is slight.

d. The Utah bituminous coal shows a pronounced maximum in tar yield as a function of final temperature. The maximum appears to occur around the relatively low final temperatures of 750°C.

e. The mix of product types (hydrocarbon gases versus oxygen-containing gases) is reflective of the functional group characteristics of the coal as revealed by infrared analysis.

f. The ratio of saturates to unsaturates in the hydrocarbon gases decreases as the coals are driven to higher final temperatures.

g. The nitrogen evolved in a light gas species is mainly in the form of HCN and is a high temperature phenomena relative to the evolution of the other species. That is, HCN evolution becomes appreciable at final temperatures of 800°C and above whereas only small increases in total weight loss are observed at these temperatures.

3. Char and Tar Characteristics

Figure 7 displays typical carbon-hydrogen-oxygen changes that occur in the char produced from the vacuum devolatilization experiments. The hydrogen and oxygen elements display the most dramatic change with final temperature. These elements are concentrated in the functional groups attached to the condensed ring structures of the coal matrix. It is these functional groups that are most susceptible to thermal rupture during the pyrolysis process. Thermal cleavage of the groups from the condensed ring structures of the coal results in a char matrix of decreasing H/C and O/C ratios.

Infrared inspection of the chars formed during the devolatilization process indicates that chars have greatly reduced functional group contents at final temperatures as low as 600°C. The vacuum tars maintain species with appreciable functional group concentrations to final grid temperatures of 900°C. However, as the coal is driven to higher temperatures with higher heating rates the tar species themselves can thermally decompose before being ejected from the decomposing coal mass. The Utah coal in particular displays this behavior. The tar yield (see Fig. 6) is at maximum for final temperatures of around 750°C. As the coal sample is driven to higher temperatures at greater heating rates the tar yield drops significantly while light gas production increases (Figs. 6 through 13). The total mass loss increases only slightly for final temperatures above 750°C implying little secondary carbon deposition of carbon from the degrading tar to the char. The evidence indicates that the tar yield and chemical characteristics are dependent not only on the coal type but also upon the heating rate to final temperature. An attempt to indirectly test this hypothesis by injection of tars into an isothermal furnace is described below.

4. Fuel Nitrogen Distribution in Devolatilizaton Products

Figure 15 displays the mass fractions of the coal nitrogen observed in the tar, char and gaseous products of the devolatilization process. By comparison of these plots to Fig. 6 it is noted that:

a. The fraction of original fuel nitrogen that remains in the char displays approximately the same temperature sensitivity as the fraction of coal mass that is converted to char within the temperature range from 500°C to 900°C.

b. At temperatures of 950°C and above the char nitrogen continues to decrease with increases in final temperature.

c. The mass fraction of the fuel nitrogen that evolves with the tar is the same as the fraction of coal mass that evolves as tar over the entire temperature range.

d. The major light gas species containing nitrogen observed is HCN.

e. It is possible that some nitrogen evolved as NH_3 is catilytically converted to N_2 by the screen, char or some combination of these.

f. The retention of nitrogen in the char devolatilization product appears to be a function of coal rank. The higher the coal rank the more coal nitrogen that is retained by the char product. Reducing char nitrogen to 10% in high rank coals requires temperatures in excess of 1400°C.

g. Residual char N - that remaining after light gas and tar evolution - requires temperatures in excess of 1100°C to evolve as NCH.

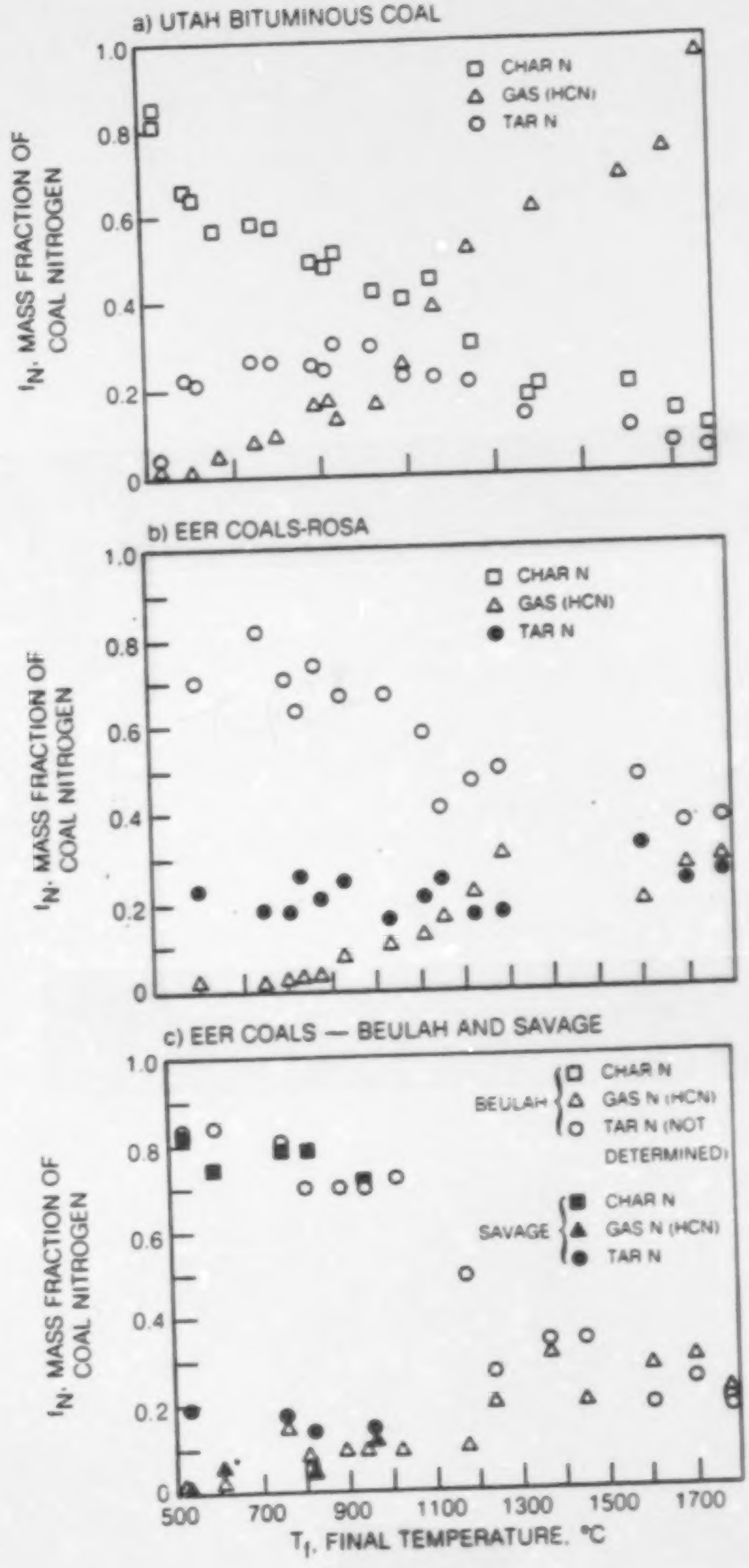
a) UTAH BITUMINOUS COAL
b) EER COALS-ROSA
c) EER COALS — BEULAH AND SAVAGE
f_N, MASS FRACTION OF COAL NITROGEN
0
0.2
0.4
0.6
0.8
1.0
CHAR N
GAS (HCN)
TAR N
BEULAH
GAS N (HCN)
TAR N (NOT DETERMINED)
SAVAGE
500
700
900
1100
1300
1500
1700
T_f, FINAL TEMPERATURE, °C

80-11-33-1

IV. COAL THERMAL DECOMPOSITION MODEL

A. Experimental Bases of the Model

1. Product Identification and Characterization, Extraction of Apparent Kinetic Constants

The vacuum devolatilization apparatus as discussed above was the reactor system used to generate the data employed in construction of the initial devolatilization model. The low resolution, rapid scan mode of the FTIR system allows identification of CO, CO_2, H_2O, CH_4, COS, SO_2, CS_2, HCN, C_2H_2, C_2H_4, C_3H_6, benzene and the presence of other light hydrocarbon species. The rapid scan feature allows the identification of these species in time as they are evolved during the devolatilization. The high resolution scan completed at the termination of the devolatilization run allows determination of the above noted species plus C_2H_6, C_3H_8 and NH_3.

First-order Arrhenius kinetic constants are extracted from the data collected in the real time scans by plotting the rise times associated with a particular species, as is shown in Fig. 16. The temperature associated with the rate constant is taken to be the final temperature of the grid. As will be discussed in more detail below, the rate constants extracted in this manner are only overall rate constants. These constants reflect the thermal environment created in time around the coal particles in the grid as well as the chemical decomposition process within the particle. Consequently, the rate parameters are termed "apparent" rate parameters.

In the case of a volatile species which is not observed directly in time, the rate constants are evaluated by standard integral techniques, using the final grid temperature as the reference temperature. The tar evolution is the primary volatile product of concern in this respect.

When possible, tar samples were collected and examined with the FTIR in the manner noted above. The similarity of low temperature tar spectra to that of the parent coal formed the basis of one of the hypothesis contained in the devolatilization model. Similarly, the rapid decay in the functional group characteristics of the parent coal upon heating, as revealed by FTIR inspection of the chars formed, also assisted in the initial understanding of the vacuum decomposition process. Further clarification was added by the results of the elemental analysis performed on the tar and char species.

In short, the experimental basis of the devolatilization model formulated consisted of a series of devolatilization experiments performed in vacuo using a heated grid apparatus. Kinetic data, chemical structural changes and product distributions were in large part the results of infrared analysis of the real time process and products formed. Elemental analysis assisted in data interpretation.

FIG. 16

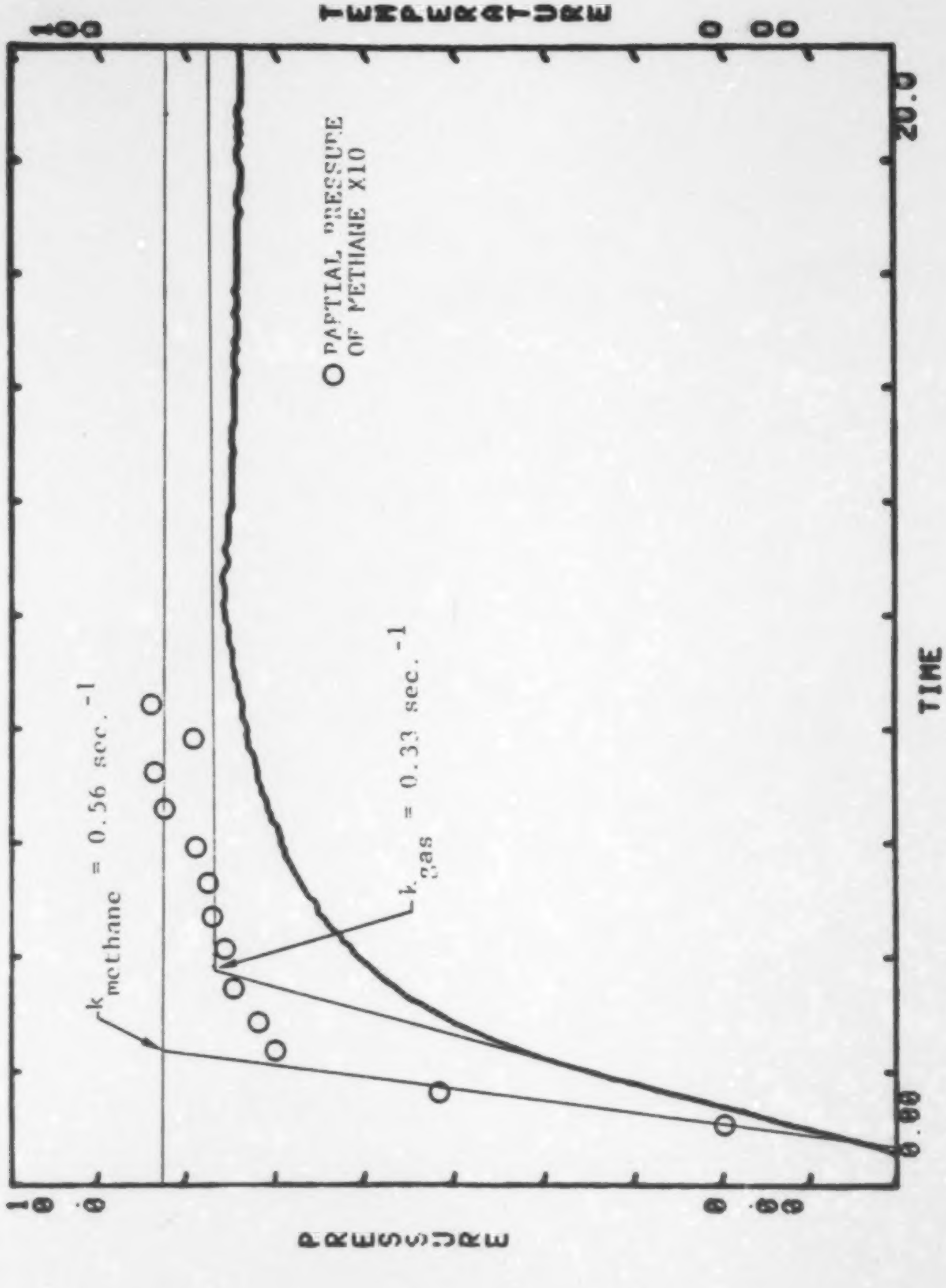
TEMPERATURE
1.00
0.00
PRESSURE
10.0
0.00
TIME
0.00
20.0
k_methane = 0.56 sec.^-1
k_gas = 0.33 sec.^-1
○ PARTIAL PRESSURE OF METHANE X10

2. Determination of Source Terms for Kinetic Expressions

In general, the source term for a particular devolatilization species is estimated in one of two manners:

a. from the high temperature, asympototic limit approached by that species;

b. from a quantitative determination of the functional group associated with that species and as revealed by an analysis (infrared, wet chemical means, etc.) of the parent coal.

In this investigation, both methods were employed in determining the source terms in the model formulated. Table XXIV lists the species and the method of determination of the source term associated with that species for vacuum devolatilization pyrolysis of the coal.

3. Observation Pertinent to Formulation of Model Hypotheses

The following experimental observations were central to the formulation of the working model of coal devolatilization which resulted from the heated grid studies.

a. The apparent rise times of a particular devolatilization species at a given final grid temperature do not vary with coal type.

b. The infrared spectra of the low temperature tars from each of the coals is very similar to the infrared spectra of the respective coal except that the tar has enhanced aliphatic content.

c. The infrared spectra of the chars formed from the devolatilization process reveals that the functional group characteristics of the coal are significantly reduced at low devolatilization temperatures.

d. The variations in the product distributions obtained from different coals reflects the variation in functional group characteristics of the coal as revealed by infrared analysis of the coal.

e. Elemental analysis of the tars and chars formed from the devolatilization process reveals that the evolved species tend to be hydrogen and oxygen rich relative to the parent coal. That is, the chars are hydrogen and oxygen poor relative to the parent coal as a result of the devolatilization process.

4. Assumptions Employed in Interpretation of Data and Model Formulation

In a process as complex as coal pyrolysis it is important to constantly review the important assumptions used as a basis to interpret the data. In the heated grid experiments and the formulation of the resultant devolatilization model these assumptions are:

TABLE XXIV

FUNCTIONAL GROUP COMPOSITION AND SOURCE DETERMINATION

Composition Parameter (dmmf)	Source
C	Elemental Analysis
H	Elemental Analysis
S (organic)	Elemental Analysis and SEM
O	By Difference
S (mineral)	SEM
CO_2 - Carboxyl	Fit to Pyrolysis Data
OH - Hydroxyl	Infrared
CO - Ether Loose	Fit to Pyrolysis Data
CO - Ether Tight	By Difference
N - Nitrogen Loose	Fit to Pyrolysis Data
N - Nitrogen Tight	By Difference
$CH_{1.8}$ - Aliphatic	Infrared
H - Aromatic H	Infrared
C - Non Volatile	By Difference
TAR	Fit to Pyrolysis Data

a. The final grid temperature is the temperature of devolatilization; that is, no significant reaction occurs during the non-isothermal heating of the grid to the final temperature.

b. Variations in heating rate to a final grid temperature have an insignificant effect on the product distributions and characteristics. In short, the behavior observed in the heated grid experiments is chemical kinetic behavior.

c. First-order Arrhenius chemical kinetic expressions can be used to adequately model the devolatilization process for the majority of evolved species. In some cases a set of parallel first order reactions may be justified.

d. As a consequence of the assumptions above, it follows that a source value for a particular volatile species can be estimated a priori by a quantitiative identification and measurement of a functional group in the parent coal that produces the species upon thermal stimulation. If such an identification is not possible then the source term can be estimated by examination of the asymptotic limit approached by that species as the parent coal is driven to near complete devolatilization.

B. Vacuum Devolatilization Model - Working Hypotheses from Vacuum Devolatilization Studies

Based on the experimental observations and results above and the assumptions used in interpretation of the data, the following hypotheses were formulated as the basis of a devolatilization model:

1. The rate of evolution of a particular species is independent of coal type.
2. First-order Arrhenius rate expressions are adequate to describe the evolution process of a particular devolatilization species.
3. Variations in product distributions are the result of variations in the functional group characteristics of the parent coal.
4. Thermal degradation of a coal results in the reduction of the functional group characteristics of the coal via the production of light gas species and the evolution of tar species.
5. It follows from the above that the vacuum devolatilization of a coal can be described by a set of universal rate parameters and a set of source terms unique to a particular coal.

Figure 17 geometrically displays the concepts of the devolatilization model. The coal is represented in an area with X and Y dimensions (Fig. 17a). The Y dimension is divided into fractions according to the chemical composition of the coal. $Y^\circ(i)$ represents the initial fraction of a particular component (carboxyl, aromatic hydrogen, etc.) and $\Sigma\, Y^\circ(i) = 1$. There are two components for ether since CO is typically evolved in two distinct steps. The evolution of each component into the gas (carboyxl into CO_2, aromatic hydrogen in to H_2, etc.) represented by the first order diminishing of the Y(i) dimension, $Y(i) = Y^\circ(i) \exp(-k_i t)$. The X dimension is divided into a potential tar forming fraction X° and a non-tar forming fraction $1 - X^\circ$ with the evolution of the tar being represented by the first order diminishing of the X dimension $X = X^\circ \exp(-k_x t)$.

The kinetic rate constants and k_i and k_X are represented by Arrhenius expressions. Values for Y°(hydroxyl), $Y^\circ(H_{ar})$ and Y°(aliphatics) are determined from quantitative infrared measurements. Y°(nitrogen) is determined from ultimate analysis. Values of X°, Y°(carboxyl), and Y°(ether-loose) are fited to the pyrolysis data. Y°(ether-tight) and the non-volatile carbon fraction $Y^\circ(C_{NVC})$ are determined by difference;

$$Y^\circ(\text{ether-tight}) = 28/16\ (O_{total} - 1/2\ O_{OH} - O_{CO_2}) - Y^\circ(\text{ether-loose}) \qquad (4)$$

$$Y^\circ(C_{NVC}) = C_{ar} - C_{CO_2} - C_{CO\text{-}tight} - C_{CO\text{-}loose} \qquad (5)$$

One-half of the hydroxyl oxygen, O_{OH} has been included with ether-tight since it has been assumed that H_2O forms by

$$\theta\text{-OH} + \theta'\text{-OH} = H_2O + \theta\text{-O-}\theta'$$

Th modeling of sulfur is complicated because of the presence of pyrite as well as organic sulfur and has not been included in recent versions of the model.

Figure 17b illustrates the initial stage of thermal decomposition during which the volatile components H_2O, CO-loose and CO_2 evolve from the hydroxyl, ether-loose and carboxyl groups, respectively, along with aliphatics and tar. At a later stage (Fig. 17c) CO-tight and H_2 are evolved from the ether-tight and H_{ar} respectively.

To simulate the abstraction of H by the tar, the aliphatic fraction in the tar is assumed to be retained together with some additional aliphatic material which may be added directly or may contribute its hydrogen. When hydrogen from the aliphatic material is contributed, its associated carbons remain with the non-volatile carbon fraction which eventually forms the char (Fig. 17d). Table XXV lists the kinetic parameters for the model.

FIG. 17

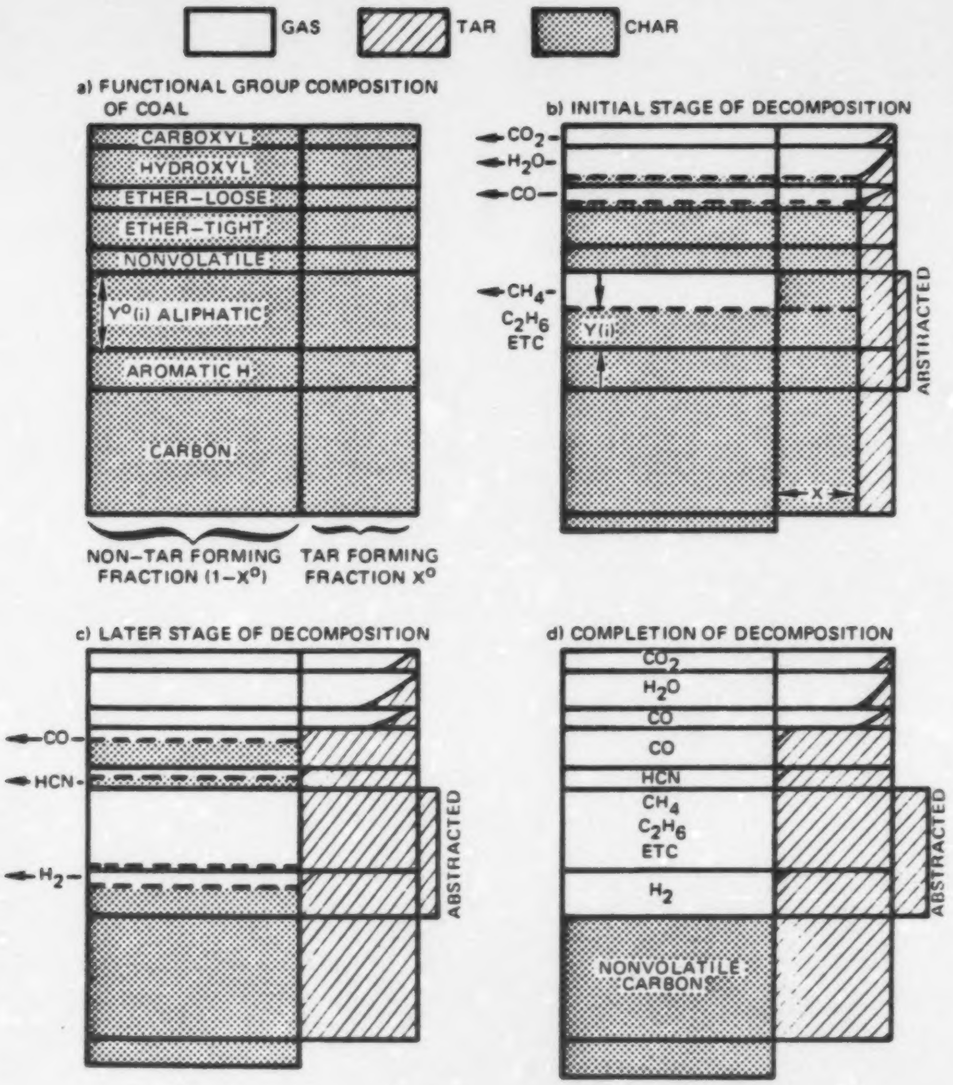
GAS
TAR
CHAR
a) FUNCTIONAL GROUP COMPOSITION OF COAL
CARBOXYL
HYDROXYL
ETHER-LOOSE
ETHER-TIGHT
NONVOLATILE
$Y^{o}(i)$ ALIPHATIC
AROMATIC H
CARBON
NON-TAR FORMING FRACTION $(1-X^{o})$
TAR FORMING FRACTION X^{o}
b) INITIAL STAGE OF DECOMPOSITION
CO_2
H_2O
CO
CH_4
C_2H_6
ETC
Y(i)
X
ABSTRACTED
c) LATER STAGE OF DECOMPOSITION
CO
HCN
H_2
ABSTRACTED
d) COMPLETION OF DECOMPOSITION
CO_2
H_2O
CO
CO
HCN
CH_4
C_2H_6
ETC
H_2
NONVOLATILE CARBON
ABSTRACTED

79-08-12-1

TABLE XXV

FUNCTIONAL GROUP POOLS AND RATES

Functional Group			Kinetic Rates
carboxyl	K(1)	=	6 exp(-4,000/T) sec^{-1}
NH_3	K(2)	=	30 exp(-4,590/T)
hydroxyl	K(11)	=	45 exp(-4,950/T)
ether loose	K(25)	=	7000 exp(-10,300/T)
ether tight	K(4)	=	400 exp(-12,000/T)
HCN	K(6)	=	200 exp(-7,600/T)
HCN	K(7)	=	290 exp(-13,000/T)
aliphatic CH_x	K(24)	=	2300 exp(-9,700/T)
aromatic H	K(15)	=	3600 exp(-12,700/T)
non volatile C	K(27)	=	0
tar	KX	=	750 exp(-8,000/T)
olfins	KOL	=	2 x 10^7 exp(-20,000/T)
acetylene	KAC	=	1.9 x 10^{10} exp(-35,000/T)
soot	KSOOT	=	4 x 10^{10} exp(-35,000/T)

C. Model Results and Discussion

The solid curves in Figs. 6 through 14 indicate the model predictions obtained for three of the four coals. The Utah bituminous coal was not modeled due to the apparently anomolous tar behavior. In examining the model curves it is to be noted that the model adequately describes product distributions as a function of final temperature and in vacuum conditions for three of the four coals investigated. However, it is also to be noted that the model a priori neglects the possible influence of physical parameters such as the finite heating rate to final grid temperature, the effect of ambient pressure on the product distributions, particle size effects on observable rates. The model is an attempt to interpret observed devolatilization behavior in terms of intrinsic chemical characteristics of the parent coal. As such, the mathematical formulation of the model reflects the assumptions employed in interpreting the data obtained from the heated grid.

The following section deals with results obtained by employing a different devolatilization apparatus in an attempt to determine the sensitivity of the devolatilization results to changes in the thermal environment and particle size of the coal sample.

D. Isothermal Furnace Studies: An Experimental Check of Model Hypotheses and Kinetic Parameters

1. Experimental Design

Figure 18 displays a schematic of the isothermal furnace, devolatilization apparatus. The apparatus allows small samples (< 50 mg) of coal to be rapidly injected (∿ 25 msec) into a preheated isothermal zone maintained at one atmosphere of pressure. Most of the devolatilization runs were performed using either N_2 or Ar as the inert gas present in the reactor. The apparatus allows variations in the initial size of the particles employed. Due to the nature of the heat transfer within the grid, the grid apparatus is limited to the particle size which can be employed. The isothermal furnace allows particle sizes in the range from 100 μm to several millimeters to be utilized.

The isothermal furnace devolatilization apparatus was designed to meet two major objectives: 1) to test the validity of the hypotheses used to generate the thermal decomposition model developed by use of the heated grid; 2) to investigate the influence which changes in associated physical parameters could have upon pyrolysis behavior. The furnace involves devolatilization under one atmosphere of pressure by coal particles heating at a rate approximately one to two orders of magnitude greater than in the heated grid experiments.

In addition to determining a more combustion-like environment in which to observe the devolatilization process, the injection apparatus allows the delivery of small pellets of tar. Thus one can observe the thermal decomposition behavior of vacuum-formed tars within the furnace.

FIG. 18

ISOTHERMAL FURNACE APPARATUS

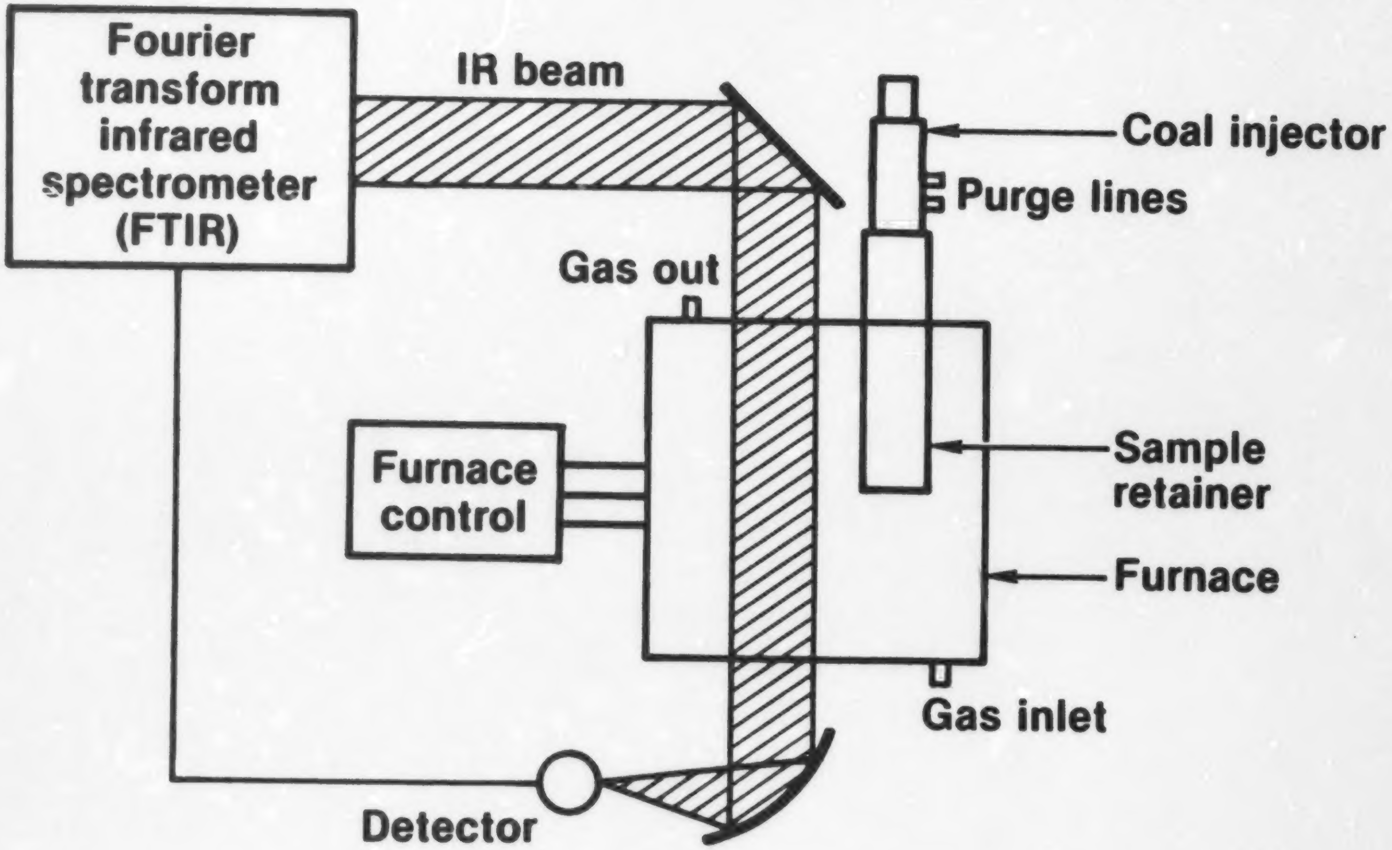
Fourier transform infrared spectrometer (FTIR)
IR beam
Coal injector
Purge lines
Gas out
Sample retainer
Furnace control
Furnace
Gas inlet
Detector

80-07-79-27

Most of the devolatilization runs were performed with the Utah Bituminous coal. Spot runs with samples of lignite and Rosa coals were also made to determine if they displayed behavior similar to that observed from the Utah coal. Runs were performed at furnace temperatures of 500°C to 1000°C and with particle size cuts of -100 + 140 mesh, -35 + 40 mesh and -20 + 25 mesh.

2. Coal Devolatilization Times, Rate Constants, Volatiles Distribution

Figures 19 through 22 are examples of real time data collected during devolatilization runs within the isothermal furnace by use of the FTIR in the rapid scan mode. Isothermal furnace devolatilization times and rate constants were extracted for the light gas species CO_2 and CH_4 in the same manner as from the heated grid data; i.e., from the rise time plots of these gases as revealed by their absorption of the infrared signal at specific wave numbers. These two particular species were chosen in comparing results from the two different reactors for several reasons: 1) they are strong absorbers of infrared radiation in the range of wavelengths made available by the two detection systems; 2) they are relatively stable from thermodynamic considerations in the temperature range employed in the investigations; 3) they are observed products of the thermal decomposition of vacuum-formed tars. The heated grid experiments with the Utah coal indicated the tar yield decreased with increase in thermal drive while the light gas yields increased. Since the thermal drive in the furnace is much greater than that of the heated grid, it is expected that CH_4 and CO_2 yields are more indicative of the decompostion process.

Figures 23 and 24 display rate constant plots constructed from data collected by use of the isothermal furnace. Examination of these plots reveals that both the magnitude and temperature sensitivity of the first-order rate constants for these species are considerably different from those observed for the heated grid apparatus. In general the rate constants are at least one order of magnitude greater the furnace than those observed at a comparable final temperature within the heated grid apparatus. Only at the lower temperatures (500°C) do the rate constants from the two reactors begin to converge. Presumably as one approaches the lower final temperature regimes in the two reactors one is moving toward a chemical control region.

The isothermal furnace rate constant plots for both CO_2 and CH_4 show a severe change in slope in the 750°C to the 800°C temperature region. As higher temperatures are employed, little change in the magnitude of either rate constant is observed. Several explanations are possible: 1) transport factors become the dominant rate-determining influence; 2) the experimental time resolution is not adequate to follow the rapid devolatilization process; 3) some combination of these factors.

The rate constant plots also indicate that the three coals tested at that time displayed very similar rate behavior. However, preliminary results of more recent investigations with other coals indicate that there is some dependence of the rate constant on the particular coal type. Verification of this dependence awaits further work.

TIME RESOLVED SPECTRA OF UTAH BITUMINOUS COAL

- 500°C
- Furnace −100 + 140 mesh, 51.9 mg

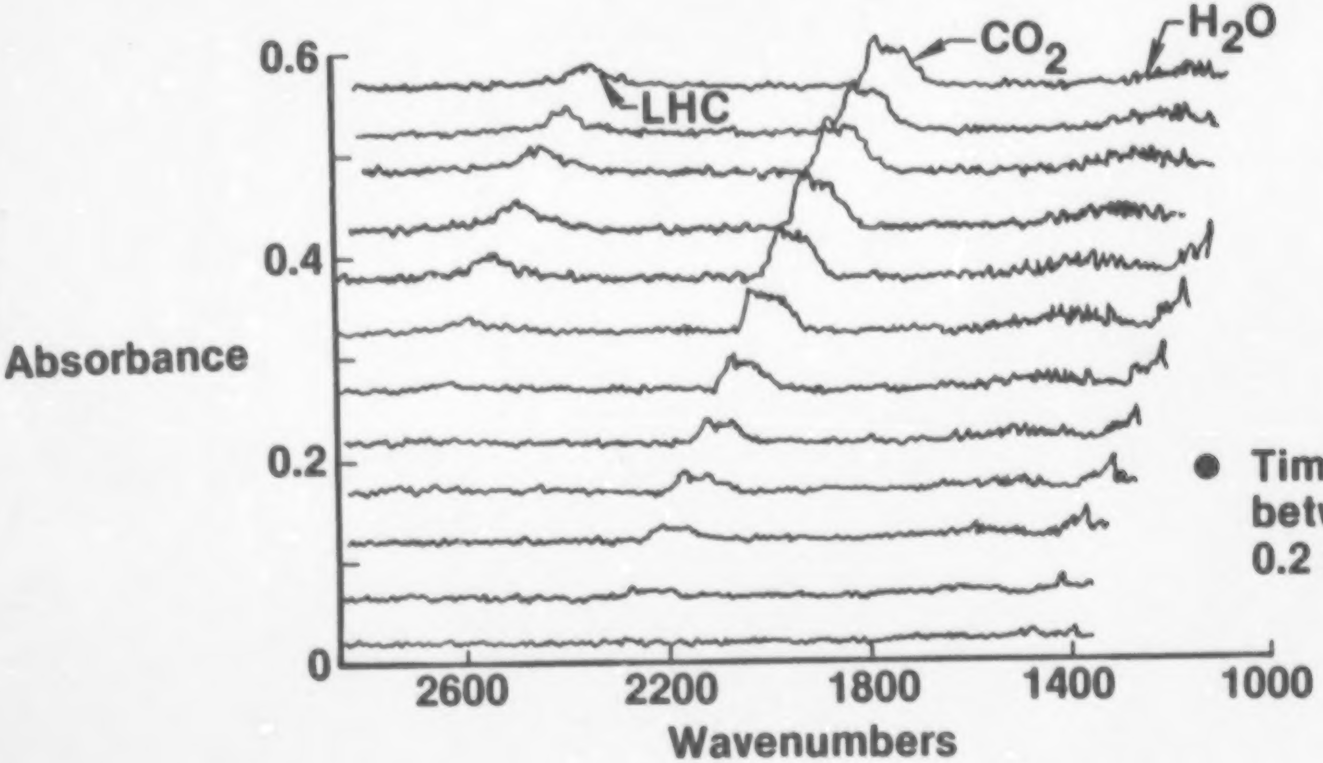

- Time resolution between spectra 0.2 sec

FIG. 19

80-8-67-9

TIME RESOLVED SPECTRA OF UTAH BITUMINOUS COAL

- 600 °C
- Furnace −100 + 140 mesh, 51.3 mg

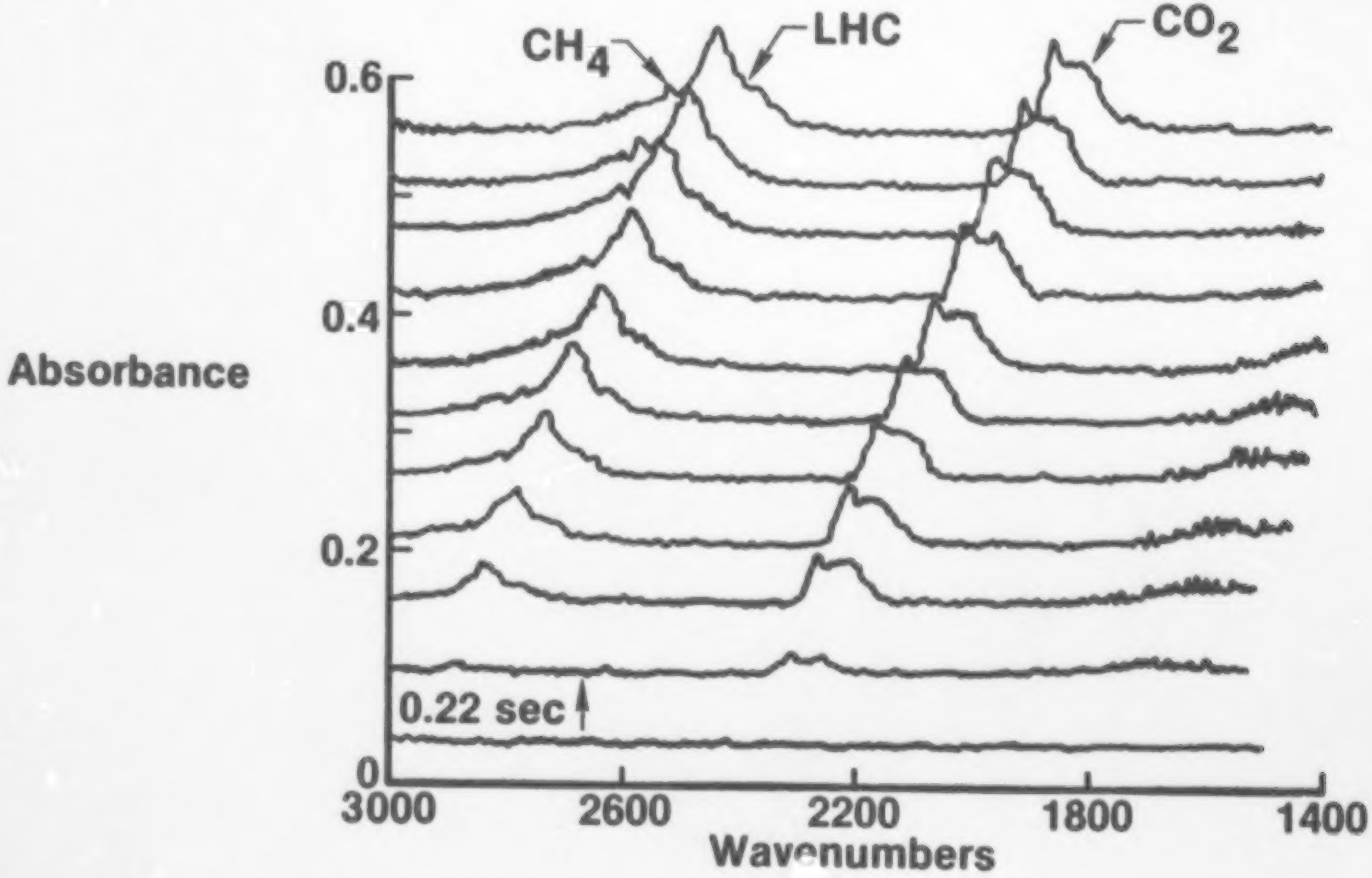

80-8-67-7

TIME RESOLVED SPECTRA OF UTAH BITUMINOUS COAL

- 700 °C
- Furnace −100 + 140 mesh, 51.4 mg

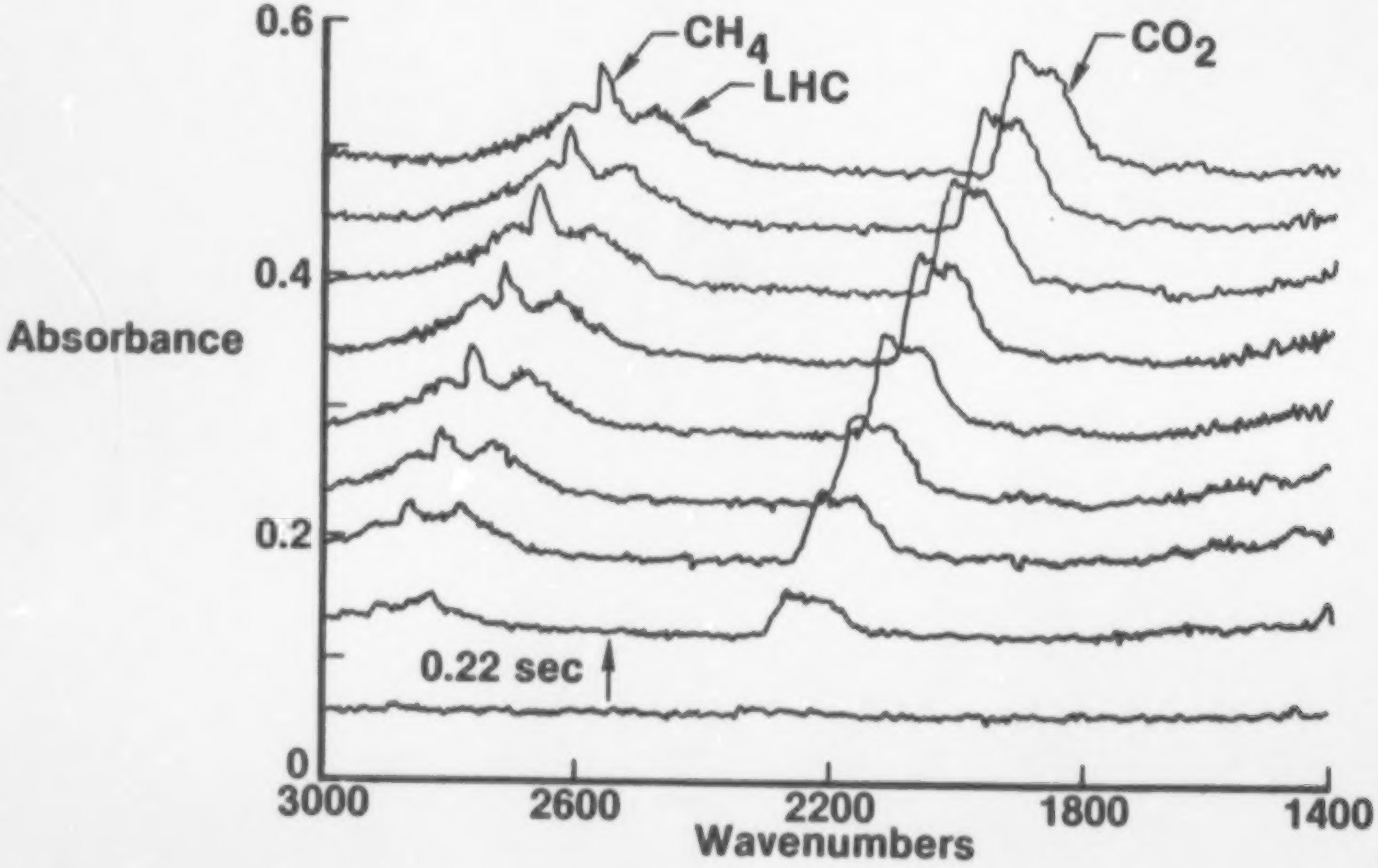

FIG. 21

80-8-67-8

TIME RESOLVED SPECTRA OF UTAH BITUMINOUS COAL

- 800°C
- Furnace −100 + 140 mesh, 50 mg

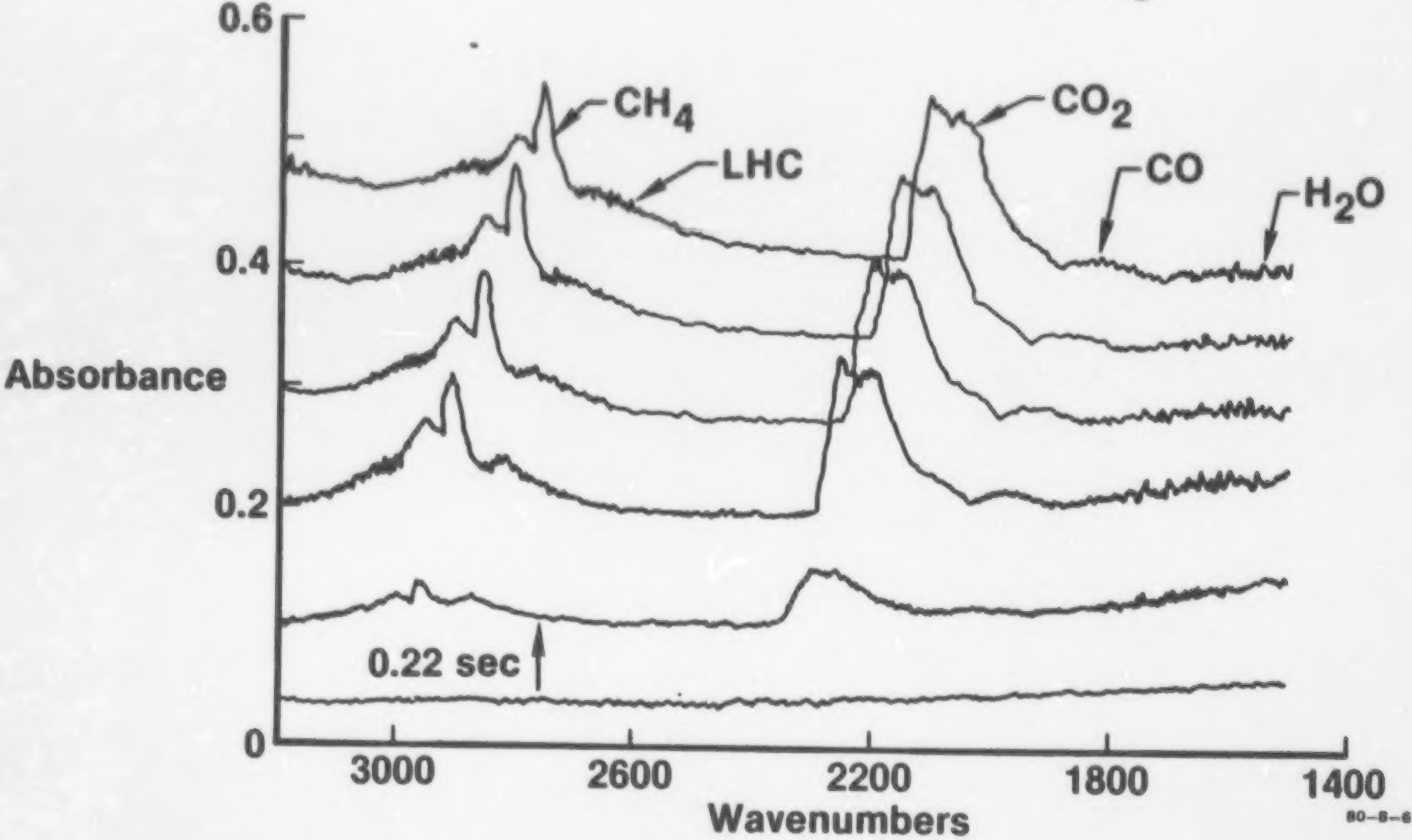

FIG. 22

80-8-67-12

RATE CONSTANTS FOR LHC EVOLUTION

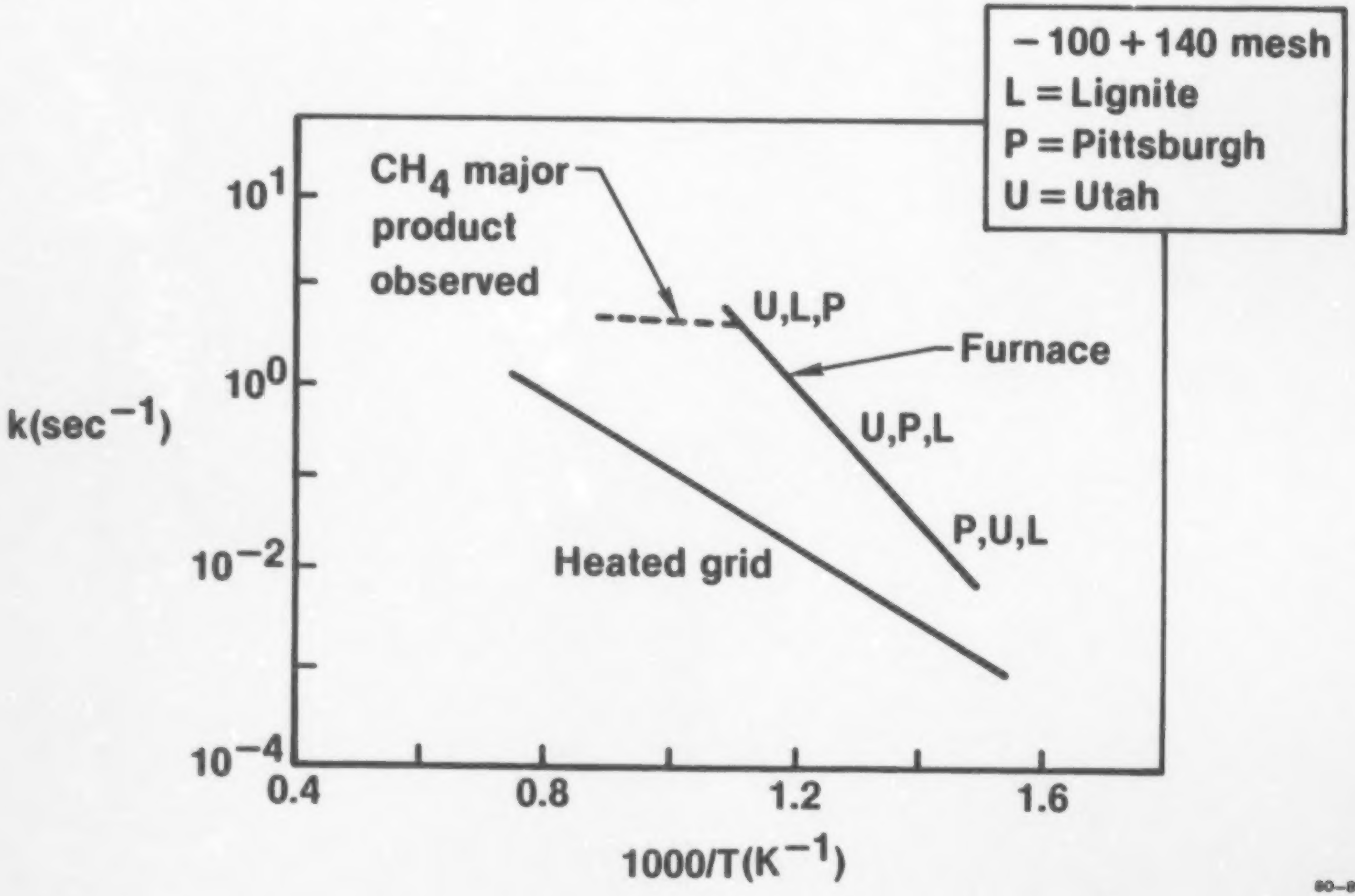

FIG. 23

80–8–67–1

RATE CONSTANTS FOR CO_2 EVOLUTION

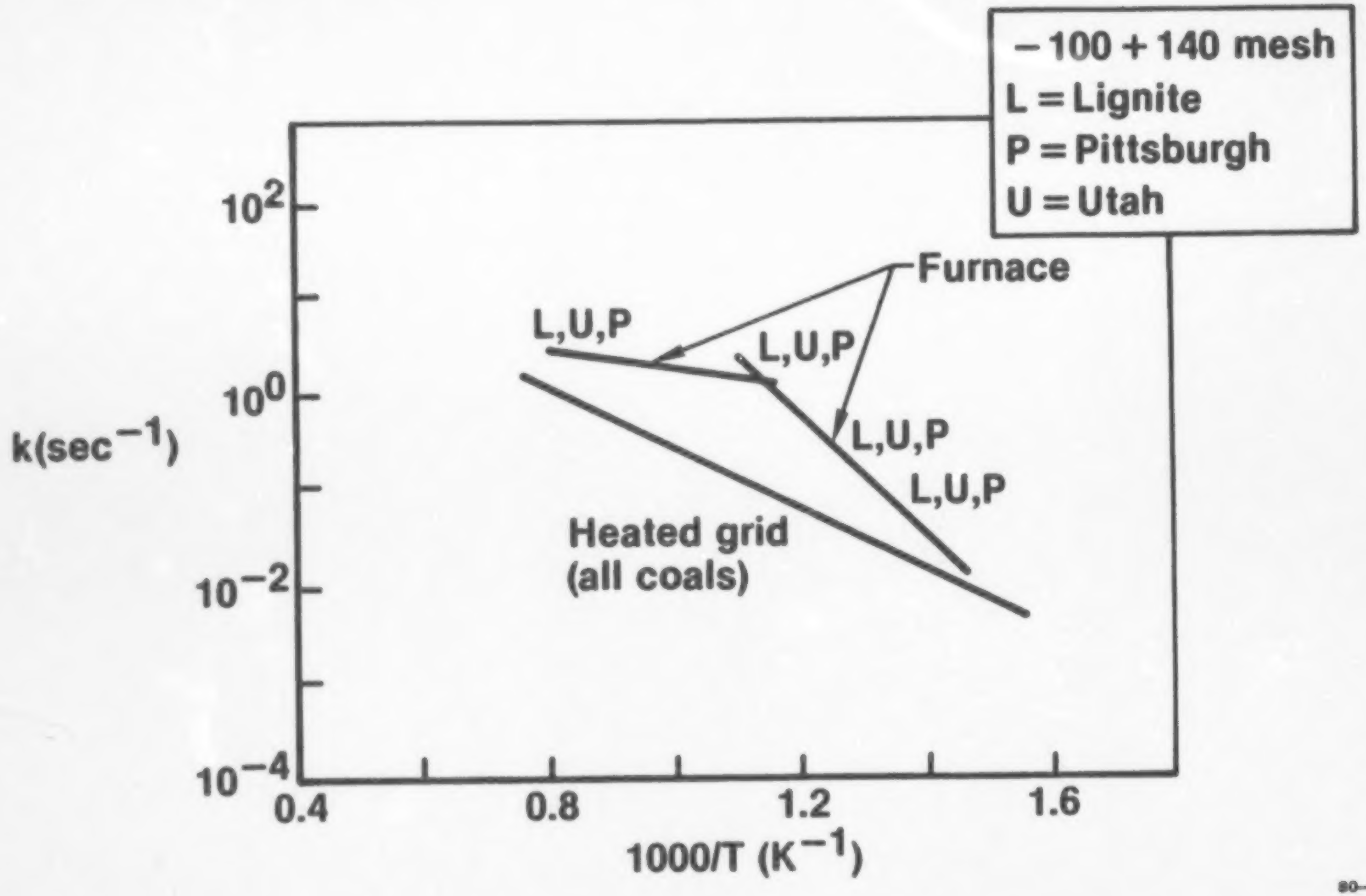

80-8-67-4

Figures 20, 25, and 26 display examples of data collected from various particle sizes of the Utah bituminous coal. It is to be noted that the initial particle size can have an effect not only on the devolatilization times, but also the mix of hydrocarbons evolved. The -20 + 25 mesh particles show a pronounced CH_4 peak in the hydrocarbon region (2800-3050 cm^{-1}). However, the smaller particle sizes (-30 + 35 mesh, -100 + 140 mesh) yield an ill-defined mix of light hydrocarbons for the same operating temperature. Apparently, the larger particle size promotes intraparticle cracking of the hydrocarbon species as they are evolved. Thus, an increase in particle size at a given operating temperature has an effect similar to an increase in operating temperature for a given particle size - cracking of the larger hydrocarbons to more thermodynamically favored species such as CH_4, C_2H_4, CO_2. It is to be noted here that the effects of ambient pressure have not been parametrically isolated in this investigation. It is to be expected that increases in ambient pressure above near-vacuum would have a significant effect on product distribution as well.

3. Tar Decomposition Studies

In order to obtain some insight into the nature of the thermal decomposition of vacuum-formed tars, a set of isothermal furnace devolatilization experiments were performed with samples of vacuum tars released from a bituminous coal. Small amounts of tar (10-30 mg) were made into a pellet and rapidly injected into a preheated furnace. The evolution of light gases was monitored by use of the FTIR. The major species observed were CH_4, CO_2, and CO. At temperatures above 700°C the evolution times of these species were comparable to those observed for the parent coal. The increase in light gas species such as CH_4, CO_2, and C_2H_4, observed in the isothermal furnace is, in part, due to the thermal degradation of the tars in the hot environemtn. The high-temperature tar decomposition contribues to an increase in these observable light gas species in a manner similar to the high-temperature cracking of the mix of light hydrocarbons observed in Figs. 21 and 22.

Discussion of Results

With respect of the main hypotheses of the vacuum devolatilization model, the experimentation performed to date with the isothermal furnace has indicated that significant modifications of these hypotheses must be made to allow for interpretation of data collected in the different environment. It has been observed that the volatiles product distribution and evolution rates are sensitive functions of physical parameters such as thermal drive, final temperature, and particle size. Thus, variations in product distributions are not simply the result of variations in the functional group mix of the parent coal. Quantitative descriptions of the evolution of light gases by first-order Arrhenius rate expressions are to be taken as a means of correlating the data, not as reflective of a fundamental chemical kinetic process. The temperature-insensitive dependence of the Arrhenius rate constants with coal type as observed within the heated grid apparatus probably reflects the thermal transport limitations imposed by the nature of the grid heating coupled to the manner in which the kinetic parameters were extracted from the data.

TIME RESOLVED SPECTRA OF UTAH BITUMINOUS COAL

- 600°C
- Furnace −35 + 40 mesh, 51.7 mg

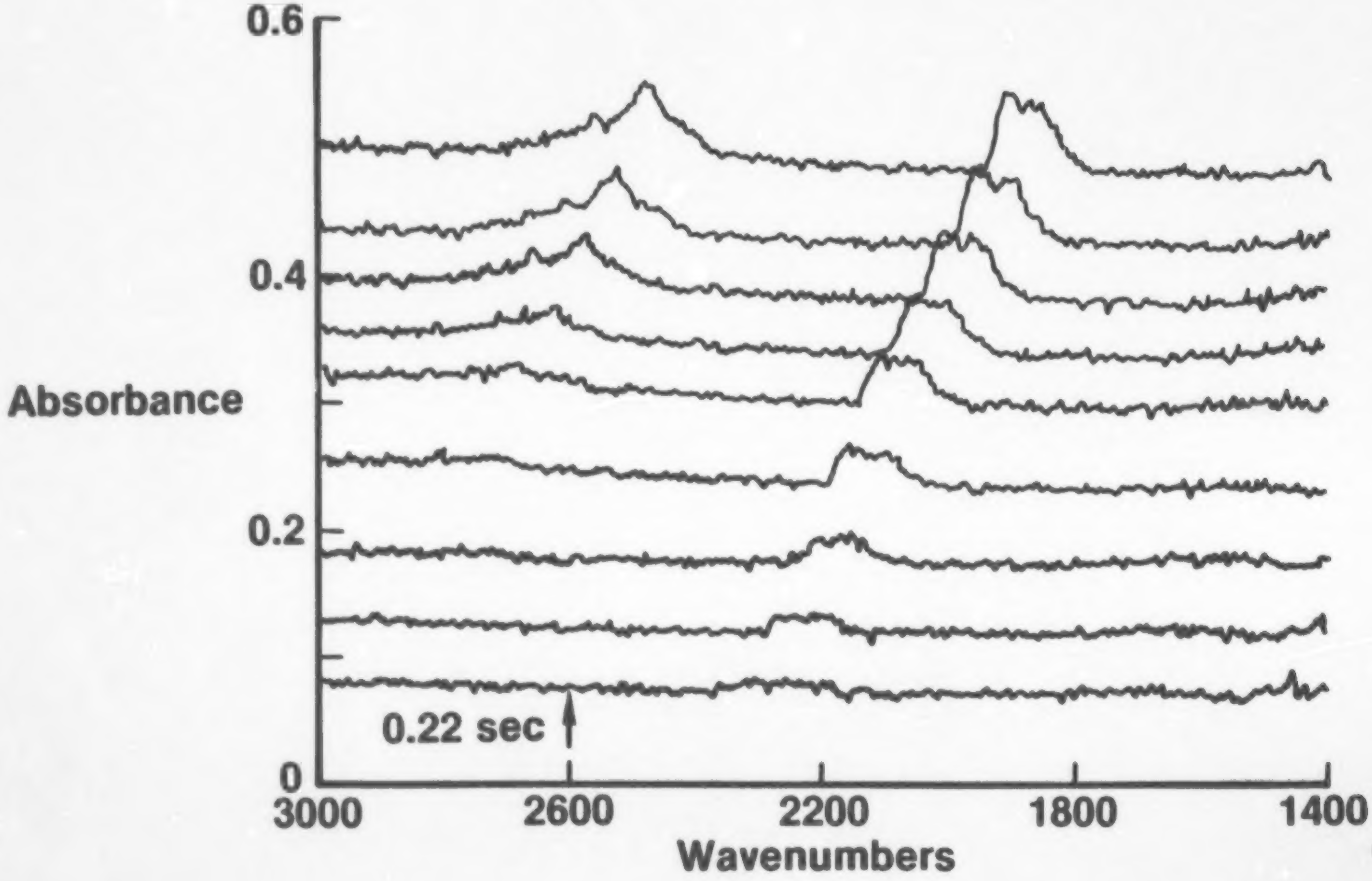

FIG. 25

80-8-67-10

FIG. 26

TIME RESOLVED SPECTRA OF UTAH BITUMINOUS COAL

● 600°C ● Furnace −20 + 25 mesh, 50.3 mg

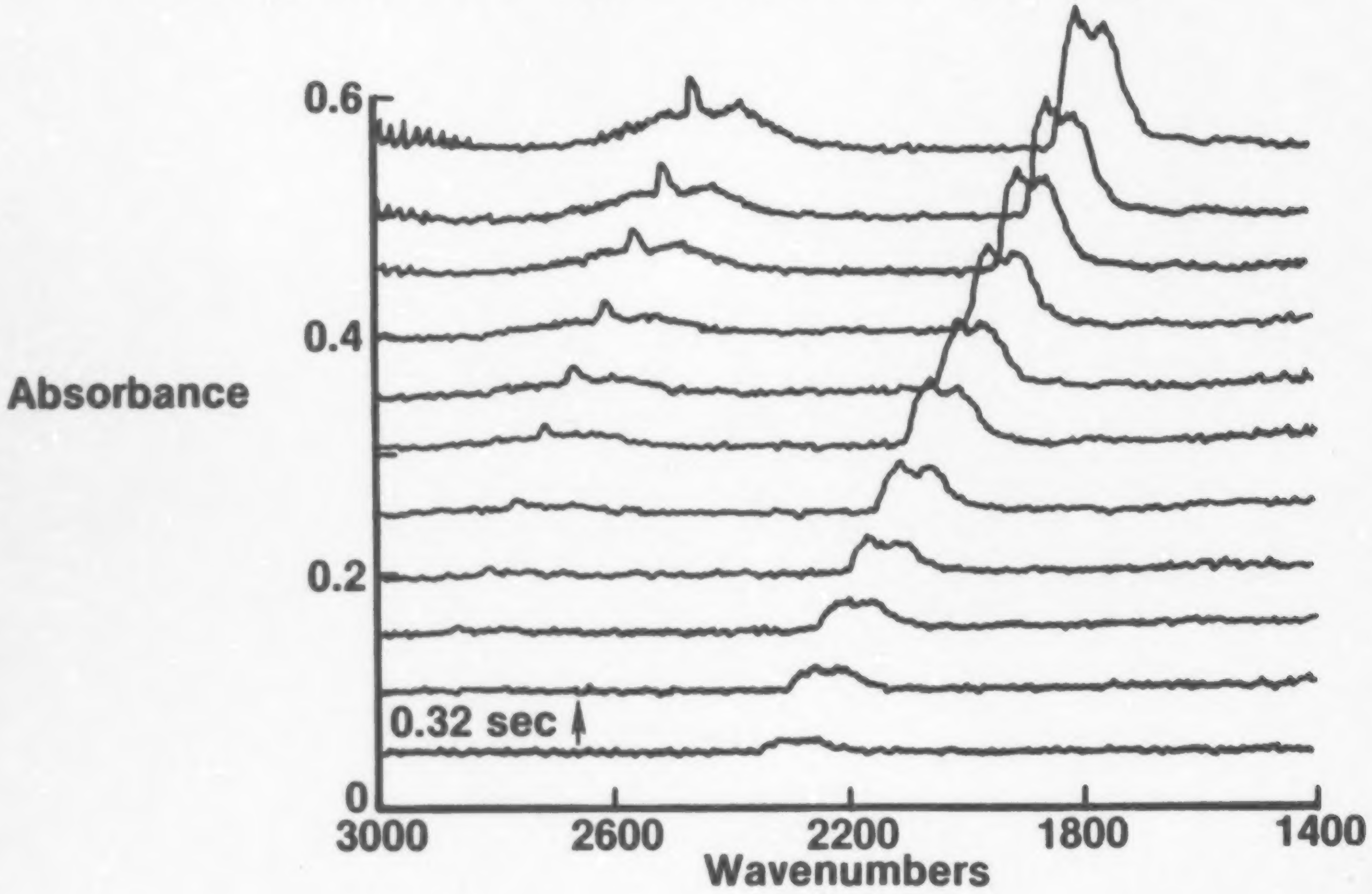

80-8-67-11

As a consequence of the above, it becomes apparent that the source terms for a kinetic model of the devolatilization process can be estimated only indirectly by an a priori process such as quantitative infrared analysis of the parent coal. One must also know the nature of the transforms introduced by the physical parameters associated with the particular pyrolysis process. The mix of functional groups revealed by infrared analysis coupled to an elemental analysis can give an estimate of the product distribution expected from a coal heated in vacuo, to a given final temperature, at a given rate. One must then know the nature of the transforms introduced by varying physical parameters such as particle size, heating rate, and ambient pressure, etc. Such parameters have been shown to influence both devolatilization rates and product mixes.

The investigations performed with the isothermal furnace indicated the rather severe limitations of the vacuum devolatilization model of coal pyrolysis. The modification of the pyrolysis environment introduced both qualitative and quantitative modifications of the observable devolatilization behavior with respect to the vacuum devolatilization behavior. Particle size and thermal flux delivered to the particle are seen to have an effect on both the rates of devolatilization and product distribution. Indeed, these effects are observed to be comparable to those observed for variations in the intrinsic chemical characteristics of the parent coal.

The primary effect of the hot environment (temperature greater than 750°C) appears to be the rapid reduction of complex hydrocarbon species to more thermodynamically favored species. As a first attempt to take into account the effects of the environment, the vacuum model has been revised to reflect this behavior.

Model Revision

To illustrate the development of the equations for the heated grid simulation and the changes for the combustion model, the potential tar forming fraction of a single component is considered in Figure 27, a and b. The values of X and Y at some instant of time are indicated by the dashed lines. For both cases the amount of char is equal to the shaded area,

$$W(I)_{char} = X*Y(I)$$

For the heated grid simulation, Figure 27a the total volatile material evolved (tar + gas) is XO*YO(I) - X*Y(I) and the division between gas and tar is given by the relative kinetic rates, i.e.,

GAS $\quad WG(I) = \left[K(I)/(KX + K(I))\right] * (XO*YO(I) - X*Y(I))$

TAR $\quad WT(I) = \left[KX/(KX + K(I))\right] * (XO*YO(I) - X*Y(I))$

FIG. 27

COAL DECOMPOSITION MODEL

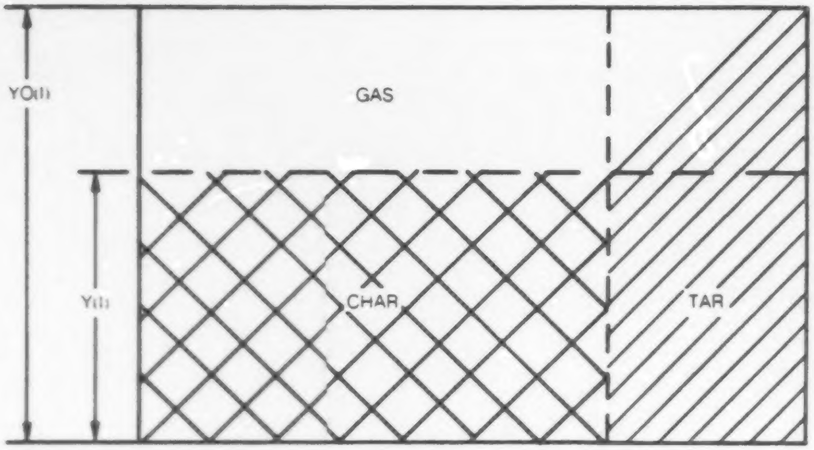
YO(I)
GAS
Y(I)
CHAR
TAR

a) HEATED GRID SIMULATION

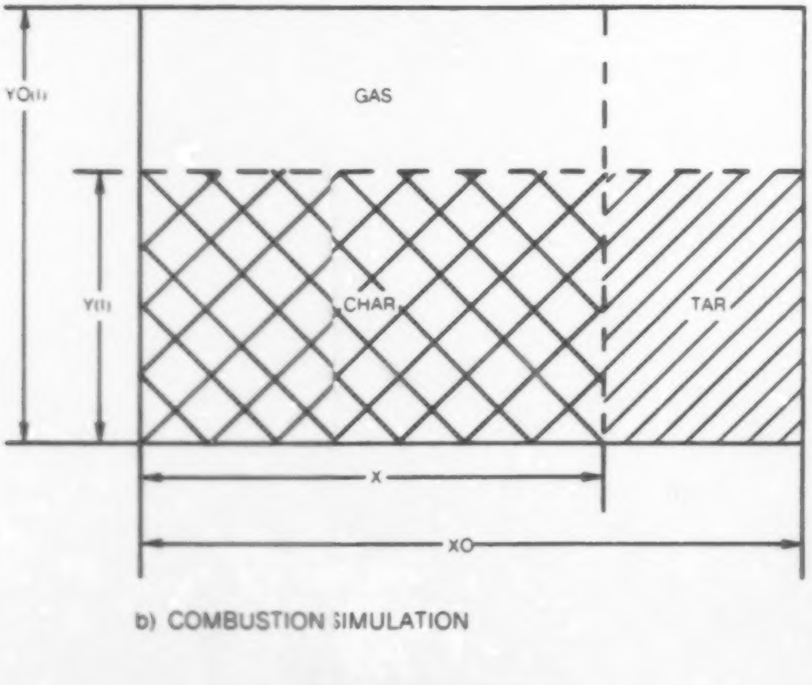
YO(I)
GAS
Y(I)
CHAR
TAR
X
XO

b) COMBUSTION SIMULATION

80–4–73–4

The equations can be verified by direct integration

$$WG(I) = \int_{0}^{X} Y(I)dX = XO*YO(I) \int_{0}^{X} - K(I)\exp\left|-(KX + K(I))t\right| dt$$

The difference for the combustion case Figure 27b is that the tar fraction can continue to thermally decompose after it is released. If it is assumed that the kinetic rate for thermal decomposition into gas is independent of whether the source is the tar or the char, the whole functional group pool is available for gas production at the rate K(I). The split between gas and tar is then modified as shown in Figure 27b and the amounts are:

$$WG(I) = XO*(YO(I) - Y(I))$$

$$WT(I) = (XO - X)*Y(I)$$

The above description considered the case where a functional group pool in the coal could thermally decompose to a gas species via two routes

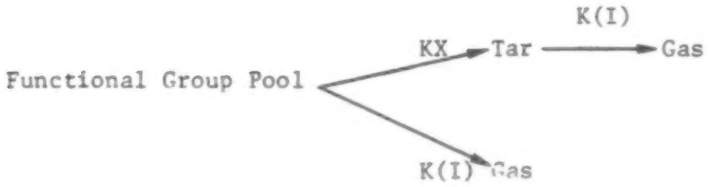

The assumption is that the split between char and tar does not affect the gas evolution.

The general case considers a volume with n dimensions representing n paths for the decomposition of the functional group pool. The most complicated case is the aliphatic pool which has the following thermal decomposition paths.

The weight fraction of the total aliphatic pool is given by the volume

XO * YO(I) * ASMALO * OLO * ACO * SOOTO

Under the conditions of the combustion simulation, each product may continue to thermally decompose as follows.

Product	Original Dimension	Dimension at time t
Tar	XO	XO = XO * exp(-KX*t)
Abstracted	ASMAL O = 1	ASMALL = ASMALO * exp(-KA*t)
Paraffin	YO(I)	Y(I) = YO(I) * exp(-K(I)*t)
Olefins + H_2	OLO = 1	OL = OLO * exp(-KOL*t)
Acetylene + H_2	ACO = 1	AC = ACO * exp(-KAC*t)
Soot + H_2	SOOTO = 1	SOOT = SOOTO * exp(-KSOOT*t)

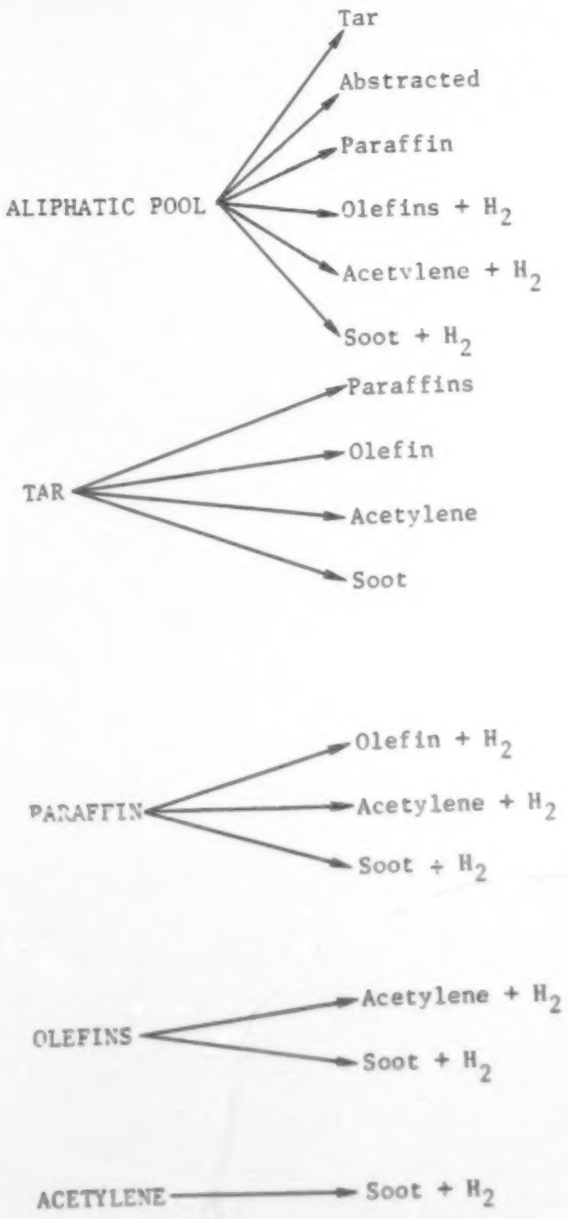
ALIPHATIC POOL
Tar
Abstracted
Paraffin
Olefins + H2
Acetylene + H2
Soot + H2
TAR
Paraffins
Olefin
Acetylene
Soot
PARAFFIN
Olefin + H2
Acetylene + H2
Soot + H2
OLEFINS
Acetylene + H2
Soot + H2
ACETYLENE
Soot + H2

The thermal decomposition equations have been derived under the assumptions that the rate for the production of a particular product (i.e. soot + H_2) is independent of the source (i.e. acetylene, olefins, paraffins, tar or the remaining aliphatic pool in the char). This results in an enormous simplification in the thermal decomposition equations. For example, the whole aliphatic pool is always available for soot production independent of the split between char, tar, paraffin, olefin and acetylene. The equation for the weight fractions from functional group pool "I" is then

$$WSOOT\ (I) = XO * ASMALO * YO(I) * OLO * ACO * (SOOTO - SOOT)$$

Except for the volume WSOOT, the remainder of the aliphatic pool XO * YO(I) * ASMALO * OLO * ACO * SOOT can be considered to be the source for acetylene production so

$$WAC(I) = XO * ASMALO * YO(I) * OLO * (ACO - AC) * SOOT$$

By the same reasoning, the weight fraction olefins is:

$$WOL(I) = XO * ASMALO * YO(I) * (OLO - OL) * AC * SOOT:$$

the weight fraction paraffins is:

$$WG(I) = XO * ASMALO * (YO(I) - Y(I)) * OL * AC * SOOT.$$

the weight fraction abstracted is:

$$WA(I) = XO * (ASMALO - ASMALL) * Y(I) * OL * AC * SOOT.$$

the weight fraction tar is:

$$WT(I) = (XO - X) * ASMALL * Y(I) * OL * AC * SOOT.$$

the weight fraction char is:

$$WC(I) = X * ASMALL * Y(I) * OL * AC * SOOT.$$

In the computer code, the tar forming fraction (considered above) and non-tar forming fraction are designated by the index J = 2 and J = 1, respectively i.e. X(1), X(2), XO(1), XO(2). The equations for the non-tar forming fraction are the same except that X(1) = XO(1).

The list of functional group pools considered in the code is given in Table XXV together with the kinetic rates for decomposition. These rates were chosen to match the heated grid simulation and will need some modification for the combustion case.

V. SUMMARY

The vacuum devolatilization experiments have shown that the product distributions obtained by the thermal decomposition of coal in such an environment are reflective of the intrinsic chemical characteristics of the coal. The distributions of products is dependent upon the functional group characteristics of the parent coal as revealed by infrared analysis with a Fouier Transform Infrared Spectrometer. These experiments have shown that apparent heating rates of the order of 10^2 °C/sec to final temperatures from 500°C to 1700°C yield product distributions reflective of the mix of functional groups present in the parent coal. The product yields as a function of final temperature in such experiments can be adequately predicted by a simple model. The model partitions the coal mass between tar-forming and a non-tar forming fractions. Collectively, these fractions are further subdivided into light gas species, the amounts of which are related to the mix of functional groups present in the coal. When the coal samples are heated at these relatively low heating rates and the kinetic parameters extracted by integral techniques, the Arrhenius first-order kinetic parameters are found to be independent of coal type. Thus, the decomposition process of any coal in such a reaction environment can be described by a single set of kinetic parameters modified by the appropriate coal-dependent source terms.

A nitrogen trace performed upon the devolatilization products formed in such a reaction environment revealed that HCN is the dominant observable light gas species containing nitrogen. The tar abstracts nitrogen on a mass fraction basis in an amount proportional to the mass fraction of coal released as tar. Results from the Utah coal indicate that at higher thermal drivers ($\sim 10^3$°C/sec and above) the tar fraction of some coals may thermally degrade as it is leaving the coal mass. The nitrogen contained in the tar fraction that is decomposed apparently evolves as HCN. A substantial fraction of the coal nitrogen (50-60%) does not evolve as HCN or as an element in the tar species. The evolution of nitrogen from the char occurs at higher temperatures ($\sim$ 1000°C and above) and is released primarily in the form of HCN. The temperature dependence of the evolution of the "char nitrogen" is apparently rank dependent, the higher rank coals tending to retain greater fractions of nitrogen at higher final temperatures.

Devolatilization experiments performed in the isothermal furnace revealed the sensitivity of observable behavior upon physical parameters such as particle size and thermal drive. Using the relative amounts of CH_4, CO_2, and C_2H_4 produced at a given set of operating parameters, for a given particle size increasing the furnace temperature (thereby increasing the thermal flux to the particle) above 600°C results in the increase production of light gases such as CH_4, CO_2, CO, C_2H_4 at the expense of less thermodynamically favored species such as tars and other hydrocarbons. At a given operating temperature increasing the particle size also results in the production of smaller light gas species at the expense of larger hydrocarbons. This is presumably due to intraparticle cracking promoted by the active internal surface of the devolatilizing particle.

It is also observed that the devolatilization times observed in the isothermal furnace are significantly lower than those observed for the corresponding conditions within the heated grid reactor. It is believed this is due to the greater heating rates produced by the furnace environment coupled to the non-isothermal nature of the devolatilization process.

At attempt to include the effects of the hot environment on the devolatilization process has been included in a first revision of the vacuum devolatilization model.

VI. SUGGESTIONS FOR FUTURE WORK

The results of this investigation have pointed to the importance of several considerations in any future work to be directed toward a fundamental and practical understanding of coal devolatilization. These are:

1. Char is always a major devolatilization product.

2. The tar species can collectively form a significant fraction of the devolatilization products initially formed in a wide variety of conditions.

3. Collectively the tar and char products can represent the major fraction of the initial calorific value present in parent coal.

4. Physical parameters such as particle size, apparent heating rate and ambient pressure can have a significant effect upon pyrolysis behavior.

5. The effect of variations in the physical parameters associated with the coal devolatilization process appears to be most readily apparent in the corresponding changes in the production of large hydrocarbon species.

Several guidelines with respect to continued experimental and mathematical modeling studies follow.

1. Due to the sensitivity of the coal decomposition process to variations in physical parameters, no one reactor design can furnish both the experimental control and parameter variation needed to arrive at an applicable model of coal devolatilization. Several reactor designs and analytical techniques used concurrently are needed to isolate the effects of chemical and physical parameters.

2. It appears that any comprehensive model of coal devolatilization will be the result of ongoing modeling efforts taking place in immediate interaction with planned experimental effort. This is the case because the equations of the model must reflect the physical conditons of the devolatilization process as well as the intrinsic characteristics of the coal utilized. Useful universal relationships will be extracted from these results.

3. Since the tar species form a significant fraction of the mass release from many coals while its characteristics and yields are sensitive to variations in physical parameters, ongoing work should make a concerted effort to characterize the tar release from coals. Such characterization should include real time data on the tar release, physical characterization of the mode of tar release and chemical characterization of the tars released.

4. Just as a greater effort should be made to characterize the tars so also should a greater effort be made to characterize the char devolatilization product. Such characterization must include physical as well as chemical characterization.

Specific recommendations include:

1. Modification of the heated grid apparatus to allow for independent variation in apparent heating rate and final temperatures. The control circuit should allow for the selection of any heating rate in the range of 10°C/sec-10^3°C/sec to any final temperature in the range from 400°C to 1500°C. Such a modification will permit the systematic investigation of the effects of either heating rate or final temperature on devolatilization rates and product distribution.

2. The heated grid chamber should be redesigned to permit real time observations of tar release in vacuo. Such a design has been made and implementation appears quite feasible.

3. Real time observations of tar release under pressure should also be made. These should be made under controlled heating rate conditions and under conditions of heating rate such as are produced in the isothermal furnace. Modification of the heated grid apparatus will permit real time observation of tars released under pressure with a controlled heating rate. Modification of the isothermal furnace will allow observations of tar release in a hot environment.

4. The heated grid should be operated in a differential mode to allow collection of differential rate data with the FTIR. Such data is more informative for a non-isothermal process such as coal pyrolysis. The data should be correlated by non-isothermal kinetic techniques.

5. A concerted effort should be made to more precisely quantify the measurement of functional groups in coal by FTIR and cross correlate these measurements with rank parameters.

6. The chemical characteristics of tars released under various conditions should include both elemental analysis and hydrocarbon group type characteristics. The FTIR used in conjunction with a High Pressure Liquid Chromatograph would provide a powerful technique for chemical characterization of the tars. Used in conjunction with the Elemental Analyzer the system developed would provide insight into the nature of the nitrogen retention in tars released under pressure conditions similar to those found in combustion systems.

7. A reactor allowing the production of large quantities of chars and tars in conditions of disperse phase rapid devolatilization should be constructed so that enough char and tar samples can be collected from devolatilization in the same environment for subsequent charactertization and reactivity studies.

REFERENCES

1. Lowry, H. H., Chemistry of Coal Utilization, Supp. Vol., Wiley, New York (1963).

2. Van Krevelen, D. W., Coal: Typology-Chemistry-Physics-Constitution. Elsevier Pub. Co., Amsterdam (1961).

3. Oswa, Y., and J. W. Shih, Fuel, 50, 53 (1971).

4. Dormans, H. N. M., F. J. Huntjens, and D. W. van Krevelen, Fuel, 63, 321 (1957).

5. Mazumdar, B. K., et al., Fuel, 41, 129 (1962).

6. Brown, J. K., and W. R. Ladner, Fuel, 39, 87 (1960).

II. VOLATILITY OF FUEL NITROGEN

Prepared by:

A. E. Axwortny, H.L.Recht, V.H. Dayan,
R, L. Gay, and C. L. Nealy

Rockwell International Corporation
Energy Systems Group
8900 De Soto Avenue
Canoga Park, California 91304

Prepared for:

Energy and Environmental Research Corporation
EER Subcontract No. EER-8318-4

CONTENTS

Page

I. SUMMARY II-1

II. INTRODUCTION II-2

III. EXPERIMENTAL DETAIL II-5

- A. FUEL PYROLYSIS APPARATUS II-5
- B. EXPERIMENTAL PROCEDURE II-6

IV. RESULTS AND DISCUSSION II-8

- A. DESCRIPTION OF FUELS II-8
- B. PROCEDURE VERIFICATION II-8
- C. PETROLEUM-BASED OILS II-11
- D. ALTERNATIVE FUELS II-16
- E. COALS II-19
- F. CORRELATION OF TEST RESULTS WITH NO_X FORMATION II-23

V. REFERENCES II-28

APPENDIX A II-29

FIGURES

Figure | Page

1. Inert Pyrolysis Reactor--Schematic.................... II-4
2. HCN Yield vs First-Stage Temperature for Oils A, B, and C.. II-12
3. HCN Yield vs First-Stage Temperature for Oils D and E.. II-13
4. HCN Yield vs First-Stage Temperature for Oils F and G.. II-14
5. HCN Yield vs First-Stage Temperature for Oils I and J.. II-15
6. HCN Yield vs First-Stage Temperature for Oils H, K, and L (Synthetics)................................. II-18
7. HCN Yie:d vs First-Stage Temperature (Second Stage at 1100°C) for Coals................................ II-21
8. HCN Yield vs First-Stage Temperature (Second Stage at 1100°C) for Coals................................ II-22
9. Percent Fuel-N to NO in Combustion vs Wt Percent N in Fuel (daf).. II-25
10. Percent Fuel-N to HCN in Pyrolysis at 1100°C vs Wt Percent N in Fuel (daf)............................. II-26
11. Percent NO in Combustion vs Percent HCN in Pyrolysis at 1100°C... II-27
A. HCN Yield vs First-Stage Temperature: A-15 Oil....... II-31

TABLES

Table | Page

1. Ultimate Analyses of Fuel Oils......................... II-9
2. Ultimate Analyses of Coals (As-Received Basis)........ II-10
3. Effect of Reaction Time on HCN Yield................. II-17
4. HCN Yield (% of Fuel N) vs First-Stage Temperature.... II-20
5. Summary of Data Related to Fuel Nitrogen Volatility and NO_x Formation................................ II-24

I. SUMMARY

An experimental program has been completed for the measurement of fuel nitrogen volatility using a quartz two-stage pyrolysis reactor. Fuel nitrogen compounds were volatilized in the first-stage of the reactor at temperatures of 300°C, 500°C, 750°C, and 1100°C. The nitrogen compounds were converted to HCN in the second-stage of the reactor, operating at 1100°C. The HCN was collected in dilute sodium carbonate solution and analyzed colorimetrically.

Nineteen fossil fuel samples were studied, consisting of petroleum-based fuel oils, synthetic oils from coal and shale, and coals. The fuel oils from petroleum produced maximum yields of HCN at a first-stage temperature of 1100°C. These yields corresponded to 44-48% of the total nitrogen in the fuel. The yield curve increased monotonically from 300°C with a slight dip at 600-750°C.

The synthetic crude oils showed much higher nitrogen evolution. The HCN yields from shale oils were 70 to 79%, while the coal liquid yielded 50%. The nitrogen species in shale oils were very volatile, giving HCN yields of about 65% at a pyrolysis temperature of 200°C.

A variety of eight bituminous and lignite coals were tested as part of this contract. In general, the coals exhibited much lower fuel nitrogen evolution than was seen from the fuel oils. Maximum coal HCN yields were about 20 to 25% obtained at a pyrolysis temperature of 1100°C.

A plot of the percentage of fuel nitrogen converted to NO during combustion (data from EERC Consultant, D. W. Pershing, of the University of Utah) vs the percentage of fuel nitrogen volatized at 1100°C was found to give a strong, linear correlation, even though a variety of coals was studied. The slope of this line is 2, indicating that twice as much NO is formed as is volatilized as HCN at 1100°C. This correlation may provide an excellent means of predicting NO formation for any given coal simply by measuring the nitrogen volatility at 1100°C. It is recommended that additional studies be done to expand and confirm this correlation.

II. INTRODUCTION

The formation of NO_x in the combustion of fossil fuels is controlled by a number of physical and chemical processes. Sarofim et al.(1) have reviewed the types of chemical processes involved and Wendt and Pershing(2) have considered the physical mechanisms governing NO_x formation in pulverized coal flames. Different types of physical processes, from those involved in coal combustion, may be important in the combustion of liquid fuels.

One of the more important "physical" factors in fuel NO_x formation is the rate at which the "volatile" fuel nitrogen is evolved from the fuel droplets or particles at various points in the combustion zone.(3) This evolution rate determines, in part, the conditions such as temperature and oxygen concentration under which the nitrogen reacts, and is believed to strongly affect the ratio of NO to N_2 formed.(1,2) The rate at which fuel nitrogen is evolved from coals under pyrolysis conditions has been measured as a function of temperature in rapid-heating experiments,(4) and the total amount of volatile nitrogen evolved has been measured in both rapid-heating and long-term experiments.(5) Similar measurements have not been reported of the volatility of the bound-nitrogen contained in liquid fuels. Based on distillation experiments, however, much of the nitrogen in coal-derived liquids and in shale oil is believed to be considerably more volatile than the fuel nitrogen contained in petroleum crudes. This difference between the volatility distributions of the fuel nitrogen compounds of alternative liquid fuels and those of petroleum-based oils may have a major effect on the amount of fuel NO_x that forms under various combustion conditions.

In order to model even semiempirically the conversion of fuel nitrogen to NO and N_2 in combustion and the effects of combustion modification techniques on this conversion, it is necessary to estimate the rate of evolution of volatile nitrogen from various fuels at each point within the combustor.(3) The most detailed method for obtaining data for coals that relate to this process appears to be that employed by Pohl, Sarofim, and Howard at MIT.(1) There is, however, a need for a simplified experimental procedure for investigating the volatility range distribution of the nitrogen in a variety of fuel samples. Such information has been obtained during the present program for a rather large number of fuels and fuel types. These data will permit the optimum combustion conditions for each type of fuel to be evaluated (by use of semiempirical models). Also, these preliminary nitrogen volatility data supplement the more detailed data to be obtained in the MIT program for selected fuel samples and include fuel types that may not be suitable for the MIT apparatus.

Another consideration is the possiblity that all of the nitrogen species evolved from fossil fuels may not be equally reactive in the formation of fuel NO_x. The evidence available at present suggests that this is not the case, but the possibility does exist. The techniques prior to our work to investigate nitrogen evolution from heated coal particles measure the amount of nitrogen remaining in the char or residue and obtain the total nitrogen loss by difference. The nature of the experimental procedure used in the present investigation is such that only volatile nitrogen species capable of further reaction to form NO_x in combustion are measured.

It was found under a previous Rockwell program (EPA 68-02-1886)(6) that in a two-stage inert pyrolysis reactor the reactive volatile nitrogen evolved from the fuel in the first-stage pyrolysis process is converted to HCN in the second stage when the second stage is held at about $1400^{\circ}K$. This two-stage reactor technique, therefore, permits the reactive nitrogen evolved at a given first-stage temperature to be measured by converting it to HCN in the second-stage and measuring the HCN formed by a very sensitive colorimetric technique. In the present program, nitrogen volatility vs temperature profiles were measured in this manner for 19 fossil fuel samples including alternative fuels derived from coals and shale oils.

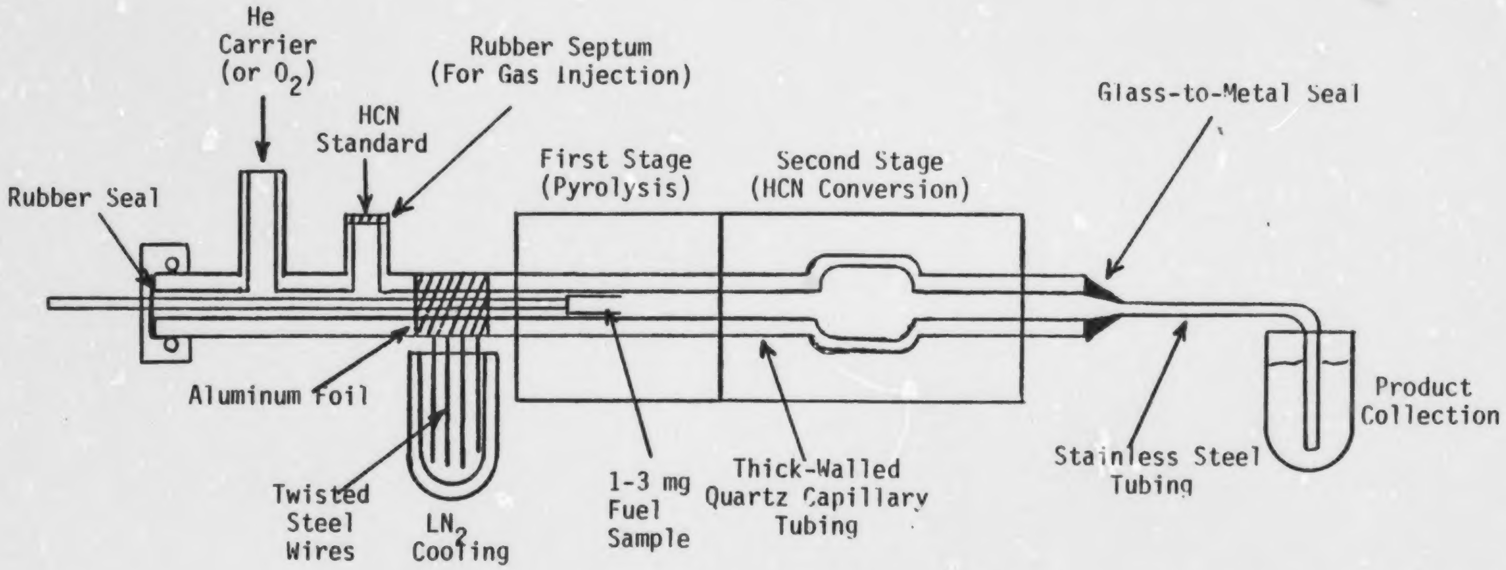
He
Carrier
(or O_2)
Rubber Septum
(For Gas Injection)
HCN
Standard
Rubber Seal
First Stage
(Pyrolysis)
Second Stage
(HCN Conversion)
Glass-to-Metal Seal
Aluminum Foil
Twisted
Steel
Wires
LN_2
Cooling
1-3 mg
Fuel
Sample
Thick-Walled
Quartz Capillary
Tubing
Stainless Steel
Tubing
Product
Collection

Figure 1. Inert Pyrolysis Reactor - Schematic

III. EXPERIMENTAL

A. FUEL PYROLYSIS APPARATUS

The fuel pyrolysis apparatus used for the initial parts of the present program, which involved testing of petroleum-based oils and alternative fuels, was the same apparatus as had been used in a previous Rockwell program. Midway through the project, the program was transferred to Rockwell's Energy Systems Group, and a new apparatus of essentially identical design was built and used in the final portion of the test program.

A schematic diagram of the pyrolysis apparatus is shown in Figure 1. The pyrolysis section of the apparatus consists of a two-zone heated quartz tube. Heating is done using muffle furnaces. The first zone is heated to the desired pyrolysis temperature. Fuel samples are inserted into the center of the first zone. The temperature at the sample position of the first zone is held constant during a given pyrolysis experiment. Typically, the temperatures studied are 300, 500, 750, and 1100°C. The second heating zone is maintained at a temperature of 1100°C in all tests in order to convert all of the pyrolyzed nitrogen to HCN. A separate muffle furnace was used to heat the second zone. Insulation around the quartz tube at the ends of the furnaces was used for thermal separation between the two zones.

The quartz tube used in these experiments was a 178 cm length of 2.0 mm ID x 10.0 mm OD capillary tubing. The first zone (the pyrolysis zone) was heated over a length of 32 cm. The second zone (conversion to HCN) was heated over a length of 51 cm. The quartz tubing was enlarged (mainly as to ID) in the center of the second zone to form a small, 5-cm long chamber of approximately 11 mm OD. The purpose of this chamber was to increase the residence time in the 1100°C region and thus insure conversion of the volatile nitrogen species to HCN.

The oil or coal sample was held in a small quartz boat or tube attached to the end of a quartz rod which fitted inside the capillary tubing. The size of the sample was usually 1 to 3 mg. The quartz rod was connected via a Teflon tube to a stainless steel rod which was used to insert the sample into the pyrolysis zone. Helium carrier gas, set at standard flow rate of 40 cc/min, was used to carry the volatile species through the system. The front end of the tube had provision for injection of gaseous HCN samples for standardization. A region of the tube at the entrance to the pyrolysis furnace was cooled by a metal conductor dipped in liquid nitrogen. Oxygen could also be admitted to the quartz tube to burn out deposits.

The exit of the quartz tube was connected by a glass-to-metal seal to 1.6-mm OD stainless steel tubing. For sample collection, the tubing was inserted in a small test tube containing 25 ml of dilute (5 g/l) sodium carbonate solution. A small amount of cadmium carbonate powder was added to the solution to remove sulfur as CdS. The HCN was collected in the sodium carbonate solution, the solids removed by centrifugation, and the supernate analyzed according to ASTM Procedure D 2036-75 (a sensitive colormetric analysis).

B. EXPERIMENTAL PROCEDURE

The pyrolysis system was tested each day prior to performing pyrolysis experiments initially using a HCN-He gas mixture and later with Ultrasystems A-15 oil, which was well known in terms of nitrogen volatility. In the work with oils, it was not necessary to further condition the quartz tube before running samples. However, in order to get reproducible results with coals, it was found that a light coating of carbon (pyrolysis products) on the walls of the tube was necessary. This was produced by pyrolyzing three to four samples (≈1 mg each) of a Conoco low-nitrogen, light-weight oil. This pretreatment was then followed by pyrolysis of the fuel samples.

Each sample was placed in the quartz holder, weighed, and then inserted in the quartz reactor tube up to the liquid N_2 cooled region. It was left there for 3 to 5 min, while being purged with He, and then quickly inserted into the center of the pyrolysis zone. The pyrolysis off-gas was then collected for 3 min. The sodium carbonate collector solution was then centrifuged to settle solids, mainly $CdCO_3$, at the bottom of the tube. Four aliquots of the collector solution were taken for analysis. Two or more of these were analyzed as required to obtain reproducible results.

Periodically, the quartz tube was cleaned of accummulated deposits by burning out with oxygen and, if required, by then rinsing the tube with concentrated hydrofluoric acid.

A detailed outline of the experimental procedure is given in Appendix A.

IV. TEST RESULTS AND DISCUSSION

A. DESCRIPTION OF FUELS

The fuels tested in this program consisted of fuel oils, synthetic oils, and coals. The ultimate analyses of the fuel oils and synthetic oils are given in Table 1. The fuel nitrogen content of these oils varied from 0.16 wt % to 1.98 wt %. The ultimate analyses of the coals are given in Table 2. The fuel nitrogen content of the coals varied from 0.54 wt % to 1.75 wt % (as received basis).

B. PROCEDURE VERIFICATION

The procedure verification consisted of testing the two-stage pyrolysis apparatus with closely coupled furnaces. The purpose of this arrangement was to permit operation of the first stage (pyrolysis) at temperatures as low as 300°C, while the second stage was held at 1100°C to give maximum conversion of volatile nitrogen to HCN. The apparatus was tested by measuring the HCN yields from Ultrasystems' No. 6 fuel oil at first-stage temperatures of 250°C to 1100°C. The results obtained are shown in Curve A of Figure 2.

The HCN yields obtained at 1100°C, 950°C, and 750°C (48%, 40%, and 34%, respectively) are in good agreement with those obtained previously with this oil (46%, 42%, and 35%) as reported in Table III of Reference 6. As the temperature is decreased below 750°C, the yield increases reaching a maximum of about 40% around 500°C. At lower temperatures, the yield decreases steadily with temperature reaching a value of 14% at 250°C.

It was not expected that an appreciable amount of the chemically-bound nitrogen in this fuel would be evolved at 250°C. This fuel oil is obtained from a Wilmington crude, and it can be seen from Figure 3 of Reference 7 that less than about 7% of the total fuel nitrogen in Wilmington crude oil is contained in the fraction that boils below 325°C. One

TABLE 1

ULTIMATE ANALYSES OF FUEL OILS

Oil	Source	C, wt %	H, wt %	N, wt %	S, wt %	Ash, wt %	O, wt % (By Difference)
A	Wilmington, California	85.41	11.44	0.77	1.63	0.043	0.71
B	Indonesian Malayasian	86.53	11.93	0.24	0.22	0.036	1.04
C	Gulf Coast	84.62	10.77	0.36	2.44	0.027	1.78
D	East Coast Essex Co.	86.54	12.31	0.16	0.36	0.023	0.61
E	Middle East (Exxon)	86.78	11.95	0.18	0.67	0.012	0.41
F	Venezuelan	85.24	10.96	0.40	2.22	0.081	1.10
G	Venezuelan (Desulfurized)	85.92	12.05	0.24	0.93	0.033	0.83
H	Synthoil	-	-	1.3	0.8	-	-
I	Rocketdyne	-	-	0.62	1.05	-	-
J	Alaskan	-	-	0.51	1.63	-	-
K	Diesel Marine Fuel (Shale)	-	-	0.24	0.51	-	-
L	Crude PARAHO Shale Oil	-	-	1.98	0.67	-	-

737-G.65/jmh

TABLE 2

ULTIMATE ANALYSES OF COALS (AS RECEIVED BASIS)

Coal	C, wt %	H, wt %	N, wt %	S, wt %	Ash, wt %	H_2O, wt %	O, wt % (By Difference)
TRW No. 2	71.57	4.94	1.33	1.09	11.66	1.87	7.54
TRW No. 1	-	-	1.34	-	-	1.29	5.88
Utah No. 1	68.49	5.20	1.24	0.64	7.40	6.39	10.64
Scranton, ND, No. 4	42.02	2.71	0.54	0.99	7.50	34.96	11.28
Beulah, ND, No. 9	43.24	2.74	0.72	0.24	4.97	34.63	13.46
Montana Savage No. 11	41.36	2.57	0.72	0.27	4.61	36.36	14.11
Rosa, AL, No. 18	74.72	4.36	1.60	0.96	6.79	8.02	3.55
Black Creek, AL, No. 19	80.27	5.09	1.75	0.74	4.45	2.25	5.45

737-G.65

explanation of the 14% yield at 250°C would be that, because of radiative heat transfer from the second stage to the first stage, the capillary may be somewhat hotter at the boat stop position than the temperature read on the thermocouple, which was suspended about 1/8 in. from the capillary at this point. Since the objective of this program was to compare the volatility characteristics of a number of fuels, this possible error in absolute temperature may not be important since it would be the same in all experiments and probably only occurs at very low first-stage temperatures.

C. PETROLEUM-BASED OILS

Nine petroleum-based fuel oils were characterized with respect to fuel nitrogen volatility using the procedure described in Section III. These oils are Oils A, B, C, D, E, F, G, I, and J. The analyses of these oils have been given in Table 1. The HCN yield curves obtained with these oils are presented in Figures 2 through 5.

The maximum yields of HCN (at a first-stage temperature of 1100°C) were between 44 and 48% for all of the oils except the two Venezuelan oils and the Alaskan oil which gave maximum yields of 35 to 39%. The dip in the yield curve that occurred at 750°C with Oil A (see Figure 2) is indicated with some of the other oils but is less pronounced. This dip is also predominant in the volatility curve for the A-15 calibration oil (see Appendix A). The yields are near their maximum values at 500°C except for Oils D and E.

At lower temperatures, greater differences exist in some of the results. At 300°C, five of the oils (A, B, E, F, and G) give HCN yields between 15 and 18%. Oil D (East Coast) and Oil I (Rocketdyne) give slightly higher yields (22% for both oils) while Oil J (Alaskan) gives slightly lower yield (7%). Oil C (Gulf Coast) is quite unusual in that it produces no volatile nitrogen at 300°C. Except for Oil C, the measured

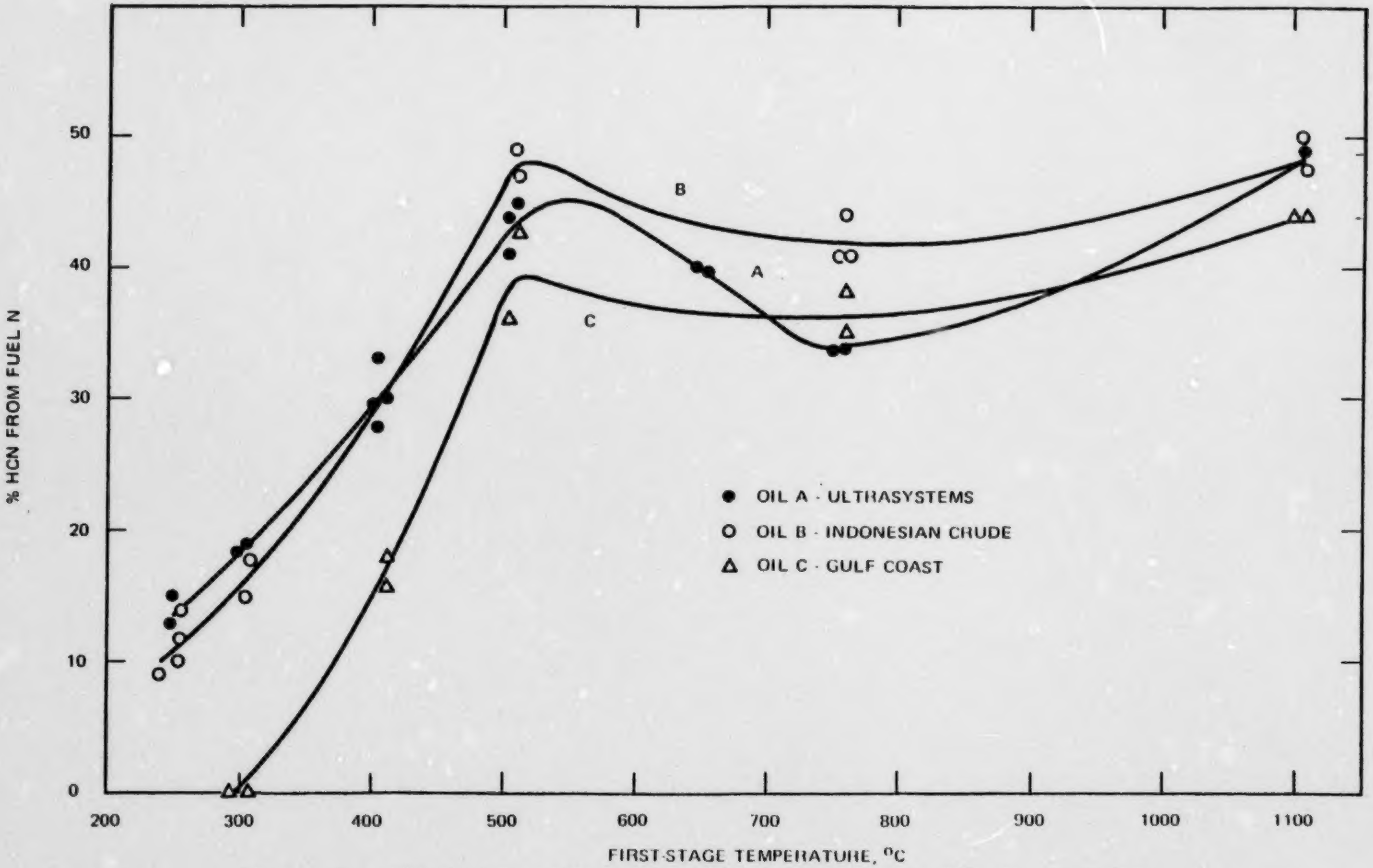

Figure 2. HCN Yield vs First-Stage Temperature for Oils A, B, and C

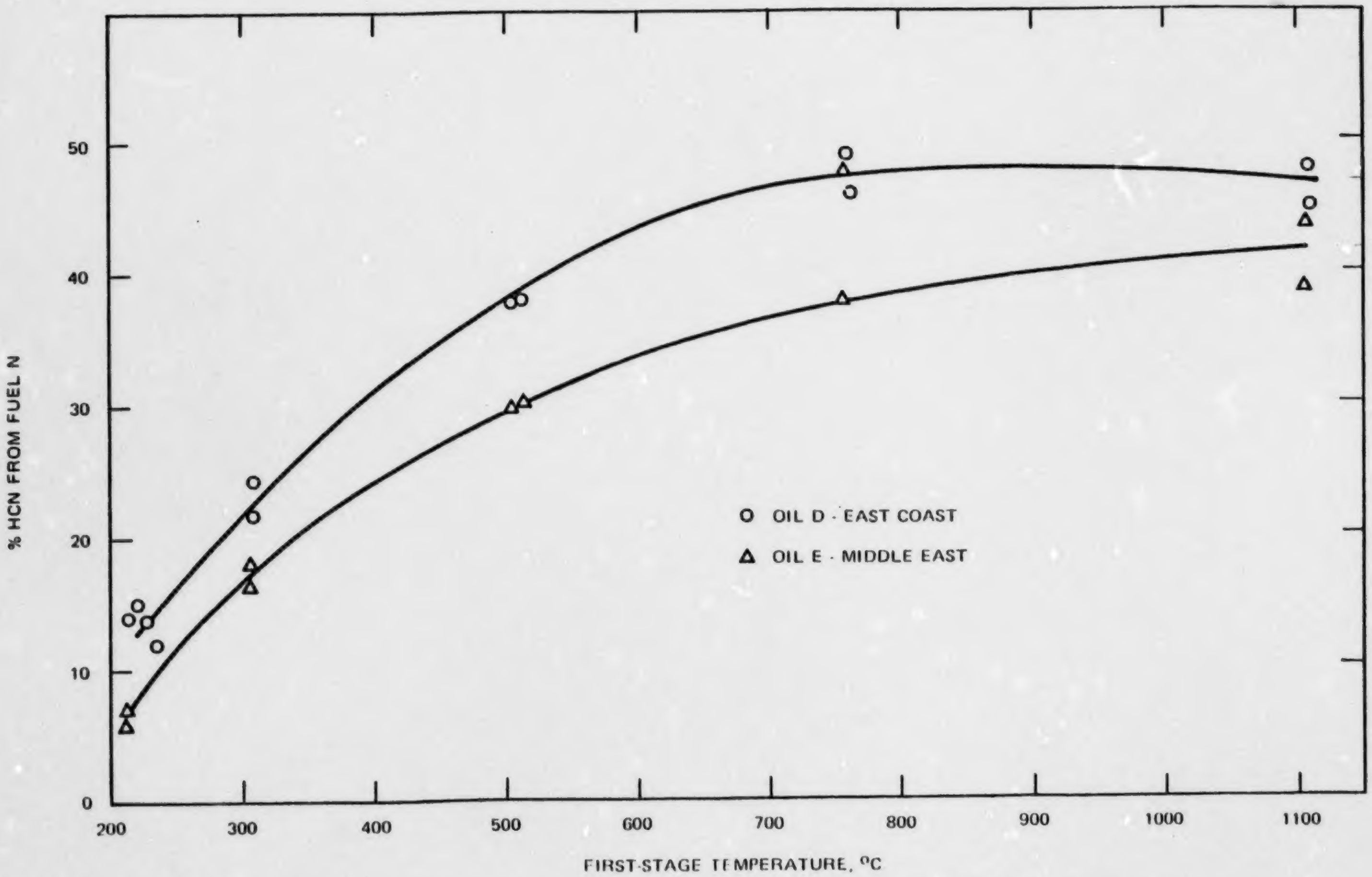

Figure 3. HCN Yield vs First-Stage Temperature for Oils D and E

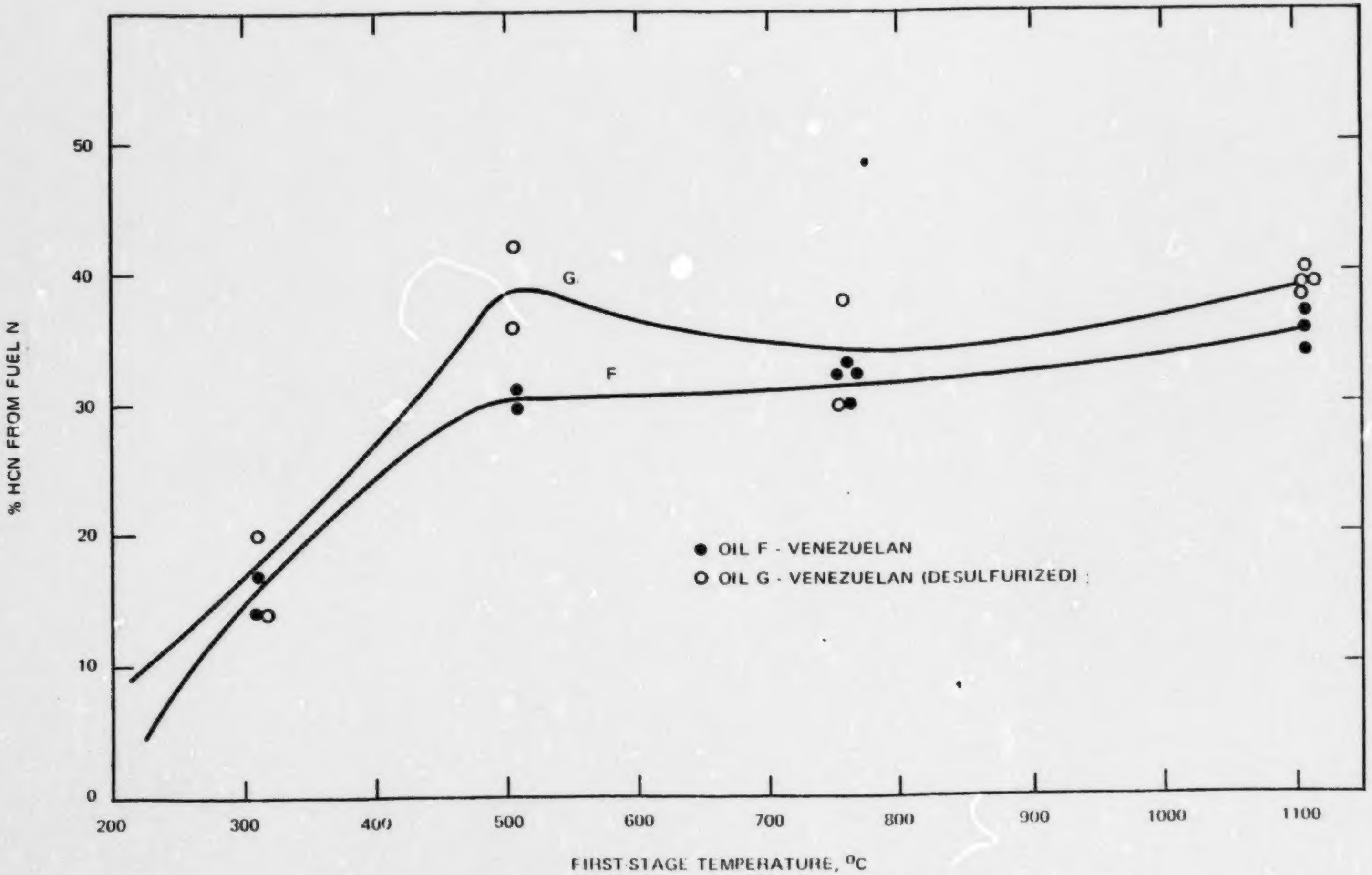

Figure 4. HCN Yield *vs* First-Stage Temperature for Oils F and G

K&E 10 X 10 TO THE CENTIMETER 18 X 25 CM
KEUFFEL & ESSER CO. MADE IN U.S.A. 46 1510

Oil J Alaskan
Oil I Rocketdyne

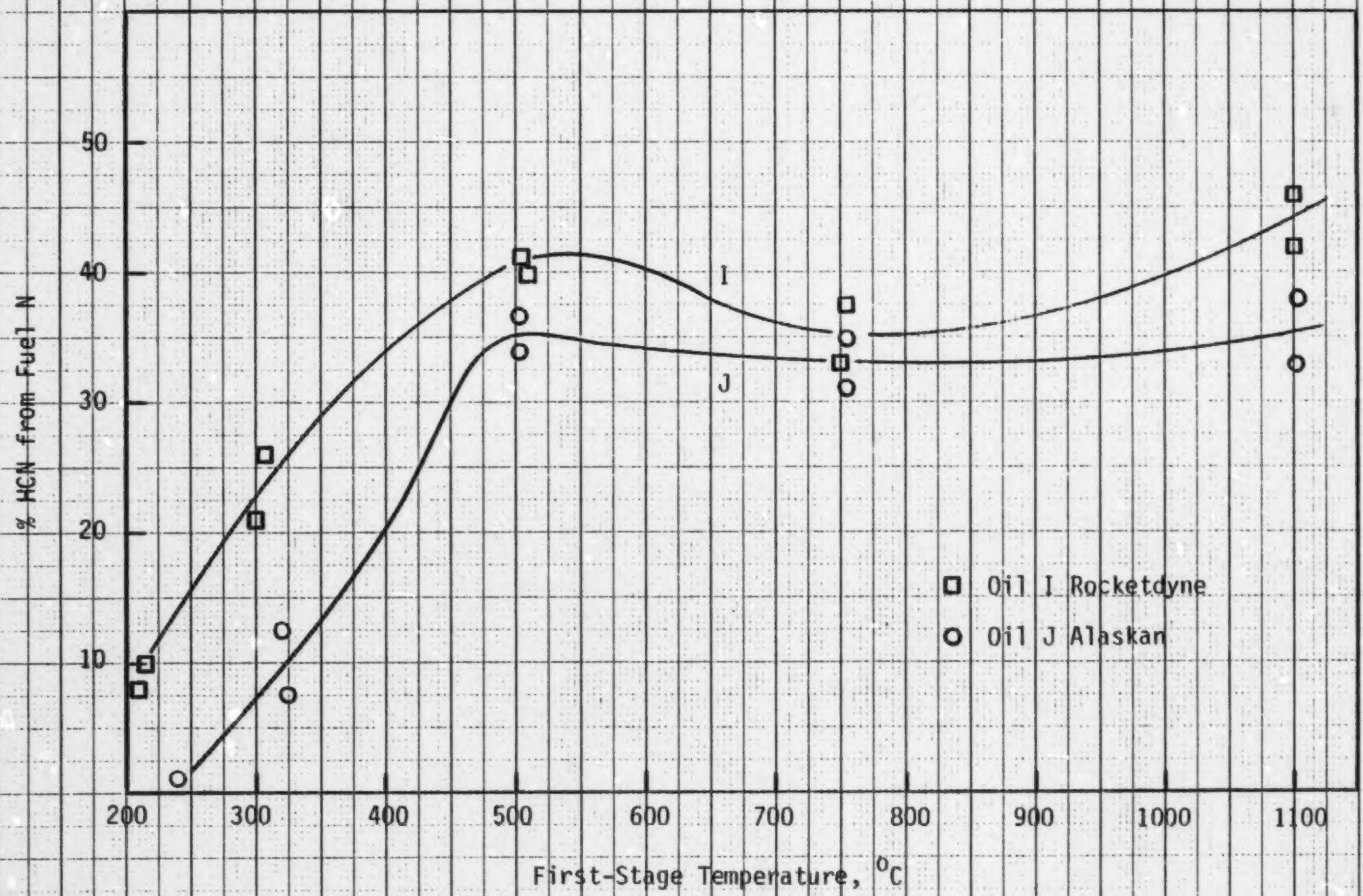

Figure 5. HCN Yield VS First-Stage Temperature for Oils I and J

Reproduced from best available copy.

HCN yields ranged from 2 to 16% at 250°C and from 6 to 10% at 200°C (for those oils run at 200°C). These results indicate that, with one major exception, the volatility characteristics of the fuel nitrogen in the petroleum-based oils are quite similar.

All of the data points in Figures 2 through 5 are from experiments in which the HCN was collected for 3 min after the oil sample was inserted into the preheated reactor. It has been demonstrated previously in higher temperature experiments that most of the HCN is formed in less than a few seconds. The 3-min collection period was chosen to allow time for any HCN that might be absorbed in the system to be evolved. One might expect that the fuel nitrogen would be evolved more slowly at the lower temperatures, and experiments were carried out to investigate this. After 3 min, the bubbler solution was removed and was quickly replaced with another solution that was left in place for at least 10 min.

It can be seen from Table 3 that, at 210°C, a considerable amount of HCN is formed after the first 3 min. At higher temperatures, the amount of HCN that is evolved after 3 min at a given temperature is much smaller. In the experiments with Oil A, the residue that remained in the boat and in the first stage of the reactor was slowly heated to 750°C, and the additional HCN evolved was measured. At each of the four temperatures, the remainder of the "volatile" fuel nitrogen was evolved giving total yields similar to those obtained in 1100°C experiments.

D. ALTERNATIVE FUELS

The alternative fuels tested in this program were SYNTHOIL (a liquefied coal), a shale-based diesel marine fuel, and a crude PARAHO shale oil. The HCN yields from these oils are plotted in Figure 6. The two shale oils show much higher HCN yields than the coal liquefaction product. At the highest pyrolysis (first stage) temperature, 1100°C, the HCN yields of the shale oils were 70 to 79%, while the coal liquid

TABLE 3

EFFECT OF REACTION TIME ON HCN YIELD

	Total HCN Yield, %		
	Oil A	Oil D	Oil G
210°C			
3 min		15	9
18 min		30[a]	13[a]
300°C			
3 min	18		
13 min	23[a]		
Inc. to 760°C (30 min)	50[b]		
400°C			
3 min	28		
13 min	33[a]		
Inc. to 750°C (20 min)	45[b]		
500°C			
3 min	41		
13 min	43[a]		
Inc. to 750°C (15 min)	47[b]		
650°C			
3 min	40		
13 min	47[a]		
Inc. to 750°C (10 min)	51[b]		

[a] Includes HCN formed during first 3 min

[b] Includes HCN formed at lower temperature

K&E 10 X 10 TO THE CENTIMETER
KEUFFEL & ESSER CO.

46 1512

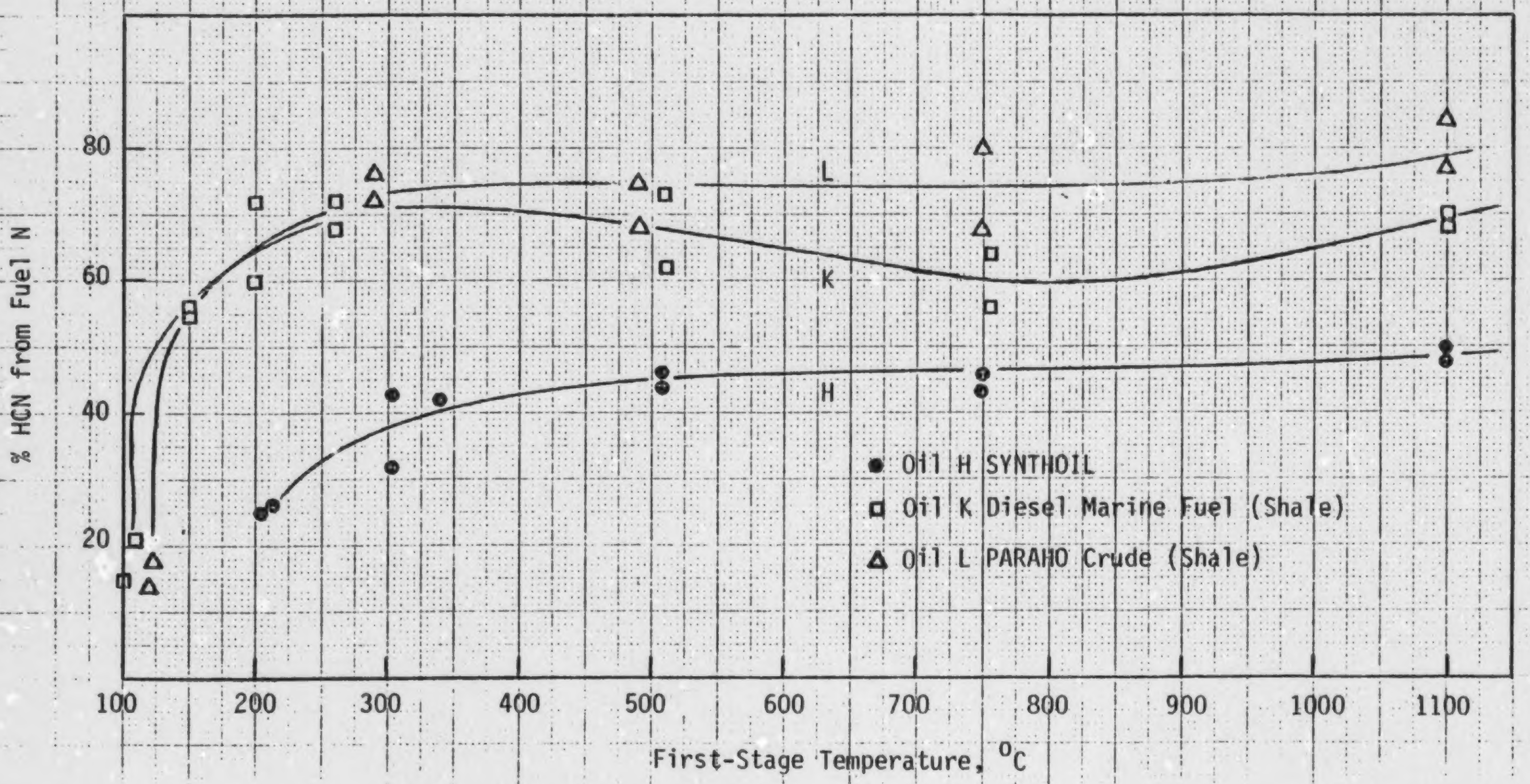

Figure 6. HCN Yield Vs First-Stage Temperature for Oils H, K. and L (Synthetics)

only yielded 50%. The SYNTHOIL and shale oil results are in agreement with previous (Program 68-02-1886) single-stage reactor results.

In contrast to petroleum-based oils, the HCN yield did not drop off appreciably until the first-stage temperature was decreased below about 350°C for the SYNTHOIL and 200°C for the shale oils. The nitrogen species in the shale oils are very volatile, giving HCN yields of about 65% at a pyrolysis temperature of 200°C.

There are large differences in volatility between the nitrogen species in shale-based fuels and in petroleum-based fuels. This suggests that the optimum combustion modification techniques for alternative fuel combustion may be quite different than those developed for petroleum-based fuels.

E. COALS

Eight coals were tested as part of this contract. The ultimate analyses of these coals are given in Table 2. The HCN yields for these coals are given in Table 4. These results are plotted for comparison in Figures 7 and 8. The coal results were obtained using the apparatus built at Energy Systems Group. Previous results for fuel oils were obtained using the apparatus at Rocketdyne.

In general, the coals exhibit much lower fuel nitrogen evolution than was seen from the fuel oils. Maximum coal HCN yields (at 1100°C pyrolysis temperature) are about 20 to 25%, as compared to 40 to 50% for the fuel oils. The scatter in the coal data at 300°C is probably not real. It is most likely due to a slight variation in temperature about the 300°C point. Further analysis of the coal results is presented in the next section where the HCN yields are compared to NO_x formation from fuel nitrogen during combustion.

TABLE 4

HCN YIELD (% OF FUEL N) VS FIRST-STAGE TEMPERATURE

Coal	300°C	500°C	750°C	1100°C
TRW No. 2	1.1	8.3	13.4	16.4
TRW No. 1	4.3	8.3	11.6	17.2
Utah No. 1	0.4	10.5	14.6	21.4
Scranton, ND, No. 4	0.3	9.7	22.0	25.5
Beulah, ND, No. 9	4.2	8.1	10.0	11.7
Montana Savage No. 11	0.9	8.1	9.7	18.9
Rosa, AL, No. 18	0.1	8.8	14.8	16.1
Black Creek, AL, No. 19	0.1	6.7	13.5	15.8

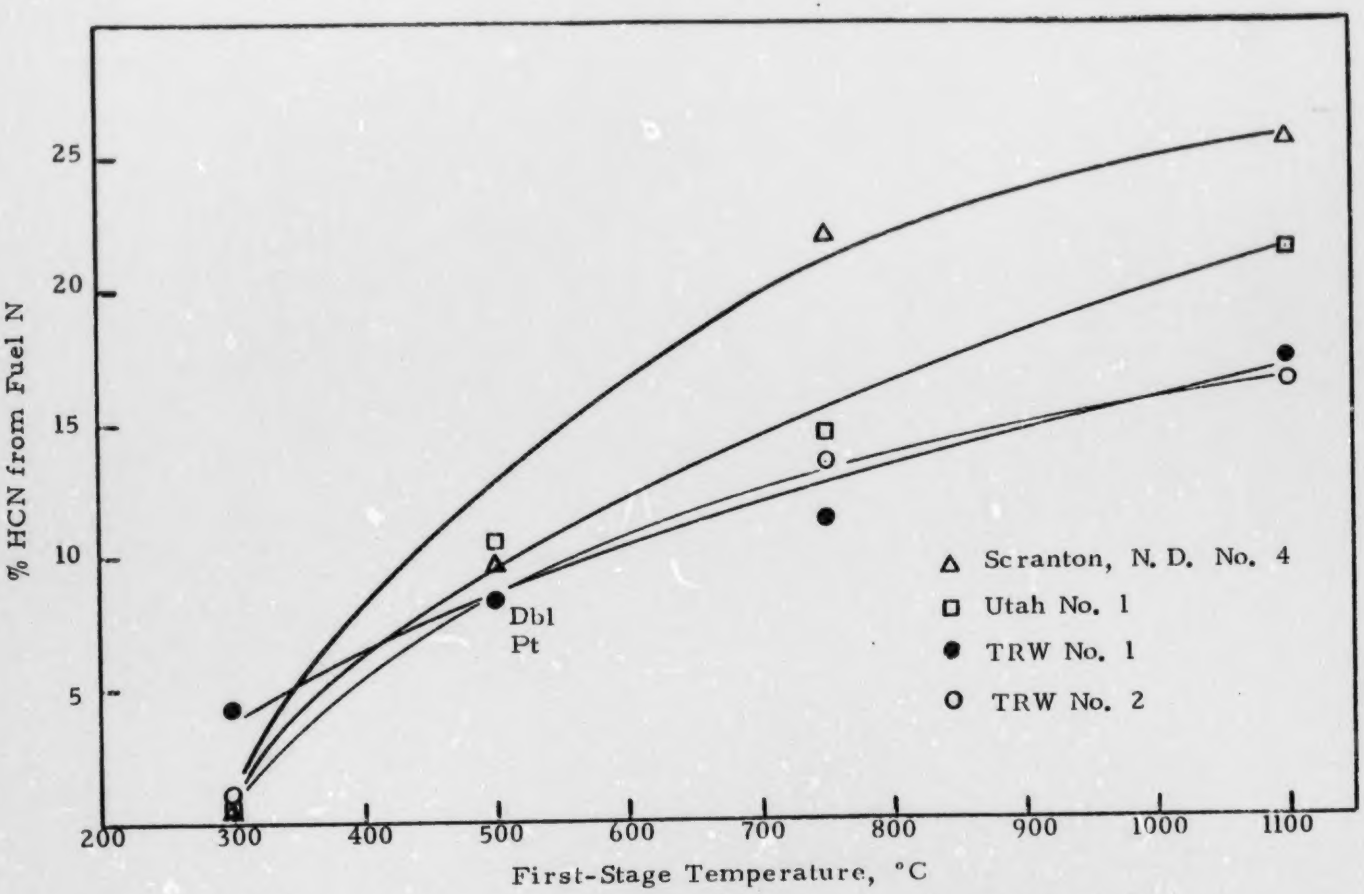

Figure 7. HCN Yield Vs. First-Stage Temperature (Second Stage at 1100°C) for Coals

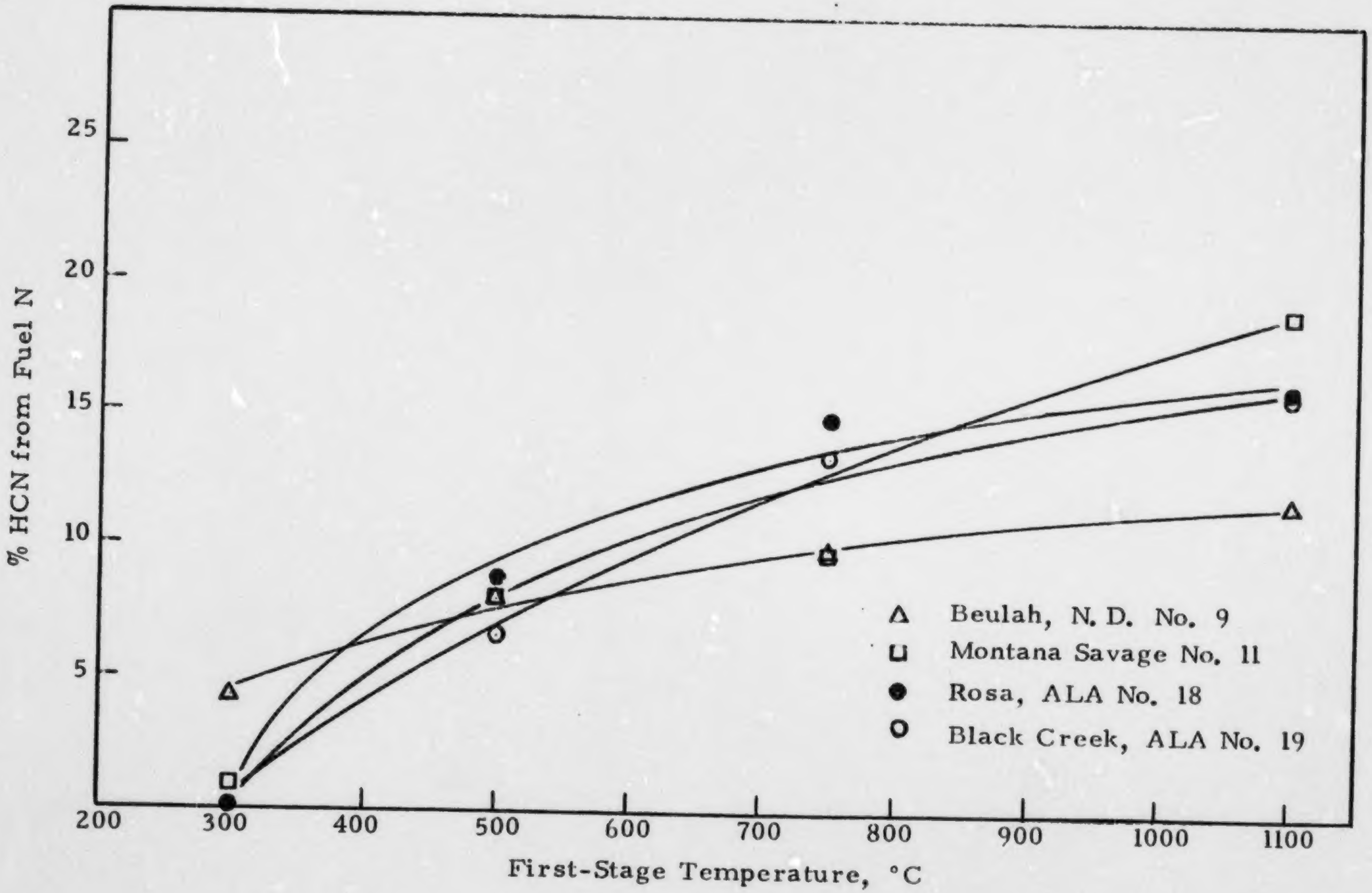

Figure 8. HCN Yield vs. First-Stage Temperature (Second Stage at 1100°C) for Coals

F. CORRELATION OF TEST RESULTS WITH NO_x FORMATION

It is of importance to the study of combustion processes and pollution control to examine the formation of NO_x from fuel nitrogen with respect to the volatility of fuel nitrogen. This is especially important for the case of coal combustion because fuel nitrogen is the major source of NO_x emissions when burning this fuel.

A summary of the data related to fuel nitrogen volatility and NO_x formation is given in Table 5. The NO data given in Table 5 are the result of combustion of the same coals used in this program. These data were reported to us by EERC Consultant, D. W. Pershing. The HCN data are the result of this program and are given in Table 4.

A plot of the percentage of Fuel N converted to NO during combustion vs the wt % N in the fuel is given in Figure 9. The data do not correlate well. A similar plot for the percentage of Fuel N volatilized at 1100°C vs the wt % N in the fuel is given in Figure 10. Again, the data do not correlate well. However, the two plots (Figures 9 and 10) are very similar.

A plot of the percentage of fuel nitrogen converted to NO during combustion vs the percentage of Fuel N volatilized at 1100°C is given in Figure 11.* There is a very strong, linear correlation between the two even though a large variety of coals was studied. The slope of this line is 2, indicating that twice as much NO is formed as is volatilized as HCN at 1100°C. This correlation provides an excellent means of predicting NO formation for any given coal simply by measuring the nitrogen volatility at 1100°C. It is recommended that additional studies be done to expand and confirm this correlation.

---

*Two values for fuel NO were received for the Scranton No. 4 coal, one early in the program, one much later. Parentheses are used to distinguish the later value. Although one value for fuel NO appears to match the correlation very well, it is still uncertain as to which value corresponds to the coal that was tested for nitrogen volatility.

TABLE 5

SUMMARY OF DATA RELATED TO FUEL NITROGEN VOLATILITY AND NO_X FORMATION

Coal	% N (DAF)	Moles Dry Comb. Prod. Per Gm (As Rec'd.)[a]	NO[b] (ppm)	Fuel-NO Per Gm Coal (m mole)	Fuel-N to Fuel-NO (%)	Fuel-N to HCN @ 1100°C (%)	% to NO / % to HCN
TRW No. 2	1.54	0.323	790	0.255	26.9	16.4	1.64
TRW No. 1	1.58	-	-	-	-	17.2	-
Utah No. 1	1.44	0.309	1230	0.380	42.9	21.4	2.00
Scranton, ND, No. 4	0.94	0.180	1070 (690)[c]	0.193 (0.121)	49.9 (31.2)	25.5	1.96 (1.22)
Beulah, ND, No. 9	1.19	0.182	630	0.115	22.3	11.7	1.91
Montana Savage No. 11	1.22	0.172	1020	0.175	34.1	18.9	1.80
Rosa, AL, No. 18	1.88	0.335	1100	0.368	32.3	16.1	2.01
Black Creek, AL, No. 19	1.88	0.361	1170	0.422	33.8	15.8	2.14

[a] Moles dry combustion products per gm = % C/12.01 + % N/14.01 + % S/32.06 + 3.727 (Z)
where Z = net moles O_2 = % C/12.01 + % H/4.00 + % N/28.02 + % S/32.06 - % O/32.00

[b] Personal communication from D. W. Pershing

[c] Values in parenthesesare a second set of NO values received for the Scranton, ND, No. 4 coal

737-G.65/jmh/sjh

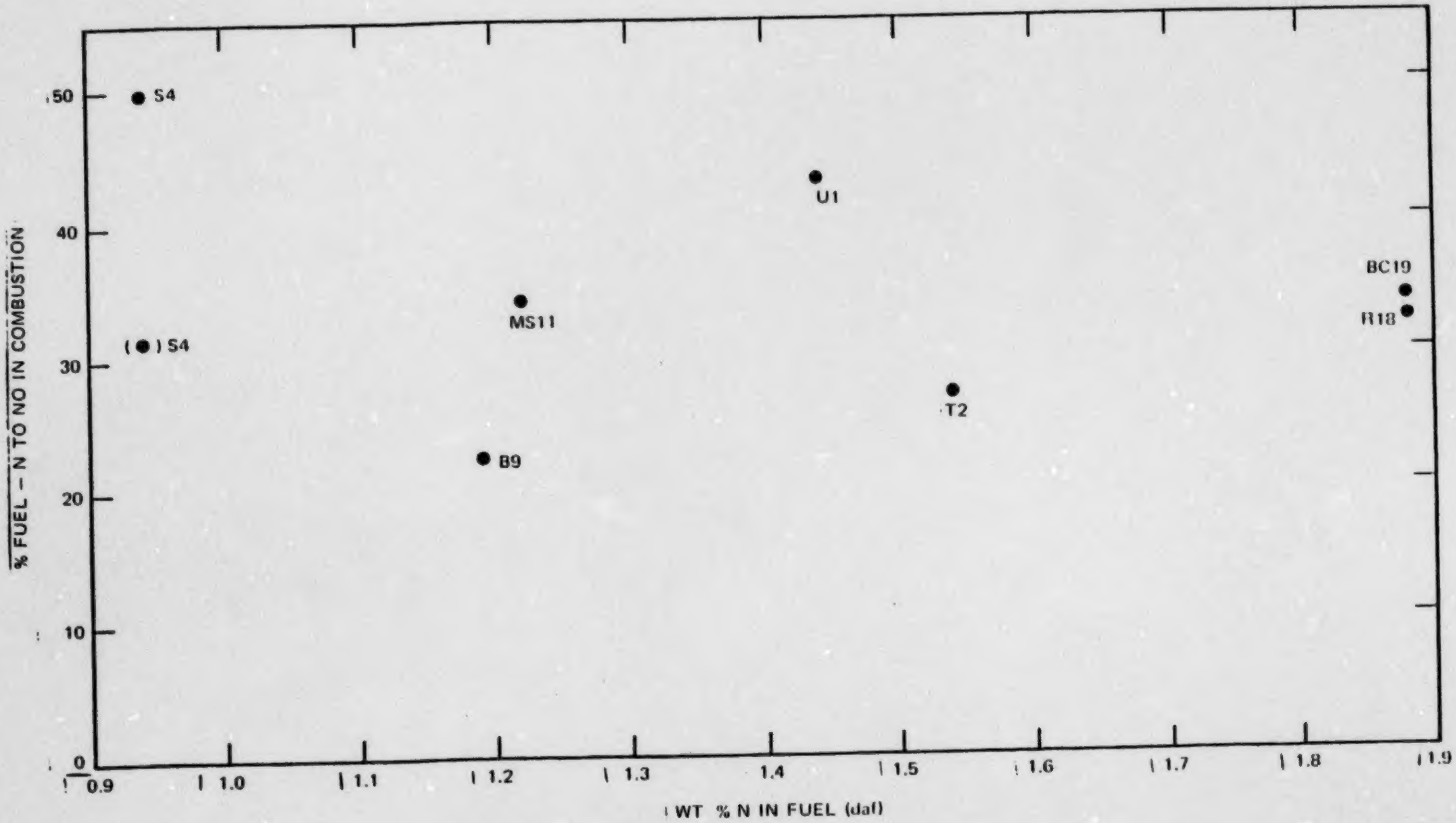

Figure 9. Percent Fuel-N to NO in Combustion vs
Wt Percent N in Fuel (daf)

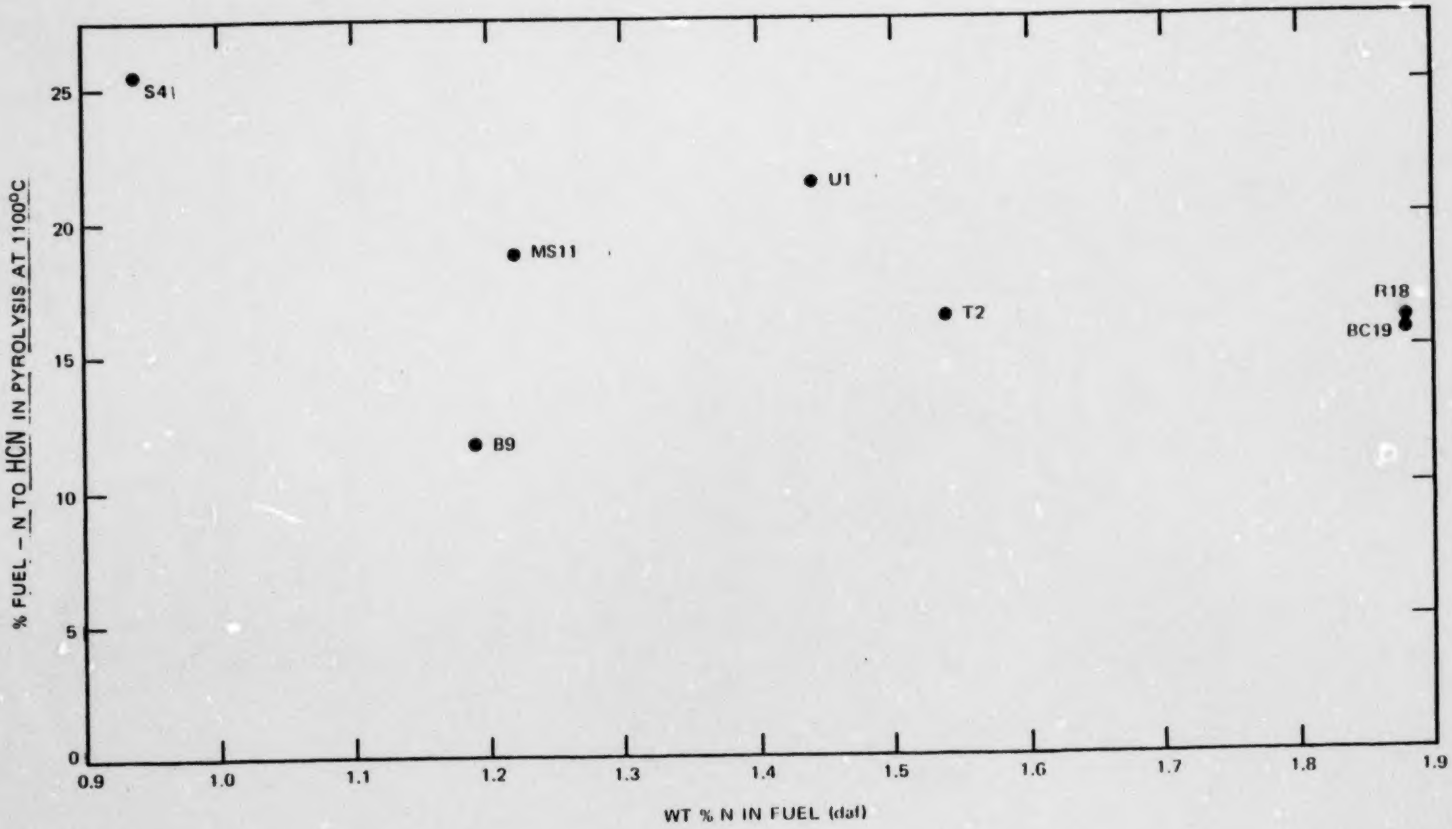

Figure 10. Percent Fuel-N to HCN in Pyrolysis at 1100°C
Wt Percent N in Fuel (daf)

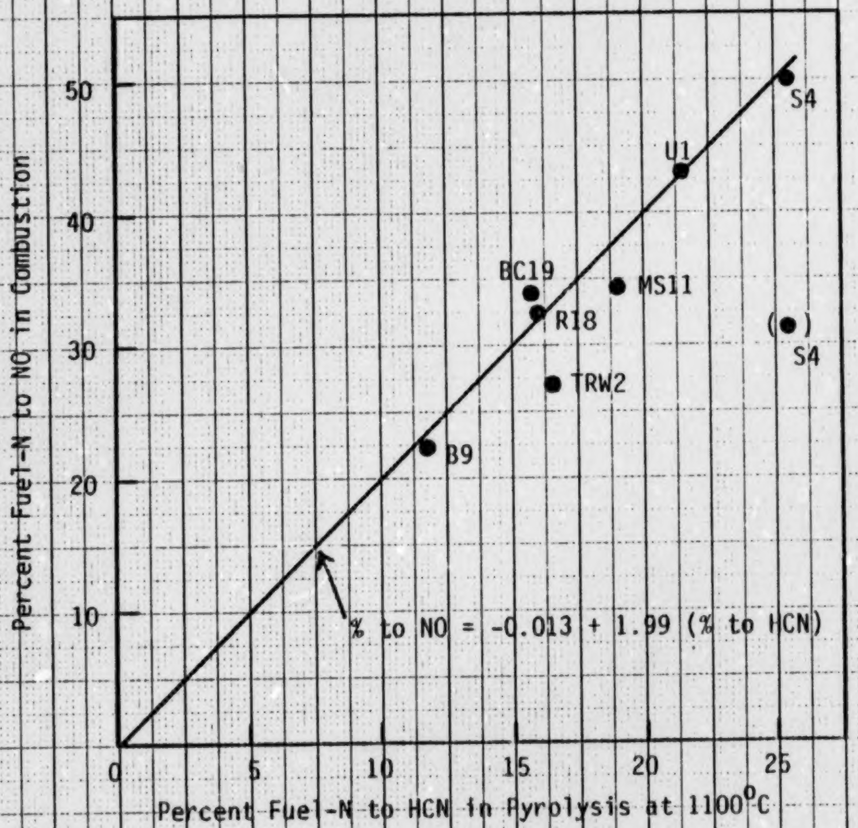

Figure 11. Percent NO in Combustion *vs* Percent HCN in Pyrolysis at 1100°C

K&E 10 X 10 TO THE CENTIMETER
46 1510

V. REFERENCES

1. A. F. Sarofim, J. H. Pohl and B. R. Taylor, "Mechanisms and Kinetics of NO_x Formation: Recent Developments," presented at the 69th Annual AIChE Meeting, November 1976, Paper No. 27D

2. J. O. Wendt and D. W. Pershing, "Physical Mechanisms Governing the Oxidation of Volatile Fuel Nitrogen in Pulverized Coal Flames," Comb. Sci. & Tech. (1977)

3. A. E. Axworthy, V. H. Dayan, and G. B. Martin, "Reactions of Fuel-Nitrogen Compounds Under Conditions of Inert Pyrolysis," Fuel, Vol. 57, pp. 29-35, January 1978

4. J. H. Pohl and A. F. Sarofim, "Devolatilization and Oxidation of Coal Particles," presented at the 16th International Symposium on Combustion, August 1976

5. D. W. Blair, W. Bartok, J. O. L. Wendt, and D. G. Lilley, "Devolatilization and Pyrolysis of Fuel Nitrogen from Single Coal Particle Combustion," presented at the 16th International Symposium on Combustion, August 1976

6. A. E. Axworthy and V. H. Dayan, "Chemical Reactions in the Conversion of Fuel Nitrogen to NO . Fuel Pyrolysis Studies," In: Proceedings of the Second Stationary Source Combustion Symposium, Vol. IV, EPA-600/7-77-073d (NTIS PB274029), p. 39, July 1977

7. A. E. Axworthy, et al., "Chemistry of Fuel Nitrogen Conversion to Nitrogen Oxides in Combustion, EPA-600/2-76-039 (NTIS PB250373), February 1976

APPENDIX A

Detailed Experimental Procedure

A. PREPARATION

1) Temperatures raised or adjusted from overnight standby to operating levels. Usual overnight T_1 and $T_2 = 500^0C$.
2) If last test prior day was with coal, 3-4 samples of Conoco low-N oil pyrolyzed in system.
3) Sample of Ultrasystems A-15 oil pyrolyzed. If HCN value at expected level, compared with Figure A, proceeded to test with coal.

B. EXTENSIVE RECONDITIONING PROCEDURE

1) If HCN value was low, 2-3 additional samples of low-N oil would have been pyrolyzed; A-15 oil retested.
2) If HCN value was still low, deposits would have been oxidized in stream of O_2. After overnight purge with He, tube conditioning with low-N oil would be repeated.
3) If Step 5 proved inadequate, a repeat of O_2 purge followed by HF treatment would be used.

C. PYROLYSIS PROCEDURE

1) Quartz sample holder cleaned in hot Fisher burner flame.
2) Sample weighed onto holder.
3) Holder mounted onto positioning rod and placed into reaction tube (ambient temperature section).
4) He purge continuously on (adjusted at temperature, if required).
5) After 3-4 min. purge, liquid-N_2 coolant put in place to cool zone just outside first furnace.
6) After 2-3 min. of cooling, sample moved to position in middle of cooled zone. Allowed to cool 3-4 min.

7) Collector Na_2CO_3 solution with $CdCO_3$ powder put in place; magnetic stirring started.

8) Sample moved to position at center of first furnace. (Move time ~5 sec).

9) Effluent gas collected for 3 min.

10) Collector solution removed from line. Sample moved to ambient temperature section of tube. Liquid-N_2 coolant removed.

11) Collector solution transferred to centrifuge tube. Centrifuged for 3-4 min.

12) Four aliquots of supernatant taken for analysis.

D. ANALYSIS

1) ASTM Procedure D2036-75 used.

2) Standard curve prepared using known CN solution; periodic rechecks made.

3) Aliquot of collector solution diluted to ~10 ml in 25 ml volumetric flask.

4) With constant stirring, additions made of:
   a) Phosphate buffer (7.5 ml)
   b) Chloramine-T solution (1 ml)
   c) Pyridine-Barbituric acid reagent (2.5 ml)
   d) Water to mark

5) Color permitted to develop for 7-8 min.

6) Read using Beckman Model 25 spectrophotometer at 578 nm.

7) Blank prepared using 50 ml volumetric flask, 4 ml of 5g/1 Na_2CO_3 solution as sample, and volumes 2X those used for collector solution.

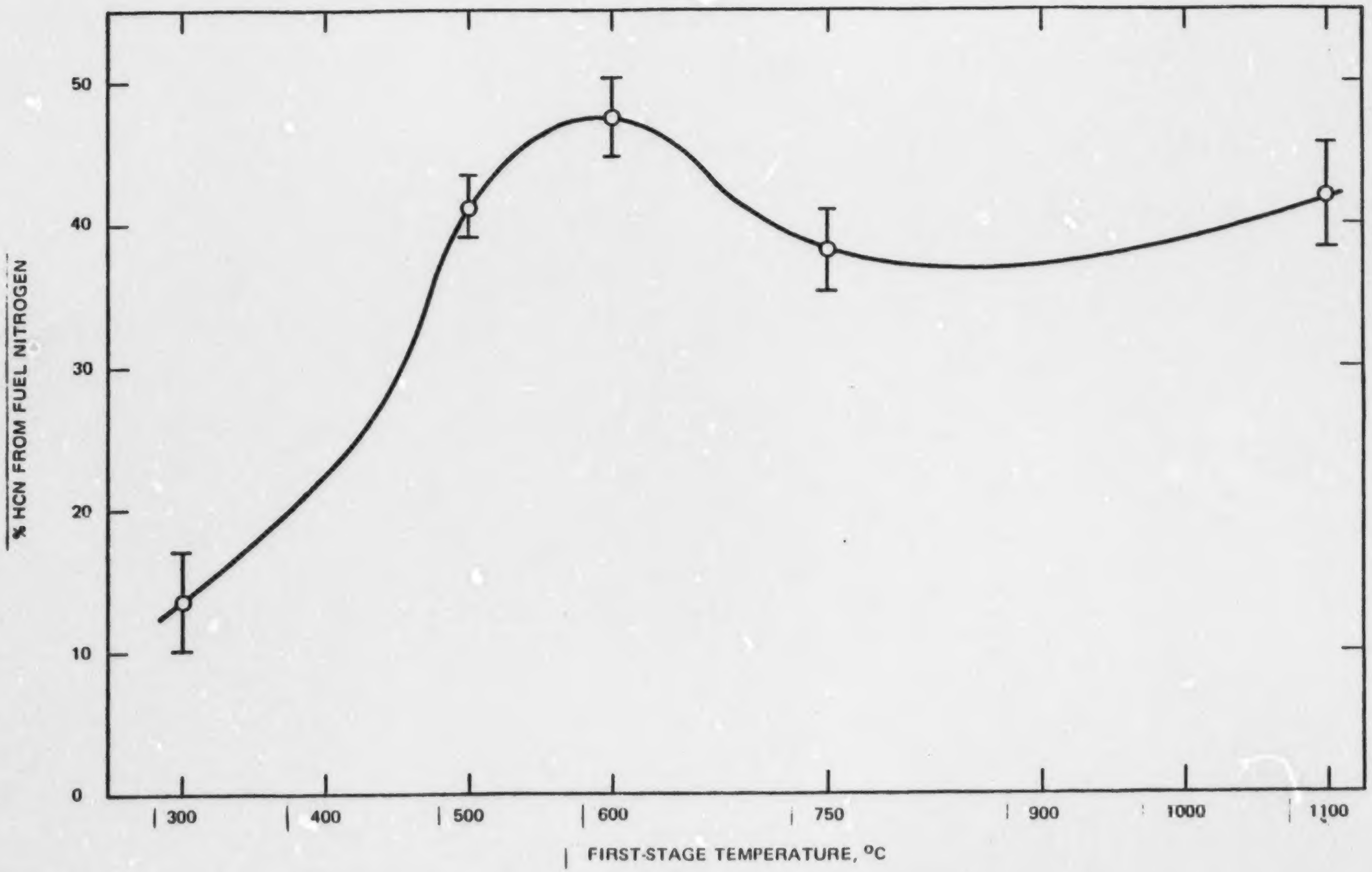

HCN Yield vs First-Stage Temperature: A-15 Oil

III. STIRRED REACTOR STUDY OF POLLUTANT FORMATION FROM COMBUSTING PULVERIZED COAL CLOUDS

Prepared by:

P. M. Golberg, P. A. Cawley,
J. T. Kelly, H. Tong, and R. M. Kendall

Acurex Corporation
Energy & Environmental Division
485 Clyde Avenue
Mountain View, California 94042

Prepared for:

Energy and Environmental Research Corporation
EER Subcontract No. EER-8318-2

TABLE OF CONTENTS

Section — Page (III-)

1 INTRODUCTION 1

1.1 Objective 1
1.2 Program Overview 4

2 COMBUSTOR DESIGN 5

2.1 Background 5
2.2 Design Considerations 6
2.3 Cold Model Designs 13

3 PRELIMINARY EXPERIMENTS 17

3.1 Gas Mixing Experiments 17
3.2 Particle Mixing Experiment 33

4 COMBUSTION EXPERIMENTAL EQUIPMENT 61

4.1 Fuel and Gas Delivery System 61
4.2 Sampling System 61
4.3 SR Combustors 66

5 EXPERIMENTAL 71

5.1 Test Procedure and SR Operating Characteristics . 73
5.2 Combustion Test Results 77

5.2.1 Temperature and Major Gas Species 82
5.2.2 Extent of Reaction 91
5.2.3 Fuel Nitrogen Reactions 99
5.2.4 Coal/Air/N2/CH4 Devolatilization Tests 114

5.2.5 Reacted Particle Size Distribution 119

6 RESULTS 121

6.1 SR Mixing Performance 121
6.2 Operating Characteristics 122
6.3 Combustion and Emissions 123

7 CONCLUSIONS AND RECOMMENDATIONS 127

7.1 Conclusions 127
7.2 Recommendations 128

TABLE OF CONTENTS (Concluded)

Section Page (III-)

REFERENCES 131

APPENDIX A -- PARTICLE MIXING DATA 135

LIST OF ILLUSTRATIONS

Figure		Page (III-)
2-1a	SR II Construction Showing Chamber Dimensions (cm) . .	9
2-1b	SR 1 Construction Showing Chamber Dimensions (cm) . . .	9
2-1c	SR Construction Showing Jet Orientations and Relative Locations	10
2-2	Injector Design	12
2-3	Predicted Injector Performance	12
3-1	Setup for Helium Tracer Experiments	18
3-2	SR II Injector Tip with Ball Socket Showing Helium Injection Configuration	20
3-3	SR II Helium Tracer Results at a Middle Jet Angle of 15°	23
3-4	SR II Helium Tracer Results at a Middle Jet Angle of 15°	25
3-5	SR II Helium Tracer Results at a Middle Jet Angle of 30°	26
3-6	Particle Mixing Experimental Setup	30
3-7	SR II Helium Tracer Results Showing Top Jet, Middle Jet, and Bottom Jet Response	31
3-8	Quick Acting Valve for Coal/Air Switching	35
3-9	Normalized Light Intensity Versus Equivalence Ratio . .	37
3-10	Data Reduction Method Schematic	38
3-11	Injector Output Signal at an SR II Airflow of 14.2 l/s, Showing Data Range and Effect of Particle Concentration 0.12 g/l; 0.29 g/l	40
3-12	SR II Response at 30 scfm	41
3-13	Predicted SR II Response Comparing Test Data with Model Selection	45
3-14	Residence Times Versus SR II Model Throughput . . .'. .	47

LIST OF ILLUSTRATIONS (continued)

Figure Page (III-)

3-15 SR I Response to Dust Injection at an Air Throughput of 9.4 l/s 49
3-16 SR I Response to Dust Injection Stopped at an Air Throughput of 9.4 l/s 51
3-17 SR I Response to Coal Injection at an Air Throughput of 14.3 l/s 53
3-18 SR I Response to Coal Injection Being Stopped at an Air Throughput of 14.3 l/s 55
3-19 Residence Time Versus SR I Model Throughput 59
4-1 Combustion Testing Experimental Setups 62
4-2 Sampling Probe 64
4-3 Sampling Probe Positioning 65
4-4 Combustor Construction Schematic 68
5-1 Utah Coal Particle Size Distribution for Two Samples Obtained by Wet Sieving 72
5-2 SR I Variations in Temperature and Gas Composition Over Test Interval 75
5-3 SR II Variations in Temperature and Gas Composition Over Test Interval 76
5-4 Measured Gas Temperature Versus Whole Coal Equivalence . . . 83
5-5a SR I Gas Composition Versus quivalence Ratio 84
5-5b SR II Gas Composition Versus Equivalence Ratio 85
5-6 SR I Temperature Measurement Along Axes 87
5-7a SR I Heat Balance Closure; Residence Time Ranges 89
5-7b SR II Heat Balance Closure; Residence Time Ranges 89
5-8 Temperature Versus Equivalence Ratio Showing the Estimated Maximum Temperature Error 92
5-9 Variation of Reaction Efficiency with Equivalent Ratio 93

LIST OF ILLUSTRATIONS (Continued)

Figure Page (III-)

5-10 Weight Loss Versus Equivalence Ratio 95

5-11 Difference Between Weight Loss, NA, and Extent of Reaction, NG, with Equivalence Ratio 96

5-12 Variations of Nitrogen Loss (NN), ASTM Volatile Matter Loss (NVM), and Hydrogen Loss (NH_2) with Total Coal Weight Loss (NA) 98

5-13 Variation of Volatile Matter and Fuel Nitrogen With Gas Temperature 100

5-14 Fuel Nitrogen Conversion to NO with 0 102

5-15 Fuel Nitrogen Conversion to HCN with 0 103

5-16 Total Maximum Conversion Versus Equivalence Ratio . . . 104

5-17 Conversion Versus Equivalence Ratio, Effect of Varying Residence Time and Temperature 105

5-18 Fuel Nitrogen Conversion Versus Reaction Efficiency, Effect of Varying Residence Time and Temperature 108

5-19 Fuel Nitrogen Conversion Versus Residence Time for Varying Equivalence Ratio 110

5-20 Ln (Fuel Nitrogen Conversion) (NOC) Versus Residence Time for Various Equivalence Ratios 112

5-21 Rate of NOC Decay Versus 112

5-22 Fuel Nitrogen Conversion Versus Reaction Efficiency . . 113

5-23 Normalized NOC Versus 113

5-24 Fuel Nitrogen Conversion (NOC) Versus Gas Phase Reaction Efficiency (NG) and Temperature for Equivalence Ratios Less than 1 115

5-25 Fuel Nitrogen Conversion (NDC + HCNC) Versus Gas Phase Reaction Efficiency (NG) 116

5-26 CH_4/Air/Coal N_2/Combustion Volatile Matter Loss (NVM), and Total Weight Loss (NA) With Time at Low Temperature 118

5-27 Comparison of Unreacted Coal Size Distribution 118

LIST OF TABLES

Table		Page (III-)
1-1	Program Outline	4
2-1	Reactor Design Parameters	8
3-1	SR II Helium Tracer Results (ms)	22
3-2	SR I Helium Tracer Results	29
3-3	Dust Residence Time Modeling Results	43
3-4	SR Global Mixing Model	46
3-5	SR Dust Mixing Conditions	48
3-6	SR I Dust Residence Time Modeling Results	58
4-1	Exhaust Gas Analysis Equilaent	67
5-1	Utah Coal Properties (As Received)	72
5-2a	SR I Results	78
5-2b	SR II Results	79
5-3	Char Analysis Results (Dry)	81

SECTION 1

INTRODUCTION

Several studies have investigated the emissions of oxides of nitrogen (NO_x) formed during the combustion of pulverized coal. These studies have ranged in scope from fundamental experiments to combustor characterization studies. However, the relationships between nitric oxide (NO) formation and the physical mechanisms of coal decomposition and reaction are still in the developmental stages. This being the case, coal combustion equipment designers must still rely on trial and error approaches to minimize NO emissions. Although some progress has been made in reducing NO emissions using this approach, a predictive coal flame model of NO formation would be of great value. It is hoped that such a model would both speed the development of low-NO_x burners, based on current concepts, as well as to provide insight into new areas of combustion modification NO_x control technology.

1.1 OBJECTIVE

The goal of this experimental program is twofold, namely:

- To provide data on NO_x formation during pulverized coal combustion, which will aid in the development of predictive models
- To provide fundamental information on the mechanisms acting during coal combustion and pollutant formation

This information was to be obtained under conditions similar to those found in the near-burner regions of a high-intensity pulverized coal burner flame.

A stirred reactor (SR) operating on pulverized coal was the combustion system selected for use in this study. The use of an SR for gathering combustion information is not new (Reference 1). However, most experimental studies using such a combustor have been primarily confined to the examination of gaseous and liquid fuels behavior. Recently an SR system has been used to investigate the mechanisms of coal dust explosion flame propagation (Reference 2).

An SR can be conceptually thought of as a region in space without concentration or temperature gradients where entering materials are dispersed rapidly. Regions of a similar nature can be shown to exist in most high-intensity burner flames (Reference 3). In fact, the presence of such stirred regions are necessary in some systems to achieve good flame stability over a range of firing rates. Therefore, it is possible to artificially separate a large-scale burner flame into several stirred regions and a downstream plug region (in the limit, infinitesimally small SR's in series represent a plug region).

The advantages of using an SR can be found in its relative simplicity from the point of view of mixing coupled with an ability to model practical combustor behavior. Of course, other experimental methods have been used to study coal combustion; however, they are more limited than the SR in terms of meeting the objectives of this study.

Experiments conducted to elucidate fundamental coal combustion and pollutant formation mechanisms have included small-scale pyrolysis (References 4, 5, and 6), laminar flow reactor (Reference 7), flat flame

(References 8 and 9), plug reactor (References 10 and 11) and well-stirred reactor (WSR) (Reference 2) studies. The pyrolysis studies (References 4, 5, and 6) provided information on the distribution of products of coal volatilization under inert conditions. These have been useful in elucidating the steps in fuel and fuel-bound nitrogen evolution. However, the environment under which these experiments were performed is not characteristic of coal combustor conditions. The laminar flow reactor studies (Reference 7), useful in determining pyrolysis steps, also suffer from a similar problem. Whether an oxidizing or inert atmosphere is used in these systems, the reaction environment surrounding the coal particles is, at best, representative of a long, thin laminar diffusion flame. Flat flame environments, though definitely of a combustion character, are typically laminar (Reference 8) flow in nature where upstream diffusion of volatile products controls the rather slow rate of combustion. Premixed plug flow reactors (References 10 and 11) have been used to study the influence of coal properties on NO_x emissions under both staged and unstaged conditions. These experiments have been useful in understanding the long time scale processes of postvolatilization NO reduction by homogeneous or heterogeneous reactions in fuel-rich environments and char NO_x formation in lean environments. However, these experiments have not covered the important time scales of early NO_x formation in detail.

The only experimental apparatus meeting the requirements of realistic combustion conditions, simple mixing conditions, and the ability to resolve processes on a short time scale characteristic of the near burner region, is the WSR.

1.2 PROGRAM OVERVIEW

During this program, two SR's, SR I and SR II, were designed to cover the operating residence time ranges of 20 to 50 ms and 50 to 100 ms,* respectively. Noncombusting mixing studies were conducted in scaled models of the combustors to verify that a high level of gas phase mixing would exist in the SR's. Once gas phase mixing performance was verified, subsequent experiments were directed at quantifying coal particle mixing behavior in the model reactor. Following this, coal combustion tests were conducted.

An overview of the experimental program by task is presented in Table 1-1. In the following sections, results of the gas phase mixing and particle mixing experiments, as well as results obtained from the coal combustion experiments, are described.

Table 1-1. Program Outline

Task	Description
1	Design SR's (two) to cover the operating residence time range of 20 to 100 ms
2	Verify (optimize) gas mixing intensity using "cold" models of the operating SR's in conjunction with helium (He) tracer methods
3	Quantify coal particle mixing behavior in the SR's using the "cold" models
4	Coal combustion testing

---

*The original goal was to attain an upper limit of 200 ms; however, experimentally 100 ms was found to be the practical upper limit for SR II.

SECTION 2

COMBUSTOR DESIGN

2.1 BACKGROUND

An SR was chosen as the combustion system to be used in this testing program. Although many different types of SR's have been developed (References 1 and 12), use of any one of these would be difficult with a pulverized fuel. This is because previous reactors were designed for gaseous fuels where gas/fuel particle inertial decoupling, wall particle impact, wall erosion, and particle fragmentation did not have to be considered. Operating these reactors on pulverized coal fuel would result in unacceptable performance in terms of gas/particle mixing and wall impact effects. Therefore, it was necessary to design an SR system specifically for this program.

The reactor design was to exhibit a high degree of gas phase mixing while operating on coal/air mixtures over a residence time range of 20 to 200 ms. Originally, one combustor was to be designed to cover the entire operating residence time range. For a fixed reactor volume, the air turndown ratio would have to be approximately 10 to 1. Based on this flow turndown requirement and its resultant effect on reactor mixing (as defined, for example, by the decrease in jet Reynolds number), it was decided that two reactors were needed to cover the specified residence time range. Two reactors would more easily produce the desired level of mixing than one reactor operated over a very wide range of air input.

2.2 DESIGN CONSIDERATIONS

Since the SR would be mixed solely by its feed jets, the parameters considered to be most influential in controlling the mixing process were:

- Jet placement and combustion chamber shape
- Jet Reynolds number (Re_j)
- Ratio of jet diameter to chamber width (d/L)

The shape of the reactor, as well as the number and placement of the jets, were selected to eliminate stagnant regions in the reactor and provide good mixing between "old" and "new" fluid. The jet orientations (angles with respect to the axes of the combustor) were set to generate various scales of turbulence between interacting jets that would provide mixing on both large and small scales. The final orientations of the jets were determined by use of the gas phase mixing tracer results described in Section 3.

It should be mentioned that combustion chamber Reynolds number was not considered to be an important parameter for the SR designs. This is because turbulence generation comes primarily from the jet flows. Therefore, jet Reynold's number, Re_j, is the major parameter for SR mixing, and chamber Reynold's number is of secondary importance.

SR testing was to be conducted primarily with mixtures of coal and air. While there is information available covering the effects of jet solids loading on mixing characteristics (References 13 and 14), it is insufficiently quantitative to estimate jet behavior inside the reactor with any accuracy. Therefore, the jet operating parameters were selected based on observed behavior of CH_4/air combusting jets (References 15 and 16). It should be noted that the jets in the reactor will not operate like free jets but will be turned and slowed down by interactions with other jets and the reactor walls. Free jet behavior is used to simply identify major jet parameters for the mixing experiments discussed in Section 3.

A minimum Re_j of 6,000 was determined to be adequate in ensuring turbulent jet flow for the SR. This value was selected after examining the values of transitional Re_j for various gaseous fuels (Reference 16). If the coal/air jet behaved in a manner similar to a CH_4/air flame, this Re_j would limit the laminar flame region (if at all present) to less than about five jet diameters.

The selection of a jet diameter to chamber width ratio is based on the decay of dynamic pressure with distance of a methane/air turbulent jet flame (Reference 15). Assuming that the dynamic pressure decay is a measure of mixing energy, uniform SR mixing requires the normalized dynamic pressure to be lost over the entire reactor length. Therefore, it is appropriate that the jet should lose about one-half of its dynamic pressure upon traversing one-half the reactor chamber length. Based on the jet dynamic pressure decay documented in Reference 15, an SR reactor chamber length to jet diameter ratio of 40 was selected for use in this study.

The operating parameters for the two SR's are listed in Table 2-1. The lower limit airflow of the large reactor, SR II, has been determined by gas phase mixing He tracer experiments described in Section 3. These experiments showed that mixing efficiency was not good below 14 l/s. The lower limit airflow of the smaller reactor, SR I, was set so as to have a partial overlap between the two SR residence time ranges. As shown in

Table 2-1. Reactor Design Parameters

Specifications	SR I	SR II	Units
Volume	1.7	7.6	l
SR diameter	13.7	22.2	cm
Number of jets	12	12	--
Jet diameter	0.13	0.22	cm
SR diam/jet diam (L/d)	40	40	--
Airflow	6.6 - 14.2	14 - 28.3	l/s
Cold residence time	0.25 - 0.12	0.54 - 0.27	s
Jet Reynolds number	$1.4 \times 10^4 - 2.9 \times 10^4$	$1.7 \times 10^4 - 3.5 \times 10^4$	--
Jet velocity	200 - 420	158 - 316	--
SR "Reynolds number" (cold)	$2.6 \times 10^3 - 5.3 \times 10^3$	$5.5 \times 10^3 - 1.1 \times 10^4$	--

Table 2-1, the reactors are similar in terms of the number of feed jets, L/d, and Reynolds numbers. Each reactor has the same relative chamber shape and jet locations as shown in Figure 2-1.

In both SR's, the top four jets are located in a horizontal plane 90^o apart. They are yawed at an angle of 20^o with respect to the diagonal. The middle jets are also separated by 90^o. They enter the chamber rotated in the horizontal plane by 45^o from the top jets. The middle jets are yawed counter to the top jets. They have a yaw angle of -20^o in the horizontal plane and are inclined upward at an angle of 15^o. The bottom jets point straight up and are separated by 90^o intervals. They are aligned so that their respective axes intersect a

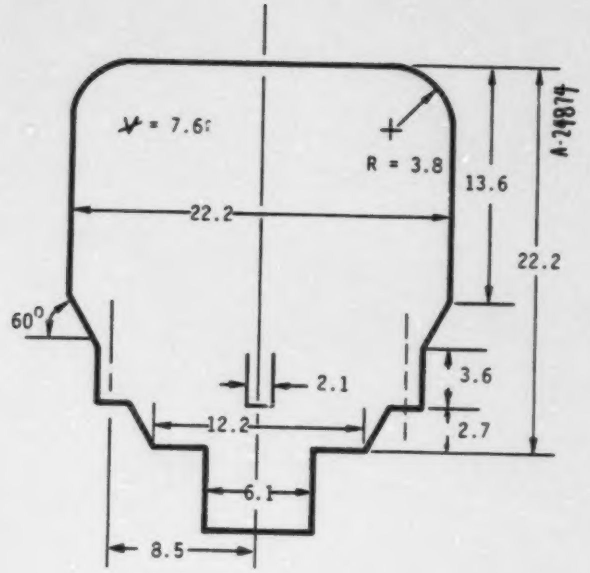
V = 7.6ℓ
R = 3.8
A-24874
22.2
13.6
22.2
60°
2.1
3.6
2.7
12.2
6.1
8.5

Figure 2-1a. SR II Construction Showing Chamber Dimensions (cm)

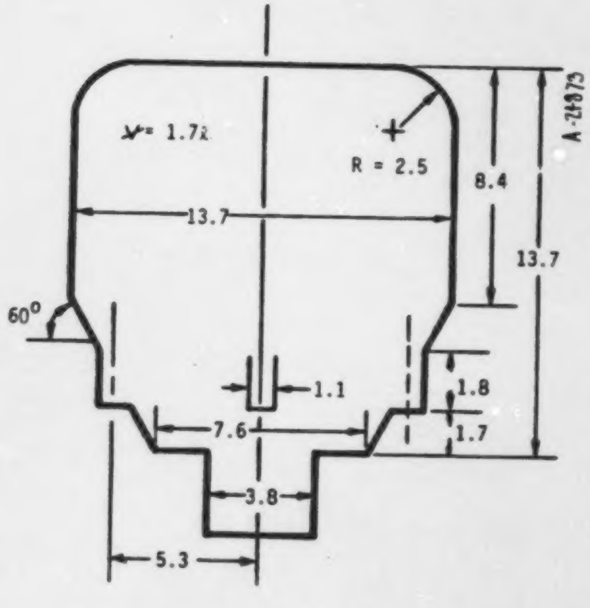
V = 1.7ℓ
R = 2.5
A-24875
13.7
8.4
13.7
60°
1.1
1.8
1.7
7.6
3.8
5.3

Figure 2-1b. SR I Construction Showing Chamber Dimensions (cm)

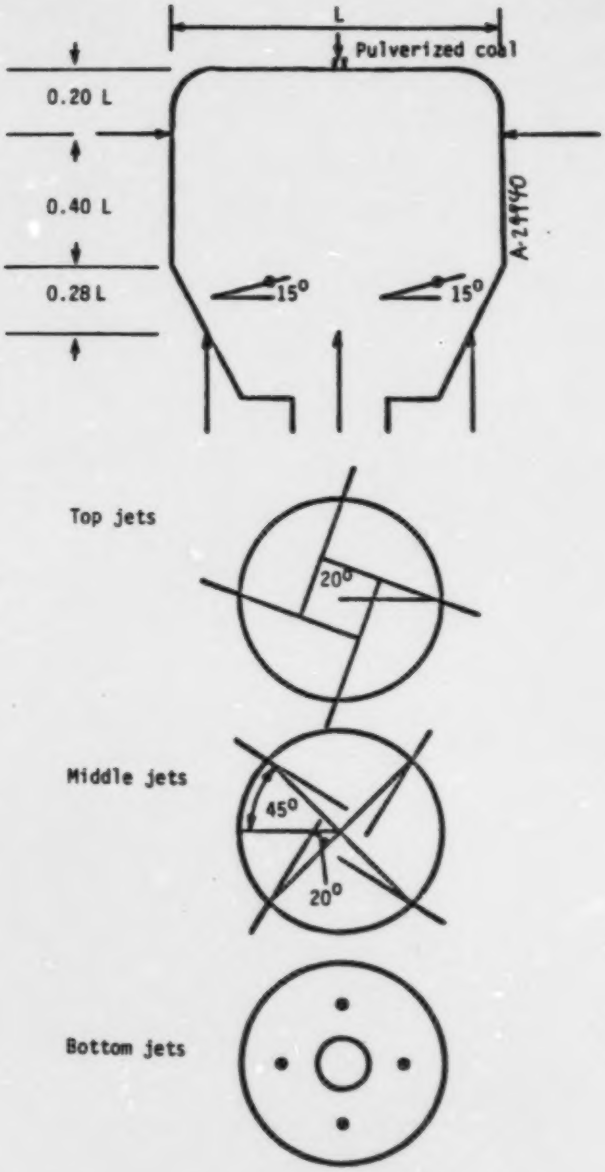
L
Pulverized coal
0.20 L
0.40 L
0.28 L
15°
15°
A-21940
Top jets
20°
Middle jets
45°
20°
Bottom jets

Figure 2-1c. SR Construction Showing Jet Orientations and Relative Locations

radial line to the entering points of the top jets. As mentioned previously, these orientations were established based on helium tracer experiments that showed the degree of stirring for each jet orientation.

Special reactor chamber injectors were designed for introducing the coal/air mixture into the SR's. Since the reactor jet gas velocities are high (Table 2-1), it was thought that wall impingement by the high velocity particles might produce particle fracture and significant chamber erosion. For good mixing efficiency, the gas velocity could not be lowered to reduce particle impact. Therefore, special injectors were designed to introduce the coal particles into the reactors at lower velocities than the gas. The injector design is shown in Figure 2-2. The particle and gas velocity values presented in Figure 2-3 are based on calculations assuming that Stokes drag on the particles applies in the cylindrical part of the injector. A standard correlation (Reference 17) between particle drag and Reynolds number was used to estimate particle behavior in the convergent section of the injector. Particle/particle interaction was not considered. As shown in Figure 2-3, calculations indicate that, for a 50-μm diameter coal particle, the coal outlet velocity is approximately one-third that of the gas. Chamber erosion should be reduced at these lower velocities.

In addition to minimizing erosion, lower particle velocities increase the chance of significant gas-particle coupling in the SR's. The high-velocity gas jet quickly slows down upon interacting with other jets or the chamber walls. Injecting the particles at lower velocities gives them more time to adjust to the gas velocity and, thereby, a greater potential for slowing down before hitting the reactor wall. If the velocity of the particles and gas were equal at all points in the reactor,

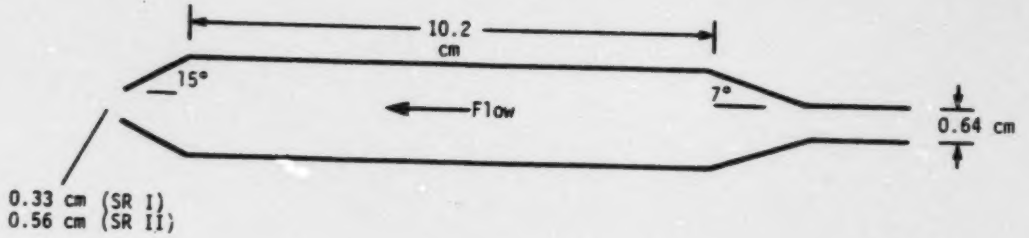
10.2 cm
15°
7°
Flow
0.64 cm
0.33 cm (SR I)
0.56 cm (SR II)

Figure 2-2. Injector Design

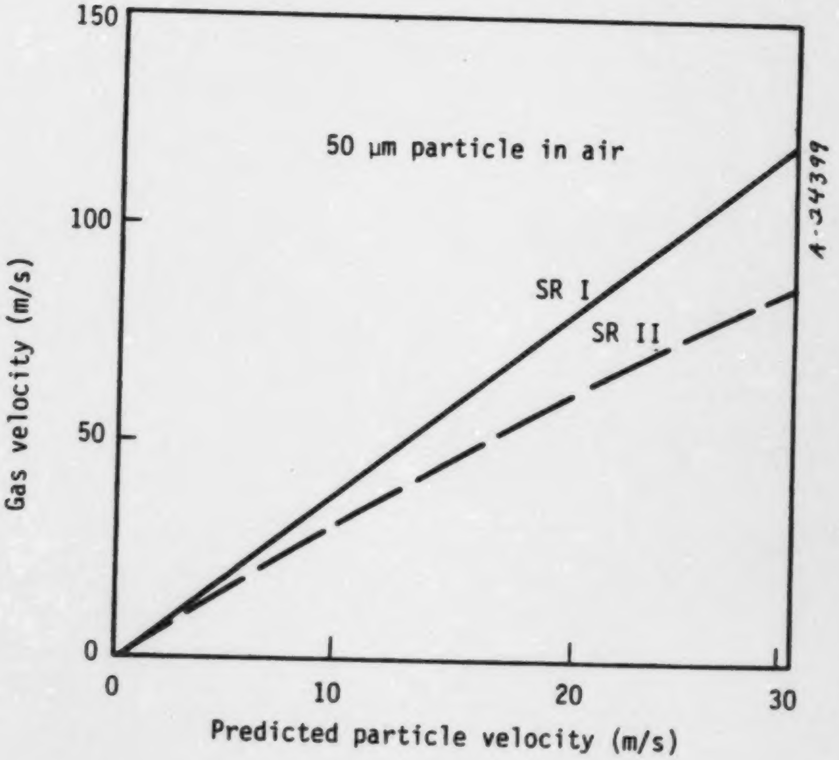

Figure 2-3. Predicted Injector Performance

as in the completely coupled case, the particles could be considered as just another "heavy" gas component. The particles would then be as well stirred as the gas.

Particles injected into the chamber at high velocities (consistent with high Re_j) will traverse the reactor in well defined paths in a short time with less dispersion than the gas, until collision with the SR wall occurs. Under these conditions it might be that the residence time of the particles will depend on free flight trajectories and wall collisions and to a large extent on the ratio of chamber surface area to exit area instead of gas flowrate and reactor temperature. Under these conditions, the mean residence time of the particles will not be influenced by gas mean residence time changes.

As shown in Figure 2-2, the main body of the injector is 10.2 cm long with a 15^o nozzle taper. Further increases in the difference between the particle and gas velocity can, theoretically, be obtained by lengthening the cylindrical section or increasing the convergence angle. However, flow experiments indicated further increases in either the angle or the length caused particle settling in the injector for the range of flow conditions used in these experiments.

2.3 COLD MODEL DESIGNS

Plexiglas models of the SR's described in Section 2.2 were constructed to allow cold gas and particle mixing measurements to be made. The use of a model was necessary so that injector orientations during mixing optimization tests could be adjusted with a minimum of effort. In addition, helium penetration into the walls and leak problems as would be experienced in a ceramic reactor were absent with the Plexiglas model. The model also allowed the use of smoke as a flow visualization aid. From a large group of scaling parameters, the following parameters were chosen as being most important to simulate cold to hot reactor mixing conditions:

- Jet Reynolds number (Re_j)
- Jet entrainment (M_x)
- Reactor residence time (τ)
- Geometric similarity (η)
- Power input/length^2 (β)

Jet Reynolds number and entrainment rate were considered important since mixing in the reactors was accomplished solely by the feed jets (injectors). Reynolds numbers need to be similar to generate the turbulence required for good mixing. Entrainment rates between the hot and cold systems must be adjusted for the effect of nonisothermal fluid entrainment in combusting systems. The well known Thring-Newby (Reference 18) adjustment to cold system jet diameter must be applied to match the entrainment rate.

Chamber residence time was thought to be an important scaling variable because of the dynamic nature of the mixing process. Geometry should be similar between the hot and cold reactors to achieve the same jet/jet and jet/wall interactions between the hot and cold systems.*

The last parameter, β, the micromixing parameter, was used as a measure of potential micromixing intensity. The parameter, β, is found by dividing the energy input per unit mass in the reactor by the reactor length scale squared. This parameter was used by Evangelista (Reference 19) to analytically predict the effects of imperfect micromixing in an SR.

---

*The shape of the chamber was similar between hot and cold systems. Only the jet radius to major chamber dimensions was a variable between the hot and cold systems.

In terms of the reactor mass input, m, length, L, and jet radius, r, the designated scaling parameters can be expressed in terms of ratio of cold to hot reactor values, denoted by subscript R, as:

- $(Re_j)_R = m_R/r_R$
- $(M_x)_R = 2.2\ m_R L_R/r_R$
- $(\tau)_R = 5\ L_R^3/m_R$
- $(\eta)_R = r_R/L_R$*
- $(\beta)_R = m_R^3/5\ r_R^4 L_R^5$

In the above relations, a temperature ratio of 1:5 between model and reactor has been assumed. Setting m_R, L_R, and r_R at 1.0, 0.6, and 1.2, respectively, the scaling parameters become:

- $(Re_j)_R = 0.8$
- $(M_x)_R = 1.0$
- $(\tau)_R = 1.1$
- $(\eta)_R = 2.0$
- $(\beta)_R = 1.2$

These results are considered to be a good compromise in modeling the hot reactor with a cold system. Based on these similarity parameter values, it was assumed the gas mixing in the cold model would simulate the mixing process occurring in the hot reactor.

The model-to-prototype scaling variables mentioned deal solely with gas phase mixing similarity. However, additional consideration must be given to the question of gas/coal particle interaction on mixing in the hot reactor. It has been reported that jet entrainment rate can be influenced by the presence of particulate (Reference 13). Gas/particle jet entrainment is affected by nozzle diameter and, to a lesser extent, particle concentration. More recent work conducted by Memmott (Reference 14) shows that the addition of particles has either none or a small enhancing effect on gas mixing rate. Hence, gas mixing rates obtained in the models can be assumed to be slightly lower than would be expected in the presence of particles.

As mentioned, the model SR's have the same shapes as their counterparts (shown in Figure 2-1) scaled down by a factor of 0.6, with the exception of the injectors. The model injectors for both the gas and particle mixing studies are identical to the reactor injectors with the exception of having an exit plane radius that was larger by a factor of 1.2. This adjustment was made to account for the entrainment rate of a hot versus cold system.

SECTION 3

PRELIMINARY EXPERIMENTS

The experimental program can be broken into two parts. The goal of the first part was to design a reactor that was well-stirred for both gas and particulate phases. After the completion of the first part, the reactor was to be used to obtain information on the fate of fuel nitrogen during coal combustion.

Successful completion of the first half of the program required two reactors of unequal size to be designed. The gas mixing characteristics were determined experimentally and jet orientations optimized by using SR models (of SR I and SR II) and a helium tracer/hot-wire anemometer technique. Particle mixing characteristics were evaluated by monitoring the attenuation of a laser beam by the coal dust particles in the reactor exhaust.

3.1 GAS MIXING EXPERIMENTS

The gas mixing study can be divided into mixing evaluation/optimization testing in the SR II and in the SR I model. A standard helium tracer cutoff method was used to evaluate mixing. However, only testing in the model of SR II was used to optimize jet configurations.

The experimental setup is shown schematically in Figure 3-1. A hot wire anemometer, having a diameter of 0.0025 cm and connected to the exhaust by a short venturi section, was used to monitor the helium

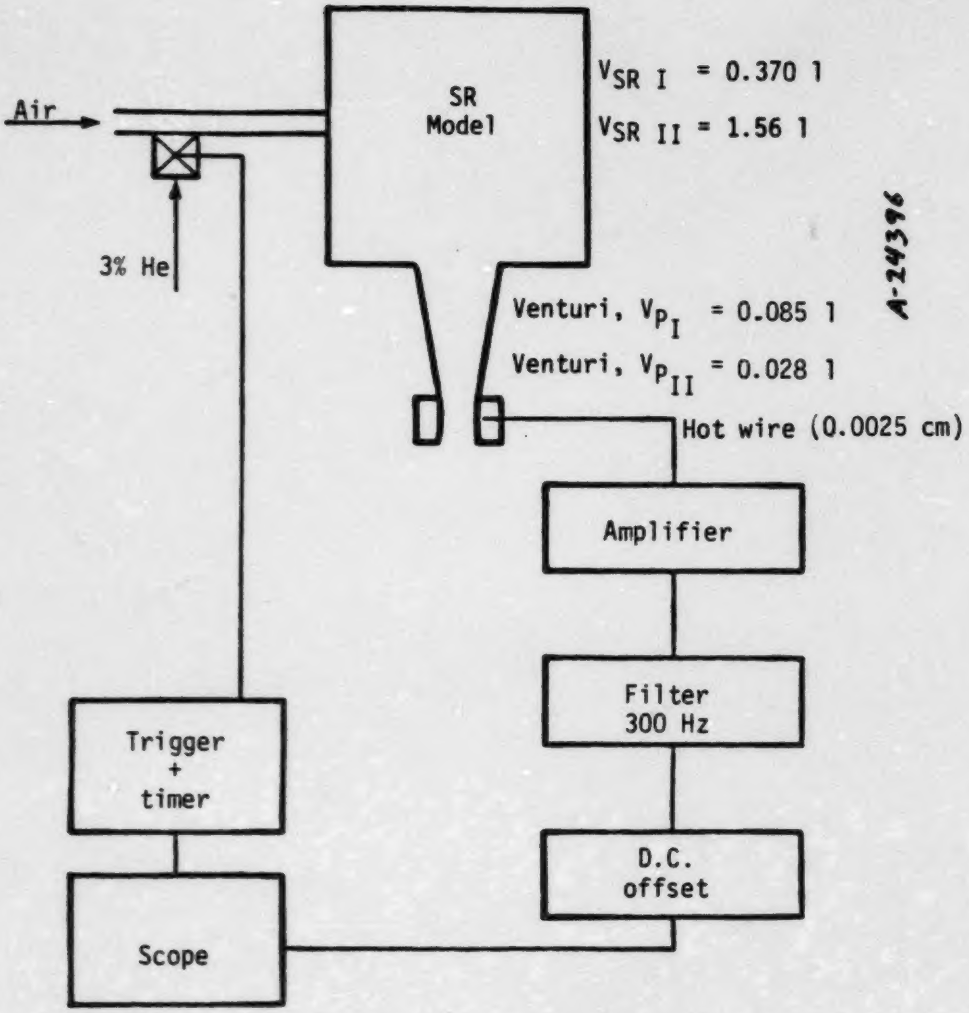
Air
3% He
SR
Model
$V_{SR\ I}$ = 0.370 l
$V_{SR\ II}$ = 1.56 l
Venturi, V_{P_I} = 0.085 l
Venturi, $V_{P_{II}}$ = 0.028 l
Hot wire (0.0025 cm)
Amplifier
Filter
300 Hz
D.C.
offset
Trigger
+
timer
Scope

A-24396

Figure 3-1. Setup for Helium Tracer Experiments

concentration in the exhaust gas. The output of the anemometer was fed into a sharp cutting filter giving a 3-dB attenuation of a 300-Hz signal. After passing through the filter, the signal was displayed on an oscilloscope.

During a test, the model input airflow was fixed at the desired level. The helium was injected into the chamber of the SR model as illustrated in Figure 3-2. The helium flowrate was equal to about 3 percent of the total airflow in the model. After a steady flow condition was reached, the helium flow was stopped using an electromagnetic valve with a response time of about 2 to 4 ms. At the same time, the oscilloscope trigger was actuated, recording the resultant helium decay signal on the scope. The display was photographed and the same cutoff experiment was repeated a number of times. The trace was then transferred to semilog graph paper and examined for mixing characteristics. A well-mixed condition would be evidenced by straight line helium decay whose plug and mean stirred flow times correspond with expected system values based on volumes and flowrates.

SR II Tests

The SR II model was constructed and tested first. The reactor model consisted of two independently rotatable stacked sections. Each of the jets in the top and middle level could be pivoted to 20^{0} in the horizontal plane and the entire injector assembly could be rotated about its major axes in 30^{0} increments.

Many injector orientations were tested before a suitable jet pattern for good mixing was found. The most common faults of the various jet orientations tried were unequal residence time traces for helium

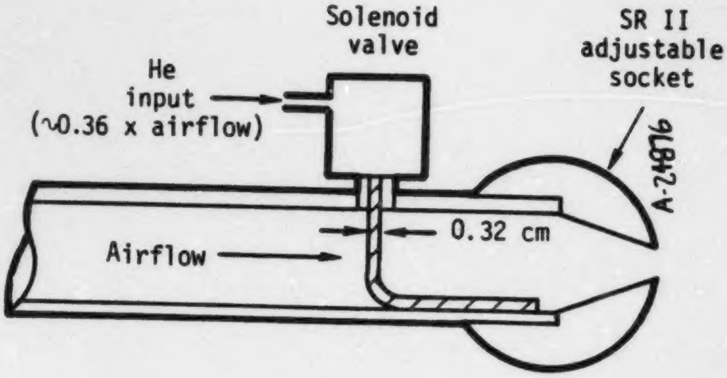

Figure 3-2. SR II Injector Tip with Ball Socket Showing Helium Injection Configuration

injection in different jets, large-scale recirculation tendencies, and short circuiting (Reference 20).

Unequal residence time traces for different jet injections of helium were evidence that mixing between jet fluids was not ideal. Jet orientation changes, altering bulk mixing, alleviated these problems.

Recirculation was evidenced by sinusoidal variations in helium concentration superimposed upon the helium decay curves. This indicated that, relative to the mean concentration, high helium concentration packets of fluid were circulating in the reactor without significant mixing with the bulk of the fluid. Jet orientation changes solved these types of problems in most cases.

Short circuiting was evidenced on the helium traces by an immediate drop in helium concentration upon cutoff of the tracer. This indicated that a portion of the flow quickly traversed the reactor and passed out the exhaust without significant mixing with the bulk of the fluid.

The short circuiting problem was most acute for the case of the bottom jets. In fact, the original SR design called for the bottom jets to be placed in the 3.0-cm flat surrounding the exhaust (Figure 2-1), and the bottom jet diameters to be approximately 1.5 times larger than the diameter of the other eight jets. After many jet orientation helium tracer experiments trying to correct this bottom jet short circuiting behavior, a smoke injection/visualization method was used to help define flow patterns and mixing in the reactor. These tests resulted in the relocation and reduction in size of the bottom jets. This helped the problem greatly but at low flowrates some degree of short circuiting was still evident. Smoke injection also helped to quickly narrow down the combination of potentially good jet orientations to be tested with the helium injection technique.

As an example of the jet configuration optimization procedure, the results of the three best jet configurations are presented in Table 3-1 and also illustrated in Figures 3-3 through 3-5. The locations and orientations of the jets are as shown in Figure 2-1c. The variable in these cases is the vertical angle of the middle jets with respect to the horizontal plane. The following three cases illustrate the effect of changing the middle angle from 70^{0} to 45^{0} to the final value of 15^{0} (Figure 2-1c).

An acceptable level of mixing in the model SR was indicated by the following criteria:

- The cutoff response of the model to helium injection through the three levels of injectors had to be similar

Table 3-1. SR II Helium Tracer Results (ms)

θ^o	Q (scfm)	Expected		Top Jet		Middle Jet		Bottom Jet		Average	
		τ_{po}	τ_{sr}	τ_p	τ_{sr}	τ_p	τ_{sr}	τ_p	τ_{sr}	τ_p	τ_{sr}
-15	17.4	6	190	-2	154	-4	163	0	151	-1 ± 2	156 ± 6
-15	20.0	6	165	-14	145	2	147	-7	149	-6 ± 8	147 ± 2
15	28.0	5	118	12	106	17	96	15	103	15 ± 3	102 ± 5
15	35.0	5	94	7	90	5	81	9	89	7 ± 2	87 ± 5
-45	17.4	6	190	0	187	-6	174	0	179	-2 ± 3	180 ± 7
45	35.0	5	94	11	97	2	127	9	112	7 ± 5	112 ± 15
70	17.4	6	190	11	159	5	200	7	181	8 ± 3	180 ± 20
70	35.0	5	94	13	100	8	82	7	110	9 ± 3	97 ± 14

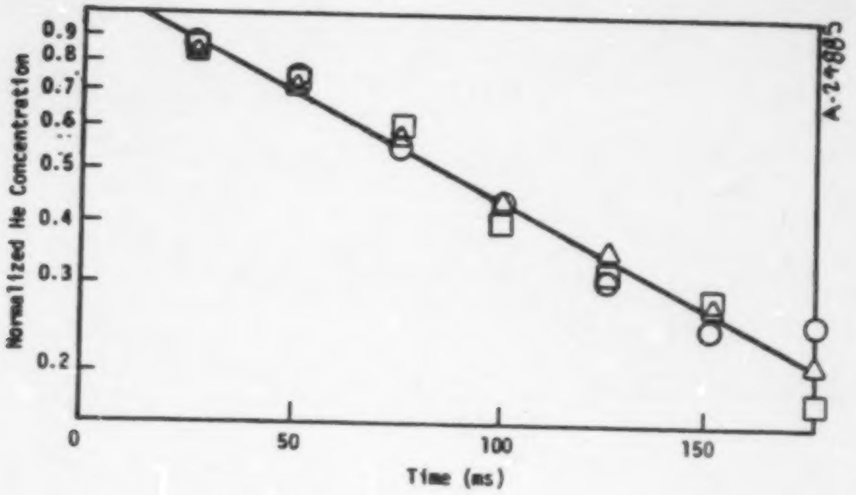

(a) Air Input of 8.2 l/s

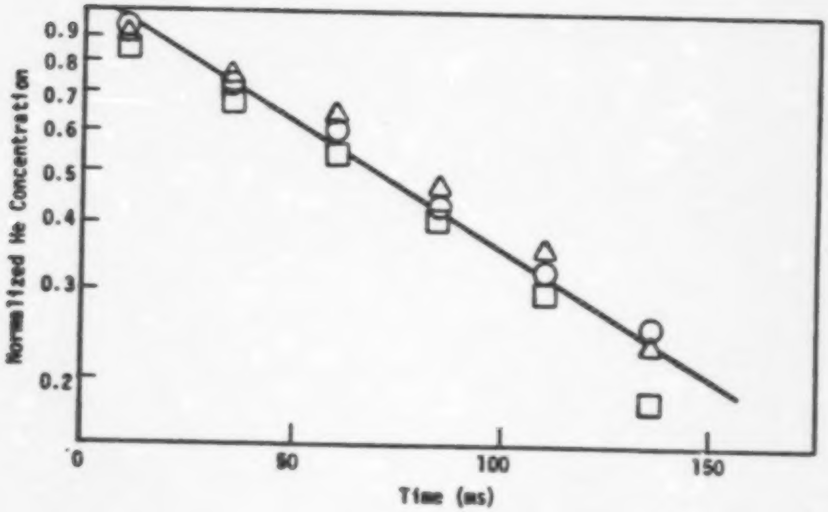

(b) Air Input of 9.4 l/s

Figure 3-3. SR II Helium Tracer Results at a Middle Jet Angle of 15°
(Top Jet ○; Middle Jet □; Bottom Jet △)

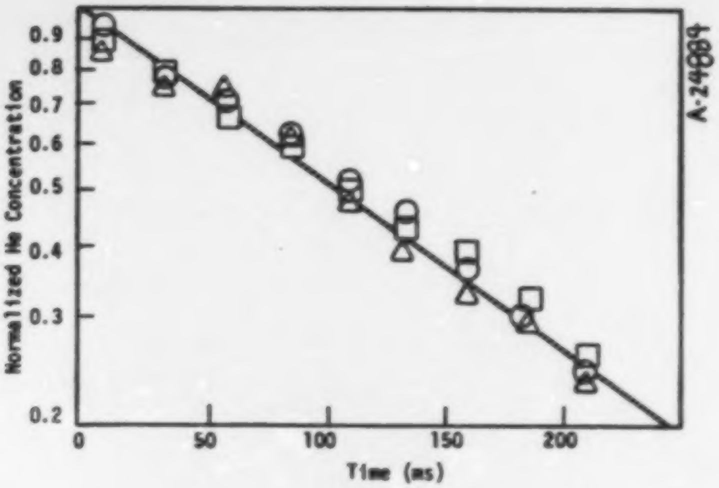

(c) Air Input of 13.2 l/s

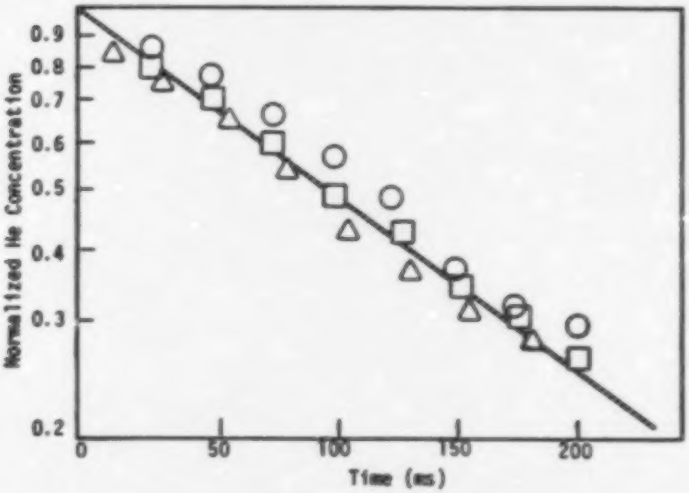

(d) Air Input of 16.5 l/s

Figure 3-3. Concluded

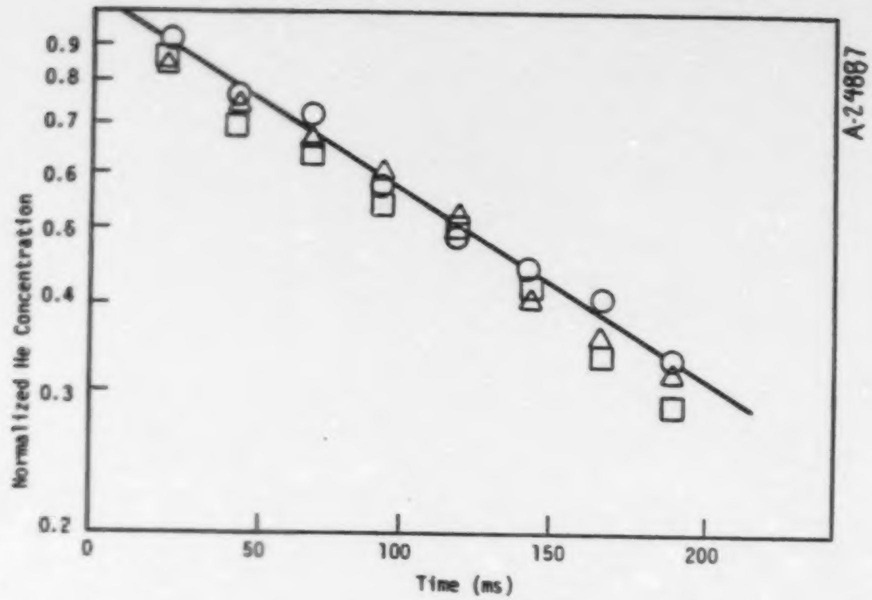

(a) Air Input of 8.2 l/s

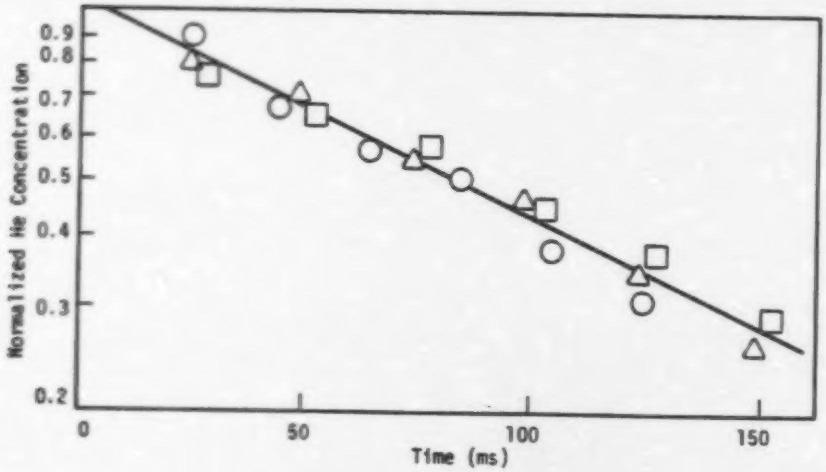

(b) Air Input of 16.5 l/s

Figure 3-4. SR II Helium Tracer Results at a Middle Jet Angle of 15° (Top Jet ○; Middle Jet □; Bottom Jet △)

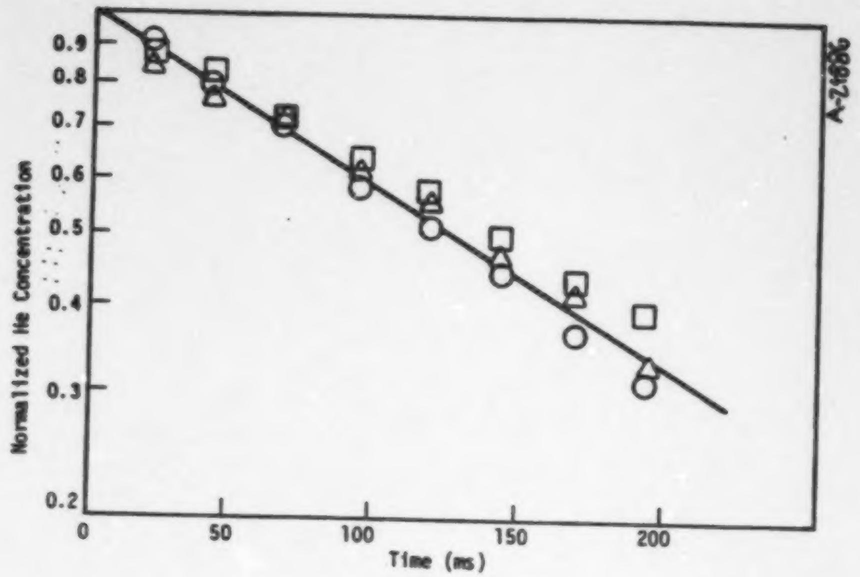

(a) Air Input of 8.2 l/s

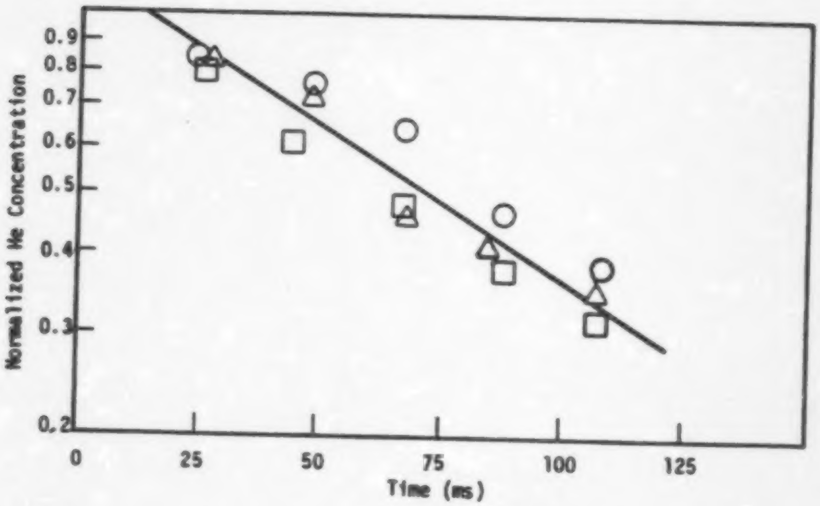

(b) Air Input of 16.5 l/s

Figure 3-5. SR II Helium Tracer Results at a Middle Jet Angle of 30°
(Top Jet ○; Middle Jet □; Bottom Jet △)

- The mean residence time of the SR determined by tracer response had to be similar to the calculated bulk residence time of the SR based on air input flowrate and reactor volume
- The plug flow time from the tracer response must be similar to the calculated plug flow times based on system plug volumes and flowrates
- The tracer decay curves must be exponential in character without significant deviations

The reduced data is presented in Table 3-1. In the table, the observed plug flow (τ_p) and stirred section (τ_{sr}) residence times for all three injector levels are compared to the calculated times. As shown in the table, the low flow conditions (8.2 and 9.44 l/s) for jet angles of 15^o and 45^o show negative plug flow times. This is indicative of short circuiting or fluid escaping the SR without mixing. The 70^o jet configuration was considered inferior to the 15^o configuration because of the large deviations in characteristic times between injectors in different elevations. The high flow condition observed at a jet angle of 45^o can likewise be excluded. The remaining two conditions 13.2 and 16.5 l/s at a 15^o jet angle are in best agreement with the expected times. Also, the deviation between injector levels for this case is acceptable. Thus, the 15^o jet configuration case was selected for combustion testing.

The data taken at the 15^o jet configuration is shown in Figure 3-3. Each data point in the figure represents the average of at least three separate cutoff experiments. The data is plotted as the normalized helium concentration versus time with the slope of the line giving τ_{sr}.

The time at which the normalized concentration becomes less than unity is τ_p. This simple relation, however, does not apply to the conditions observed for the 8.2 and 9.4 l/s flows. For these flows, short circuiting of fluid in the reactor is evident, and plug flow times are determined as negative from the helium traces.

At both 13.2 and 16.5 l/s, the results of each jet falls close to the average results. However, at the lower throughput, the traces seem less straight and the experimental times differ from the expected times by about 12 percent. At 16.5 l/s, the traces are straight (semilog) and the experimental and expected times agree fairly well. Since it is expected that Reynolds number effects will dominate mixing, then good mixing will persist as throughput is increased above 16.5 l/s. Based on these results, it was decided to increase the lower limit air input to SR II for good mixing to 14.2 l/s. This corresponds to an upper limit hot residence time of approximately 100 ms.

SR I Tests

The helium tracer tests of the SR I model were conducted in the same manner as the SR II tests with the following exceptions:

- The jets were fixed in the "optimum" (15^o) condition as dictated by the results of the SR II tests
- The 300-Hz filter was not used during the SR I testing
- A 15-ms delay was added between the scope trigger and valve trigger

The results of these tests are presented in Table 3-2 and shown graphically in Figure 3-6. As seen in Table 3-2, expected and observed τ_p and τ_{sr}^{-} agree very well with the exception of the results of the 6.6 l/s test. This can also be seen in Figure 3-7. At the lowest

Table 3-2. SR I Helium Tracer Results

Residence Times (seconds)										
Flow (scfm)	Expected τ_p	Expected τ_{sr}	Top Jet τ_p	Top Jet τ_{sr}	Middle Jet τ_p	Middle Jet τ_{sr}	Bottom Jet τ_p	Bottom Jet τ_{sr}	Average τ_p	Average τ_{sr}
14	28	55	20	48	24	48	23	65	22	54
19	24	41	24	41	25	40	23	45	24	42
24	23	33	23	37	23	37	27	39	24	38
29	21	27	24	30	21	30	22	34	22	31

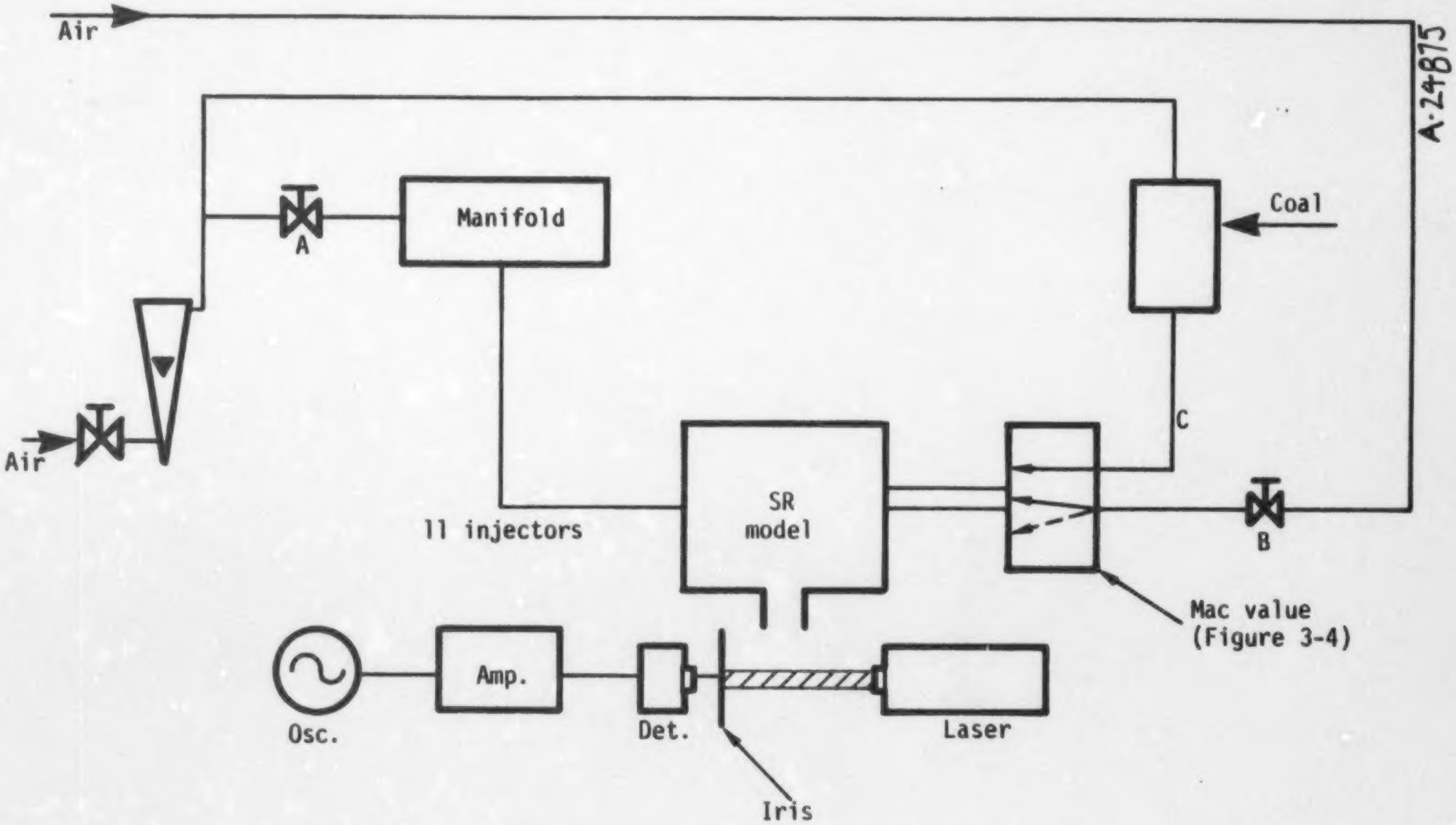
A·24875
Air
Air
A
Manifold
Coal
C
11 injectors
SR
model
B
Mac value
(Figure 3-4)
Osc.
Amp.
Det.
Laser
Iris

Figure 3-6. Particle Mixing Experimental Setup

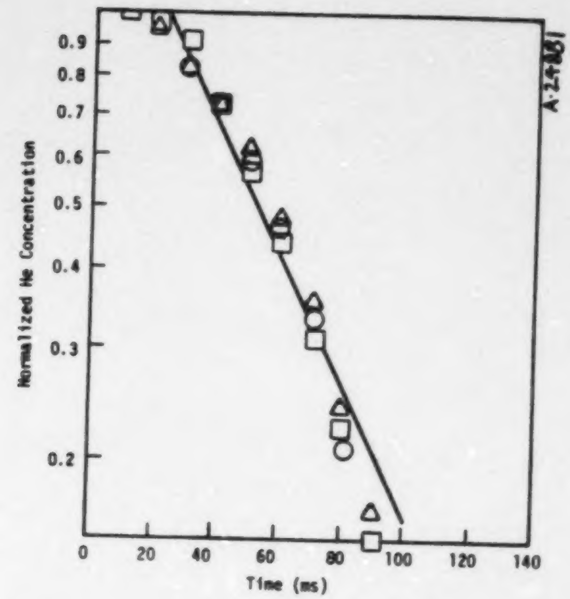

(a) Air Input of 6.6 l/s

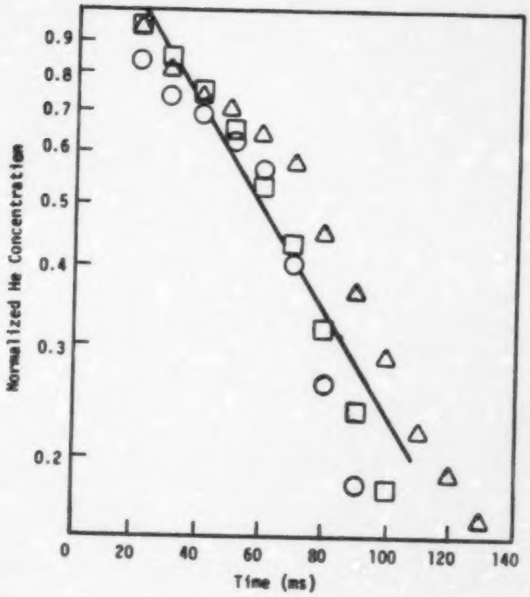

(b) Air Input of 9.0 l/s

Figure 3-7. SR II Helium Tracer Results Showing Top Jet○, Middle Jet□, and Bottom Jet△ Response

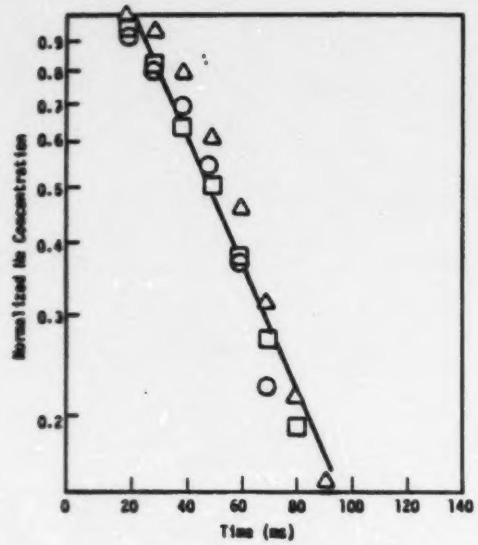

(c) Air Input of 11.3 l/s

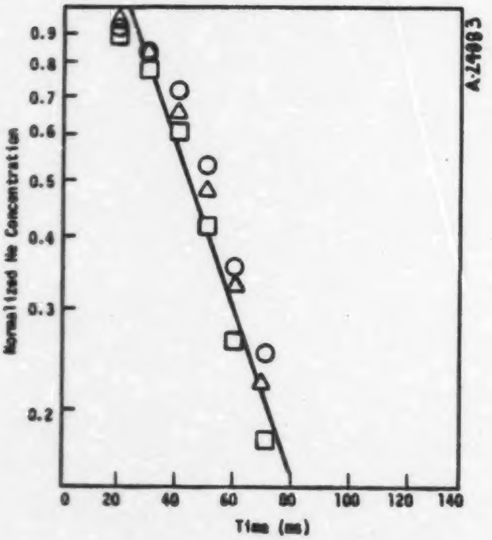

(d) Air Input of 13.1 l/s

Figure 3-7. Concluded

flowrate, the data exhibit the most nonuniformity. However, at the higher flows, the data become more uniform. There is some evidence of relatively long time scale recirculation at all, but the highest, flowrate. This is evidenced by the slight sinusoidal type helium concentration variation about the linear (logarithmically) helium decay line. However, the degree of recirculation was considered to be at an acceptable level for the test program. Hence, the SR I model was considered to be suitably mixed at flows of 8.9 l/s and above.

3.2 PARTICLE MIXING EXPERIMENT

For these experiments, coal was used as a "tracer" to characterize particle mixing in the SR models. The experimental setup for these tests is shown in Figure 3-6. Particle mixing behavior was examined by both cutting off and turning on the coal flow and observing the change of coal concentration with time in the model reactor exhaust. Coal was injected into the SR model through one injector. The coal concentration in this injector was very high compared to the 10 percent coal mass in the reactor. In addition, the coal was either totally on or off with this system. This approach was, in part, dictated by system limitations. Initial experiments indicated relatively small pulsations in the coal feed rate due to auger rotation. A valve having a response time of about 10 ms was used to turn the coal flow on or off by exchanging a flow of air for a balanced flow of coal and air. The particle concentration history was monitored using light attenuation. As was the case in the gas mixing experiments, the switching valve and oscilloscope were connected to a common trigger. The amplifier output was photographed from the oscilloscope display for later data reduction.

During these experiments, the plastic model and injectors were used with coal as the particulate material. It is realized that the use of the plastic reactor and coal particulate does not constitute ideal cold-to-hot modeling conditions. The major modeling uncertainty concerns itself with particle aerodynamics. Grossly speaking, the factors most likely to influence particle behavior are gas viscosity, particle density, and particle size. Little consideration was given to factors such as cloud motion, jet deceleration, and the effects of combustion on velocity fields because of uncertainties in predicting their effects. Changes in viscosity (at high temperatures) could be offset by using lighter or smaller particulate. However, the benefits of doing this would most likely be adversely compensated for by a mismatch in the particle size distribution. Therefore, the standard coal fuel supply was used in these dust mixing experiments.

Prior to conducting a test, the airflow passing through the rotameter was adjusted to the desired level (Figure 3-6). Valve A in Figure 3-6 was then adjusted to produce the correct flowrate splits between the 11 injectors using air and the test injector using a coal/air mixture. Valve B was used to set the auxiliary airflow to the test injector equal to the flow through line C (controlled by valve A). The flowrate balances were confirmed at the exit of the valve using a hot-wire anemometer.

A diagram of the valve is given in Figure 3-8. This valve was used to interchange a flow of air for a flow of coal dust and air. The switching time of the valve was measured by monitoring the movement of the spool. From these experiments, it was found that the solenoid energization time varied between 8 and 9 ms. The travel time of the spool

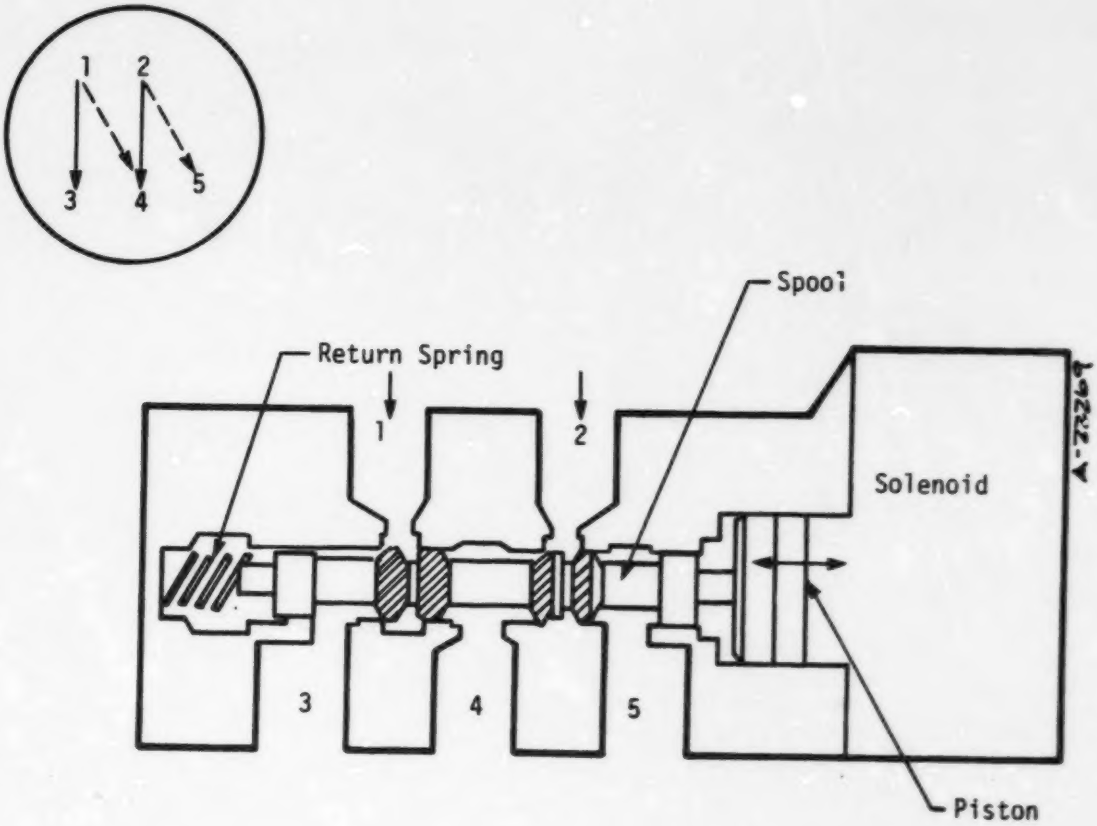
1
2
3
4
5
Spool
Return Spring
1
2
Solenoid
A-72269
3
4
5
Piston

Figure 3-8. Quick Acting Valve for Coal/Air Switching

(from start to stop) ranged from about 2 to 4 ms. These times were found to be unaffected by changes in input airflow or changes in coal concentration (up to 0.6 g/l solids).

Prior to performing dust mixing experiments, the ability to monitor dust concentration using light attenuation was checked. Ideally, the attenuation should be governed by the relation:

$$I/I_0 = e^{-\pi/d^2 \; N_pL/4}$$

where I/I_0 is the normalized intensity; d the mean diameter of the particles; N_p the particle number; and L, the path length. To check the experimental technique, light attenuation tests were run for constant coal flowrate through the reactor. The experimental results are shown in Figure 3-9. The result is the expected logarithmic relation. However, the slope of the line is greater than was expected based on the above relationship. The calculated results could be lower due to assumptions of uniform particle size and extinction based simply on the projected areas of the particles fully absorbing the light. The important aspect of correlating light attenuation with dust concentration is evident from the data and this relationship is the only important consideration for reducing data.

Several tests were performed at all three injector elevations. A complete set of data for a given jet location and flow condition consisted of injector dust input and SR dust output concentration histories.

The method by which SR dust mixing was evaluated is illustrated in Figure 3-10. The injection and SR output particle concentration history is determined experimentally. With the system "stimulus/response" known,

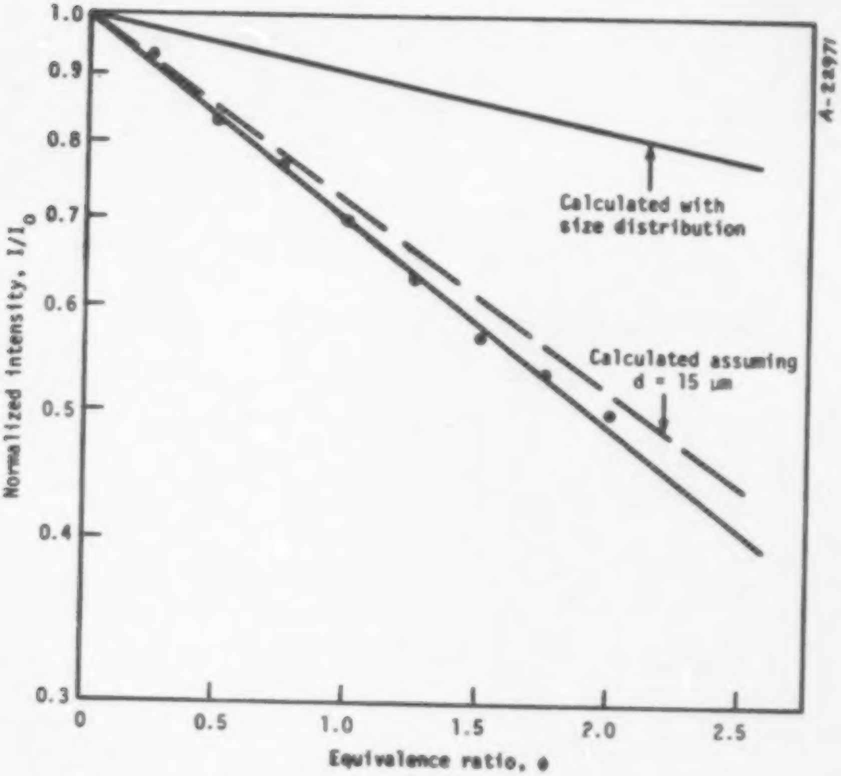

Figure 3-9. Normalized Light Intensity Versus Equivalence Ratio

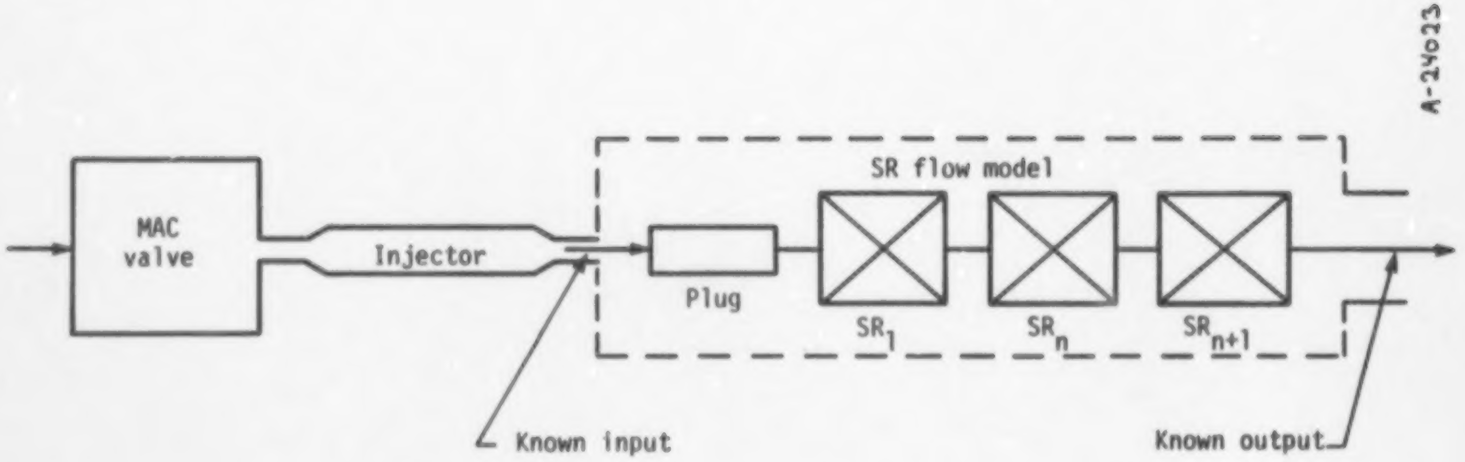
A-24023
MAC valve
Injector
SR flow model
Plug
SR_1
SR_n
SR_{n+1}
Known input
Known output

Figure 3-10. Data Reduction Method Schematic

a mixing model was then used to approximate the type of system observed. Equal volume SR's in series were used to approximate the system behavior. A model was assumed to apply when the experimentally determined input into the mixing model correctly predicted the observed system response.

To fit various data, it was possible to vary the number of reactors in series, the total apparent chamber volume and the mixing delay (plug flow) time. As was the case in the helium tracer experiments, the SR II model was tested first. In the SR II tests the effect of changing coal concentration, air input, and injector location was examined. In the case of the SR I model tests, only the latter two parameters were varied. As a result, the data from SR II tests is more numerous than from SR I tests. The results of all the testing follows. However, while SR I results are presented graphically in their entirety, only representative SR II test results are illustrated. A complete listing of the data taken during the particle mixing tests is presented in Appendix A.

SR II Dust Mixing

A typical set of SR II model injector output signals is shown in Figure 3-11. The corresponding SR output signals are shown in Figure 3-12. Figure 3-11(a) shows the injector response to the coal flow being turned off. Figure 3-11(b) shows the injector response to coal being turned on. From the figures it can be seen that the concentration decay takes much longer than the concentration rise. This is not due to the switching mechanism or measurement technique.

A possible reason for the long-time concentration decay upon coal cutoff might be the reentrainment of coal dust deposited in the injector prior to coal cutoff. A similar type of effect might also be present in

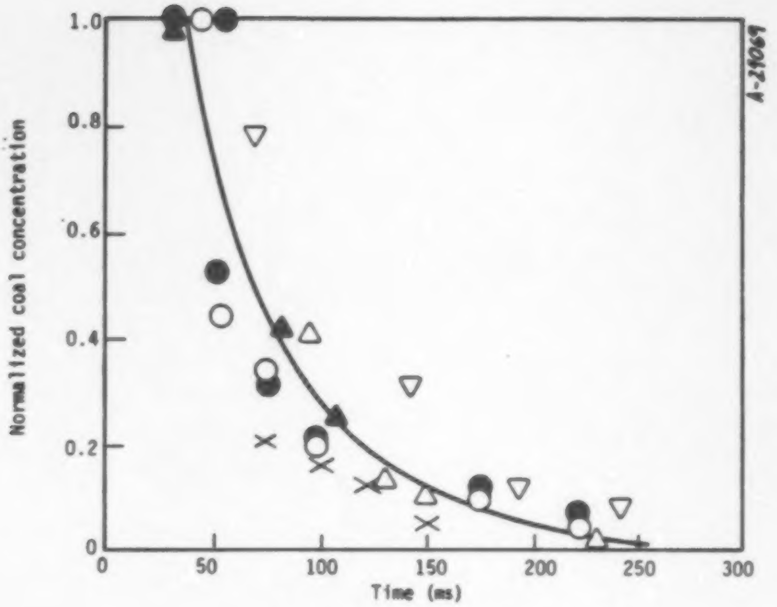

(a) Coal Flow Stopped

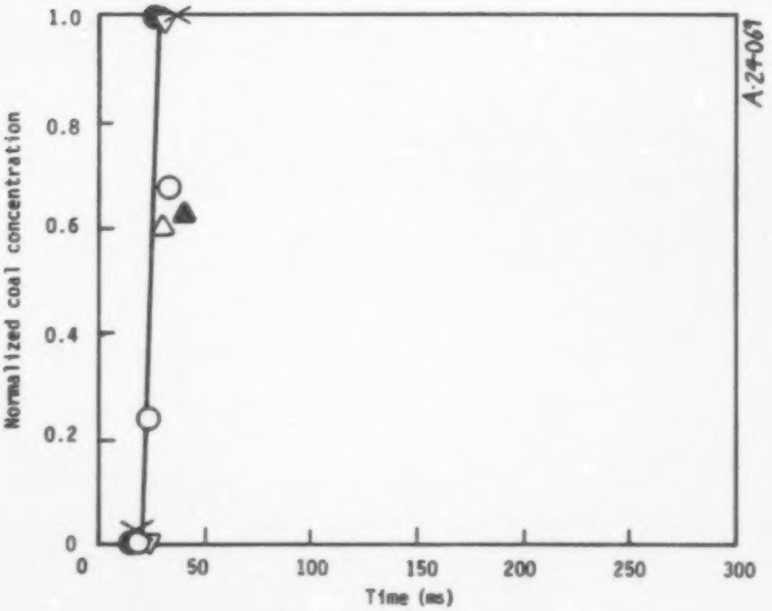

(b) Coal Flow Started

Figure 3-11. Injector Output Signal at an SR II Airflow of 14.2 l/s, Showing Data Range and Effect of Particle Concentration 0.12 g/l, ●, ✕, ○; 0.29 g/l, △, ▲, ▽

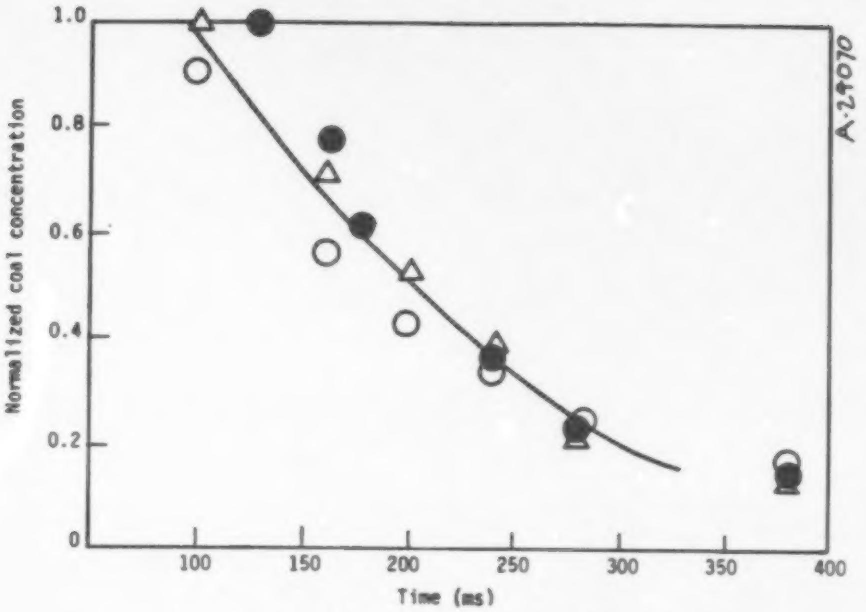

(a) Coal Turned Off

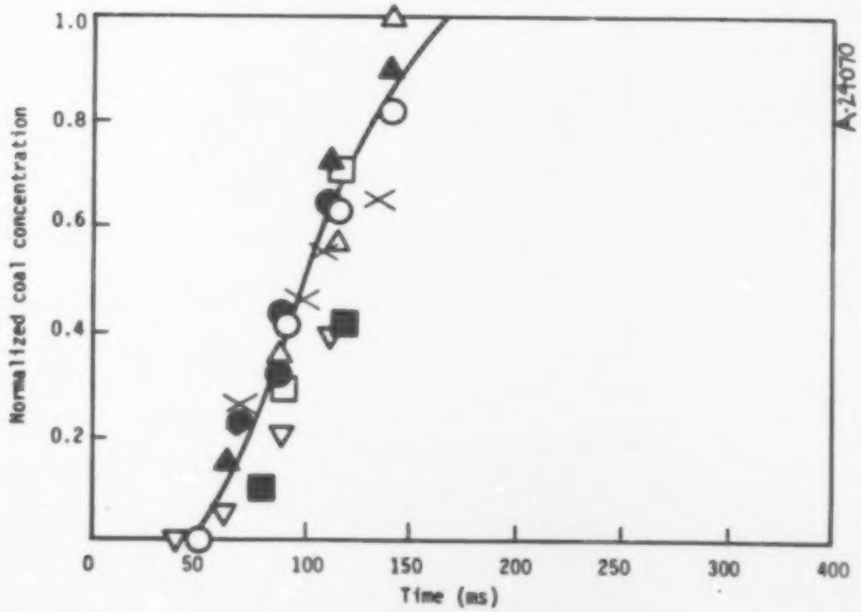

(b) Coal Turned On

Figure 3-12. SR II Response at 30 scfm

the reactor for the case of coal cutoff. Dust concentrations at the reactor exhaust are given in Figure 3-12.

The solid lines in Figure 3-12 are the smoothed measured injector concentration time histories used in fitting a mixing model to the data shown in Figure 3-12. The solid lines in Figure 3-12 indicate the chosen mixing model response to the injector signal. All results were analyzed in this manner.

Table 3-3 presents the results of the mixing studies. Tests were performed at 14.1 and 23.5 l/s. At certain jet locations, several dust loadings (equivalence ratios) were studied ranging from 0.12 to 0.24 g/l. These values represent total concentrations and therefore injector coal concentrations were substantially higher. At a given injector location and flow condition, dust loading did not noticeably affect mixing behavior.

The results presented in Table 3-3 show that there are large dust concentration history differences between stopping the coal flow and starting the coal flow. Possible reasons for these differences are the accumulation of dust in the reactor system and reentrainment upon dust cutoff and the reactor mass loading changes as the coal flow is turned on or off. When coal flow is turned on, reactor mass loading is increased by roughly 10 percent due to the solids loading, and the particles initially enter a gas-only environment. When coal flow is turned off, the reactor mass loading decreases by 10 percent with the particle concentration initially being high. The roughly 10 percent change in mass loadings and the effect of particle concentration decoy or buildup on mixing could cause the differences noted in Table 3-3.

Table 3-3. Dust Residence Time Modeling Results

Jet Location	Top	Middle	Bottom	Top	Middle	Bottom
Coal flow stopped						
Airflow (scfm)	30	30	30	50	50	50
Number of reactors in series	1	1	1	1	1	2
Total apparent volume (ft^3)*	0.055	0.055	0.055	0.055	0.055	0.055
Mixing delay time (ms)	40	15	50	55	40	40
Coal flow started						
Airflow (scfm)	30	30	30	50	50	50
Number of reactors in series	5	3	3	1	3	3
Total apparent volume (ft^3)*	0.040	0.055	0.055	0.095	0.055	0.062
Mixing delay time (ms)	0	20	20	0	15	20

*Includes stirred volume only

It might be speculated that the initial behavior of the coal cutoff case might be more representative of mixing conditions than the coal turn-on case. For coal cutoff, coal concentrations in the reactor are high and the material is initially dispersed at a uniform concentration. Particle/particle interactions and particle effects on gas phase mixing are uniform across the reactor. For coal turn-on, coal concentration is initially very high near the single coal injector and particle/particle and particle/gas mixing effects are localized in this region. Because of the significant initial nonuniformities in the coal turn-on case, these results are not as good as the more uniform turn-off case. An additional potential problem with the coal cutoff case is the reentrainment of deposited injector and reactor particulates as the coal concentration diminishes.

In the trials where dust flow was cut off, the mixing behavior was similar. The system behaved like a single SR having an apparent volume equal to the system volume of 1.56 l. Results obtained from the bottom jet at a flow of 23.6 l/s were slightly different. All of these tests exhibited a characteristic mixing delay time ranging from 15 to 55 ms.

In the trials where dust flow was started, the number of reactors in series varied from one to five, the apparent volume varied from 1.13 to 1.76 l. The mixing delay time varied from 0 to 20 ms.

For a given flow condition, the mixing models for the three injector elevations were combined and averaged numerically so that the SR behavior with all jets operating could be predicted. These results are presented in Figure 3-13. The points in the figure represent numerical averaging of the mixing behaviors listed in Table 3-3. The curves represent a fit of the data, giving global SR mixing performance.

The SR global mixing models are presented in Table 3-4. The results obtained in the coal cutoff tests show that the system behaves like an SR having the correct chamber volume. At 14.2 l/s, there is a 35-ms mixing delay time while at 23.6 l/s, the delay time increases to 45 ms. The results obtained by turning the coal flow on are much different. At 14.2 l/s the system acts like three SR's with a delay time of 5 ms. At 23.6 l/s, the system acts like an SR with a delay time of 30 ms.

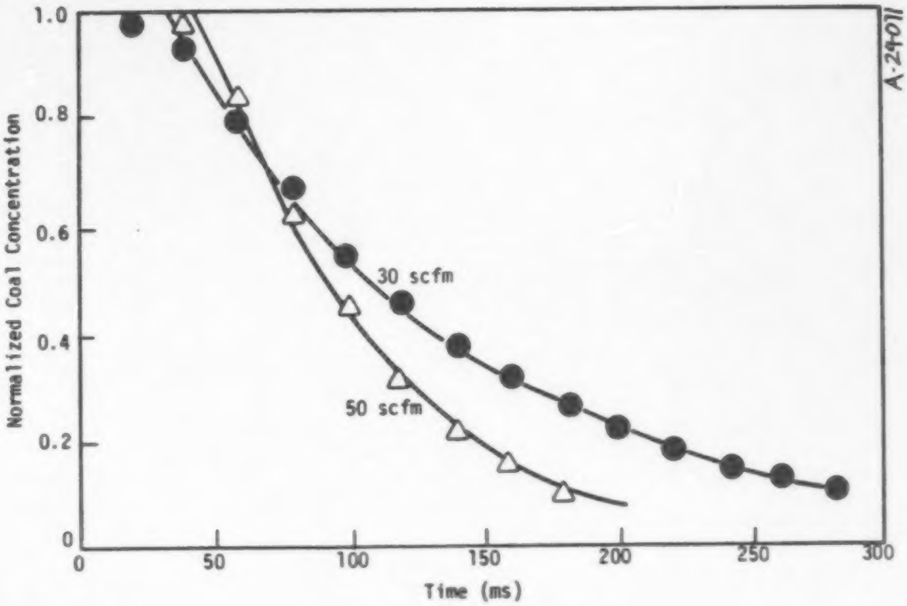

(a) Coal Turned Off

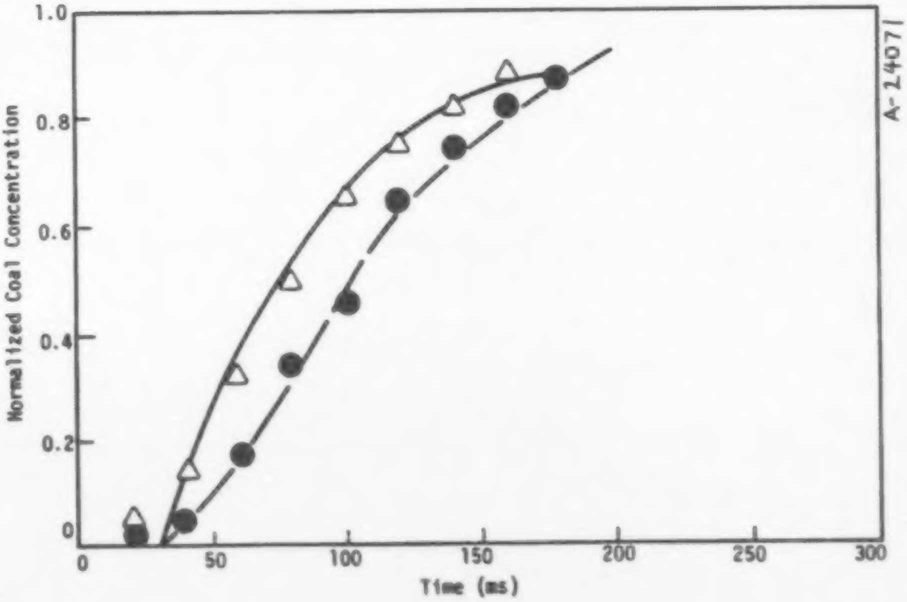

(b) Coal Turned On

Figure 3-13. Predicted SR II Response Comparing Test Data with Model Selection

Table 3-4. SR Global Mixing Model

	Coal Flow Stopped		Coal Flow Started	
Airflow (scfm)	30	50	30	50
Number of reactors in series	1	1	3	1
Total apparent volume (ft^3)	0.055	0.055	0.055	0.055
Mixing delay time (ms)	35	45	5	30

Although the two test methods give different results, there are similarities. A major point of similarity appears to be the existence of an apparent plug flow region inside the SR II model. This time ranges to about 50 ms and may be a significant contribution to the total particle residence time in the chamber.

Figure 3-14 presents the calculated particle residence time behavior in the SR II model based on the model given in Table 3-4. Aside from the fact that this particle time does not match the gas residence time, it also shows that the variation in particle residence time with airflow is much less than that of the gas. The case where the particle flow is stopped gives a wider range of residence time for the airflows measured but is up to a factor of two higher than the gas results.

The test method for dust mixing measurements was found to have significant limitations. Though quantitatively limited, they do show that there may be a significant difference between particle and gas mean residence times. A listing of particle mixing conditions examined during the SR II-tests are presented in Table 3-5. A complete data set is presented in Appendix A.

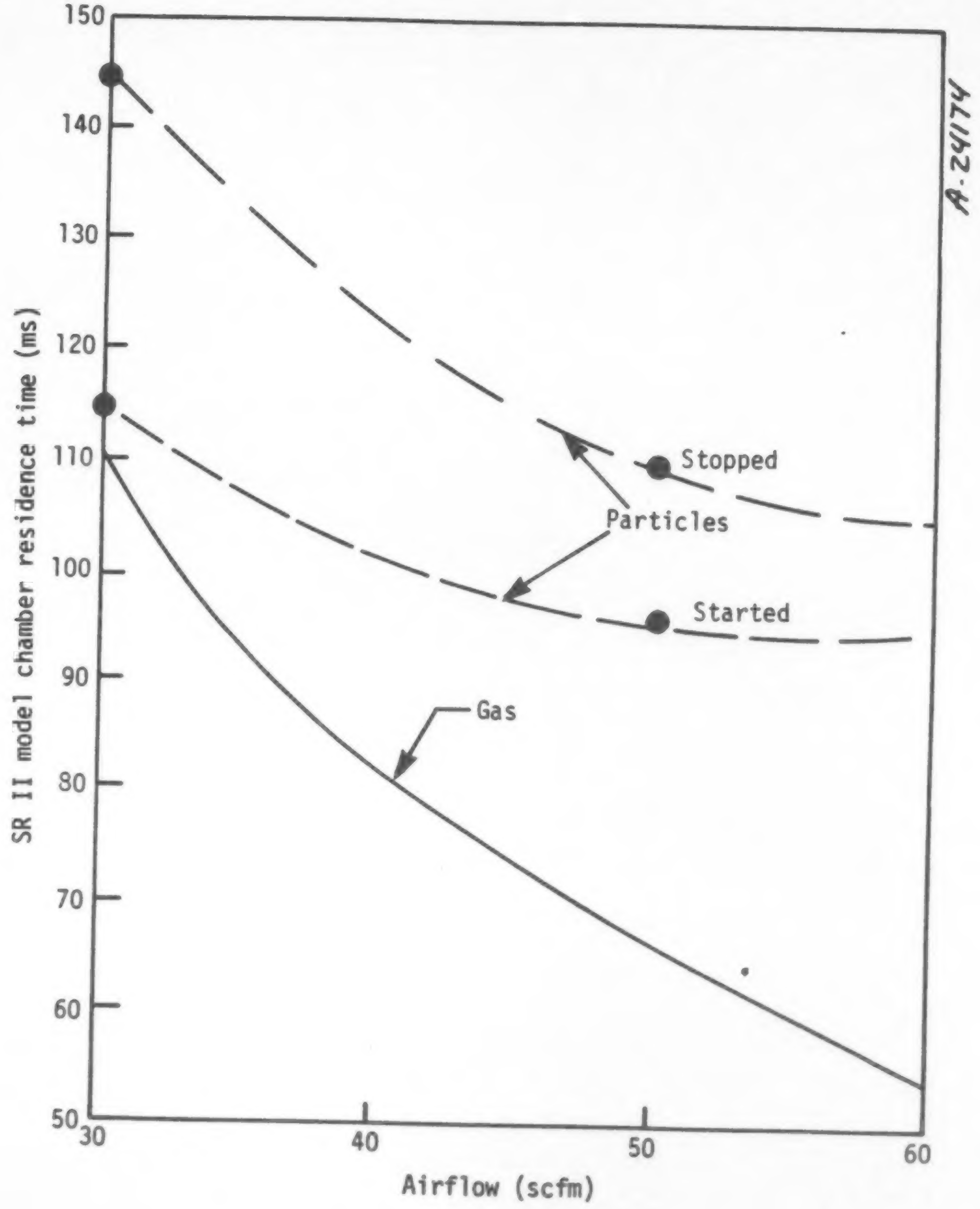

Figure 3-14. Residence Times Versus SR II Model Throughput

Table 3-5. SR Dust Mixing Conditions

Model	Jet Location	Airflow (l/s)	Overall Coal Conc. (mg/l)
SR II	Top jet	14.2	0.12
		14.2	0.18
		14.2	0.29
		23.6	0.12
SR II	Middle jet	14.2	0.12
		23.6	0.20
SR II	Bottom jet	14.2	0.12
		23.6	0.05
		23.6	0.12
		23.6	0.17
SR I	Top jet	9.4	0.10
		14.2	0.09
SR I	Middle jet	9.4	0.10
		14.2	0.09
SR I	Bottom jet	9.4	0.10
		14.2	0.09

SR I Dust Mixing

Particle mixing experiments in the SR I model were conducted in the same manner as the SR II model tesing. Since SR II test results showed little, if any, discernable effect of changing coal concentration, this parameter was fixed at a value of 0.09 to 0.10 g/l. The mixing conditions examined in the SR I tests are listed in Table 3-5. A complete listing of data is presented in Appendix A.

The SR I Model response to dust injection is presented in Figures 3-15 through 3-18. These figures illustrate the degree of variability of

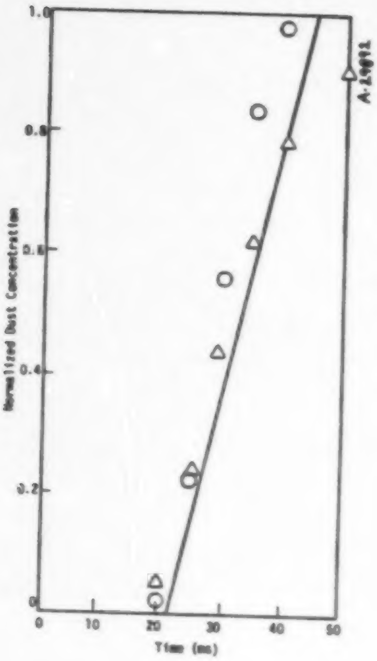

(a) Injector Output

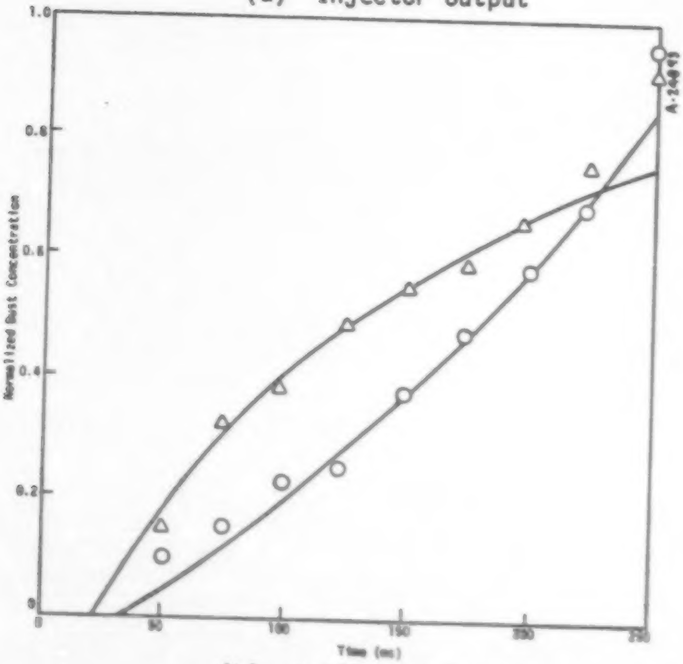

(b) Middle Jet Output

Figure 3-15. SR I Response to Dust Injection at an Air Throughput of 9.4 l/s

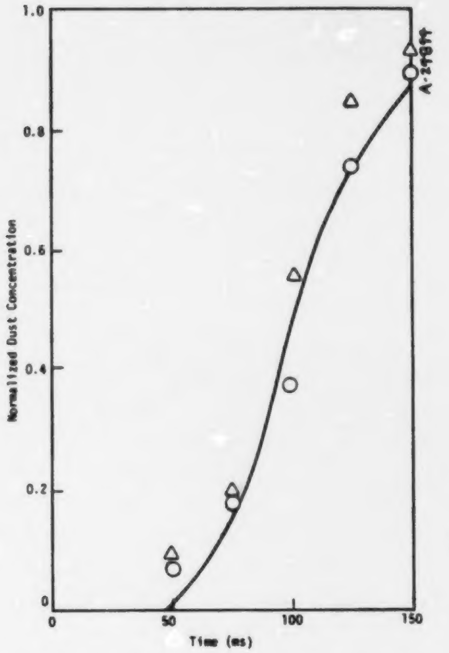

(c) Top Jet Output

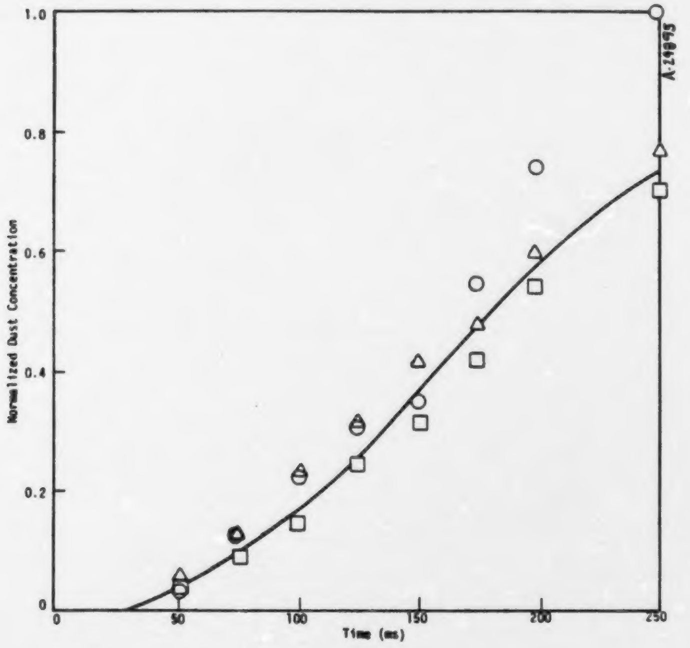

(d) Bottom Jet Output

Figure 3-15. Concluded

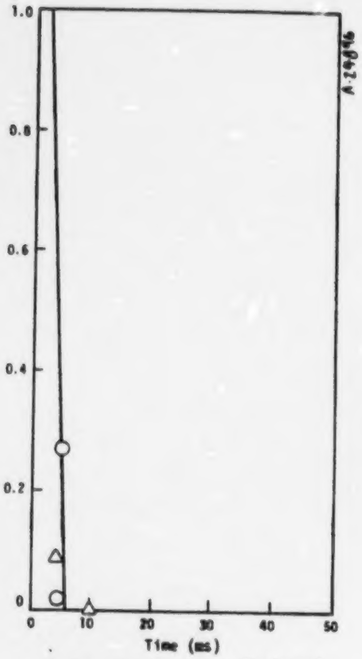

(a) Injector Output

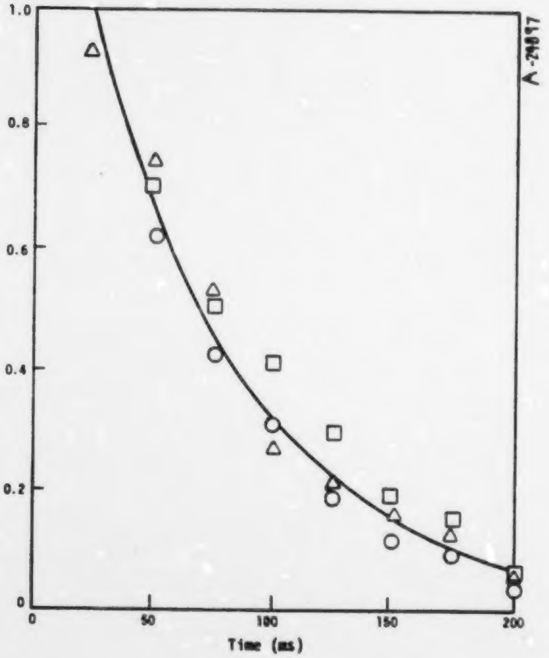

(b) Top Jet Output

Figure 3-16. SR I Response to Dust Injection Stopped at an Air Throughput of 9.4 l/s

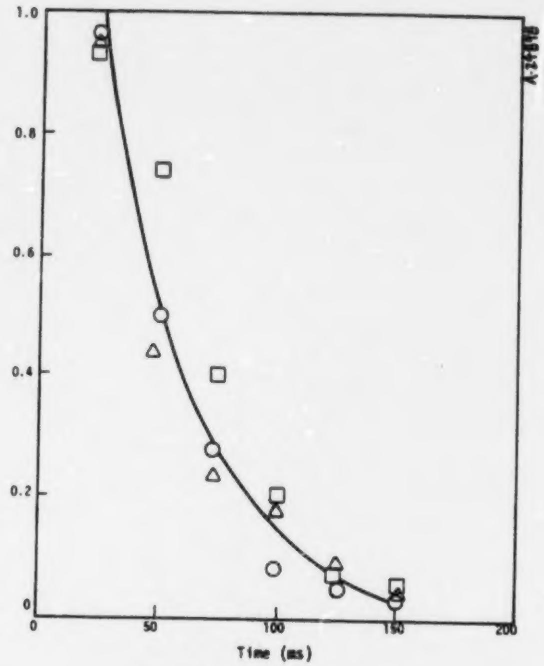

(c) Middle Jet Output

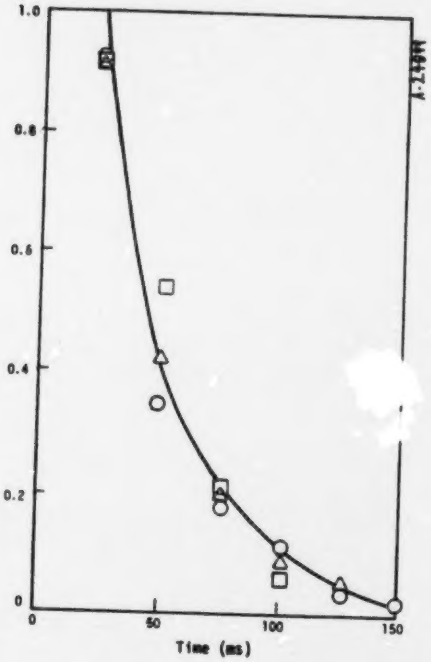

(d) Bottom Jet Output

Figure 3-16. Concluded

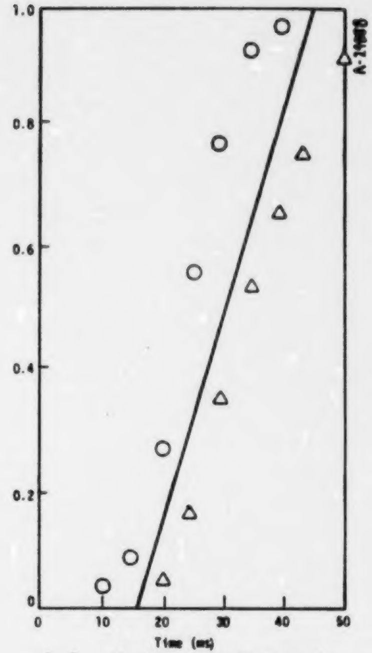

(a) Injector Output

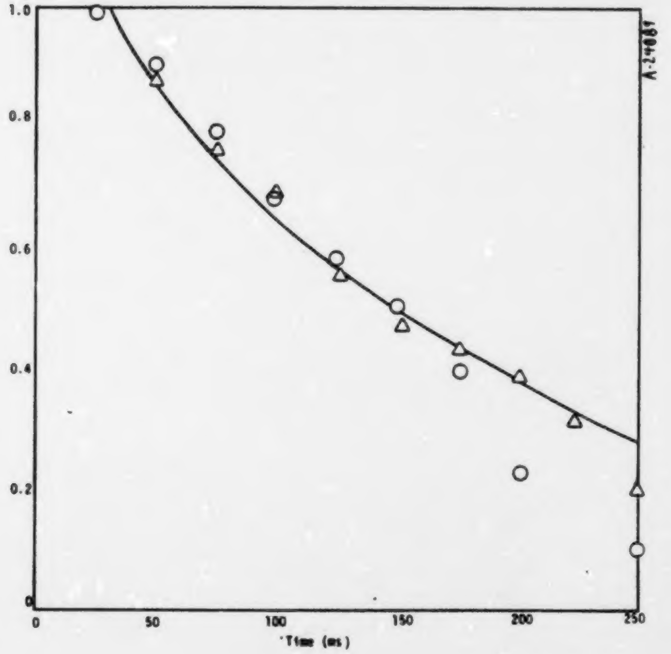

(b) Top Jet Output

Figure 3-17. SR I Response to Coal Injection at an Air Throughput of 14.3 l/s

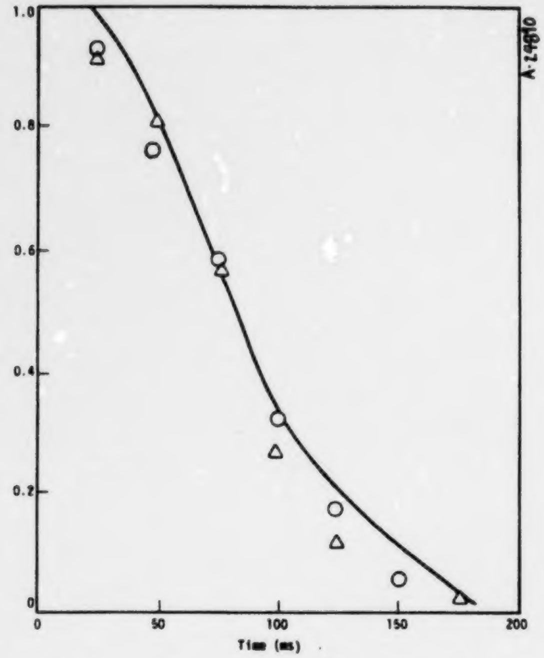

(c) Middle Jet Output

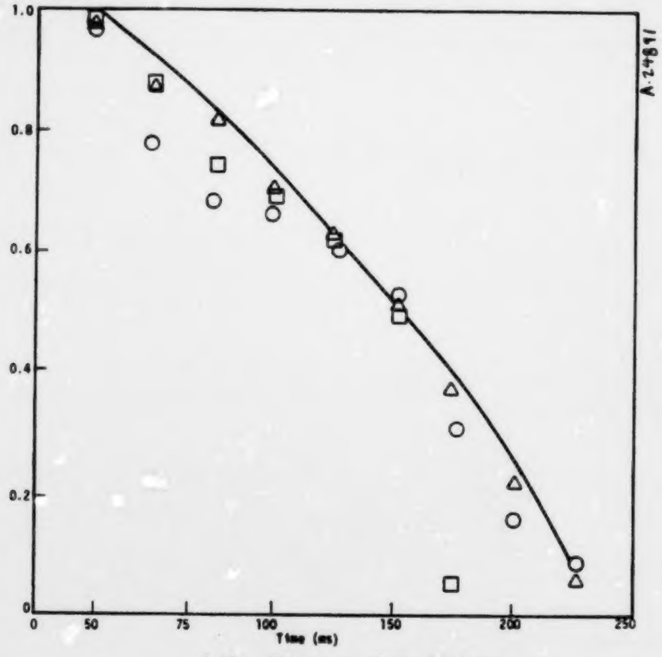

(d) Bottom Jet Output

Figure 3-17. Concluded

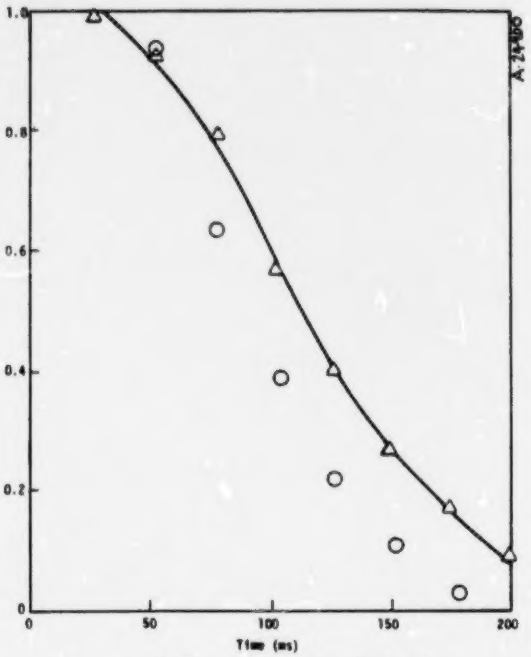

(a) Injector Output

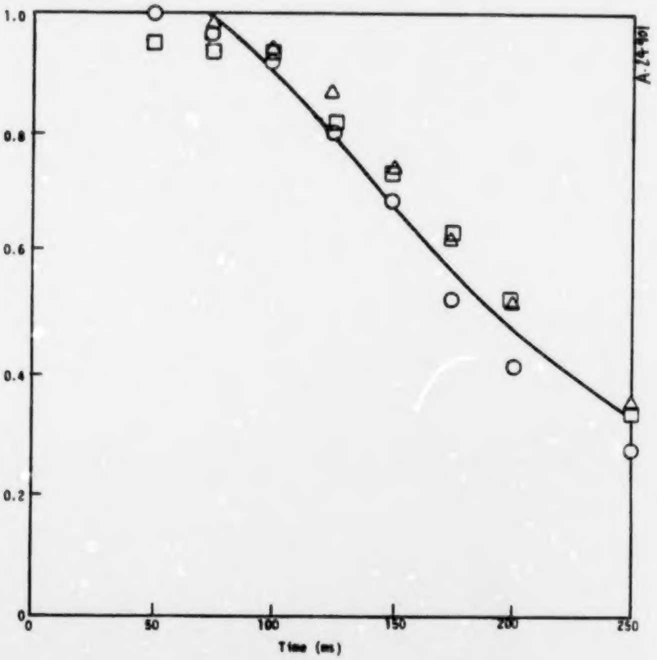

(b) Top Jet Output

Figure 3-18. SR I Response to Coal Injection Being Stopped at an Air Throughput of 14.3 l/s

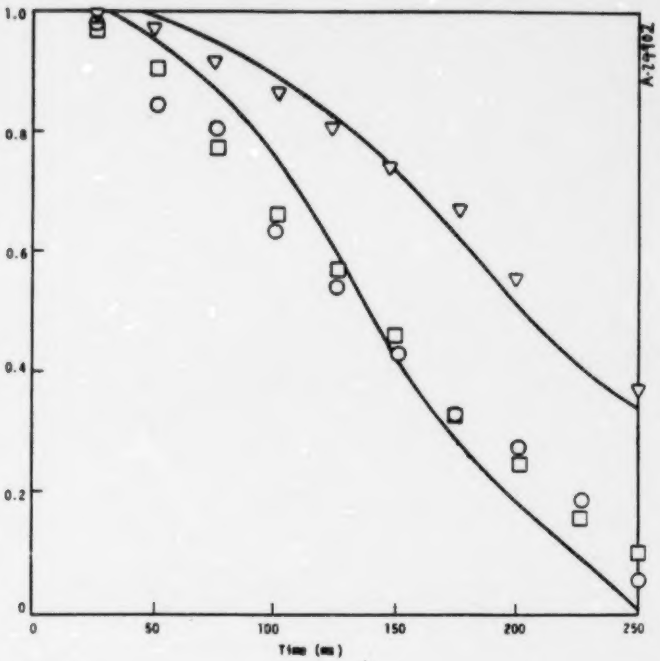

(c) Middle Jet Output

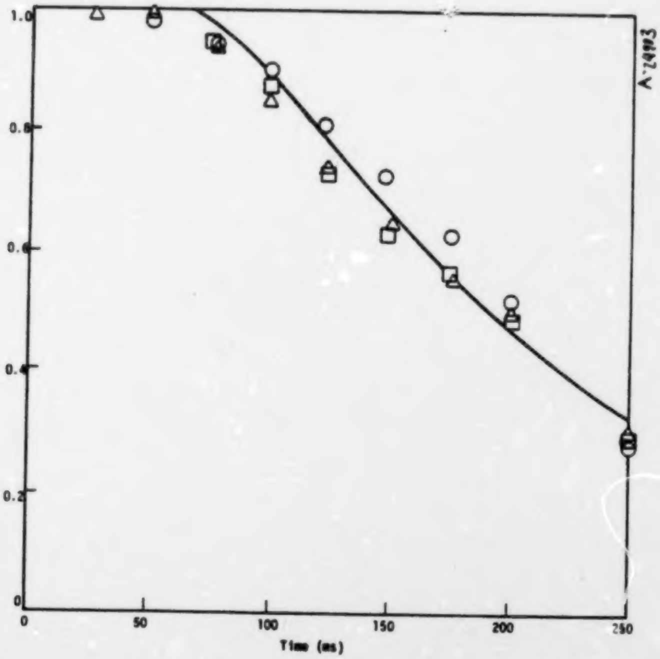

(d) Bottom Jet Output

Figure 3-18. Concluded

the injector signal as well as the SR I model response. Each type of data symbol represents a different trial.

As in SR II tests, mixing models have been fitted to the SR I model input/output data. The results are shown in Table 3-6 and Figure 3-19. In the case of two tests, two sets of model parameters have been listed; this is because of a wide spread in SR I output data. No attempt has been made to subsequently check the validity of either of the models showing dual characteristics.

Although the SR I model had a volume of about 0.37 to 1, the results in Table 3-6 indicate the apparent model has a much larger volume. This gives particle residense times larger than expected (as in the SR II experiments).

Although the absolute magnitudes of the SR I and SR II particle residence times can be disputed, the results of the SR I and SR II tests strongly support the case for particle residence times being greater than that of the gas.

If the particles do have different residence time than the gas, it is safe to assume the particles are decoupled from the gas during a fraction of their time in the reactor and a significant fraction of particles suffer wall collisions. If this is the case, an important scaling parameter would be SR width. This was not matched between SR I and SR II in these experiments.

Table 3-6. SR I Dust Residence Time Modeling Results

Jet Location	Top	Middle	Bottom	Top	Middle	Bottom
Coal flow stopped						
Airflow (l/s)	9.4	9.4	9.4	14.2	14.2	14.2
Number of reactors in serires	1	1	1	1	1 (1)	1
Total apparent[a] volume (l)	2.60	1.84	1.56	1.61	1.61 (0.04)[a]	1.61
Mixing delay time (ms)	0.025	0.022	0.055	0	0 (6)	0
Coal flow started						
Airflow	9.4	9.4	9.4	14.2	14.2	14.2
Number of reactors in series	7	1 (7)[b]	2	1	2	1
Total apparent[a] volume (l)	0.76	1.47 (1.64)[b]	1.64	2.55	0.99	2.26
Mixing delay time (ms)	0	0 (0)	0	0	0	0

[a] Includes stirred volume only

[b] Alternate model behavior to data variability

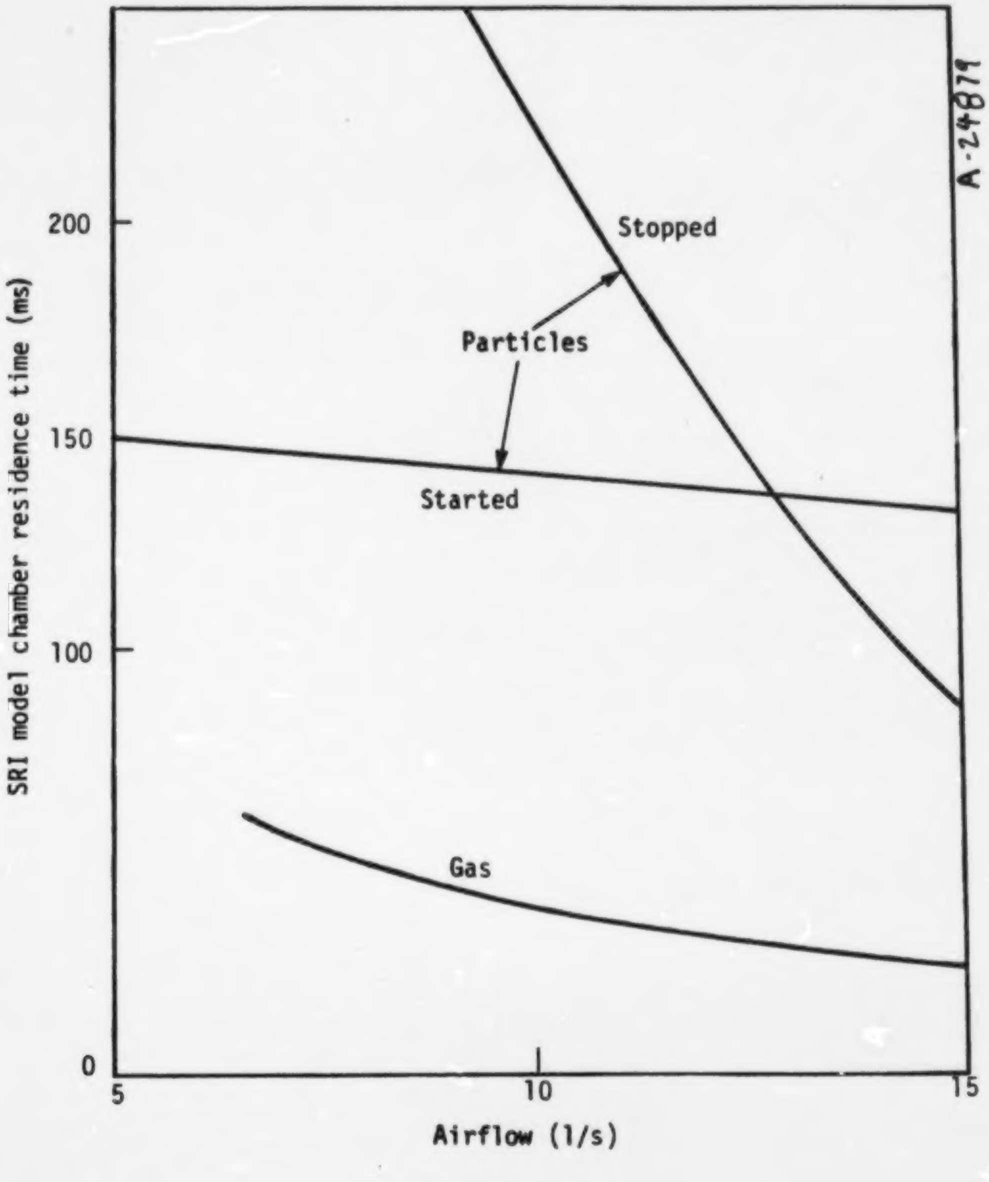

Figure 3-19. Residence Time Versus SR I Model Throughput

(This page intentionally blank)

SECTION 4

COMBUSTION EXPERIMENTAL EQUIPMENT

A schematic diagram of the SR combustion system is presented in Figure 4-1. The system can be divided roughly into three parts, namely the fuel and gas delivery system, the sampling system, and the combustor (SR I and SR II).

4.1 FUEL AND GAS DELIVERY SYSTEM

Natural gas, air, and nitrogen flows are metered by three rotameters. Coal is fed to the SR using an Acrison 105Z screw feeder. A combination coal mixing chamber/air distribution manifold (aerosolizer) is attached to the end of the screw feeder discharge tube. Air and nitrogen can be fed into the aerosolizer. The flow exits through 12 equal lengths of plastic tubing connected to the SR injectors. Air and nitrogen are fed to the SR through the aerosolizer whether or not coal is being fed. The uniformity of air distribution was checked using a hot-wire anemometer. All 12 flows were found to be uniform within 5 percent of the average flow.

Unlike the air and nitrogen flows, the natural gas flow is directly routed to only the top jet level SR injector.

4.2 SAMPLING SYSTEM

The sampling system can be divided into the sampling probe, continuous monitors, and the absorption system.

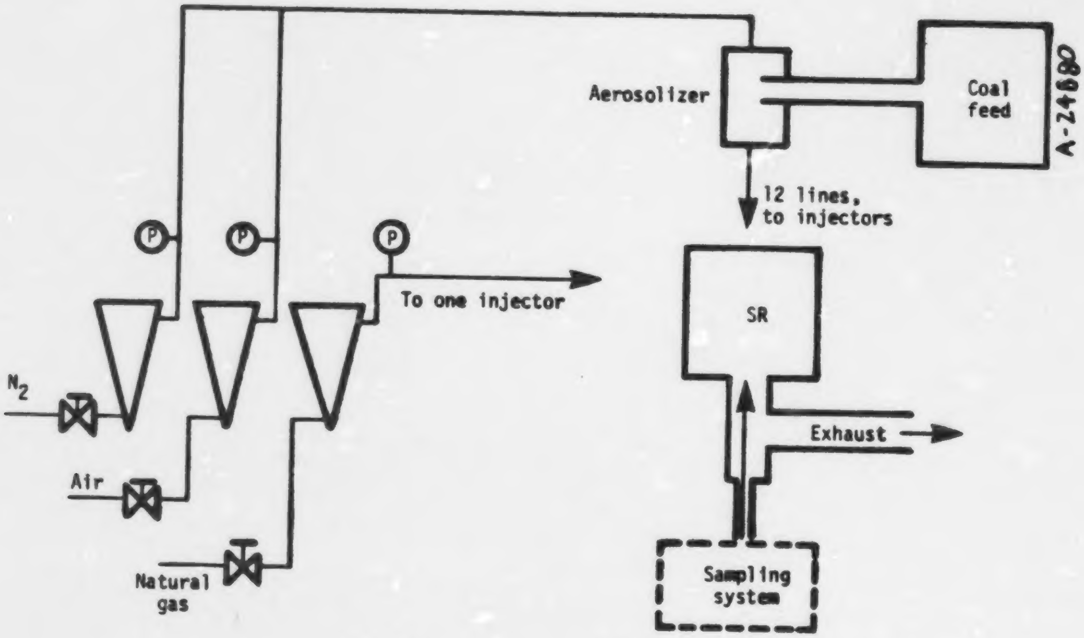
Aerosolizer
Coal feed
A-24680
12 lines, to injectors
P
P
P
To one injector
SR
N_2
Exhaust
Air
Natural gas
Sampling system

Figure 4-1. Combustion Testing Experimental Setups

The sampling probe is used to collect gas samples, cool the exhaust gases, and indirectly collect char samples. A detailed schematic of the probe is presented in Figure 4-2.

The tip of the probe is designed to aerodynamically separate coal particles from the sampled gases. The ceramic cap on the top of the probe was intended to enhance this separation as well as to protect the tip from damage due to the hot exhaust stream. However, it was found that the ceramic cap was unnecessary for correct probe operation and the probe was used without the cap for the majority of tests. The probe body is fabricated from two concentric 316 stainless steel tubes. The inner tube is used as the sampled gas passage. Water flows up through the annular passage between the tubes. At the top of the probe, the water is sprayed downward directly into the exhaust stream. The water serves to cool the sampled gases as well as to quench any reactions occurring in the exhaust. It should be mentioned that the water flows used are sufficient to keep the majority of the water in the liquid phase, with only a very small percentage being turned to steam. As shown in Figure 4-3, the char/water mixture is drained from the bottom of the exhaust tube. This mixture can be collected to allow analysis of the char.

The position of the sampling probe with respect to the SR combustion chamber is also shown in Figure 4-3. The tip of the probe sits about 10 cm away from the exit of the SR combustion chamber. The transit time of the gas from the chamber exit to the probe is very small compared to the SR residence time.

After passing through the sampling probe, the gas sample is passed through particulate filter and, to either continuous gas monitors or an

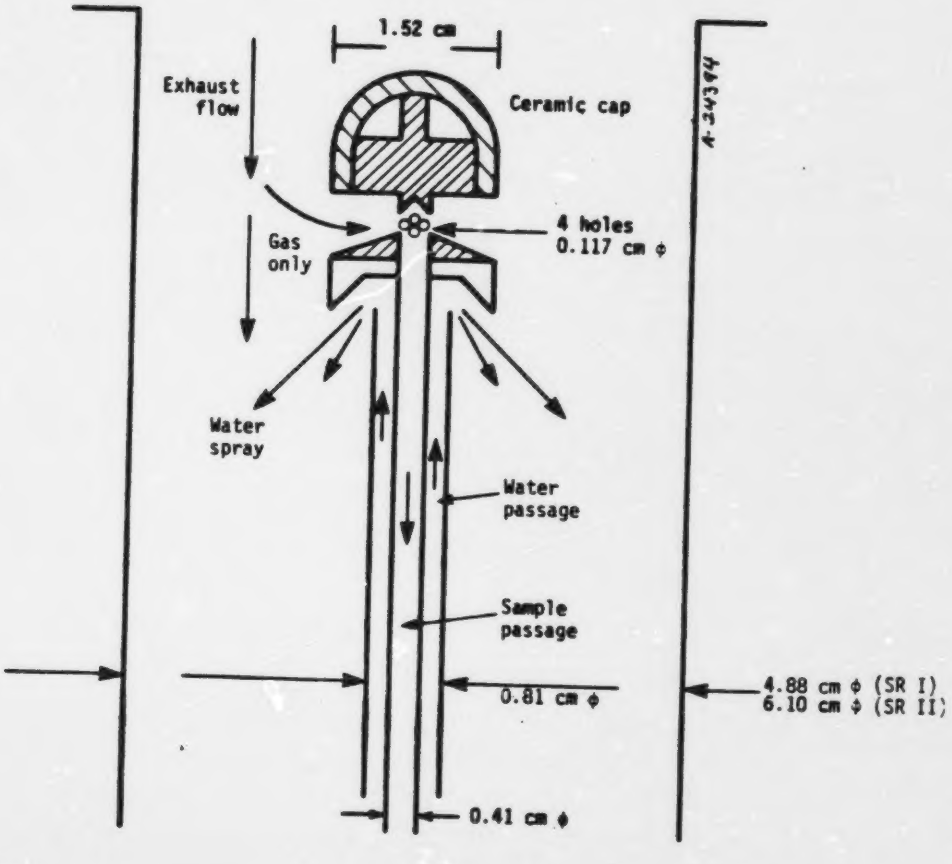
1.52 cm
Exhaust flow
Ceramic cap
A-24394
4 holes 0.117 cm ϕ
Gas only
Water spray
Water passage
Sample passage
0.81 cm ϕ
4.88 cm ϕ (SR I)
6.10 cm ϕ (SR II)
0.41 cm ϕ

Figure 4-2. Sampling probe

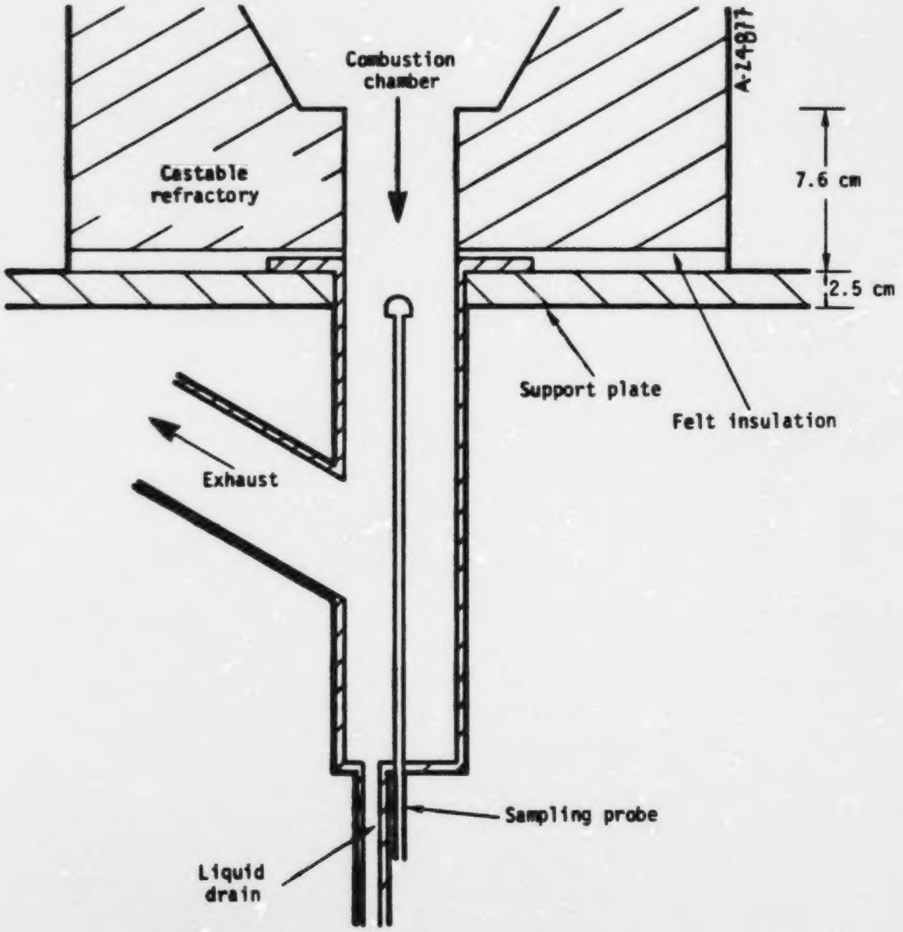
A-24877
Combustion chamber
Castable refractory
7.6 cm
2.5 cm
Support plate
Felt insulation
Exhaust
Sampling probe
Liquid drain

Figure 4-3. Sampling Probe Positioning

adsorption system used for the measurement of HCN and NH3. Table 4-1 lists the gas analysis monitors.

The technique used to trap NH_3 and HCN was a modification of a technique recommended by Energy and Environmental Research Corporation (Reference 21). This technique was used, rather than the standard technique, in hopes of reducing sulfur/HCN interference.

In measuring HCN and NH_3, exhaust gases from the probe are bubbled through four impingers. The first three impingers each contain 200 ml of deionized water together with 6g $PbCO_3$. The fourth impinger contains 200 ml of 0.005 N H_2SO_4. The supernatant from the first three impingers and the solution in the fourth impinger are analyzed by specific ion electrodes.

4.3 SR COMBUSTORS

Both SR I and SR II type combustors were fabricated using castable refractory (SHASTA KAST). The chamber dimensions for the SR's were presented in Figure 2-1. A construction diagram is presented in Figure 4-4. Each SR was cast in two halves. During assembly of the unit, the halves were stacked with a piece of fiberfax serving as a gasket between the mating surfaces. As shown in Figure 4-4, 1.27-cm support plates and compression rods were used to firmly hold the two reactor halves together.

Both SR I and SR II were cast with a wall thickness of 7.6 cm. This was the minimum distance between the combustion chamber surface and the outer wall. The wall thickness of SR I and SR II was in part, determined by heat loss, as well as weight versus strength considerations. The wall thickness was arrived at by the necessity of keeping wall heat loss below 10 percent. A compromise was also struck

Table 4-1. Exhaust Gas Analysis Equipment

Species	Instrument Manufacturer	Measurement Ranges
Carbon dioxide -- CO_2	Beckman 215 A (NDIR)	0.20 percent
Carbon monoxide -- CO	Beckman 315B (NDIR)	0-1500 ppm, 0-15 percent
Oxygen -- O_2	Teledyne 326A	0-5, 0-10, 0-25 percent
Nitrogen oxides -- NO_x	Teco 10A (chemiluminescent)	0-10,000 ppmv, change
Unburned hydrocarbons	Beckman 400 (FID)	0-100,000 ppmv

Note: The sample gases are transported to the analyzers via heat-traced lines and a Teco Model 600 gas conditioning cart. Refrigeration drying is provided at the cart to remove combustion-generated water vapor prior to analysis.

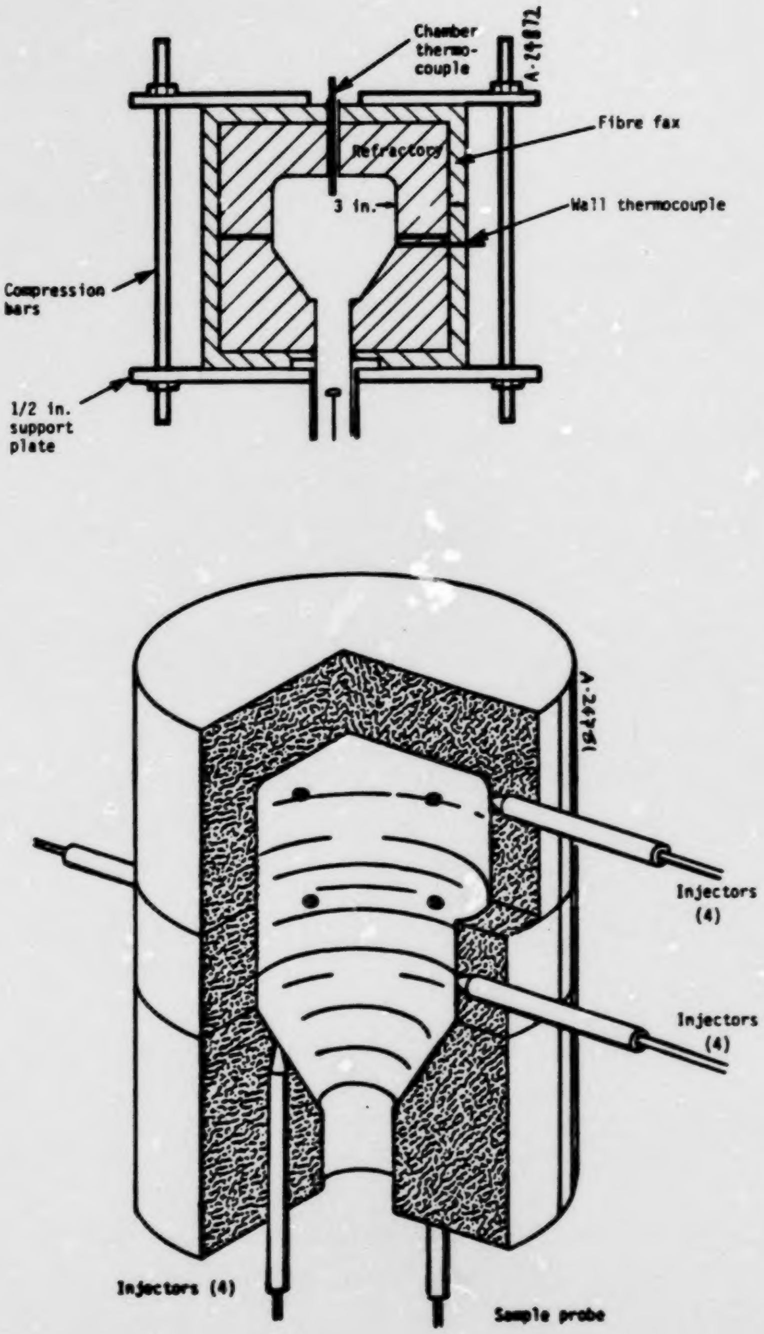
Chamber thermo-couple
A-24872
Fibre fax
Refractory
3 in.
Wall thermocouple
Compression bars
1/2 in. support plate
A-24781
Injectors (4)
Injectors (4)
Injectors (4)
Sample probe

Figure 4-4. Combustor Construction Schematic

between keeping the walls strong enough to avoid cracking as well as keeping the SR's light enough to be assembled with an acceptable level of effort.

The ratio of the SR inner to outer diameter determines resistance to fracture. This ratio for SR I was about 2.1, and 1.7 for SR II. Therefore, in an attempt to strengthen SR II, the reactor halves were cast with refractory anchors around the chamber perimeter. A 1.9-cm cylindrical opening at the top centerline was used to insert a Type R thermocouple into the chamber. A thermocouple was used to monitor the inside wall temperature and several thermocouples were attached to the outer surface of the reactor.

(This page intentionally blank)

SECTION 5

EXPERIMENTAL

In all, 42 test conditions were examined using SR combustors. These experiments were conducted using a Utah bituminous coal and mixtures of air, natural gas, and nitrogen. These tests covered whole coal equivalence ratios, for the most part, from 0.8 to 2.5. Mean residence times, based on gas flowrate, were varied from 20 to 100 ms and temperatures spanned the range from $1,400^{\circ}$ to $1,900^{\circ}K$.

Experiments conducted in SR II used air (or air plus nitrogen) flows of 14.1, 21.2, and 28.2 l/s. Tests in SR I used airflows of 6.6, 9.4, and 14.1 l/s. Although helium tracer experiments indicated that the mixing level in SR I became less well-stirred below about 9.4 l/s, tests were conducted at 6.6 l/s throughput to allow an overlap in SR I and SR II residence times.

During the tests, continuous monitors were used to determine concentrations of O_2, CO_2, CO, NO, and unburned hydrocarbons. In the majority of tests, char samples were collected and analyzed for chemical composition. In 25 tests, a liquid adsorption/ion electrode technique was used to measure concentrations of HCN and NH_3 in the exhaust gas.

Table 5-1 lists the chemical composition of the coal used in these experiments, while Figure 5-1 illustrates the coal size distribution obtained by wet sieving. This Utah bituminous coal was supplied to Acurex

Table 5-1. Utah Coal Properties (As Received)

Moisture (%)	2.82
Carbon (%)	66.65
Hydrogen (%)	4.86
Nitrogen (%)	1.41
Sulfur (%)	0.89
Ash (%)	10.60
Oxygen (by difference) (%)	12.77
Volatiles (%)	41.8
20% Oversize (µm)	67
20% Undersize (µm)	22
Mean size (µm)	44
High heating value (Cal/g)[a]	7,543

[a] HHV obtained using Dulong's formula

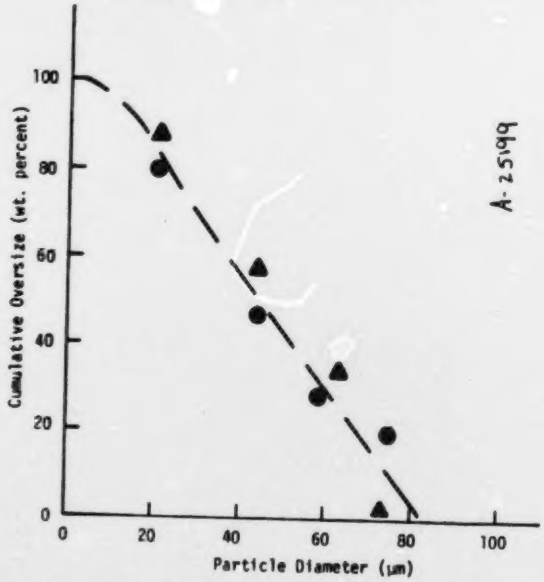

Figure 5-1. Utah Coal Particle Size Distribution for Two Samples Obtained by Wet Sieving

by Energy and Environmental Research Corporation. This coal was chosen for use in this study because it has been used in several other Environmental Protection Agency (EPA) programs (for example, Reference 22) and is fairly well characterized.

Prior to shipment, the coal was bulk-classified in an attempt to get a narrow size cut (64 to 88 μm). However, wet sieving tests show only about 30 percent of the coal to be in this range with the remainder being much finer.

5.1 TEST PROCEDURE AND SR OPERATING CHARACTERISTICS

Prior to burning coal in either SR I or SR II, the combustor is heated for over an hour using a natural gas/air mixture at 15 or 30 kW firing rate, respectively. The initial light-off of the SR is accomplished using a pilot flame which is inserted into one of the top jet openings. After the pilot is inserted (with the main airflow on), the natural gas is started. After ignition, the pilot is removed and the jet is reinserted into its socket in the SR wall. At the end of the heating period, the airflow is adjusted to the desired value and the coal feed is gradually increased while the natural gas flow is gradually decreased to zero (in tests where coal was the only fuel). The time required to reach steady state temperature conditions is on the order of 4 hours and is much longer than the actual heating time used in these experiments. However, the slight transient conditions are not expected to influence the results.

After the heating period, test conditions are set. About 5 minutes later, the exhaust emissions are measured, char/water samples are collected (Figure 4-3), and temperatures are monitored.

A single coal test condition is usually run for 15 to 20 minutes. As mentioned previously, this period is insufficient to reach steady state conditions. However, this relatively short test time is mandated by the fairly rapid slagging rate in the SR. The accumulation of slag in the SR could reduce the chamber size; however, ash accumulation on the chamber walls seemed to reach an equilibrium thickness of approximately 1/8 inch, causing a maximum decrease in chamber volume of no more than 10 percent. Of greater importance was the accumulation of slag at the exit of the SR, which blocked the exhaust passage, thereby terminating testing.

Slagging in the SR exhaust is more likely to occur at lower air flowrates and/or high coal loadings. Once slagging of the exhaust begins, the exhaust can become completely blocked in less than 5 minutes. This process has been observed several times when using SR II. The end result, if the fuel flow is not shut down immediately, is severe cracking of the chamber walls.

Due to the relatively short duration of an individual test, SR I and SR II temperature and gas composition histories were examined for the effect of nonsteady conditions. Figures 5-2 and 5-3 show the changes in these parameters during a typical test. As shown in the figures, the exhaust composition reaches a quasi-equilibrium condition fairly rapidly. In general, NO concentrations are the most stable while CO_2 and O_2 concentrations do vary slightly.

In both the large and small SR's, gas temperatures are monitored by a bare type R thermocouple as shown in Figure 4-4. Generally temperatures recorded by this thermocouple can vary up to $\pm 14^{\circ}K$ from minute to minute; however, the longer term trend is for temperature to increase with time. The average of the temperatures recorded during the interval from 5 to 15 minutes after a coal test condition has been reached is considered to be the average temperature of the test. This average temperature is

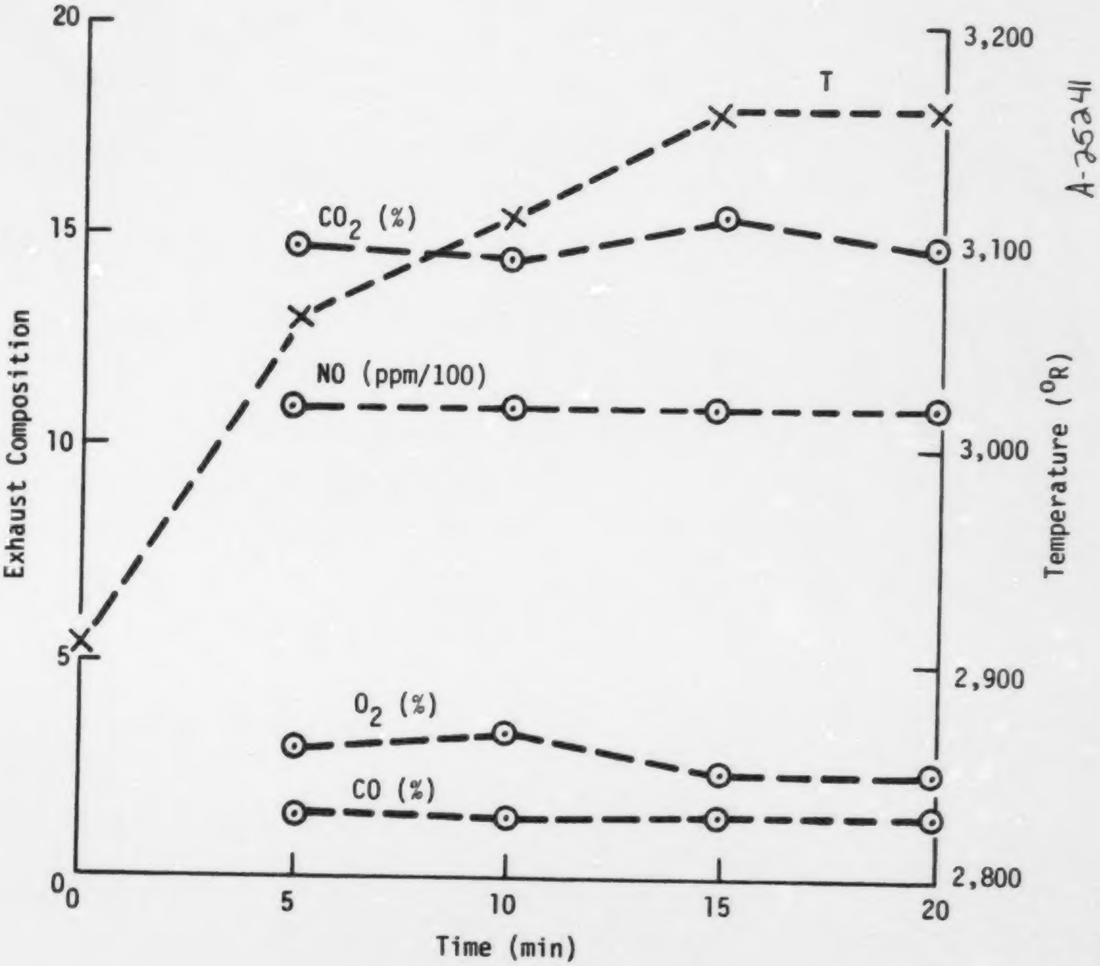

A-25241

Figure 5-2. SR I Variations in Temperature and Gas Composition Over Test Interval

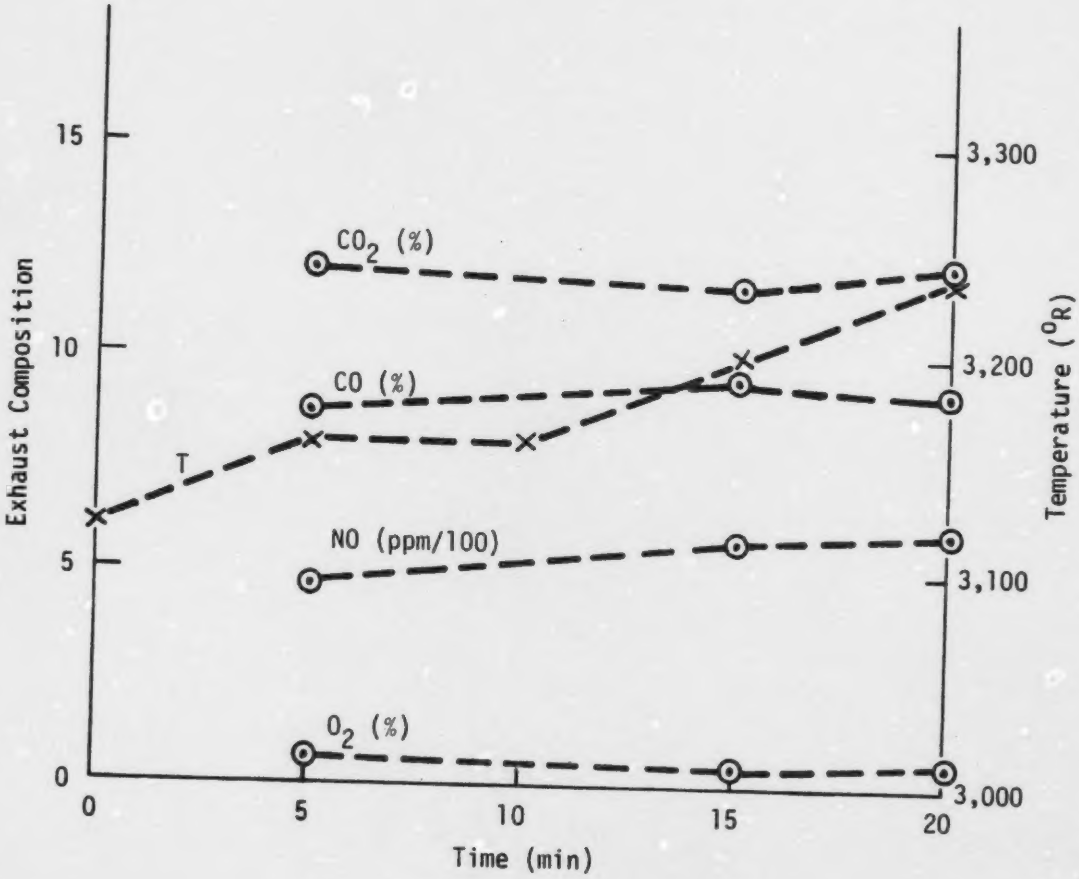

A-25242

Figure 5-3. SR II Variations in Temperature and Gas Composition Over Test Interval

generally within 28°K of the end temperature and is considered to be sufficiently close to the final temperature. The subject of thermocouple placement and temperature measurement accuracy will be addressed further in the following sections.

5.2 COMBUSTION TEST RESULTS

The coal combustion tests were performed using both SR I and SR II combustors having chamber volumes of about 1.7 and 7.6 l, respectively. During the course of testing, five similar 7.6-l SR's were used, while only one 1.7-l SR was used during experimentation. In general, SR replacement was mandated by cracking of the SR walls.

Since several materials have been shown to exhibit a catalytic effect on certain nitrogenous (Reference 23) and hydrocarbon species, some initial concern was directed to the fact that SR I and SR II have different surface area/volume ratios. In addition, heat loss would be different between the two reactors. Combustion test results in overlapping parameter regions for the two reactors have indicated these effects to be small and, in general, results from SR I and SR II are presented together.

The majority of tests were conducted using coal in air/nitrogen mixtures with the nitrogen flow being much less than the airflow. Some tests were conducted with air/N_2 ratios ranging from 3:1 to 1:1. Three of these tests were an attempt to lower the particle temperature and thereby the extent of decomposition of the particles. The results of these tests will be reviewed separately in Section 5.2.4.

Table 5-2 lists some of the data taken from both SR I and SR II tests. The data presented in the table will be referred to in the following section.

Table 5-2a. SR I Results

Test No.	Equiv. Ratio	Q_{air} (scfm)	RT (s)	Temp. (^oR)	NG (%)	NVM (%)	NN (%)	NA (%)	O_2 (%)	CO_2 (%)	CO (%)	NO (ppm)	NOC (%)	HCNC (%)	NH_3C (%)
1	1.2	30.0	0.020	3,390	71.0	92.9	97	68.2	3.2	14.7	1.0	1,350	33.9	--	--
2	1.2	20.0	0.31	3,260	70.2	--	--	--	3.6	14.5	1.1	1,250	31.2	0.3	0.0
3	1.2	14.0	0.49	3,010	74.2	--	--	--	2.9	14.9	1.4	1,100	27.8	1.1	0.3
4	1.7	30.0	0.020	3,400	62.6	95.9	100	77.3	1.0	14.0	5.3	1,250	22.0	3.3	0.8
5	1.8	20.0	0.030	3,385	63.3	--	--	--	0.4	14.2	6.3	930	15.6	6.7	0.0
6	1.8	14.0	0.044	3,330	62.1	--	--	--	0.4	14.1	5.8	887	15.0	9.4	0.0
7	2.6	30.0	0.020	3,385	48.2	94.0	100	75.2	0.7	11.3	10.1	750	8.9	4.1	0.0
8	2.5	20.0	0.032	3,250	49.7	--	--	--	0.3	11.2	10.5	600	7.2	19.9	0.1
9	2.5	14.0	0.045	3,230	49.2	--	--	--	0.5	11.7	9.7	580	7.0	20.3	0.0

Table 5-2b. SR II Results

Test No.	Equiv. Ratio	Q_{air} (scfm)	Q_{CH_4} (scfm)	Q_{N_2} (scfm)	RT (s)	Temp. (°R)	NG (%)	NVM (%)	NN (%)	NA (%)	O_2 (%)	CO_2 (%)	CO (%)	NO (ppm)	NOC (%)	HCNC (%)	NH_3C (%)
1	1.7	60.0	0.0	0.0	0.044	3,410	62.6	97.2	--	76.3	1.2	13.5	5.8	850	14.9	--	0.0
2	1.3	60.0	0.0	0.0	0.045	3,360	71.2	--	--	--	2.6	16.0	0.9	950	22.3	--	0.0
3	1.0	30.0	0.0	0.0	0.090	3,335	85.6	--	--	80.6	3.1	14.4	1.9	840	24.6	1.1	0.0
4	0.8	60.0	0.5	0.0	0.045	3,300	86.3	--	100	78.4	5.4	12.8	0.6	850	33.5	6.1	0.0
5	1.2	45.0	0.0	0.0	0.061	3,300	82.2	--	--	--	1.5	16.7	1.6	960	24.1	--	--
6	1.3	30.0	0.0	0.0	0.091	3,300	79.1	--	98.2	86.2	0.7	14.9	3.8	760	17.8	3.1	0.1
7	1.7	30.0	0.0	0.0	0.090	3,330	67.4	97.3	93.1	79.0	0.5	12.2	8.5	450	7.9	7.5	0.1
8	1.8	45.0	0.0	0.0	0.061	3,300	63.9	96.8	0.0	78.7	0.8	13.2	6.9	740	12.7	--	--
9	2.5	30.0	0.0	0.0	0.091	3,300	51.9	84.7	82.8	77.6	1.0	11.1	11.0	320	3.9	--	--
10	1.8	30.0	0.0	0.0	0.091	3,290	59.4	94.2	86.5	81.1	1.8	15.1	4.2	620	10.4	--	--
11	2.5	45.0	0.0	0.0	0.061	3,280	51.8	--	93.3	79.8	0.2	11.4	10.7	385	4.7	1.6	0.0
12	2.5	60.0	0.0	0.0	0.046	3,260	50.9	96.2	--	75.5	0.2	11.5	10.2	590	7.3	19.9	0.1
13	2.5	60.0	0.0	0.0	0.046	3,250	50.2	96.2	--	76.1	0.3	12.4	9.1	580	7.2	--	0.0
14	2.3	45.0	0.0	0.0	0.062	3,220	52.8	96.9	79.9	79.6	0.3	11.9	9.3	590	7.8	16.0	4.3
15	1.2	45.0	0.0	0.0	0.063	3,200	61.4	--	--	--	6.6	13.3	0.1	870	21.9	--	0.0
16	0.9	45.0	0.0	0.0	0.064	3,110	87.1	94.0	87.5	87.7	5.6	13.4	0.5	1,050	36.9	--	--
17	3.0	45.0	0.0	0.0	0.064	3,110	42.9	94.5	89.6	74.5	0.3	10.3	11.7	420	4.2	25.6	0.1
18	1.3	45.0	0.0	4.5	0.058	3,110	66.6	94.9	92.6	76.6	3.4	12.2	1.9	800	20.7	2.4	0.0
19	1.8	30.0	0.0	4.5	0.085	3,085	58.6	--	--	--	1.6	11.4	4.8	600	11.7	2.5	0.0
20	2.4	30.0	0.0	2.0	0.091	3,080	48.7	--	--	--	0.5	11.9	7.3	530	7.1	20.4	0.0
21	1.2	30.0	0.0	2.0	0.092	3,070	81.1	97.1	95.1	76.4	3.1	13.2	4.0	720	18.8	12.3	0.2
22	0.7	45.0	0.0	0.0	0.065	3,060	83.4	--	--	--	8.0	11.1	0.4	730	29.6	2.2	0.1
23	0.8	60.0	0.0	0.0	0.050	3,010	78.0	95.2	86.2	85.2	8.9	11.0	0.1	745	29.1	--	--
24	0.9	45.0	0.0	0.0	0.068	2,935	69.3	--	--	--	9.8	10.8	0.1	678	23.8	--	--
25	0.8	30.0	0.0	0.0	0.103	2,910	74.4	93.1	92.2	92.3	9.1	10.5	0.0	668	26.1	--	--
26	1.9	24.0	0.0	11.0	0.095	2,715	59.0	--	--	--	0.2	9.1	4.7	260	5.9	19.3	0.1
27	1.2	24.0	0.0	10.4	0.097	2,700	75.0	95.1	--	72.5	2.3	10.0	1.3	540	19.8	10.4	0.0
28	2.6	26.6	0.0	8.0	0.099	2,630	43.2	--	--	--	1.4	9.0	5.6	300	4.6	9.9	0.0
29	6.5	40.0	3.2	21.0	0.055	2,550	29.6	82.1	87.2	65.9	0.7	7.0	3.0	300	11.3	--	--
30	15.5	30.0	2.8	10.5	0.085	2,460	32.6	92.1	81.5	73.9	1.0	6.5	5.5	140	6.0	--	--
31	31.0	25.0	2.4	8.8	0.102	2,440	24.0	91.5	84.2	70.5	0.8	6.6	4.9	180	6.4	--	--
32	0.6	45.0	0.0	0.0	0.083	2,405	55.8	--	--	--	15.7	5.4	0.8	297	14.2	--	--

The respective gas flows listed in the table are based on rotameter readings. The equivalence ratio in tests without CH_4 addition is based on a stoichiometric air requirement of 0.136g coal (as received)/l air. When CH_4 is added, it is assumed to react immediately, effectively reducing the amount of oxygen available for coal combustion.

The residence time (RT) listed in the table is calculated based on the chamber volume, indicated gas temperature (TEMP), and input gas flow. Gas compositions are reported on a dry basis and NG is the extent of coal reaction based on a carbon balance. NN, NA, and NVM are weight losses for fuel-bound nitrogen, combustibles, and volatile matter, respectively, based on a chemical analyis of the char.

These quantities are defined as:

$$NG = \frac{\text{Mass carbon in CO and CO}_2}{\text{Mass of carbon input into the reactor in coal}}$$

$$NA = 1 - \frac{\text{Combustibles/ash}}{\text{Initial combustibles/ash}}$$

$$NN = 1 - \frac{\text{Mass nitrogen in char/ash}}{\text{Initial mass nitrogen in char/ash}}$$

$$NVM = 1 - \frac{\text{Mass volatile in char/ash}}{\text{Initial mass volatile in char/ash}}$$

Table 5-3 lists the results of the char analyses, also to be referred to later.

Table 5-3. Char Analysis Results (Dry)

Test	VM	Ash	Carbon	Hydrogen	Nitrogen	Sulfur
SR I						
1	6.90	27.8	66.6	0.40	0.10	--
4	5.02	35.0	62.1	0.30	0.0	--
7	6.97	33.1	65.0	0.40	0.0	--
SR II						
1	3.32	34.09	--	--	--	--
3	--	38.70	--	--	--	--
4	--	36.18	60.2	0.40	0.0	--
6	--	47.0	53.6	0.30	0.10	--
7	3.52	36.8	58.3	0.30	0.30	--
8	4.10	36.5	--	--	--	--
9	18.97	35.4	57.6	0.63	0.72	0.77
10	8.02	39.2	58.6	0.48	0.63	0.64
11	--	37.7	59.6	0.40	0.30	--
12	4.45	33.3	--	--	--	--
13	4.52	33.8	--	--	--	--
14	4.13	37.4	61.1	0.41	0.89	--
16	10.54	49.8	48.8	0.39	0.74	--
17	6.23	32.4	62.3	0.50	0.40	--
18	6.18	34.3	62.7	0.40	0.30	--
21	3.49	34.1	63.7	0.40	0.20	--
23	7.56	45.2	53.1	0.54	0.74	0.47
25	14.86	61.5	35.3	0.60	0.57	0.61
27	5.30	30.8	--	--	--	--
29	16.62	26.4	62.3	0.70	0.70	--
30	8.88	31.9	62.1	0.70	0.70	--
31	8.72	29.3	64.8	0.70	0.55	--

5.2.1 Temperature and Major Gas Species

As mentioned, SR combustion chamber temperature was monitored by a bare type R thermocouple inserted into the chamber from 2.5 to 4.0 cm as shown in Figure 4-4.

Figure 5-4 shows that gas temperatures indicated by this thermocouple rise steeply between ϕ equaling 0.6 and about unity. At the low temperature condition, the flame was bordering on extinction. At equivalence ratios greater than unity, temperature is seen to level out at about $1,833^{o}K$ ($3,300^{o}R$). The temperature drops slightly as ϕ is increased to 3.0. The shorter residence (τ_{sg}) higher heat release rate cases appear to give higher temperatures for both SR I and SR II with the trend for SR I being most clear. The SR I and SR II 44- to 50-ms residence time cases do not correspond, indicating the higher surface area to volume SR I reactor has proportionally greater heat loss. Figure 5-5 shows SR I and SR II exhaust concentration versus ϕ. Comparison of Figure 5-5a to 5-5b shows that the concentrations of O_2, CO_2, and CO for the two reactors (SR I versus SR II) are in agreement. The fairly close agreement between SR I and SR II results for different residence times could be fortuitous and might be due to compensating factors. As residence time decreases, mass flow through the reactor increases and the proportional amount of heat loss decreases. Thus, as shown in Figure 5-4, as residence time decreases, reactor gas temperature increases. The increase of reaction rate (thermal decomposition and char oxidation) with temperature is then offset by the attendent reduction in residence time yielding CO_2, CO, and O_2 concentrations roughly comparable between reactors SR I and SR II.

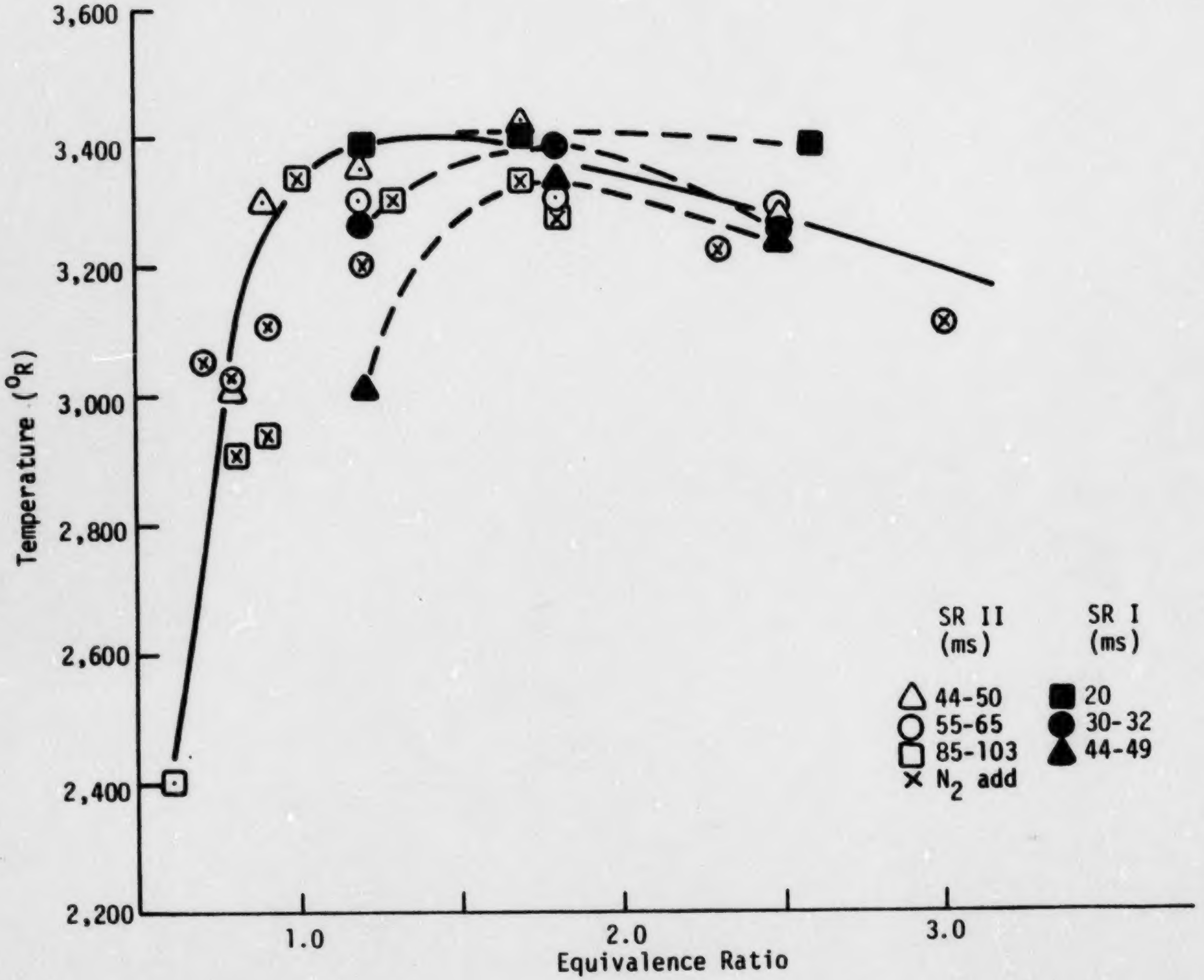

Figure 5-4. Measured Gas Temperature Versus Whole Coal Equivalence

A-251 95

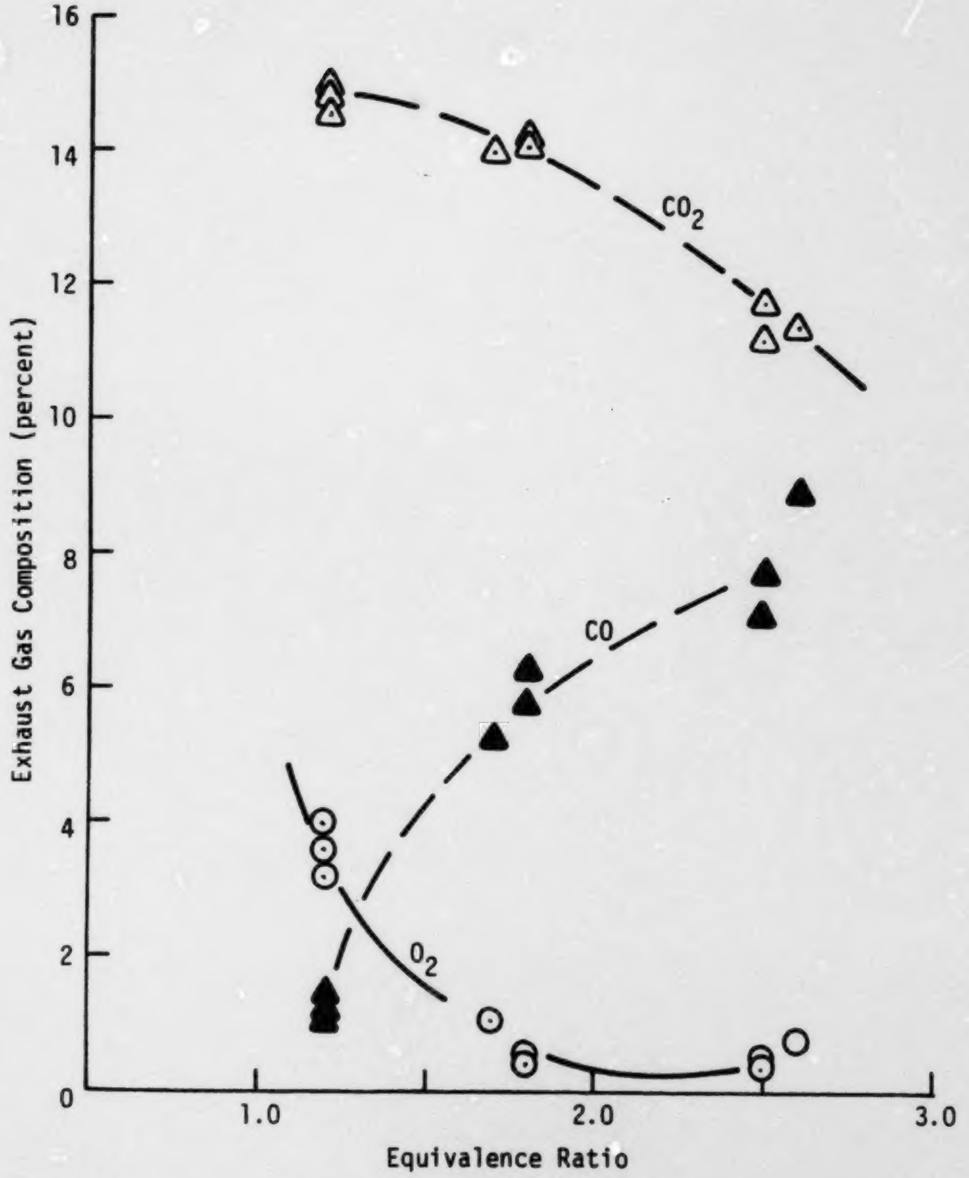

A-25189

Figure 5-5a. SR I Gas Composition Versus Equivalence Ratio Showing ▲ CO; △ CO_2; ⊙ O_2

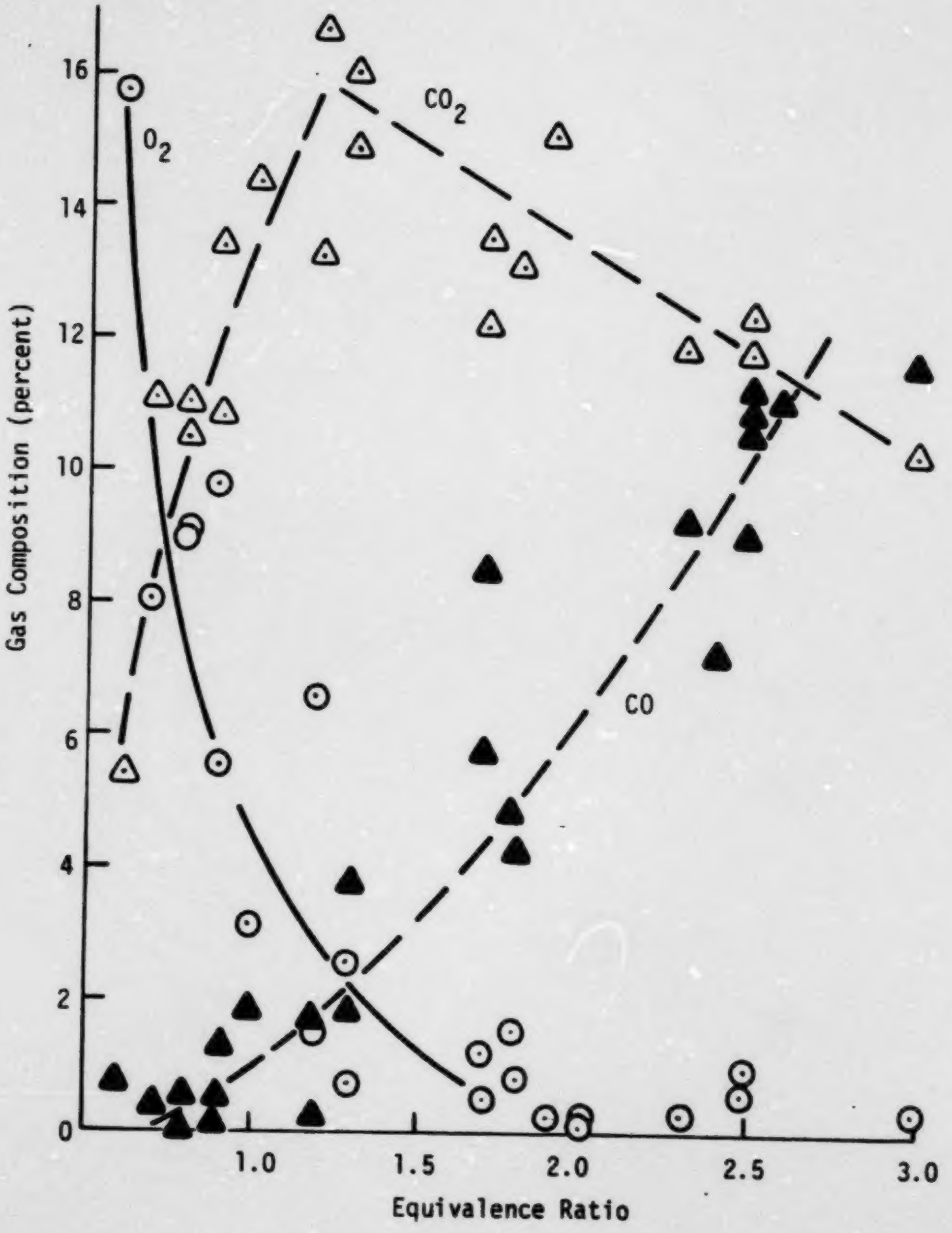

A-2519D

Figure 5-5b. SR II Gas Composition Versus Equivalence Ratio Showing △CO; ⊙ CO_2; ▲O_2

The curves suggest that "true" stoichiometric conditions seem to lie in the region between ϕ_{wc} of about 1.3 to 1.5. This is probably due to the presence of unburnt combustible material in the exhaust. It might be envisioned that combustion in the SR is primarily associated with the coal volatiles. The stoichiometric air requirements of the volatile component of the fuel is estimated to be at a whole coal ϕ of 1.4. This corresponds to some extent with the true stoichiometric conditions referred to here.

The fact that both SR I and SR II show the same trends with ϕ implies either the coal concentration in the chamber is less than expected or easily evolved volatiles play the primary role in combustion. The longer residence time of the particles versus the gas in the reactor found in the mixing studies would tend to support a greater concentration of particles in the reactor rather than a smaller concentration. Thus, volatiles must be strongly dominating the combustion results.

Temperature, as given in Figure 5-4, does not show the characteristic high peak expected based on the exhaust composition. Although the correct trend is present, it appears to be muted. This temperature smoothing is characteristic of measurements made where the thermocouple reading is strongly influenced by radiation from the surrounding combustor walls.

The two most likely factors to influence temperature measurement accuracy are thermocouple placement in the SR's and/or the magnitude of radiation errors. The temperature profile down the center of SR I was obtained by a thermocouple traverse. The results are shown in Figure 5-6.

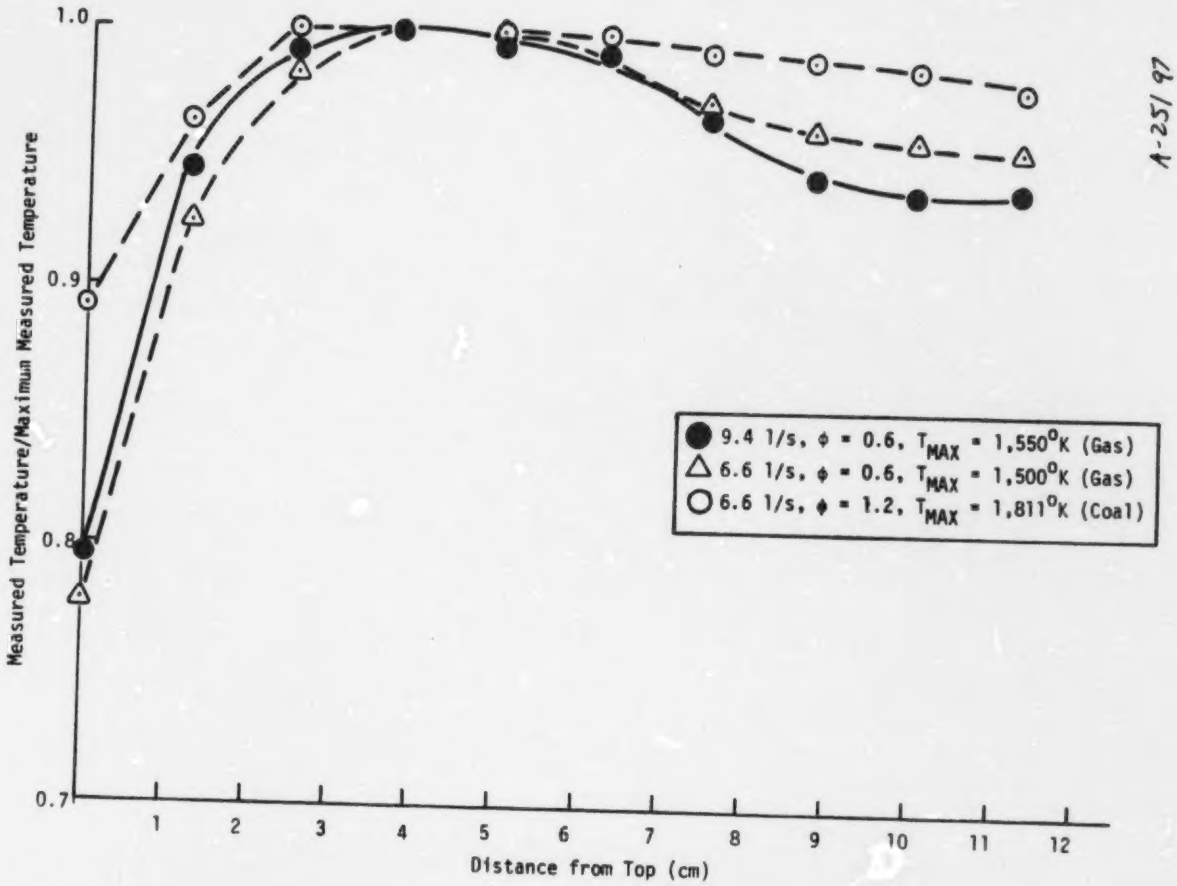

A-25197

Figure 5-6. SR I Temperature Measurement Along Axes

The temperature profiles obtained during coal combustion show characteristic differences from natural gas combustion results. During both modes of combustion, the indicated temperature rises to the maximum value at about 2.5 cm below the top of the chamber. However, the coal temperature profile remains relatively flat beyond this point, whereas the gas temperature profile shows a slight drop at about 7 cm. This may be because natural gas was only introduced through one injector, or that radiative transfer from the coal dominates convective heat transfer.

Under ideal circumstances, it is possible to make a reasonable estimate of thermocouple error due to radiation to bounding walls. However, uncertainties about particle surface areas, slag emissivities, and combustion chamber wall temperatures (due to slag accumulation) did not justify the attempt. However, a simple bounding estimate indicated that under the most (reasonably) unfavorable conditions, the radiation error could lower the thermocouple temperature by about $250^{\circ}K$.

A heat balance was performed on all the test points. The balance considers the chemical energy released from the coal, based on a carbon balance and corrected for CO emissions, and the sensible heat of the exhaust gases. The balance does not include wall losses, which are expected to account for between 7 and 10 percent of the heat generated. While the SR's were fitted with thermocouples to measure wall losses, operational difficulties prevented this information from being obtained.

The results of the heat balance are shown in Figure 5-7a and b. In both the SR I and SR II data, closure ranges from about 70 to 90 percent with closure generally being lower at $1.0 < \phi < 1.5$. The SR I data also show indications that closure is increased with increasing SR I jet

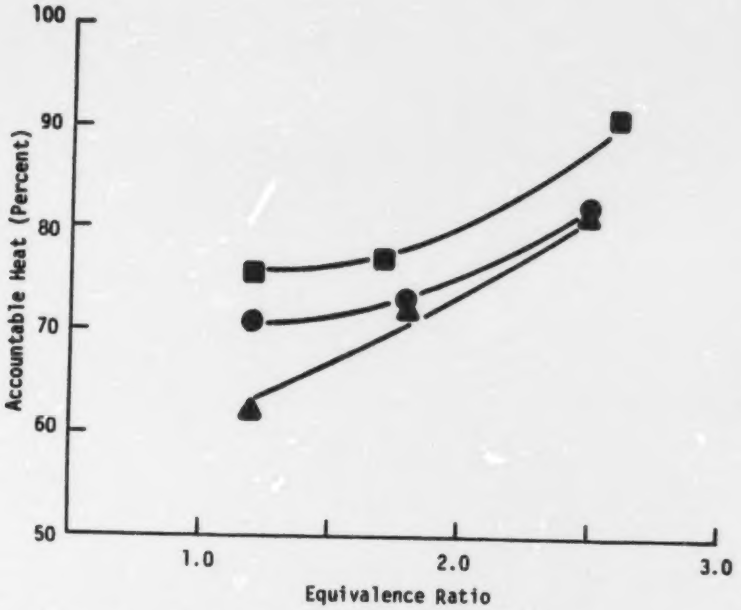

A-251 88

Figure 5-7a. SR I Heat Balance Closure; Residence Time Ranges: ■ 20 ms; ● 30 to 32 ms; ▲ 44 to 49 ms

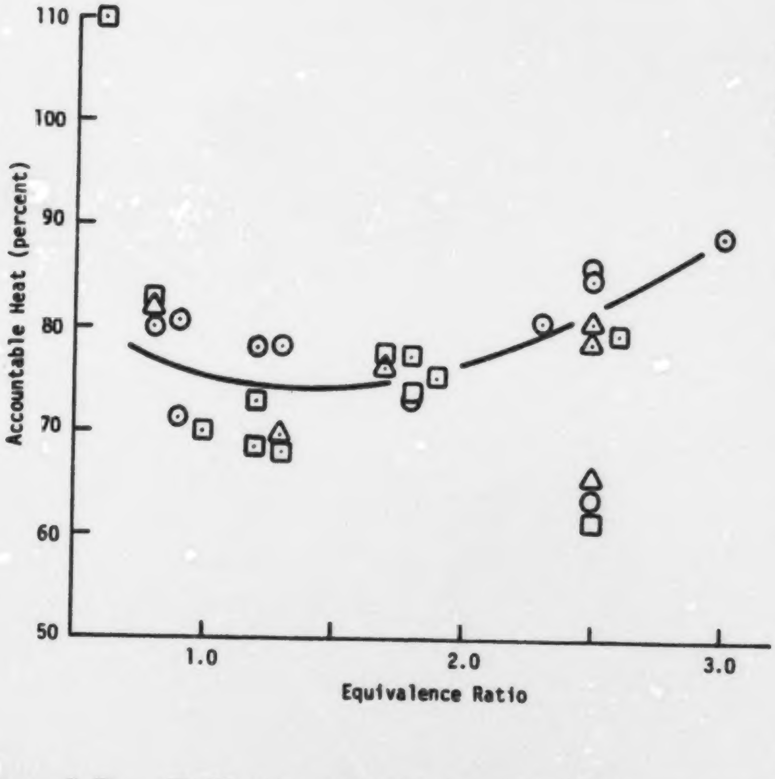

A-251 96

Figure 5-7b. SR II Heat Balance Closure; Residence Time Ranges: △ 44 to 50 ms; ○ 55 to 60 ms; □ 85 to 103 ms

velocity (or gas throughput). This is an indication of increasing convective transfer on the thermocouple.

The difference between the gas and thermocouple temperature, ΔT, can be expressed in terms of the wall temperature, T_w, and thermocouple temperature, T_t, in the following simplified manner:

$$\Delta T = (T_t - T_w) \times \frac{h_w^r}{h_g^r + h_g^c}$$

where h_w^r is the radiative transfer coefficient between the wall and thermocouple, h_g^r is the radiative transfer coefficient between the gas cloud and thermocouple, and h_g^c is the convective transfer coefficient between the gas and thermocouple. Due to the thermal mass of the SR (which was not operated at steady state temperatures), the difference between T_g and T_w will be largest over the region of maximum specific heat release ($1.2 < \phi < 1.5$). This would account for the concave shape of the accountable heat curves.

The line of maximum temperature, shown in Figure 5-4, was used in conjunction with the estimate of accountable heat (SR II) to predict the maximum possible level of SR II temperatures. For this prediction, 10 percent was uniformly added to the accountable heat values to account for wall heat loss. The maximum temperatures, T_{max}, were calculated using the relation:

$$T_{max} = T \times (200 - Q_{acct})/100$$

Both T, and Q_{acct} are functions of ϕ with their values being taken from Figure 5-4 and Figure 5-7, respectively. The results of this calculation are shown in Figure 5-8. As illustrated, maximum estimated differences of up to about $306^{o}K$ may occur between actual and measured temperatures.

5.2.2 Extent of Reaction

The degree to which the coal samples have been reacted, or the extent of reaction, has been determined by a standard carbon balance as well as by using a standard ash tracer method. The carbon balance results yield an estimate of combustion conversion (to CO and CO_2) while the ash tracer method, under ideal circumstances, gives an indication of gasification efficiency (weight loss).

Weight loss values based on ash, NA, is subject to uncertainty. The uncertainty exists due to questions about ash vaporization at high temperatures as well as particle accumulation in the SR combustion chamber, which impacts particle sample accuracy.

The effect of weight loss error due to ash vaporization is most likely to be negligible (Reference 24) due to the nonlinear dependence of calculated weight loss. Based on char ash content, NA, vaporization of 5 percent of the ash results in NA uncertainties of less than 5 percent at high values of NA. Particle accumulation in the combustion chamber affects the accuracy of NA only if char particles selectively deposit their ash components on the combustor walls or slag formed in the chamber finds its way into the char sample stream. Both of these possibilities are considered unlikely. The results presented in the following paragraphs are self-consistent supporting this view.

The values of reaction efficiency based on a carbon balance, NG, are presented in Figure 5-9. As shown in the figure, NG tends to increase as ϕ decreases from 3.0 to 1.0. At ϕ less than unity, NG decreases due to incipient extinction. The reaction efficiencies for SR I and SR II do not

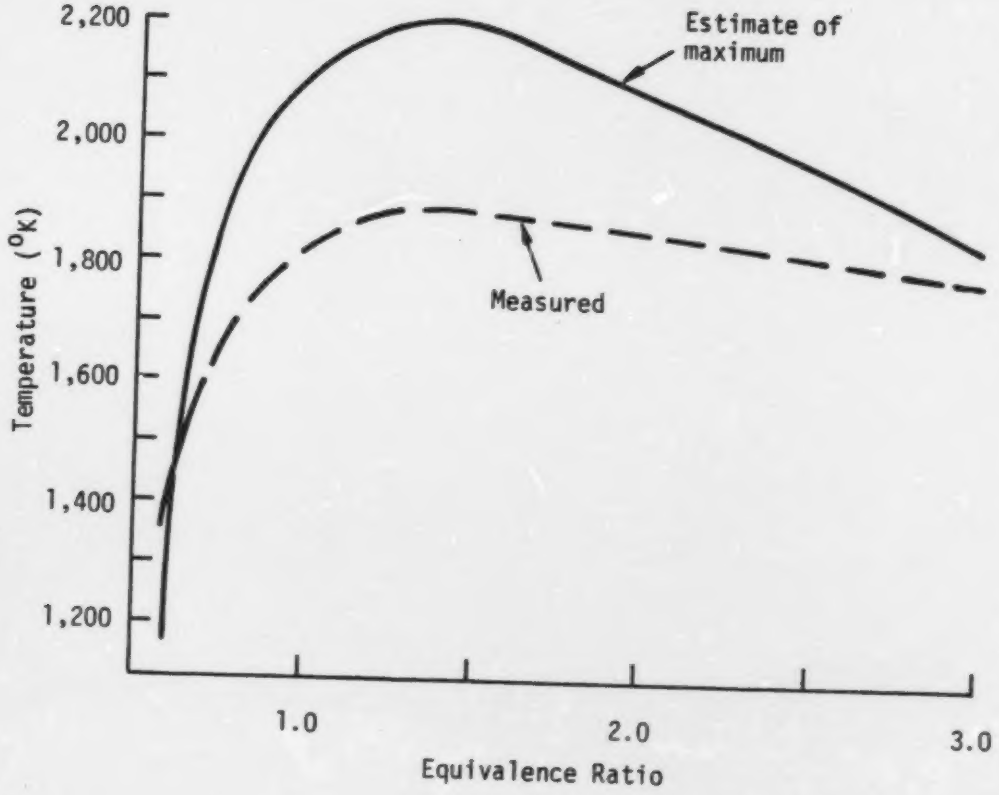

A-25198

Figure 5-8. Temperature Versus Equivalence Ratio Showing the Estimated Maximum Temperature Error

A-251 87

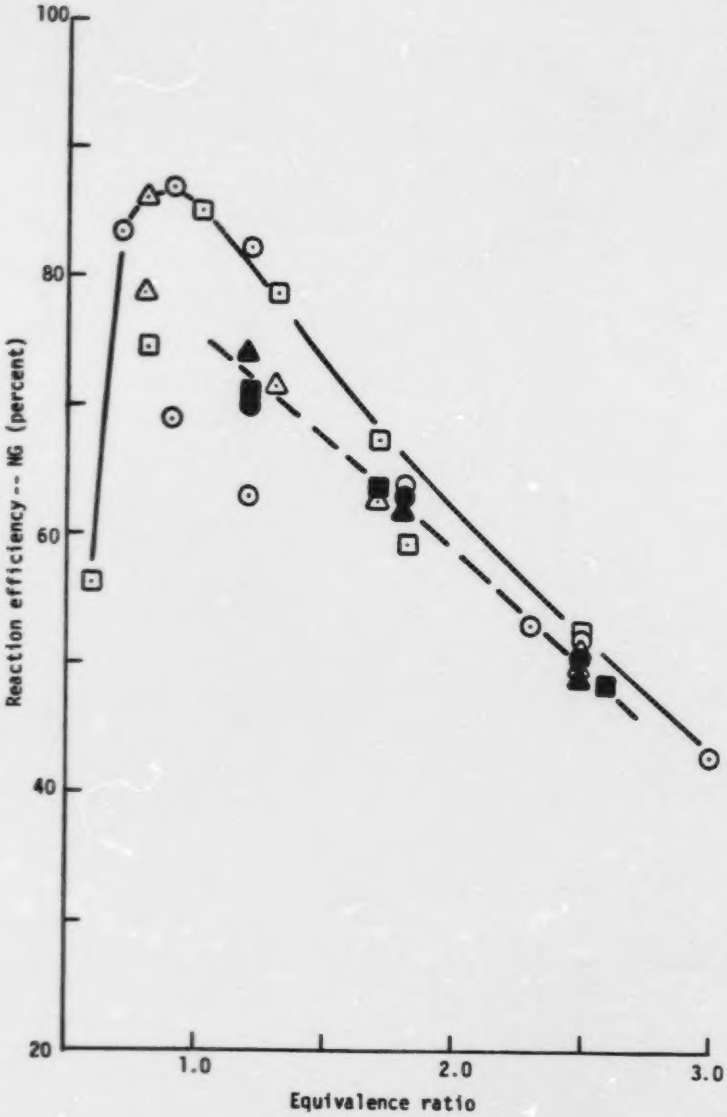

Figure 5-9. Variation of Reaction Efficiency with Equivalent Ratio; Residence Time Ranges: SR II: △ 44 to 50 ms; ○ 55 to 60 ms; ☐ 85 to 103 ms; SR I: ■ 20 ms; ● 30 to 32 ms; ▲ 44 to 48 ms

appear to have any clear trend with residence time. However, the shorter residence time SR I results show a lower reaction efficiency than the SR II results at the same ϕ. As shown in Figure 5-4, the SR I short residence time gas temperatures are comparable to SR II gas temperatures. The shorter residence time SR I results at the equivalent reactor temperature then yields the lower reaction efficiency shown in Figure 5-9.

Weight loss based on the ash content of the char, NA, versus ϕ is shown in Figure 5-10. The trend is for NA to increase gradually from a value of 76 percent at a ϕ of 3.0 to about 85 percent at a ϕ of 0.8. Although not a clear trend, it appears that weight loss increases with residence time. The decrease in reaction efficiency with ϕ is a result of the limited oxygen available for carbon burning at high ϕ. The results at high ϕ and low oxygen availability may indicate an ultimate volatile yield under SR conditions on the order of 75 percent.

This level of volatilization has been shown to be attainable for bituminous coal under high-temperature rapid pyrolysis conditions (Reference 7). As can be seen from Figures 5-9 and 5-10, this is not the case since NA is generally greater than NG. It can be speculated that the unaccounted combustibles escape the char sampling system in the form of tars or soot, which are not easily captured by the water spray in the exhaust.

The difference between NG and NA, for data where NA values are available, are plotted in Figure 5-11. The figure shows that the amount of evolved uncombusted material rises to about 30 percent at ϕ equals 3.0. This amount falls to zero or slightly less between ϕ equaling 1.0 and 1.2, indicating complete combustion of all material not associated with the char. The negative values found between ϕ equals 1.0 and 1.2 are

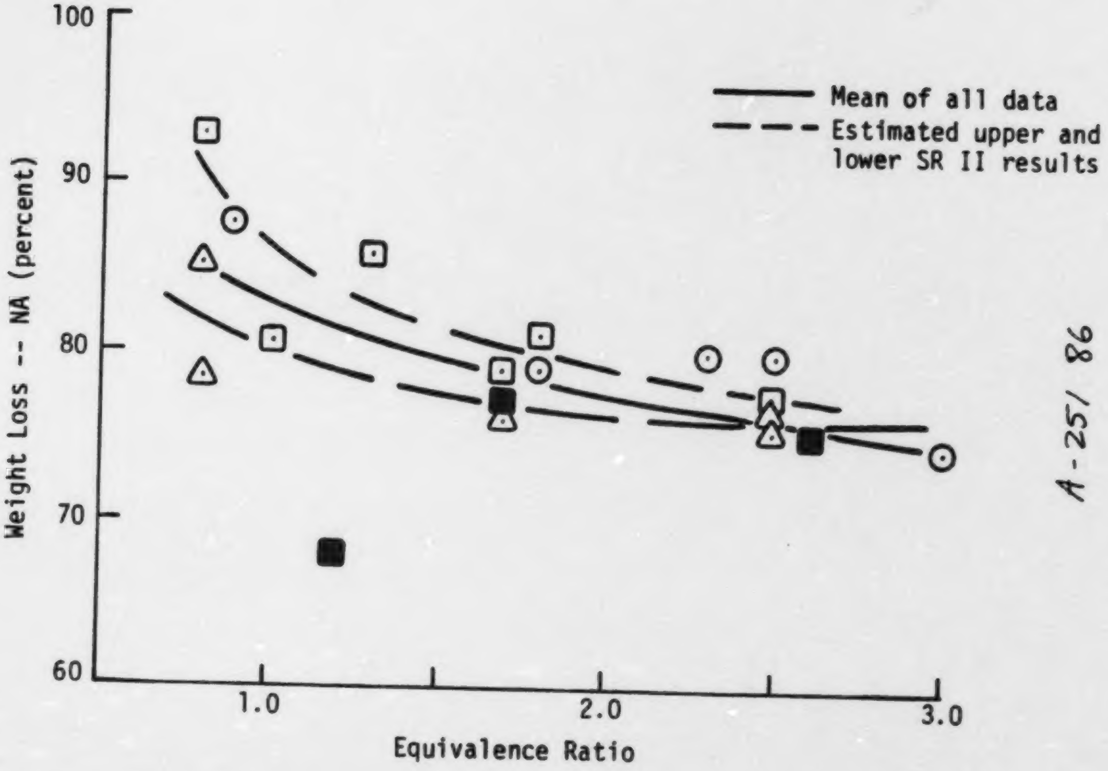

A-251 86

Figure 5-10. Weight Loss Versus Equivalence Ratio; Residence Time Ranges:
SR II: △ 44 to 50 ms; ○ 55 to 60 ms; □ 85 to 103 ms;
SR I: ■ 20 ms

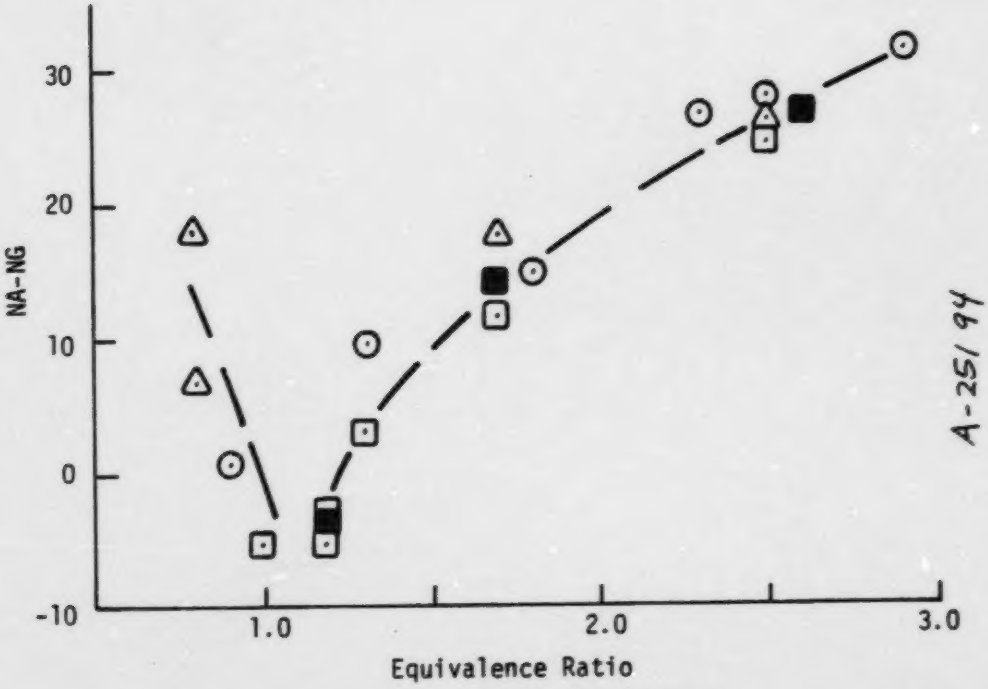

A-25194

Figure 5-11. Difference Between Weight Loss, NA, and Extent of Reaction, NG, with Equivalence Ratio; Residence Time Ranges: SR II: △ 44 to 50 ms; ○ 55 to 60 ms; □ 85 to 103 ms; SR I: ■ 20 ms

a result of either the inaccuracies associated with the calculation of NG, or low values of NA due to ash loss. The positive values at ϕ equals 0.8 might be due to poor combustion efficiency as the reactor approaches extinction. The SR II results show that as residence time increases, the amount of uncombustibles decreases. Uncombusted matter from the SR I reactor is comparable to the SR II results. For the SR I results the lower reaction efficiencies, observed in Figure 5-9, are compensated for by the lower weight losses, observed in Figure 5-10, yielding equivalent uncombustibles as compared to SR II results. This indicates that the lower reaction efficiencies for SR I are due to lower particle weight loss and not due to lower gas phase reaction rates.

Figure 5-12 shows the char hydrogen reaction efficiency, NH, char volatile matter reaction efficiency, NVM, and char nitrogen reaction efficiency, NN, versus weight loss based on ash, NA. The volatile matter reaction efficiency is based on the ASTM volatile measurement technique. This measurement is made at much lower temperatures than combustion temperatures. Pyrolysis studies (Reference 7) have shown that the ultimate volatile yield is strongly dependent on the volatilization temperature. Therefore, the ASTM volatile measurement is a measurement of the relative degree of volatilization, with the ultimate volatilization at combustion temperatures probably being greater than this value.

In the case of hydrogen and volatile matter, the char contains less than 10 percent of the original amounts of material. The loss of hydrogen and volatiles are fairly constant over the range of weight loss with ϕ, residence time, dilution, and reactor size not influencing the results significantly.

A-25176

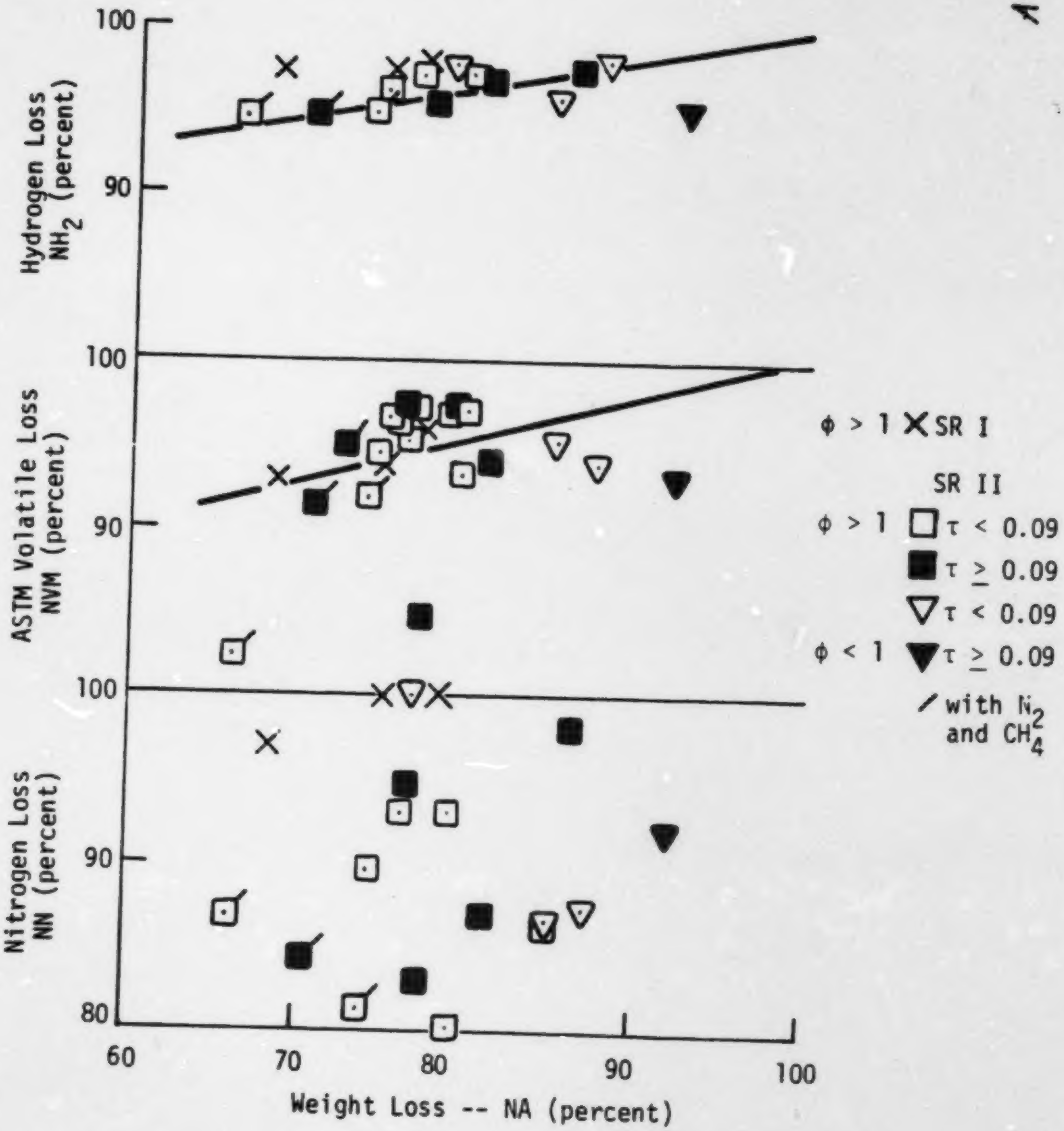

Figure 5-12. Variations of Nitrogen Loss (NN), ASTM Volatile Matter Loss (NVM), and Hydrogen Loss (NH$_2$) with Total Coal Weight Loss (NA)

The fuel nitrogen loss results show a much broader spread in data over the measured weight loss range. No clear trend of nitrogen loss, with ϕ or residence time is evident from the data. However, the high values for SR I results and the low values for SR II results with dilution indicate a possible variation with temperature.

Figure 5-13 shows the variation of fuel nitrogen and volatile matter with temperature. There appears to be some evidence for an increase in fuel nitrogen loss with increasing temperature. The volatile matter loss, except for a few points, seems to be independent of temperature.

These results indicate that, for all conditions where particle compositions were measured, volatilization was nearly complete for both SR I and SR II. The nitrogen loss results show that, for even at the lowest temperature, over 80 percent of the fuel nitrogen has been removed from the coal either by pyrolysis or oxidation. Also, at the highest temperatures measured, nearly all of the nitrogen is removed from the coal. Two SR I conditions at high temperature show 100 percent loss of fuel nitrogen.

5.2.3 Fuel Nitrogen Reactions

One of the primary goals of this program was to provide information on the mechanisms of fuel nitrogen conversion to NO. In this regard, NO emissions were measured in all 41 tests, while HCN and NH_3 concentrations were measured in 24 of the tests. All coal combustion tests were conducted using gas mixtures of air with nitrogen and/or natural gas, or air alone. No attempt was made to burn coal in gases without nitrogen although it is realized that nitrogen in the combustion air can contribute (Reference 10) to total NO production.

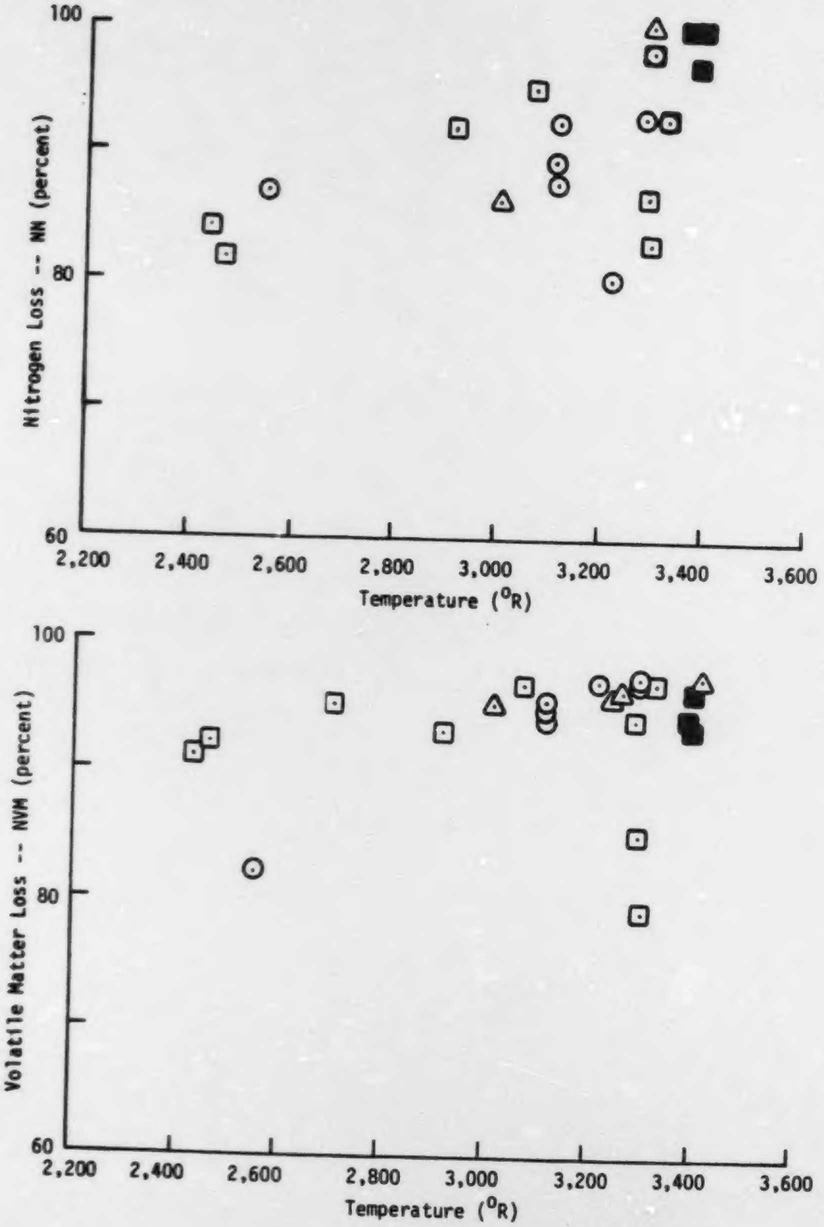

A-251 94

Figure 5-13. Variation of Volatile Matter and Fuel Nitrogen with Gas Temperature; Residence Time Ranges: SR II: △ 44 to 50 ms; ○ 55 to 60 ms; □ 85 to 103 ms; SR I: ■ 20 ms;

Percent nitrogen conversions to NO (NOC) HCN, (HCNC), and NH_3 (NH_3C) have been calculated based on the input flows of gas and coal nitrogen according to the following relation:

$$\text{Percent Conversion (NOC, HCNC, NH}_3\text{C)} = \frac{\text{Concentration (NO, HCN, NH}_3\text{)}}{\text{Maximum Nitrogen Conversion}}$$

$$\text{Maximum Nitrogen Conversion} = \frac{\dot{N}_{NC}}{\dot{N}_{air} + \dot{N}_{N_2} + \dot{N}_{N_G}}$$

where $\dot{N}$ is a substance molar flowrate and the subscripts NC and NG represent coal nitrogen and natural gas. This expression cannot be considered exact due to molar increases primarily because of the formation of CO. However, the associated error should be less than 3 percent of the maximum conversion due to presence of atmospheric nitrogen. The results are reported in terms of maximum conversion although NN was found to be less than 100 percent. Where values of NN exist, differences will be noted. Based on nitrogen of the char, the difference between NOC (or HCNC or NH_3C) and the true maximum conversion is less than 6 percent.

For all data, NOC versus ϕ is plotted in Figure 5-14. Likewise, the HCNC values are shown in Figure 5-15. Values for NH_3C are not plotted since it is always less than 0.1 percent with the exception of one point (4.3 percent).

Figure 5-14 shows NOC generally decreasing with ϕ. The data shows wide variations for each ϕ specified. As will be shown later, the variation in NOC is due primarily to residence time effects.

Figure 5-14 also shows that the lowest nitrogen conversion results agree with results obtained in a laminar flow reactor study using bituminous and lignite coals (Reference 25). Conversion results obtained

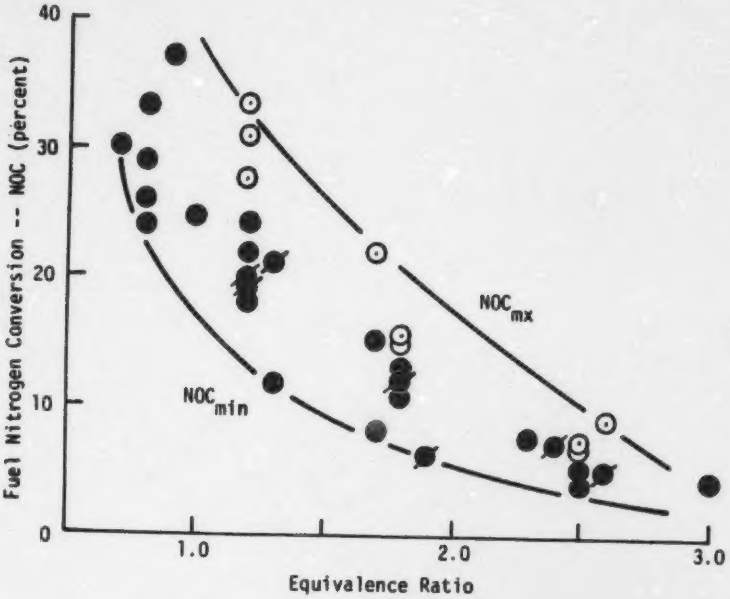

A-251 92

Figure 5-14. Fuel Nitrogen Conversion to NO with ϕ SR I Data ○ ; SR II data ●, with N_2 Addition ⊘

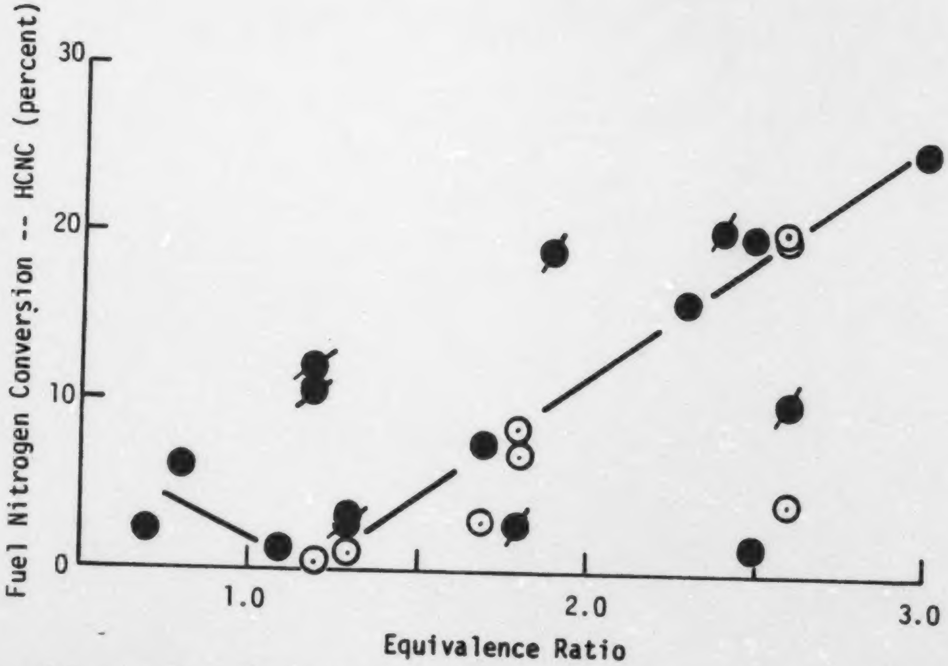

A-251 91

Figure 5-15. Fuel Nitrogen Conversion to HCN with ϕ SR I Data ○; SR II Data ●, with N_2 Addition ⊘

at shorter residence times fall above the laminar flow reactor results. The lower nitrogen conversion values are associated with the longer residence time SR II reactor results. The HCN data (Figure 5-15) shows the opposite trend with HCNC increasing with ϕ. Its value tends to zero near apparent stoichiometric conditions. Values of HCNC during N_2 addition seem slightly above and below values obtained without N_2 addition. Also, less variation is seen due to changes in τ_{sg} (SR I versus SR II). As can be seen in Table 5-2, the SRI results shows that HCNC definitely increases with τ_{sg}.

The general relations between $HCNC_{avg}$ and NOC_{mx} (SR I) and NOC_{min} (SR II) versus ϕ have been transferred to Figure 5-16 and the sum of $HCNC_{avg}$ and NOC_{mx} and NOC_{min} have also been plotted. The sum for NOC_{mx} remains flat at about 29 percent between ϕ equaling 1.8 and 3.0 with HCNC and NOC_{mx} emissions counterbalancing. At values of ϕ less than 1.8, the sum increases due to increases in NOC_{mx}. Because of the much sharper drop of the longer residence time NOC_{min} results, the sum of NOC_{min} and $HCNC_{avg}$ exhibits a minimum at an equivalence ratio of approximately 1.3. The minimum observed at long residence times and the lack of a minimum at short residence time is similar to behavior observed for staged coal combustion where first stage residence time and ϕ were varied (Reference 22).

Figure 5-17 shows NOC versus ϕ for groupings by residence time range. Also indicated are measured temperature ranges. As mentioned earlier, NOC values were calculated assuming complete removal of all fuel N. Also, NOC ignores the NO contributions from atmospheric N conversion. The variability of NOC because of incomplete fuel N ejection is also shown

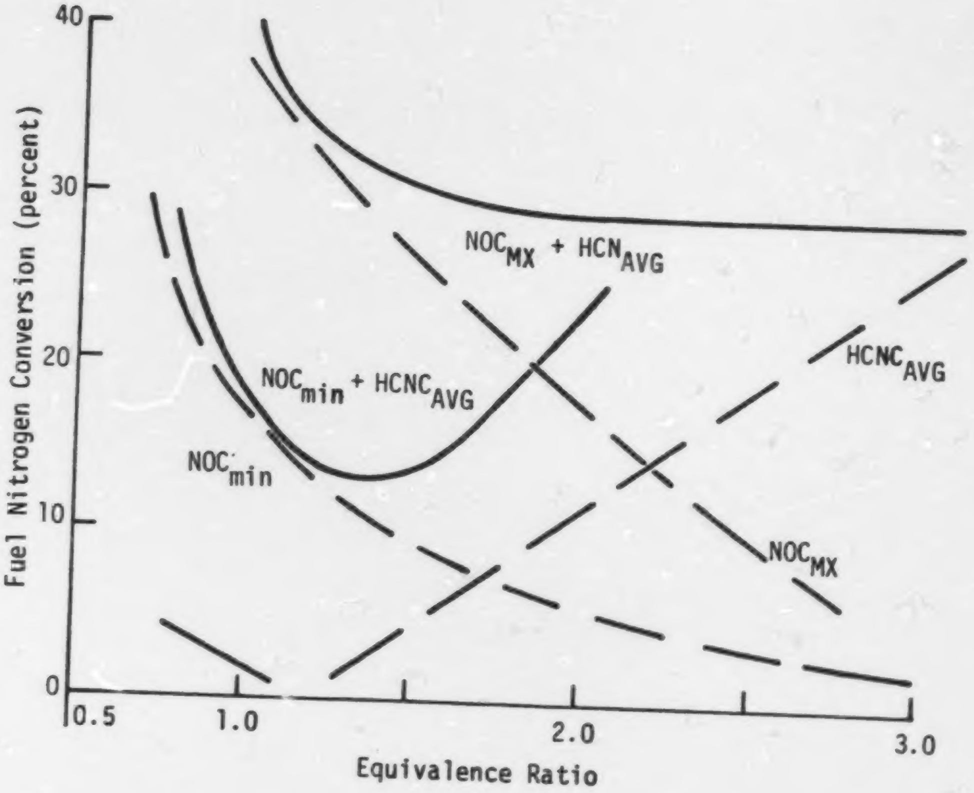

A-25191

Figure 5-16. Total Maximum Conversion Versus Equivalence Ratio

A-251 82

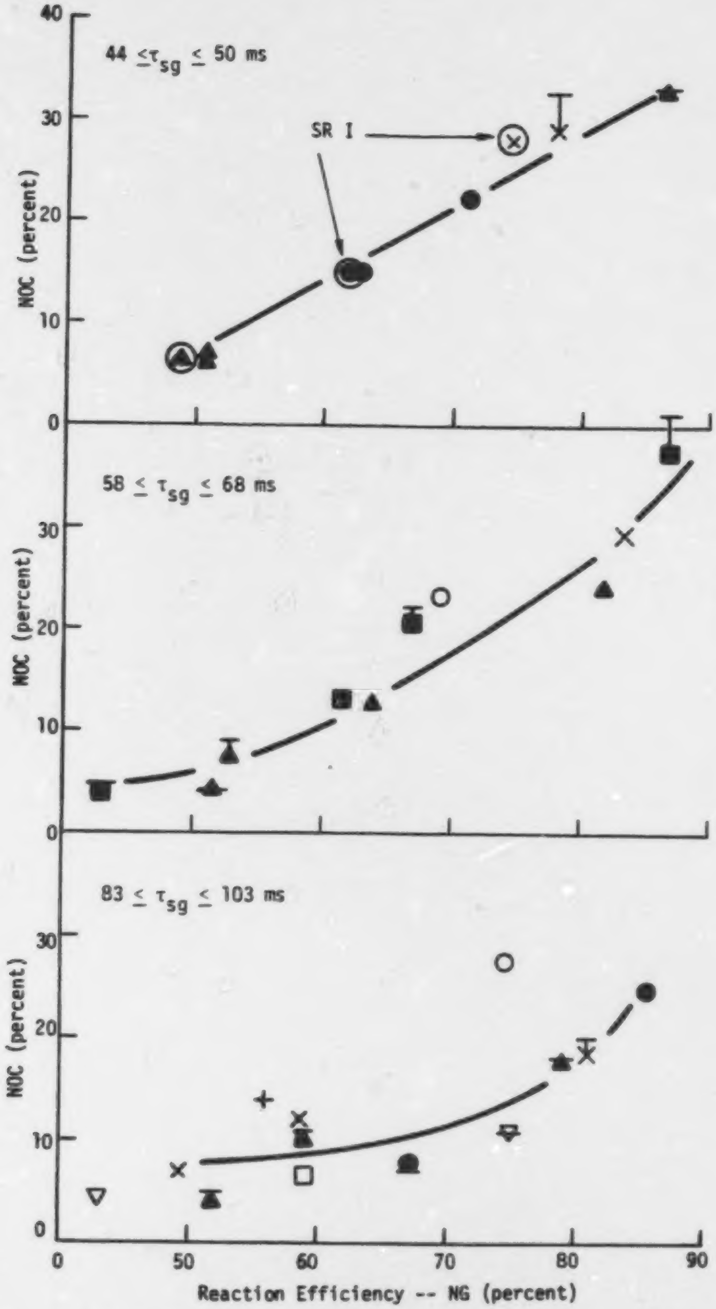

Figure 5-17. Fuel Nitrogen Conversion Versus Equivalence Ratio, Effect of Varying Residence Time and Temperature; ● 3,400° to 3,301°R; ▲ 3,300° to 3,201°R; ■ 3,200° to 3,101°R; × 3,100° to 3,001°R; ○ 3,000° to 2,901°R; △ 2,900° to 2,801°R; □ 2,800° to 2,701°R; ▽ 2,700° to 2,601°R; + 2,405°R (Conversion correction due to char nitrogen content indicated by (-))

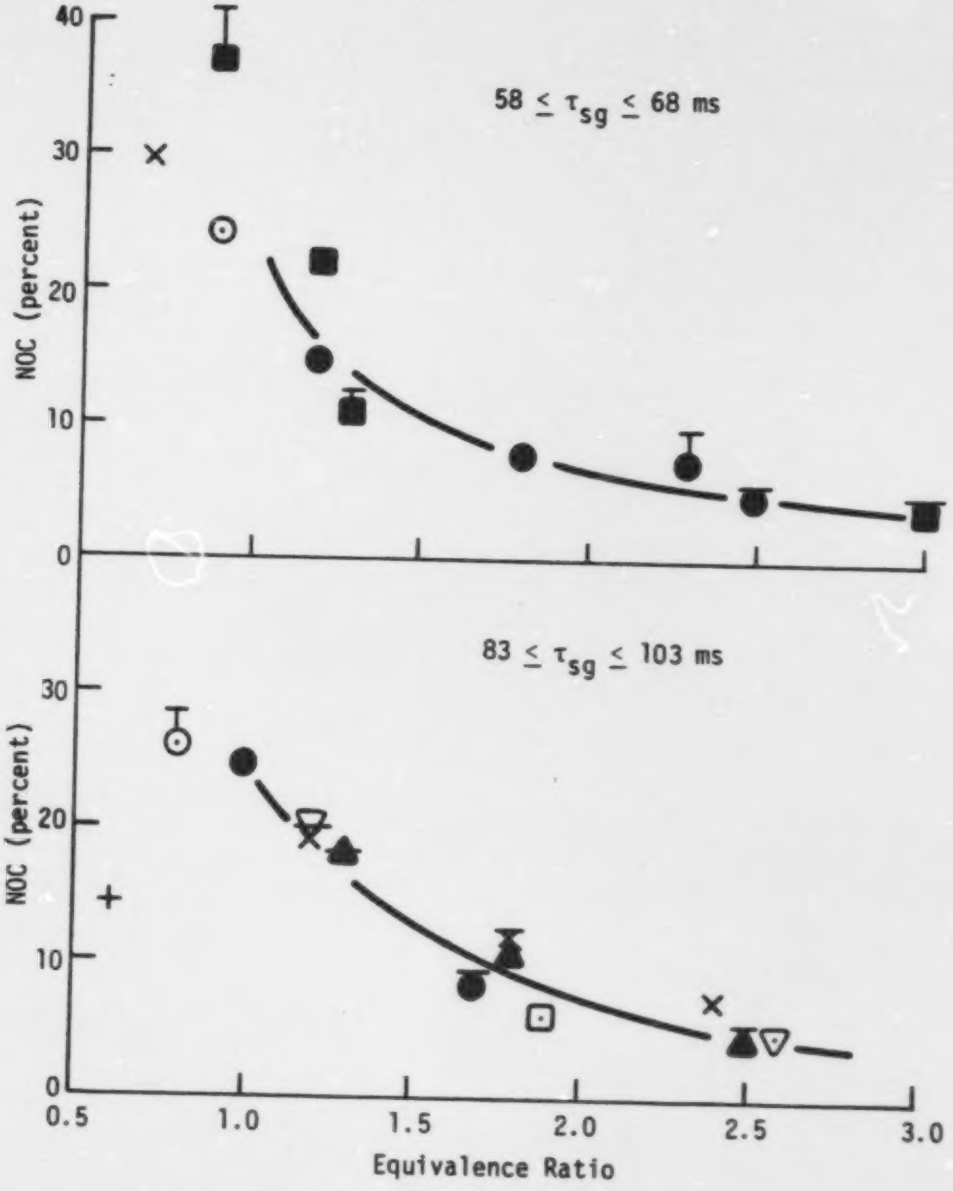

A·257 84

Figure 5-17. Continued

in the figure and for the most part, consideration of NN does not seem to increase NOC by more than about 3 percent.

These results show that the values of NOC do not seem to be strongly influenced by temperature in any clearly observable manner, possibly with the exception of data taken at ϕ below unity. For ϕ less than one, lower T, for cases possibly near extinction, gives lower NOC. In addition, the curves formed by the data ($\phi > 1$) are fairly well defined and show similarity between τ_{sg} ranges. The general shape of the curve of NOC versus ϕ has been observed in other studies (Reference 25). It tends to decrease as ϕ increases. Generally, the levels of NOC (for ϕ fixed) decrease with increasing τ_{sg}.

Figure 5-18 shows NOC plotted against calculated gas phase reaction efficiency, NG, in a manner similar to the previous figure. The curves generally are similar to those to be expected after examining Figure 5-17. However, at the longer residence times, the data exhibits a greater degree of nonuniformity (as compared to NOC versus ϕ). The points at ϕ less than one show less scatter indicating that the lower conversion for reduced T at ϕ less than one is a reaction efficiency effect.

A plot of NOC versus τ_{sg} for various values of ϕ (Figure 5-19) clearly shows the effect of τ_{sg}. As τ_{sg} increases, NOC decreases with the rate of decrease being less rapid as ϕ increases. However, the maximum value of NOC (at small τ_{sg}) increases with decreasing ϕ. Figure 5-19 also suggests that the peak in NOC occurs at τ_{sg} less than 20 ms. Probing results in coal flames show NO increasing at times under 200 ms (Reference 26). However, resolution in these experiments was such that it did not permit investigation of NOC at shorter times.

A-35183

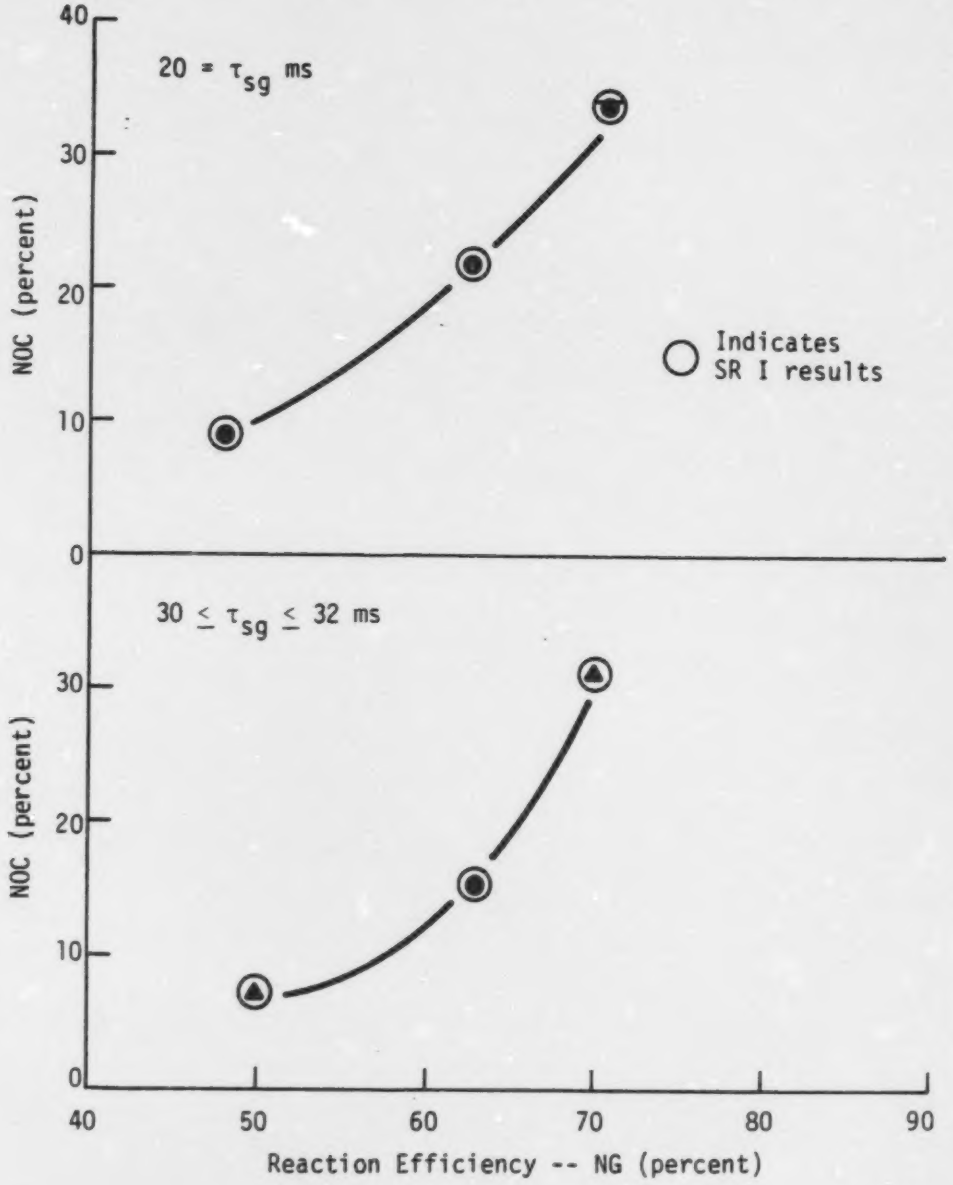

Figure 5-18. Fuel Nitrogen Conversion Versus Reaction Efficiency, Effect of Varying Residence Time and Temperature; ● 3,400° to 3,301°R; ▲ 3,300° to 3,201°R; ■ 3,200° to 3,101°R; × 3,100° to 3,001°R; ○ 3,000° to 2,901°R; △ 2,900° to 2,801°R; □ 2,800° to 2,701°R; ▽ 2,700° to 2,601°R; + 2,405°R (Conversion correction due to char nitrogen content indicated by (-))

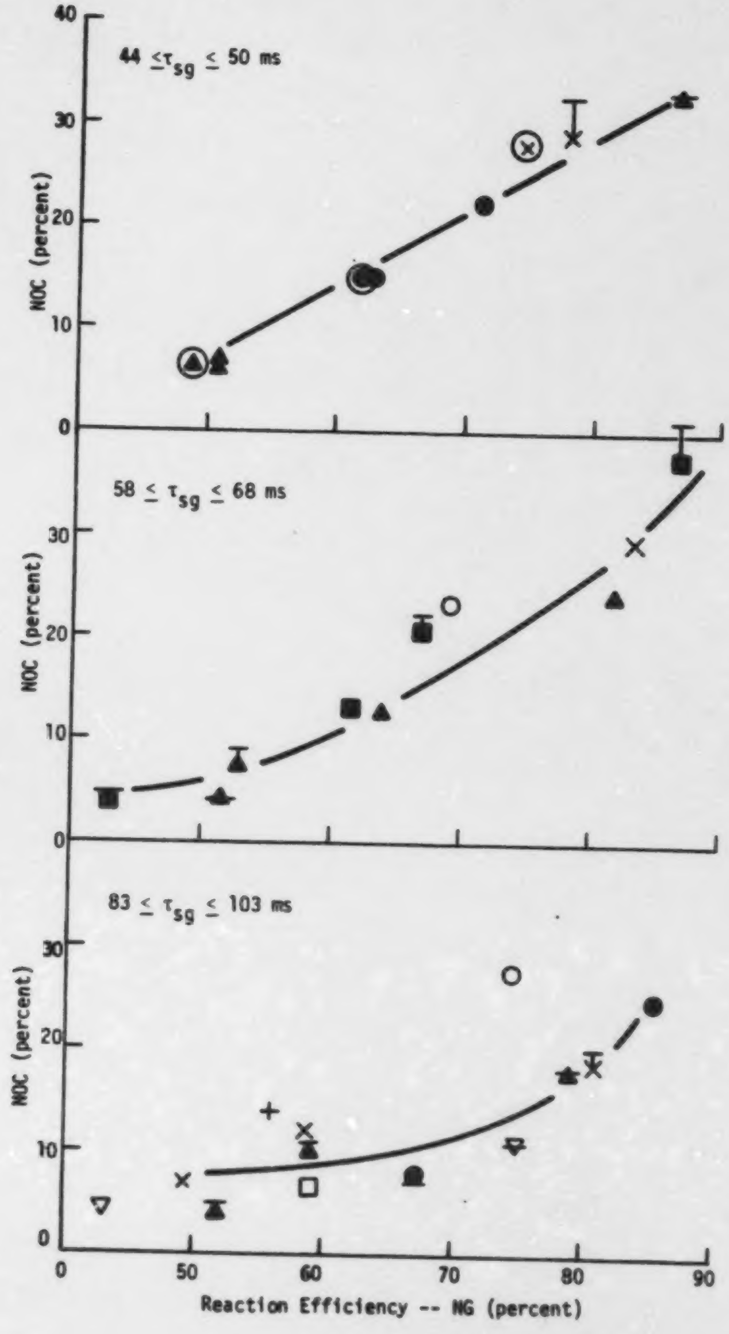

A-251 82

Figure 5-18. Continued

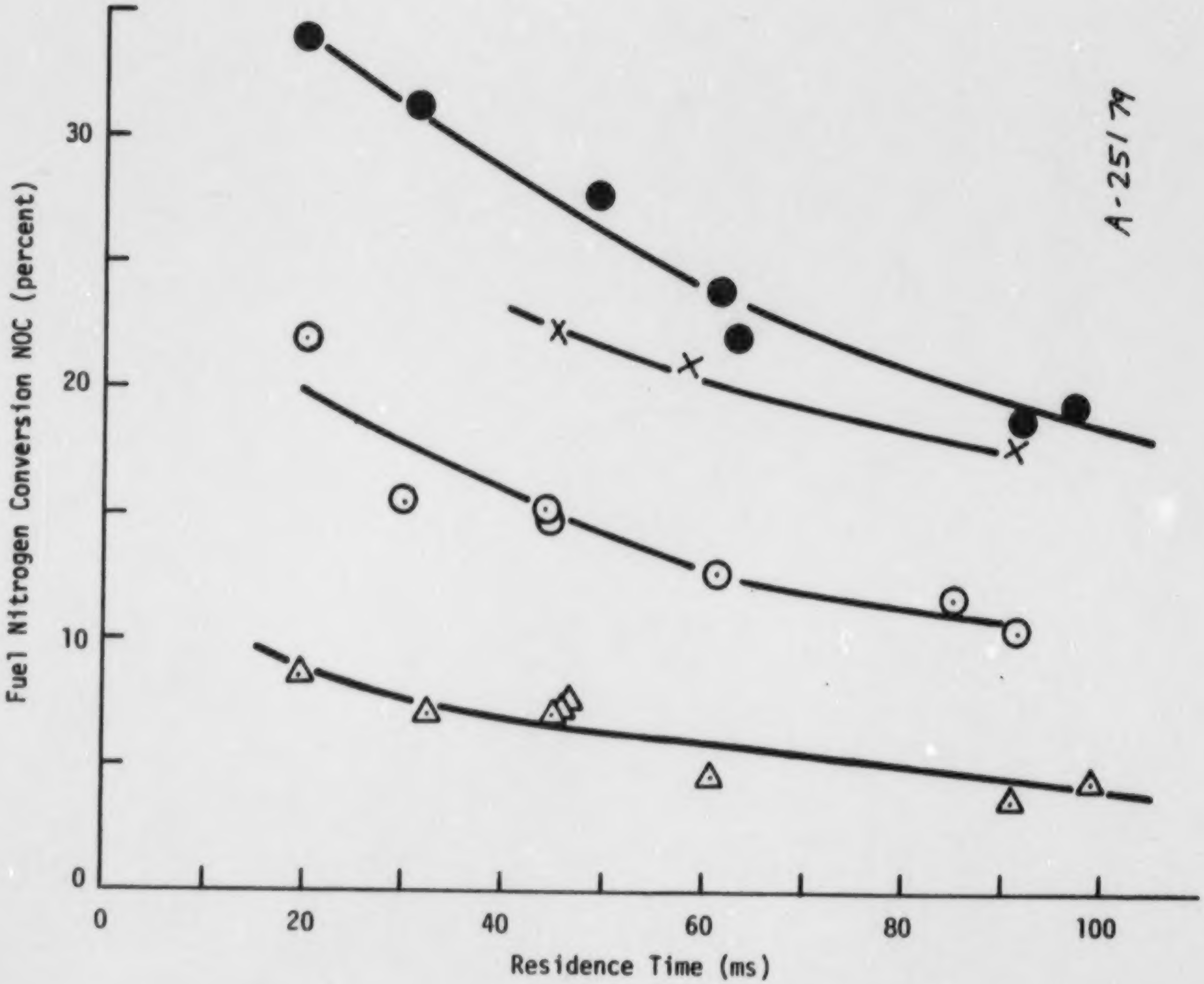

A-25179

Figure 5-19. Fuel Nitrogen Conversion Versus Residence Time for Varying Equivalence Ratio of ● 1.2; x 1.3; ○ 1.7 to 1.8; △ 2.5 to 2.6

The maximum value of NOC can be determined using a simple approach. The ln (NOC) versus τ_{sg} is plotted for various values of ϕ. The result is shown in Figure 5-20. The points form a fairly straight line when plotted in this manner, and with the exception of the data for ϕ equaling 1.3, the Y-intercept values decrease with increasing ϕ. The straight line behavior indicates a decay rate directly proportional to NOC. The rate of reduction (percent/ms) also decreases with increasing ϕ. Figure 5-21 shows the decrease of this decay rate as ϕ approaches 1. Limited data at $\phi = 0.8$ indicates that the decay, though smaller, is still possible for ϕ less than 1. Figure 5-22 gives NOC as a function of reaction efficiency. As can be seen from this figure, both early time fuel lean ($\phi < 1$) and rich ($\phi > 1$) conditions correlate somewhat linearly with reaction efficiency, NG. Later time NOC results fall below early time results. The relatively linear correlation of the early time NOC results with reaction efficiency might indicate that, as the fuel is oxidized to CO_2, CO, and H_2O, a fraction of the nitrogen components associated with these fuel components are oxidized to NO. The other fraction might react to form HCN, N_2, or pass out of the reactor in a more complex molecular form.

Taking reaction efficiency, NG, as a measure of the degree of fuel oxidation, fuel nitrogen conversion to NO, NOC, is normalized by NG and plotted versus ϕ in Figure 5-23. These results show that, for a given residence time, normalized NOC decreases with equivalence ratio. However, instead of an exponential type decrease, the normalized NOC decreases almost linearly with ϕ. This slower linear decay with ϕ shows that NOC is not as strongly varying with when the oxidation potential, as measured by NG, is considered.

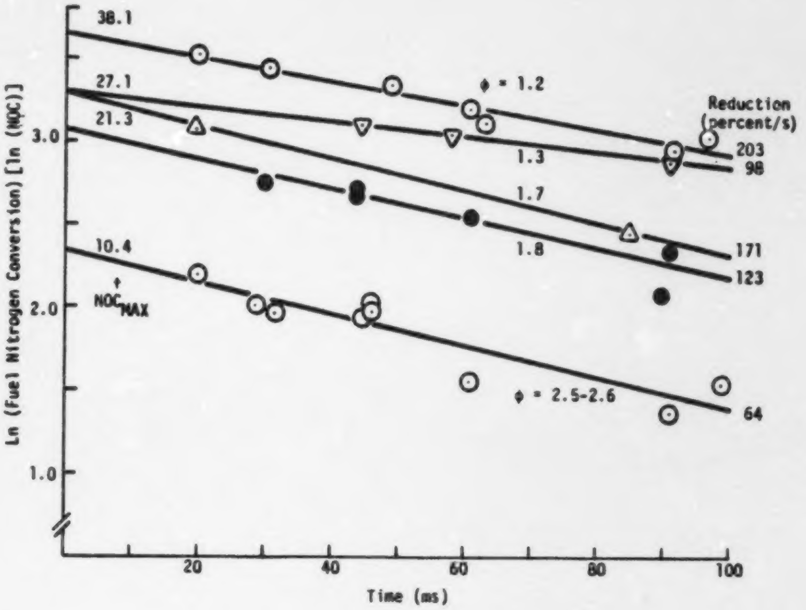

A-251 75

Figure 5-20. Ln (Fuel Nitrogen Conversion) (NOC) Versus Residence Time for Various Equivalence Ratios

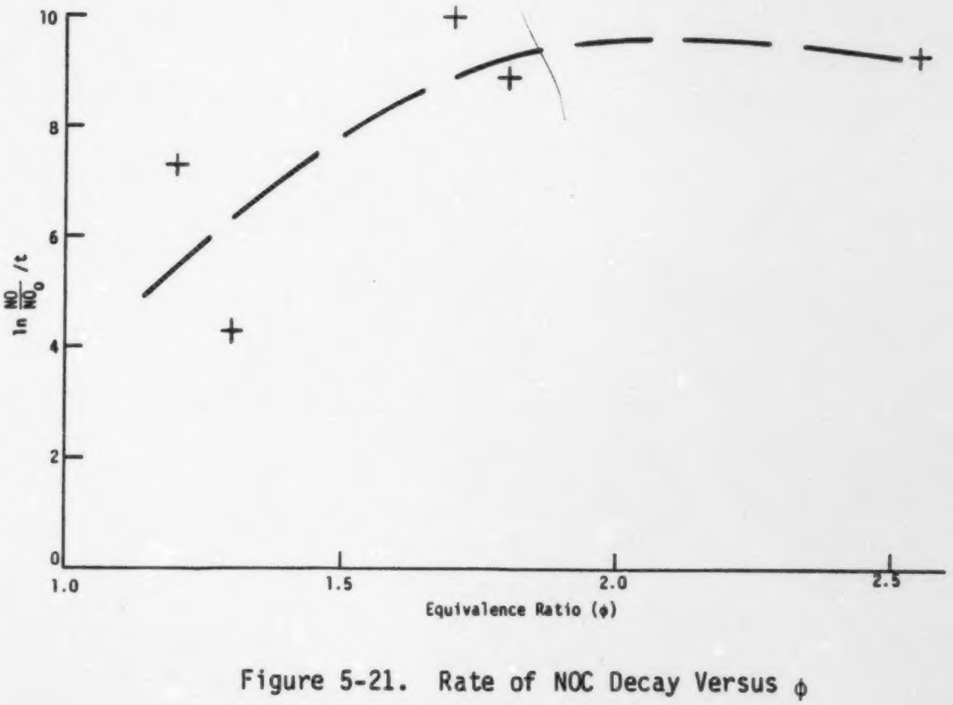

A-257 81

Figure 5-21. Rate of NOC Decay Versus ϕ

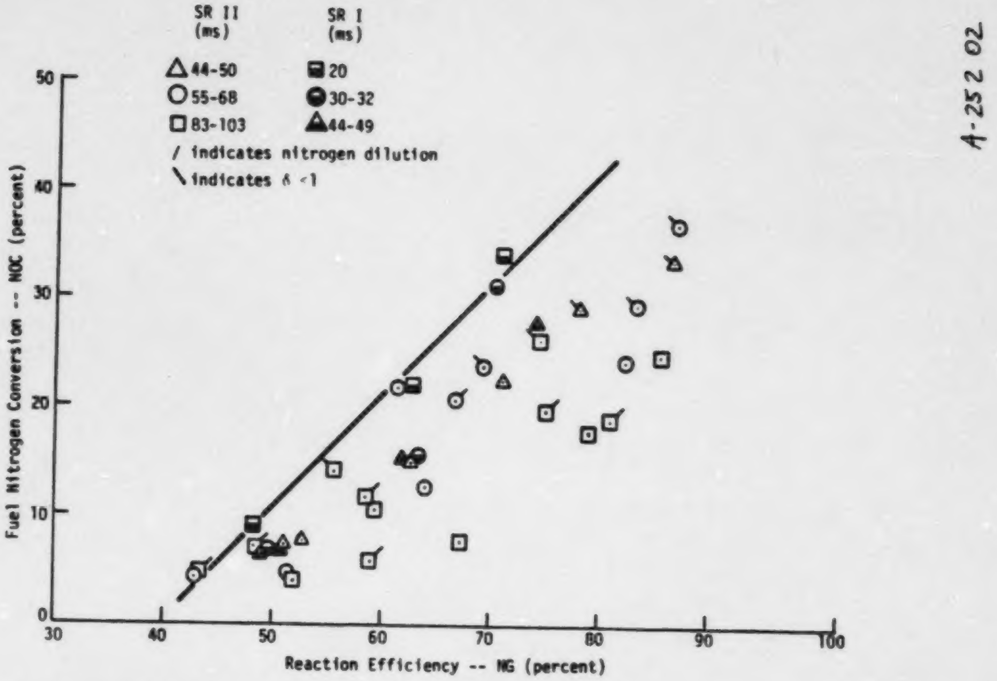

Figure 5-22. Fuel Nitrogen Conversion Versus Reaction Efficiency

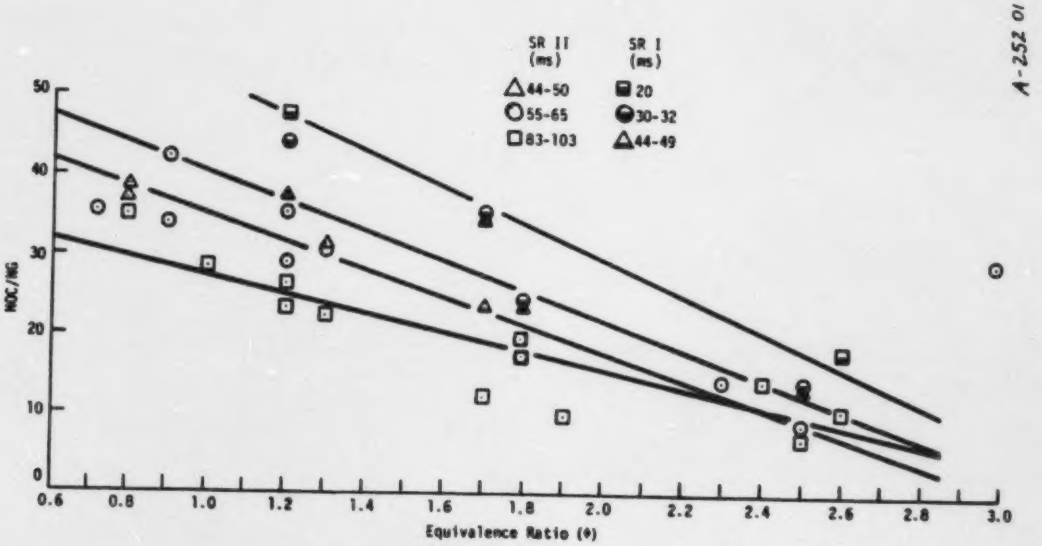

Figure 5-23. Normalized NOC Versus ϕ

Recognizing the strong variation of NOC with reaction efficiency, NG, the cyanide conversion efficiency, HCNC, is added to NOC and plotted with respect to NG in Figure 5-24. The sum of NOC and HCNC presented in Figure 5-24 does not show a trend with NG except that the highest sums appear to fall near highest NGs. From this figure it can be concluded, with some exceptions, that from roughly 13 to 32 percent of the fuel, nitrogen can be converted into NO and HCN over the range of ϕ and τ_{sg} tested.

As mentioned, while at ϕ greater than 1, the relation between NOC, ϕ, and τ_{sg} was fairly predictable, it was also shown that temperature did not directly affect NOC. The relationship between NOC, NG, ϕ and temperature at ϕ less than 1.0 does not follow the same patterns as for ϕ greater than 1.0.

Figure 5-25 shows NOC versus NG and temperature for data where ϕ is less than unity. In the figure, NOC increases with increasing NG, and temperature. The insensitivity with τ_{sg} is probably due to the limited amount of NOC decay with time for ϕ less than 1. The good correlation of NOC with temperature might reflect the strong correlation of temperature and reaction efficiency for ϕ less than 1. As shown in Figure 5-25, NOC is linearly related to NG, which is probably the dominant parameter for ϕ both greater and less than 1.

5.2.4 Coal/Air/N_2/CH_4 Devolatilization Tests

Three tests were performed in SR II using coal/air/N_2/CH_4 mixtures. They correspond to SR II test numbers 29, 30, and 31 (Table 5-2). These tests were conducted primarily to investigate particle decomposition effects in a low available oxygen environment. The CH_4/air equivalence ratio for these tests ranged from 0.8 to 1.0. It

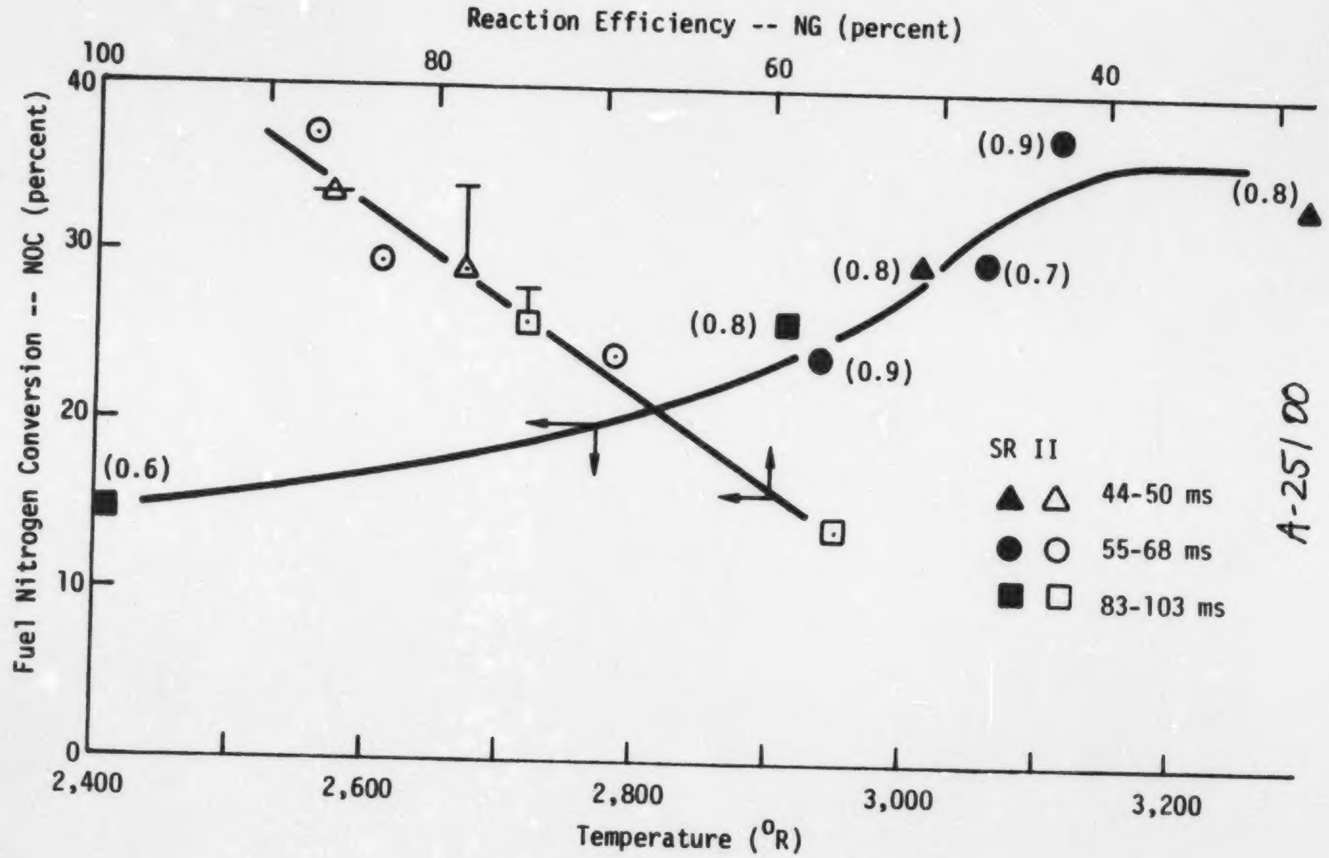

A-25100

Figure 5-24. Fuel Nitrogen Conversion (NOC) Versus Gas Phase Reaction Efficiency (NG)and Temperature for Equivalence Ratios Less than 1 (Equivalence ratios shown in parenthesis, conversion correction for char nitrogen content indicated by (-))

A-251-80

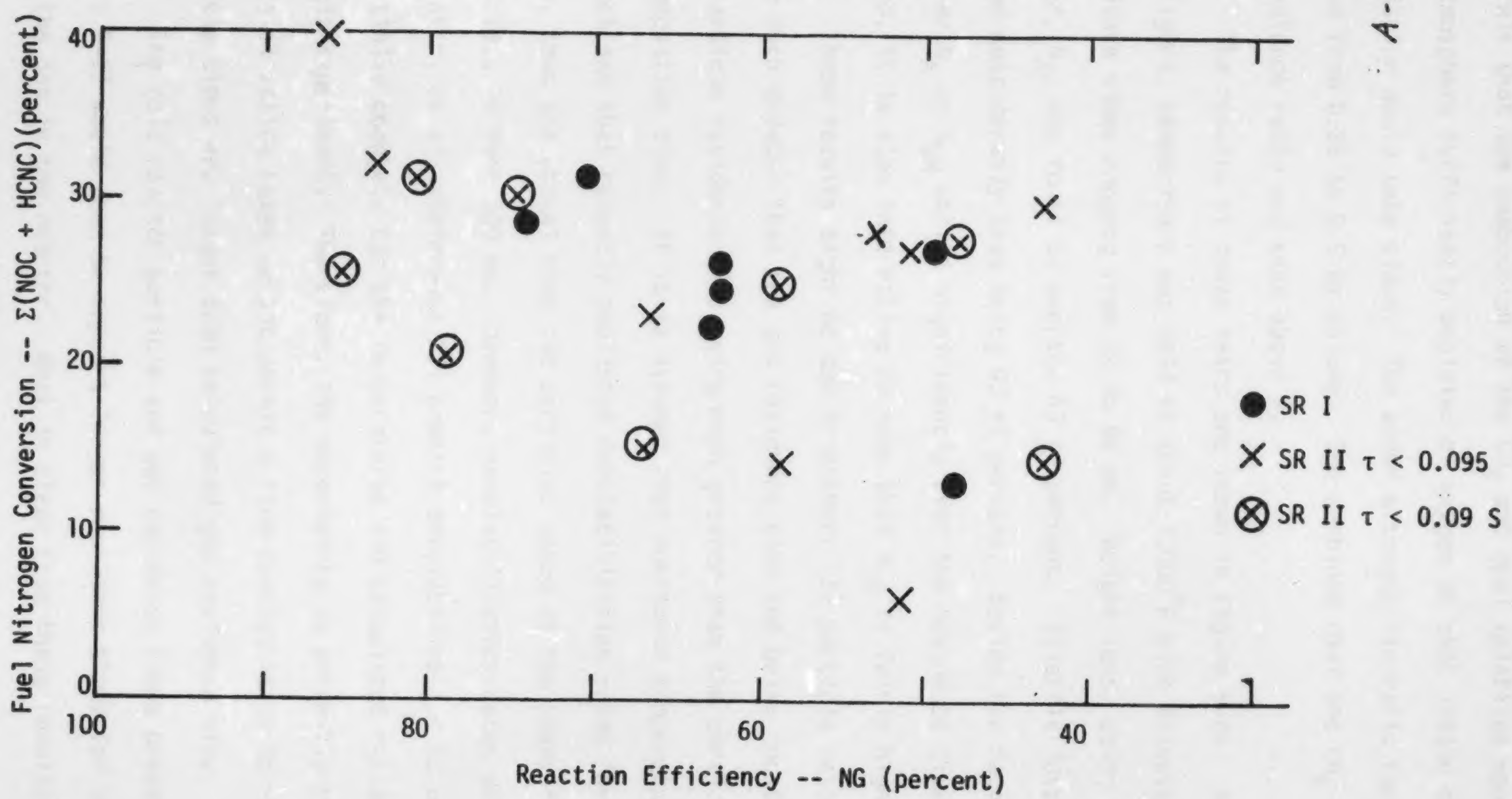

Figure 5-25. Fuel Nitrogen Conversion Σ (NOC + HCNC) Versus Gas Phase Reaction Efficiency (NG)

was felt that the combustion of the CH_4 and coal volatiles would provide an atmosphere sufficiently depleted of oxygen so that little char combustion would take place. The added nitrogen/air ratio for the tests ranged from 0.35 to 0.5 by volume. The combined coal and CH_4 equivalence ratio was kept above 2.

The results of these tests are shown in Figure 5-26. As shown in the figure, temperature was held at about 2,000^oF with calculated gas residence times ranging from 52 to 96 ms. Weight loss, using ash as a tracer, N_A, was found to average 63 ±8 percent. Volatile loss, N_{VM}, varied considerably less being 93 ±2 percent. Beside the fact that neither N_A or N_{VM} varied significantly over the residence times tested, it is also interesting to note that N_{VM} is fairly high.

These results might be due to either: (1) particle residence time being much greater than the gas residence time and being constant, or (2) particle residence time being much greater than the particle decomposition time. If it is assumed that monitored temperatures are correct and that recently published devolatilization rates (Reference 7) apply, then the actual time the particles spend in the chamber must, in all cases, be over 100 ms. However, devolatilization rates obtained by Ubhayakar, et al. (Reference 27) predict devolatilization to be essentially complete for the temperatures and calculated residence times of this experiment. Therefore, the uncertainty in presently known devolatilization rates do not permit a firm conclusion as to whether particle times are longer than calculated gas residence time.

The cold reactor particle and gas residence times presented in Figure 5-27 would seem to support longer residence times for the particles than the gas in the reactor. What is clear from these results is that,

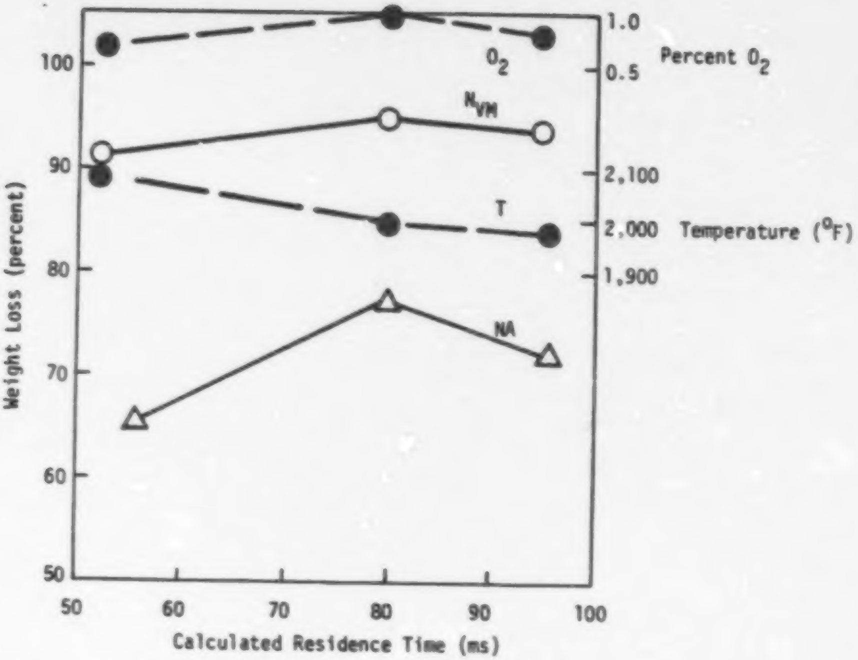

A-25178

Figure 5-26. CH_4/Air/Coal N_2/Combustion Volatile Matter Loss (NVM), and Total Weight Loss (NA) With Time at Low Temperature

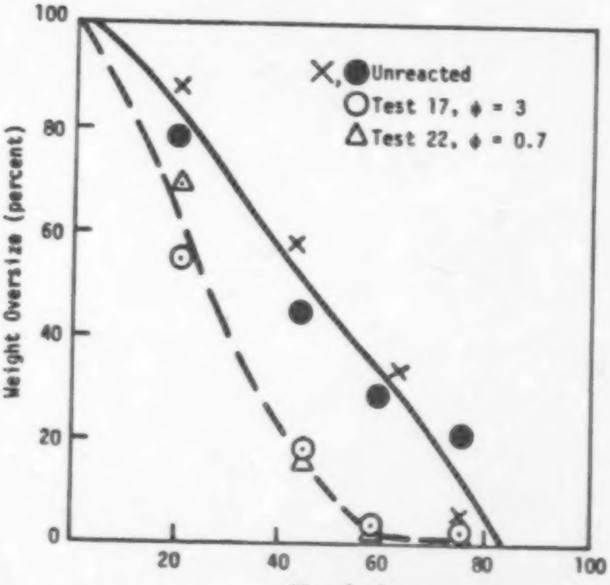

A-25177

Figure 5-27. Comparison of Unreacted Coal Size Distribution, ●, X, with Coal Reacted at Equivalence Ratios of 0.7 △ (SR II Test 22) and 3.0 ⊙

even for low temperatures and limited oxygen concentrations, particle decomposition is essentially complete for the residence times tested. In addition, the dominant processes influencing the results are gas phase reactions and gas phase/char reactions, not decomposition reactions.

5.2.5 Reacted Particle Size Distribution

Two of the char samples collected during SR II testing were classified using wet sieving. The results are shown in Figure 5-27. As indicated in the figure, the size distributions of the two reacted samples are very similar. The reacted sample has a smaller mean particle size of about 30 μm. The original mean particle size was 50 μm. From Table 5-2, tests 17 and 22, it is seen that the residence times and temperatures are similar; however, equivalence ratios (and NG) significantly differ.

Particle swelling and surface combustion change particle size. Particle consumption results presented in Figure 5-10 show that particle weight loss does not vary widely for ϕ between 0.7 and 0.3. This constancy of particle consumption might be the reason for the nearly equivalent particle size distributions for the reacted particles presented in Figure 5-27. The smaller mean size of the reacted particle distributions might be due to the roughly same degree of carbon consumption or particle fracture between the two cases tested or particle deposition in the reactor.

It is possible that the larger particles do not follow the gas and impact with the reactor walls more readily than the smaller particles. With the walls hot and covered by a slag layer, a fraction of these large particles might stick and burn on the wall leading to a smaller particle size distribution exiting the reactor. This particle wall sticking explanation of the smaller particle size distribution is consistent with the observed small buildup of slag on the inside of most reactors tested and is probably the mechanism acting to reduce the particle size distribution.

SECTION 6

RESULTS

6.1 SR MIXING PERFORMANCE

Under cold conditions, the helium tracer tests showed SR I and SR II model reactors to be well mixed (gas phase) over the range of residence times tested. This tracer study also showed that a single reactor probably cannot cover a wide range of residence times and remain well mixed. The best approach is to use multiple reactors of similar geometry, as was done in this study, or optimize several reactor and jet geometries for each residence time range. Parameters found to influence reactor mixing included reactor geometry, feed, jet size, number, placement, and orientation.

Particle mixing studies were not as successful as the gas mixing studies. Both particle flow startup and shutoff tests were attempted to define particle residence time. Instrumentation sensitivity prevented low concentrations of particles from being used as a tracer. This adversely affected the particle startup results. The particle shutoff results were strongly influenced by the reentrainment of deposited particulate. The particle startup and shutoff tests gave different particle residence times for the same calculated gas phase residence time. However, both techniques did show that the particles are in the reactor longer than the gas. This is reasonable for the small diameter reactors where high velocity injected particles probably decouple from the gas and impact with the reactor walls. After one or several collisions with the walls, the particles lose sufficient velocity to allow a coupling with the gas phase. The time spent when the particle is decoupled from the gas then represents the increase in particle residence time over the gas phase residence time. In addition to the increase in residence time, the particles, because of the decoupling with the gas, will also have a higher particle concentration in the reactor than what would be calculated based on inlet flowrates.

The particle decoupling observed under cold conditions should be somewhat improved under hot conditions where gas phase viscosity, and thereby small particle drag coefficients, are improved. Some full-sized combustors will also probably experience some form of gas/particle decoupling as was observed in this study, particularly in highly back-mixed regions near the high velocity fuel jet.

6.2 OPERATING CHARACTERISTICS

There are several problems associated with operation and data acquisition of the reactor system. Basically, these problems relate to slagging and temperature measurement. Slagging caused the bridging and clogging of the reactor exhaust resulting in a dangerous buildup of pressure in the reactor and subsequent cracking. A larger reactor exhaust seemed to alleviate this problem. Temperature measurement of the gases in the reactor is in error because of the close proximity of cooler reactor walls. A shielded thermocouple or other nonintrusive technique is needed to more accurately measure gas temperatures. Both of these problems can be overcome through careful system redesign.

6.3 COMBUSTION AND EMISSIONS

Combustion and emission test results show continuity between SR I and SR II results in their range of overlap. Gas composition (CO, CO_2, O_2, NO, HCN) and particle results (weight loss and composition) are consistent in common residence time regimes for the two reactors. There is some difference in thermal effects between the two reactors because of surface area to volume ratio differences. However, the overall agreement between reactor results is adequate.

Generally, the combustion results suggest that particle comsumption is significant for all conditions, with volatilization nearly complete even for relatively low reactor temperatures and residence times. CO, CO_2, and O_2 concentrations were found to be independent of residence time. Particle weight loss and composition (volatile fractions, hydrogen, nitrogen) also appeared not to vary significantly with residence time. Particle consumption varied from 74 to over 90 percent depending on ϕ with the remaining volatiles in the particle being less than 10 percent. These results suggest that particle thermal decomposition events are nearly complete for the residence times tested. Therefore, variations of reactor properties with time are due to slow gas phase reactions and heterogeneous or catalyzed gas phase reactions on the char particle surface.

Examining the particle consumption and extent of fuel oxidation (CO, CO_2) results, it is evident that at ϕ's above 1, considerable unburned fuel components are present in the reactor exhaust. At a ϕ of 3.0, up to 30 percent of the fuel is in the gas phase in a form other than CO, CO_2, and H_2O. This significant fuel fraction can have a considerable impact on NO emission events.

Nitrogen conversion to NO or NOC results obtained in this study at long residence times (~100 ms) are comparable to results obtained elsewhere in laminar flow reactors (Reference 27). These results have a typical exponential type behavior with increasing ϕ. Early residence time NOC results are higher than these late time results and exhibit a decay with time to the longer residence time results. A log plot of the NOC results with time for fixed ϕ exhibits a linear decay. The NOC decay rate is strongest for high ϕ with the initial NOC levels highest for ϕ near 1. The initial NOC for ϕ both greater and less than 1 appears to correlate with extent of reaction as determined from CO and CO_2 concentrations. As fuel components are oxidized, it appears that fuel-bound nitrogen components associated with these components are also oxidized to NO. However, the fraction oxidized to NO does vary with the extent of reaction or ϕ.

Ammonia concentrations for all conditions were small, being less than 4 percent of the fuel nitrogen concentration. The hydrogen cyanide concentration, HCN, was significant, particularly for high values of ϕ. The experimental results showed that the hydrogen cyanide conversion, HCNC, increased linearly with ϕ up to levels of 25 percent at ϕ equal to 3. There was some evidence from the SR I results that HCNC increases rapidly to a plateau level as residence time increases. However, the effect of residence time on HCNC is not as clear as the effect of residence time on NOC decay.

Taking the plateau level of HCNC and the long residence time NOC results and summing the two, a curve of fuel nitrogen conversion exhibiting a minimum at a ϕ of 1.3 is produced. This behavior of fuel nitrogen conversion is consistent with long time scale staged coal combustor results obtained elsewhere (Reference 22). Similarly, taking the sum of the plateau level HCNC results and the short residence time NOC results produces a curve of fuel nitrogen conversion versus ϕ that does not have a minima. The shape of these results are consistent with short residence time staged combustion results obtained elsewhere (Reference 22).

A substantial amount of data have been gathered on combustion and emission events in a coal-fired stirred reactor. Extraction of significant mechanistic and rate information from these data requires a considerable effort using computer analyses and known elementary rate data for chemical steps. This study generated a significant amount of data that requires more detailed analysis. However, it is appropriate at this time to briefly speculate on some potential mechanisms that might operate to produce the observed reactor emissions.

As discussed previously, particle decomposition events are substantially completed for the residence times and ϕ's examined in this study. Therefore, fuel component and fuel nitrogen evolution from the particles are nearly complete for all conditions tested. As shown by the data, NO, HCN, and NH_3 production is fast, and these gases exist at the earliest residence times tested. NO concentrations exhibit their highest levels at these early times. These nitrogen compounds are immersed in an environment consisting of significant CO and unburned gaseous fuel components, including gaseous nitrogen components, for ϕ greater than or less than 1 and significant char particle concentrations for all ϕ. In this environment, the NO, HCN, and NH_3 interact chemically with CO, unburned fuel, unreacted fuel nitrogen, and char particles, and also with each other. These interactions appear to lead to a regular decay of NO with HCN remaining nearly constant with time. Mechanisms whereby this would occur are postulated below.

NO reacting with fuel nitrogen or HCN and NH_3 (Reference 28) depletes NO, HCN, and NH_3 with the major product being N_2. NO reacting with gaseous hydrocarbons (Reference 29) depletes NO and can potentially produce HCN. NO reacting either heterogeneously with the char or catalyzed by the char depletes NO and produces N_2 (Reference 23). Of course, some of the fuel nitrogen, HCN and NH_3, can be oxidized to NO. However, for the low oxygen concentrations at ϕ greater than 1, this is not favored over reduction processes noted above. In addition, HCN and NH_3 can be generated from the fuel nitrogen as residence time is increased.

These brief comments show that there are several processes deleting NO and several processes both producing and deleting HCN under rich conditions. It may then be speculated that NO decay is assured at high ϕ, whereas production and reduction processes keep HCN concentrations invariant over the residence time conditions tested in this study. At much longer residence times, as NO decays to lower levels, HCN might then begin to decay with time. Experiments at longer residence times and detailed computer analyses of the results are needed to confirm these speculations.

SECTION 7

CONCLUSIONS AND RECOMMENDATIONS

7.1 CONCLUSIONS

A unique experimental system has been developed to study pulverized coal combustion and NO_x emission formation events under a well mixed gas condition. Gas tracer experiments under cold conditions have shown the gas phase to be well stirred over the reactor system conditions tested. Particle tracer studies are not conclusive on particle mixing since there is some question surrounding the application of this technique. Initial evidence is that the particles are not fully coupled dynamically to the gas and may therefore spend more time in the reactor than the mean gas residence time.

Combustion results show that significant particle decomposition and consumption occurs even for gas residence times less than 100 ms. CO, CO_2, and O_2 gas concentrations and particle properties (volatilization, hydrogen, and nitrogen content) do not vary strongly with residence time but are primarily a function of ϕ. NO formation is rapid (NO peaks occur earlier than 20 ms, the minimum residence time measured) and decay is significant. The initial NO concentrations increase as ϕ decreases to one and the normalized decay rate increases as ϕ increases. The long residence time NO results varying with ϕ are comparable to laminar flow reactor results obtained elsewhere (Reference 25). The short residence time results represent new data on early NO decay.

NH_3 emissions were small compared to NO. HCN emissions were significant and increased linerarly with ϕ to levels of up to 25 percent at ϕ equal to 3. The HCN results did not show a strong variation with residence time except for an initial rapid rise from 20 to 30 ms for the small reactor results.

It is speculated that homogeneous and heterogeneous NO decay processes are more significant than NO production processes leading to a net decay of NO with time for the ϕ conditions tested. In the residence time ranges tested, HCN decay and production processes, some of which can be associated with NO decay, are in balance and HCN appears invarient with time.

7.2 RECOMMENDATIONS

In this study, a rather significant amount of coal combustion data were obtained under characterized reactor conditions. Due to limited resources, these data have not been fully analyzed and, therefore, have not been used to their maximum advantage.

The first and strongest recommendation is to perform an in-depth analysis of the current data to elucidate the mechanisms and rates for the fundamental processes leading to the observed results. Where possible, computer techniques and analytical models should be used to cast the final results in a form that is as near as practicable to directly applicable prediction techniques for real burners.

Since the particle residence time calibrations demonstrated a possibly poor coupling between particles and gases and since some anomalies were noted in the calibration results, more refined methods for measuring particle residence times, preferably under combustion conditions, should be examined. Simultaneously, methods to improve this coupling by changes in injector designs, stirred reactor configurations, or smaller mean particle sizes should be examined.

Based on the incomplete coupling between coal particles and gases in the reactor, an experiment can be designed such that a steady stream of pulverized coal (in a plug flow) can be passed through a hot, highly mixed combustion environment. In many respects, this would simulate the region very close to the injector of a high back-mixing pulverized coal burner. Methods identical to those used in this study can be used to quench and trap partially combusted coal particles for subsequent chemical analysis.

Since the techniques for handling and combusting coal in a stirred reactor have been developed in this study, several coals different from the current Utah coal should be examined to assess the effects of coal composition on NO_x formation.

The poor particle/gas coupling observed in the current experiments was to some degree expected based on estimates using other particle/gas coupling results. These past results showed that poor coupling would occur for particle size greater than approximately 30 μm. These same estimating procedures show that the coupling would be acceptable for particle sizes less than approximately 20 μm. Although these small particle sizes are not normal for pulverized coal, they can be obtained for liquid fuels when atomizing injectors are used. The current reactor configuration should, therefore, be applicable to the study of NO_x formation from liquid fuels. Since reactor residence times less than particle burnout times can be attained, exhaust gas trapping of unburned matter can show the relative contribution of early release volatile matter to NO_x formation.

From the results obtained to date, the stirred reactor has been shown to be a useful tool for obtaining early time combustion data. Techniques for operations and sampling have been worked out and can now logically be applied to a number of other important fundamental studies. A few of the possible studies have been suggested previously for obtaining a better understanding of early time NO_x formation in fuel oil and pulverized coal burners.

REFERENCES

1. Longwell, J. P., and M. A. Weiss, Industrial and Engineering Chemistry, Vol. 47, 1955, p. 1634.

2. Goldberg, P. M., and R. A. Essenhigh, Seventeenth Symposium (International) on Combustion, the Combustion Institute, Pittsburgh, Pennsylvania, 1978.

3. Beer, J. M., and K. B. Lee, Tenth Symposium (International) on Combustion, the Combustion Institute, Pittsburgh, Pennsylvania, 1965, p. 1187.

4. Solomon, P. R., and M. B. Colket, "Coal Devolatization," Seventeenth Symposium (International) on Combustion, the Combustion Institute, Pittsburgh, Pennsylvania, 1979.

5. Suuberg, E. M., W. A. Peters, and J. B. Howard, "Production Compositions and Formation Kinetics in Rapid Pyrolysis of Pulverized Coal -- Implications for Combustion," Seventeenth Symposium (International) on Combustion, the Combustion Institute, Pittsburgh, Pennsylvania, 1979, p. 117.

6. Blair, D. W., J. O. L. Wendt, and W. Bartok, "Evolution of Nitrogen and Other Species During Controlled Pyrolysis of Coal," Sixteenth Symposium (International) on Combustion, the Combustion Institute, Pittsburgh, Pennsylvania, 1976.

7. Kobayashi, H., J. B. Howard, and A. F. Sarofim, Sixteenth Symposium (International) on Combustion, the Combustion Institute, Pittsburgh, Pennsylvania, 1976, p. 411.

8. Smoot, L. D., et al., "Propagation of Laminar Pulverized Coal-Air Flames," Sixteenth Symposium (International) on Combustion, the Combustion Institute, Pittsburgh, Pennsylvania, 1976.

9. Altenkirch, R. A., R. E. Peck, and S. L. Chen, "The Appearance of Nitric Oxide and Cyanide in One-Dimensional Coal Dust/Oxidizer Flames," Combustion Science and Technology, Vol. 20, 1979.

10. Pershing, D. W., and J. O. L. Wendt, "Pulverized Coal Combustion: The Influence of Flame Temperature and Coal Composition on Thermal and Fuel NO_x," Sixteenth Symposium (International) on Combustion, the Combustion Institute, Pittsburgh, Pennsylvania, 1976.

11. Wendt, J. O. L., J. W. Lee, and D. W. Pershing, "Pollutant Control through Staged Combustion of Pulverized Coal," DOE/FE-1817-4, 1977.

12. Jenkins, D. R., V. S. Yumlu, and D. B. Spalding, Eleventh Symposium (International) on Combustion, the Combustion Institute, Pittsburgh, Pennsylvania, 1967, p. 779.

13. Boothrayd, R. G., Flowing Gas Solid Suspensions, Chapman and Hall, Ltd., London, 1971.

14. Memmott, V. J., and L. D. Smoot, "Cold Flow Mixing Rate Data for Pulverized Coal Reactors," AIChE J., Vol. 21, p. 372, 1975.

15. Chiger, N. A., and Stroken, Combustion Science and Technology, Vol. 9, 1974, p. 111.

16. Lewis, B. and G. von Elbe, Combustion, Flares and Explosions of Gases, Academic Press, New York, 1961.

17. Crawford, M., Air Pollution Control Theory, McGraw Hill Book Co., New York, 1976.

18. Beer, J. M., and N. A. Chiger, Combustion Aerodynamics, Applied Sciences Publications, London, 1972.

19. Evangelista, J. J., R. Shinnar, and S. Katz, Twelfth Symposium (International) on Combustion, the Combustion Institute, Pittsburgh, Pennsylvania, 1969, p. 901.

20. Levenspiel, O., Chemical Reactor Engineering, John Wiley & Sons, Inc., New York, 1972.

21. Dee Rees, Energy & Environmental Research Corporation, Personal Communication, 1979.

22. Brown, R. A., et al., "Pilot Scale Evaluation of NO_x Combustion Control for Pulverized Coal: Phase II Final Report," EPA-600/7-79-132 (NTIS PB299325), June 1979.

23. De Soete, G. G., "Mechanisms of Nitric Oxide Reduction on Solid Particles," In: Proceedings of the Fifth Fundamental Combustion Research Contractors Workshop, EPA-600/9-83-001 (NTIS PB83-164483), January 1983.

24. Rees, D. P., L. D. Smoot, and W. S. Harding, "Pollutant Measurements in Coal Nitrogen," Sixteenth Symposium (International) on Combustion, the Combustion Institute, Pittsburgh, Pennsylvania, 1976.

25. Pohl, J. H., and A. F. Sarofim, "Devolatilization and Oxidation of . Laboratory Pulverized Coal Combustor and Gasifier," Paper presented at 1977 Spring Meeting Western States Section Combustion Institute, Seattle, Washington, April 18-19, 1977.

26. Wendt, J. O. L., D. W. Pershing, J. W. Lee, and J. W. Glass, Seventeenth Symposium (International) on Combustion, the Combustion Institute, Pittsburgh, Pennsylvania, 1979, p. 77.

27. Ubhayakar, S. K., D. B. Stickler, C. W. Von Rosenberg, Jr., and R. E. Gannon, Sixteenth Symposium (International) on Combustion, the Combustion Institute, Pittsburg, Pennsylvania, 1976, p. 427.

28. Wendt, J. O. L., et al., "Reduction of Sulfur Trioxides and Nitrogen Oxides by Secondary Fuel Injection," Fourteenth Symposium (International) on Combustion, the Combustion Institute, Pittsburgh, Pennsylvania, 1976, p. 897.

29. Myerson, A., "Reduction of NO_x by Hydrocarbons," Fifteenth Symposium (International) on Combustion, the Combustion Institute, Pittsburgh, Pennsylvania, 1975.

(This page intentionally blank)

APPENDIX A

PARTICLE MIXING DATA

In this section, the reduced data from all of the particle mixing studies are presented. Data were collected as described in Section 3.2. During this process, 99 photographs were analyzed for SR II and 46 photographs were analyzed for SR I.

The particle mixing test schedule for SR II is shown in Table A-1. The schedule for SR I is shown in Table A-2. The order of the lists corresponds to the chronological order of the tests.

As mentioned in Section 3.2, light attenuation was used to determine particle concentrations (normalized to the maximum concentration) at the SR model exhaust. The photo detector used in these experiments produced a voltage (V) directly proportional to light intensity (I). Then, for a given particle concentration, Np, I is related to the maximum intensity (Np = 0), I_{MX}, by the relation:

$$I = I_{MX}e^{-CNp} \text{ or } V = V_{MX}e^{-CNp}$$

where C is a constant given for a given particle size and path length. At a given time, t, the normalized particle concentration, Np/Npx, is found by:

$$Np^{(t)}/Npx = \frac{\ln\left(V^{(t)}/V_{mx}\right)}{\ln\left(Vo/V_{mx}\right)}$$

where Vo is the voltage recorded at the maximum particle concentration, Npx. The data presented in Tables A-3 and A-4 present values of Np/Npx versus time for the given test conditions listed in Tables A-1 and A-2, respectively. When SR II data are presented, no outright distinction has been made between tests where the particle flow was stopped or started. However, these conditions correspond to Np/Npx decreasing or increasing, respectively.

Table A-1. SR II Particle Mixing Test Schedule

No.	Location	Airflow (1/s)	Overall Coal Concentration (mg/1)
1	Nozzle test	14.2	0.12
2		23.6	0.12
3	Middle jet	23.6	0.2
4		14.2	0.12
5	Nozzle test	14.2	0.12
6	Bottom jet	14.2	0.12
7		23.6	0.05
8		23.6	0.12
9		23.6	0.17
10	Nozzle test	14.2	0.12
11	Top jet	14.2	0.12
12		14.2	0.18
13		14.2	0.29
14	Nozzle test	14.2	0.29
15		23.6	0.12
16	Top jet	23.6	0.12

Table A-2. SR I Particle Mixing Test Schedule

No.	Location	Airflow (1/s)	Overall Coal Concentration (mg/1)	Coal Signal
1	Nozzle test	9.4	0.10	on/off
2	Middle jet	9.4	0.10	on/off
3	Top jet	9.4	0.10	on/off
4	Bottom jet	9.4	0.10	on/off
5	Nozzle test	9.4	0.10	off/on
6	Middle jet	9.4	0.10	off/on
7	Top jet	9.4	0.10	off/on
8	Bottom jet	9.4	0.10	off/on
9	Nozzle test	9.4 14.2	0.10 0.09	off/on off/on
10	Middle jet	14.2	0.09	off/on
11	Top jet	14.2	0.09	off/on
12	Bottom jet	14.2	0.09	off/on
13	Nozzle test	14.2	0.09	off/on
14	Nozzle test	14.2	0.09	on/off
15	Middle jet	14.2	0.09	on/off
16	Top jet	14.2	0.09	on/off
17	Bottom jet	14.2	0.09	on/off
18	Nozzle test	14.2	0.09	on/off

Table A-3. SR II Particle Mixing Data

No.	t	Np/Npx
1	30	1.0
	55	0.57
	80	0.34
	105	0.14
	130	0.11
	155	0.06
	180	0
1	40	1.0
	65	0.53
	90	0.40
	115	0.26
	140	0.13
	165	0.05
	190	0
1	30	1.0
	55	0.62
	80	0.37
	105	0.24
	130	0.12
	155	0.07
	180	0
1	4	0
	12	0
	16	0.26
	20	1.0
1	4	0
	12	0
	16	0.06
	20	0.60
	24	1.0
1	4	0
	8	0
	12	0
	16	0.28
	20	1.0
2	4	0
	8	0.27
	12	1.0
2	4	0
	10	1.0
2	4	0
	8	0.05
	12	1.0
2	4	0
	8	0.05
	12	1.0
2	14	1.0
	24	0.81
	34	0.57
	44	0.46
	54	0.25
	64	0.20
	74	0.13
	84	0.09
	94	0.04
	104	0
2	4	1.0
	14	0.88
	24	0.71
	34	0.53
	44	0.36
	54	0.23
	64	0.11
	74	0.07
	84	0.04
	94	0.02
	104	0
2	4	1.0
	14	0.89
	24	0.77
	34	0.55
	44	0.44
	54	0.26
	64	0.17
	74	0.13
	84	0.09
	94	0.04
	104	0
3	40	0
	45	0.12
	70	0.32
	95	0.62
	120	0.81
3	40	0
	45	0.20
	70	0.39
	95	0.71
	120	0.83
3	40	0
	45	0.14
	70	0.88
3	50	1.0
	65	0.87
	90	0.57
	115	0.41
	140	0.35
	165	0.18
3	90	1.0
	100	0.67
	125	0.56
	150	0.36
	175	0.27
	200	0.27
	225	0.20
	250	0.18
4	100	1.0
	115	0.72
	140	0.58
	165	0.42
	190	0.38
	215	0.39
	240	0.28
	265	0.13

Table A-3. Continued

No.	t	Np/Npx
4	100	1.0
	115	0.8
	140	0.64
	165	0.64
	190	0.48
	215	0.44
	240	0.37
	265	0.33
4	50	0
	60	0.08
	70	0
	85	0.42
	110	0.42
	135	0.68
	160	0.80
	185	0.88
4	100	1.0
	110	0.84
	135	0.70
	160	0.51
	185	0.42
	210	0.33
	235	0.27
	260	0.23
4	60	0
	70	0.10
	95	0.22
	120	0.38
	145	0.50
	170	0.50
	195	0.62
	220	0.69
	245	0.69
	270	0.74
	295	0.85
4	55	0
	60	0.08
	85	0.35
	110	0.42
	135	0.60
	160	0.86
	185	0.90
5	10	0
	20	0.10
	30	0.12
	40	0.14
	50	0.16
	60	0.18
	70	0.21
	80	0.33
	90	0.43
	100	0.60
	110	1.0
5	10	0
	20	0
	30	0.55
	40	0.72
	50	1.0
5	10	0
	20	0
	30	0.55
	40	0.70
	50	1
5	10	1.0
	20	1.0
	30	1.0
	40	1.0
	50	0.26
	60	0.19
	70	0.12
	80	0.06
	90	0.03
	100	0
5	10	1.0
	20	1.0
	30	1.0
	40	0.66
	50	0.55
	60	0.24
	70	0.11
	80	0
5	10	1.0
	20	1.0
	30	1.0
	40	1.0
	50	0.29
	60	0.17
	70	0.12
	80	0.05
	90	0
6	60	0.13
	85	0.26
	110	0.54
	135	0.84
6	50	0
	60	0.06
	85	0.33
	110	0.40
	135	0.58
	160	0.69
	185	0.77
6	60	0
	70	0.16
	95	0.47
	120	0.55
	145	0.88
6	150	1.0
	165	0.45
	190	0.39
	215	0.35
	240	0.21
	265	0.14
6	150	1.0
	165	0.50
	190	0.36
	215	0.29
	240	0.23
	265	0.17
	290	0.11

Table A-3. Continued

No.	t	Np/Npx
6	130	1.0
	165	0.53
	190	0.32
	215	0.26
	240	0.26
	265	0.22
	290	0.18
7	40	0
	45	0.9
	70	0.68
	95	0.89
7	30	0
	45	0.21
	70	0.36
	95	0.54
	120	0.65
	145	0.81
7	80	1.0
	100	0.74
	125	0.49
	150	0.39
	175	0.29
	200	0.24
7	70	1.0
	90	0.77
	115	0.65
	140	0.43
	165	0.32
	190	0.21
7	70	1.0
	90	0.70
	115	0.56
	140	0.36
	165	0.19
	190	0.11
8	80	1.0
	100	0.58
	125	0.46
	150	0.38
	175	0.26
	200	0.09
8	100	1.0
	115	0.65
	140	0.38
	165	0.31
	190	0.05
8	60	1.0
	90	0.65
	115	0.48
	140	0.31
	165	0.15
	190	0.12
8	40	0
	60	0.17
	85	0.17
	110	0.32
	135	0.36
	160	0.56
	185	0.77
8	30	0
	60	0.42
	85	0.54
9	70	1.0
	90	0.61
	115	0.40
	140	0.29
	165	0.28
	190	0.16
	215	0.16
	240	0.12
	265	0.08
9	80	1.0
	90	0.73
	115	0.32
	140	0.20
	165	0.15
9	50	1.0
	65	0.69
	90	0.47
	115	0.24
	140	0.24
	165	0.24
	190	0.12
	215	0.12
	240	0.05
9	45	0.10
	70	0.29
	95	0.35
9	20	0
	45	0.47
	70	0.62
	95	1.0
9	30	0
	45	0.17
	70	0.38
	95	0.67
10	30	1.0
	40	1.0
	50	0.77
	60	0.56
	70	0.23
	80	0.04
	90	0
10	30	1.0
	40	1.0
	50	0.84
	60	0.62
	70	0.15
	80	0.05
	90	0
10	30	1.0
	40	1.0
	50	0.61
	60	0.38
	70	0.19
	80	0.09
	90	0

Table A-3. Continued

No.	t	Np/Npx
10	10	0
	20	0
	30	1
10	10	0
	20	0
	30	1
10	10	0
	20	0
	30	1
10	35	1
	50	0.53
	70	0.31
	95	0.21
	120	0.16
	170	0.12
	220	0.08
10	45	1.0
	70	0.21
	100	0.17
	120	0.13
	145	0.05
10	40	1.0
	55	0.44
	70	0.36
	95	0.19
	170	0.10
	220	0.05
10	15	0
	20	0.44
	25	1.0
10	15	0
	30	1.0
10	20	0
	25	0.24
	30	0.68
	35	1.0
11	40	0
	70	0.23
	90	0.43
	115	0.64
11	50	0
	70	0.26
	95	0.46
	110	0.56
	130	0.66
11	100	1
	140	0.79
	190	0.54
	240	0.39
	290	0.25
	390	0.13
11	100	1
	160	0.86
	180	0.72
	250	0.38
	280	0.27
	380	0.16
11	100	1
	160	0.60
	240	0.35
	280	0.24
	380	0.16
12	80	0.82
	130	0.60
	180	0.38
	280	0.25
	380	0.13
12	100	1
	110	0.77
	180	0.44
	200	0.36
	280	0.21
	300	0.17
12	100	1.0
	180	0.62
	230	0.47
	280	0.27
	380	0.23
12	50	0
	90	0.41
	115	0.64
	140	0.82
12	40	0
	90	0.36
	115	0.59
	140	1.0
12	40	0
	65	0.17
	90	0.34
	115	0.73
	140	0.91
13	40	0
	65	0.06
	90	0.20
	115	0.39
	140	0.80
13	60	0
	95	0.31
	115	0.71
13	60	0
	80	0.11
	90	0.23
	120	0.41
	130	0.84
13	100	0.67
	180	0.45
	280	0.21
	380	0.21

Table A-3. Concluded

No.	t	Np/Npx
13	120	1.0
	180	0.61
	240	0.33
	280	0.22
	380	0.16
	480	0.09
13	140	1.0
	180	0.62
	230	0.41
	280	0.29
	380	0.17
	480	0.11
14	40	1
	90	0.42
	95	0.28
	120	0.17
	170	0.09
14	30	1
	80	0.42
	105	0.26
	130	0.14
	150	0.11
	180	0.06
	230	0.03
14	40	1.0
	70	0.79
	140	0.32
	190	0.14
	240	0.09
	290	0.07
14	20	0
	30	0.61
14	20	0
	40	0.62
14	25	0
	30	1
15	20	1
	40	0.45
	80	0.24
	130	0.12
	180	0.06
15	15	1
	40	0.29
	70	0.15
	120	0.07
15	10	1
	20	0.59
	50	0.22
	70	0.10
	120	0.05
15	10	0
	30	1
15	10	0
	30	1
15	15	0
	20	1
16	80	1.0
	140	0.49
	180	0.33
	280	0.17
	380	0.14
	480	0.03
16	60	1.0
	140	0.49
	180	0.33
	280	0.21
	380	0.03
16	60	1.0
	110	0.75
	150	0.51
	230	0.31
	280	0.23
	380	0.16
	480	0.08
16	70	0
	110	0.16
	160	0.45
	200	0.78
16	80	0
	105	0.16
	180	0.45
	240	0.71
16	70	0
	150	0.27
	180	0.52
	250	0.81

Table A-4. SR I Particle Mixing Data

No.	t	Np/Npx
1	0	1
	5	0.27
	10	0.02
1	0	1
	5	0.08
	10	0.01
2	25	0.96
	50	0.51
	75	0.28
	100	0.08
	125	0.05
	150	0.03
2	25	0.96
	50	0.44
	75	0.23
	100	0.18
	125	0.09
	150	0.04
2	25	0.93
	50	0.74
	75	0.42
	100	0.19
	125	0.07
	150	0.04
3	50	0.60
	75	0.41
	100	0.30
	125	0.19
	150	0.12
	175	0.09
	200	0.05
3	25	0.93
	50	0.73
	75	0.52
	100	0.27
	125	0.21
	150	0.16
	175	0.13
	200	0.06
3	50	0.69
	75	0.51
	100	0.41
	125	0.29
	150	0.19
	175	0.15
	200	0.07
4	25	0.92
	50	0.35
	75	0.18
	100	0.11
	125	0.04
	150	0.02
4	25	0.92
	50	0.43
	75	0.20
	100	0.10
	125	0.05
4	25	0.92
	50	0.56
	75	0.20
	100	0.05
5	20	0.02
	25	0.22
	30	0.55
	35	0.84
	40	0.97
6	50	0.10
	75	0.15
	100	0.23
	125	0.25
	150	0.37
	175	0.47
	200	0.57
	225	0.68
	250	0.95
6	25	0.03
	50	0.16
	75	0.56
	100	0.95
6	50	0.14
	75	0.33
	100	0.39
	125	0.49
	150	0.56
	175	0.59
	200	0.67
	225	0.75
	250	0.93
7	50	0.17
	75	0.65
	100	0.94
7	50	0.07
	75	0.18
	100	0.37
	125	0.73
	150	0.89
7	50	0.09
	75	0.19
	100	0.56
	125	0.87
	150	0.93
8	50	0.96
	75	0.87
	100	0.78
	125	0.69
	150	0.65
	175	0.46
	200	0.27
8	50	0.95
	75	0.86
	100	0.77
	125	0.69
	150	0.58
	175	0.52
	200	0.40
	250	0.25
	300	0.05

Table A-4. Continued

No.	t	Np/Npx
8	50	0.06
	75	0.09
	100	0.15
	125	0.24
	150	0.31
	175	0.42
	200	0.54
	250	0.69
	300	0.86
9	20	0.06
	25	0.25
	30	0.44
	35	0.63
	40	0.79
	50	0.89
9	10	0.03
	15	0.08
	20	0.26
	25	0.55
	30	0.77
	35	0.92
	40	0.96
10	25	0.07
	50	0.23
	75	0.42
	100	0.68
	125	0.83
	150	0.94
10	25	0.08
	50	0.19
	75	0.44
	100	0.73
	125	0.88
	150	0.94
	175	0.97
10	25	0.10
	50	0.68
	75	0.94
	100	0.97
11	25	0.02
	50	0.12
	75	0.22
	100	0.33
	125	0.42
	150	0.50
	175	0.61
	200	0.78
	225	0.91
11	25	0.01
	50	0.13
	75	0.25
	100	0.32
	125	0.44
	150	0.52
	175	0.57
	200	0.61
	225	0.68
	250	0.80
	275	0.89
11	25	0.10
	50	0.45
	75	0.87
	100	0.97
12	25	0.04
	50	0.22
	75	0.33
	100	0.34
	125	0.39
	150	0.47
	175	0.69
	200	0.84
	225	0.91
	250	0.95
12	25	0.03
	50	0.12
	75	0.18
	100	0.29
	125	0.37
	150	0.49
	175	0.61
	200	0.78
	225	0.95
12	25	0.03
	50	0.13
	75	0.25
	100	0.29
	125	0.38
	150	0.50
	175	0.94
13	20	0.05
	25	0.15
	30	0.35
	35	0.53
	40	0.66
	45	0.74
	50	0.88
14	50	0.07
	75	0.36
	100	0.61
	125	0.78
	150	0.89
	175	0.96
15	25	0.02
	50	0.16
	75	0.21
	100	0.38
	125	0.46
	150	0.57
	175	0.67
	200	0.73
	225	0.81
	250	0.93

Table A-4. Concluded

No.	t	Np/Npx
15	25	0.03
	50	0.09
	75	0.23
	100	0.34
	125	0.44
	150	0.55
	175	0.68
	200	0.76
	225	0.84
	250	0.90
	300	0.97
15	25	0.01
	50	0.03
	75	0.08
	100	0.14
	125	0.19
	150	0.25
	175	0.33
	200	0.44
	250	0.62
	300	0.76
	350	0.90
16	100	0.07
	125	0.20
	150	0.31
	175	0.48
	200	0.58
	250	0.73
	300	0.87
	350	0.93
16	100	0.06
	125	0.13
	150	0.26
	175	0.37
	200	0.47
	250	0.64
	300	0.79
	350	0.93
16	100	0.06
	125	0.18
	150	0.26
	175	0.37
	200	0.47
	250	0.65
	300	0.78
	350	0.87
	400	0.97
17	75	0.10
	100	0.17
	125	0.30
	150	0.48
	175	0.61
	200	0.70
	250	0.86
	300	0.93
	350	0.96
17	75	0.05
	100	0.10
	125	0.18
	150	0.27
	175	0.37
	200	0.48
	250	0.73
	300	0.87
	350	0.93
17	75	0.05
	100	0.13
	125	0.26
	150	0.36
	175	0.44
	200	0.51
	250	0.70
	300	0.90
	350	0.97
17	100	0.12
	125	0.19
	150	0.32
	175	0.38
	200	0.51
	250	0.68
	300	0.87
	350	0.93
18	25	0.02
	50	0.07
	75	0.20
	100	0.44
	125	0.60
	150	0.72
	175	0.81
	200	0.88
	250	0.92
	300	0.96

IV. POLLUTANT FORMATION FROM COMBUSTION OF FUEL OILS IN A WELL-MIXED COMBUSTOR

Prepared by:

M. J. Murphy, A. A. Putnam,
A. Levy, and J. R. Overley

BATTELLE
Columbus Laboratories
505 King Avenue
Columbus, Ohio43201

Prepared for:

Energy and Environmental Research Corporation
Subcontract No. EER-8318-1

TABLE OF CONTENTS

Page (IV-)

SUMMARY vii

INTRODUCTION 1

- NO_x Formation 1
- Objective 2
- Technical Approach 2

COMBUSTOR DESIGN 4

- Air Jet Construction 5
- Fuel Jets 5

EVALUATION OF REACTOR MIXING 8

- Gas-Phase Mixing 8
  - Cold Flow Model 8
  - Droplet Lifetimes During Combustion 8
  - NO_2 Tracer Tests 9
- Droplet Mixing 18
  - Experimental Setup 18
  - Experimental Results - Time Constants Greater than 500 msec 20
  - Experimental Results - Time Constants of 200 msec 33

EXPERIMENTAL APPARATUS 39

- Combustor Construction 39
  - Casting 39
  - Wall Temperature Measurements 39
  - Combustor Insulation 39
  - Combustor Jacket 42
  - Air Jet Mounting 42
  - Fuel Nozzle Mounting 42
- Flow Measurement System 42
- Afterburner 46
- Prediction of Combustion Products 46
- Data Acquisition System 48

TABLE OF CONTENTS
(Continued)

Page (IV-)

FUEL 49

- Natural Gas 49
- Number 2 Oil 49
- Residual Oil 50
- Fuel Nitrogen Analysis 50

EMISSIONS MEASUREMENT 52

- Sample System 52
- HCN and NH_3 Analysis 52

RESULTS 54

- Initial Test Firings 54
  - Natural Gas 54
  - Number 2 Oil 54
  - Residual Fuel Oil 54
- NO_x Test Firings 55
  - Natural Gas Data 55
  - Emission Index for NO 55
  - Example 55
  - Operation with Number 2 Oil 63
  - Operation with Number 5 Oil 64
  - Emissions Data for Number 5 Oil 65
  - HCN and NH_3 Measurement 65
  - Conversion of Fuel Nitrogen 74
  - Soot Formation 75

CONCLUSIONS 76

- Implications for NO_2 Control 77

FUTURE WORK 78

ACKNOWLEDGEMENTS 79

REFERENCES 80

LIST OF TABLES

Page (IV-)

TABLE 1. Summary of NO_2 Mixing Measurements in Cold Flow Model 15

TABLE 2. Reactor Time Constants 23

TABLE 3. Reactor Time Constants Taking Deposition of DOP on the Walls into Account 31

TABLE 4. Predicted Product Mole Fractions for $CH_{1.72}$ Fuel, $T = 873$ K, $P = 101$ kPa, $= 1.6$ 47

TABLE 5. Analysis of Number 2 Oil 50

TABLE 6. Analysis of Residual Fuel Oil 51

TABLE 7. Emissions Data for Number 2 Oil 63

LIST OF FIGURES

Page

Figure 1. Sketch of Air Jets in Well-Stirred Reactor 6

Figure 2. Sketch of 8 Liquid Fuel Jets in Well-Stirred Reactor 6

Figure 3. Air Jet Alignment Path 12

Figure 4. Decay of NO_2 Absorption for Cold Flow Model Reactor for 8 mm Nozzles at Station No. 2 with Nominal Flow Rate of 28 g/s 13

Figure 5. Plot of Absorption Decay for 8 mm Nozzles at Station No. 2 with Nominal Flow Rate of 28 g/s 16

Figure 6. Plot of Absorption Decay for 12 mm Nozzles at Station No. 2 with Flow Rate of 35 g/s 17

Figure 7. MIE Scattering Experimental Setup 19

Figure 8. Solenoid Current and Scattered Light Detector Traces for a Typical Decay Test 21

Figure 9. I/I_o Versus Time for Run Number 1 24

LIST OF FIGURES
(Continued)

Page (IV-)

Figure 10. I/I_o Versus Time for Run Number 2 24

Figure 11. I/I_o Versus Time for Run Number 3 25

Figure 12. I/I_o Versus Time for Run Number 4 25

Figure 13. I/I_o Versus Time for Run Number 5 26

Figure 14. Photographs of DOP Droplets for Runs 2, 3, 4, and 5 27

Figure 15. Location and Alignment of the Sonicore Nozzles 34

Figure 16. Scattered Beam Detector Output Trace During a Decay Test 35

Figure 17. I/I_o Versus Time 36

Figure 18. Exploded View of Combustor I 40

Figure 19. Combustor II 41

Figure 20. Air Jet Mounting 43

Figure 21. Sonicor Nozzle Mounting 44

Figure 22. Flows to Well-Stirred Combustor 45

Figure 23. Sample System 53

Figure 24. Oxygen vs. Equivalence Ratio 56

Figure 25. Carbon Dioxide vs. Equivalence Ratio 57

Figure 26. Carbon Monoxide vs. Equivalence Ratio 58

Figure 27. Total Hydrocarbon vs. Equivalence Ratio 59

Figure 28. Nitric Oxide vs. Equivalence Ratio 60

Figure 29. EI_{NO}, $\frac{\text{g mol NO}}{\text{g fuel}}$ vs. Equivalence Ratio 61

Figure 30. Combustor Temperature vs. Equivalence Ratio 62

LIST OF FIGURES
(Continued)

Page (IV-)

Figure 31. Oxygen vs. Equivalence Ratio 66

Figure 32. Carbon Dioxide vs. Equivalence Ratio 67

Figure 33. Carbon Monoxide vs. Equivalence Ratio 68

Figure 34. Nitric Oxide vs. Equivalence Ratio 69

Figure 35. Temperature vs. Equivalence Ratio 70

Figure 36. EI_{NOx}, $\frac{\text{g mol NO}}{\text{g fuel}}$ vs. Equivalence Ratio 71

Figure 37. Apparent Percent Conversion of Fuel Nitrogen 72

Figure 38. Typical Data Results 73

SUMMARY

Battelle's Columbus Laboratories, working as a subcontractor under the United States Environmental Protection Agency's "Fundamental Combustion Research Applied to Pollution Control" program, is responsible for studying the conversion of fuel nitrogen to NO_x during the firing of residual fuel oil. Residual fuel oil combustion in industrial and utility boilers occurs under dynamic and constantly changing flowing and mixing conditions which are difficult to control and describe. In order to simplify the study of fuel N conversion to NO_x, a combustor was designed and constructed in which the factors affecting combustion, namely, residence time, stoichiometry, temperature, and fuel droplet size distribution, could be consistently controlled, and described mathematically.

A well-stirred (backmix) reactor was selected for the purposes of this study as the best system to meet the above conditions. Since achieving and evaluating perfect mixing in a reactor is much more difficult than establishing plug flow, the first phase in the overall fuel NO_x program was involved with the design and evaluation of a well-stirred reactor.

Battelle's combustor was designed to fire natural gas or fuel oil at firing rates between 0.5 and 4.0 g/s (20 kW-200 kW). The combustion chamber is cylindrical in shape, 250 x 250 mm, with four fuel and four air jets at each end. The jets are located to promote intense shear on turbulence as a means of producing well-stirred conditions.

A cold flow model was built to test the mixing characteristics of both single-phase (gas) and two-phase (droplet/air) systems. The single-phase mixing characteristics were evaluated using the concentration decay of a tracer gas after a step change decrease in the tracer gas input. The results showed the tracer concentration decayed exponentially, per ideal well-stirred reactor theory, and experimental time constants were at worst within eight percent of the theoretical values. Thus, the combustor mixing could be characterized as a well-stirred system.

Dual-phase mixing behavior was also evaluated using concentration decay tests; for this case liquid droplets of dioctyl phthalate, a low volatility liquid, were used as the tracer. Results indicated that the concentration decay was exponential, but that the experimental time constants were less than

theoretical values by a factor of two. This large deviation between experimental and theoretical time constants is attributed to deposition of between 40 and 75 percent of the dioctyl phthalate on the cold walls of the reactor model. Further analysis of the droplet deposition on the walls of the cold flow model was not pursued because such a behavior was felt to be related to the cold walls of the model and would not occur on the hot walls of the actual combustor.

The combustor was fired with natural gas, Number 2 oil and Number 5 oil; burning was smooth for all three fuels. The combustor was operated rich and lean on all three fuels at residence times of 50 ms and 200 ms. Measurable amounts of HCN were observed only for the residual oil burning under very rich conditions (ϕ = 2,28)*; no NH_3 was observed.

For the natural gas, the EI_{NO}, defined as moles NO per gram of fuel burne times 10^6, ranged from 36 to 54 with the peak occurring at ϕ = 1.2. The shorter residence time gives a higher EI_{NO}.

For the residual oil, the EI_{NO} ranged from 102 to 163 with the peak occurring near stoichiometric. The shorter residence time gives a higher EI_{NO} when burning rich but not when burning lean.

Taking the difference between EI_{NO} from residual oil and EI_{NO} from natural gas as a measure of fuel NO, the apparent fraction conversion of fuel bound nitrogen to NO was calculated and found to range from 9 to 71 percent. The apparent conversions for the 50 and 150 ms residence times gave two smooth curves of similar magnitudes but with the peak for the 150 ms residence time at ϕ = 0.7 and for the 50 ms residence time at ϕ = 0.9.

---

* In this report, equivalence ratio (ϕ) is defined as $\frac{m_F/m_A}{m_F/m_A)_{st}}$, where

m_F = mass of fuel and m_A = mass of air.

POLLUTANT FORMATION FROM COMBUSTION OF FUEL OILS IN A WELL-MIXED COMBUSTOR

by

M.J. Murphy, A.A. Putnam
A. Levy, and J.R. Overley

This report is submitted as specified by Subcontract No. EER-8318-1 between Energy and Environmental Research Corporation and Battelle's Columbus Laboratories. The report describes the design, construction, and evaluation of a well-stirred combustor and the emissions data for natural gas Number 2, and Number 5 oil burned in this combustor, and covers the contract period from December 1, 1977 to August 15, 1980.

INTRODUCTION

NO_x FORMATION

Residual oil combustion in packaged and field-erected industrial and utility boilers is a significant source of nitrogen oxides. These compounds are not only noxious by themselves but contribute to the formation of photochemical smog. Their control has been a challenge to the combustion engineer since measures which have traditionally been used to insure "good" combustion may complicate the NO_x control problem; for example, using a fuel-rich primary heat release zone, may cause excessive amounts of soot and char.

The situation is made more complex by two characteristics of nitrogen chemistry in flames. The first is that there are a number of fixed nitrogen species that may be formed. These include NO_2 and NO, collectively called NO_x, as well as HCN and NH_3. These last two are both combustible and may be oxidized in the combustion products to form NO. The term fixed-nitrogen is used to refere to all non-elemental nitrogen compounds including the four mentioned above.

The second characteristic of nitrogen chemistry in flames is that the fixed-nitrogen formed may originate in different ways. Some arises from the union of oxygen and nitrogen in the air as mediated by various combustion reactions. Or, if the fuel contains nitrogen compounds, the pyrolysis and burning of these compounds may produce fixed-nitrogen species. This latter situation occurs when residual oils are burned, since the nitrogen-containing compounds in petroleum tend to be concentrated in the highest boiling fractions(1).

In order to assist in the development of NO_x control strategies, the U.S. Environmental Protection Agency has set up a Fundamental Combustion Research Program aimed at studying the generation of NO_x during the firing of a variety of fuels. Battelle's participation in this program is concerned with studying the generation of fuel NO_x during the firing of residual fuel oils. The main goal of Battelle's program is to determine the effects of residence time, temperature, reactant stoichiometry, and spray characteristics, and fuel properties on the conversion of fuel nitrogen to NO_x.

OBJECTIVE

The overall objective of this study was to relate production of NO_x from the burning of heavy residual oils to the fuel-N in these fuels and to the combustion system variables of spray droplet size, droplet history, gas temperature, gas velocity and turbulence level, and fuel properties. More specifically, this study was designed to identify the sources of NO formation relative to the fuel-N components in the fuel and the char under conditions which correspond closely to a well-stirred reactor.

During the first year of this program, a combustor was constructed which met the requirements of a classic well-stirred reactor. The objective of the second-year study was to carry out a parametric examination of the dependent variables which most influence fuel NO_x production from the combustion of residual fuel sprays. The information collected will ultimately be needed to define the path of the nitrogen species in the fuel.

TECHNICAL APPROACH

Residual fuel oil combustion in industrial and utility boilers occurs under varied and constantly changing flowing and mixing conditions. These different flow patterns can have a dramatic effect on NO_x production by oil burners(2). Therefore, as a prerequisite to evaluation of the effect of the combustion variables mentioned above, it was necessary to develop a combustion system in which these variables could be easily altered and controlled and one for which the mixing characteristics could be mathematically described. Such a system would allow the investigation of NO_x formation in a cloud of liquid droplets under conditions representative of specific regions within practical combustion devices.

The classic examples of flowing reactor systems which can be theoretically analyzed are the well-stirred reactor, in which all reacting elements are exposed to an identical environment, but over a distribution of residence times, and the plug flow reactor, in which all reacting elements have the same residence time in the reactor, but are exposed to a changing environment, due to reaction, as they pass through the reactor. The well-stirred reactor was chosen for use in this program so that evaporation, pyroloysis, and initial stages of combustion could be carried out in a uniform, well-characterized environment.

The first phase of this fuel NO_x program was therefore devoted to developing a well-stirred combustor for use by the project. In the second phase the combustor was instrumented and emissions measurements were taken for gas, light oil and heavy oil.

COMBUSTION DESIGN

Practical combustors are not homogeneous chemical reactors but rather contain regions of quite different conditions due to the pattern of fuel injection and aerodynamic mixing, including recirculation patterns, turbulence, staged air admission, etc. As a consequence, the identification of the source and mechanisms of NO_x formation is complex. It is recognized that mixing processes and the time-temperature environment of reactants and products strongly influence emission levels of NO_x. Thus, proper control of fuel and air inlet parameters can lead to reduction and control of NO_x emissions. This is complicated, however, by the fact that NO_x can arise from two different sources, fuel nitrogen and atmospheric nitrogen, by different mechanisms. Further, these mechanisms respond individually tot he different conditions in various regions of any combustor. This program is directed toward studying the mechanisms of fuel NO formation, since roughly 80 percent of the NO_x produced from the combustion of residual fuel oil is from the fuel nitrogen.

Evaluation of these mechanisms requires that we know how such system inlet parameters as fuel spray characteristics, fuel/air ratios, turbulence levels, and mixing patterns influence the time-temperature history of fuel drops and char particles, and that we relate these parameters to their influence on such intermediates as HCN and NH_3, which ultimately are converted to NO_x or N_2. Such a correlation requires that we perform experiments in a manner that the variables can be separated for the major reaction regions of the combustor and related to NO_x formation. The well-stirred reactor, also referred to as the backmix reactor, satisfies the required reactor conditions.

In the well-stirred reactor one can vary and control although not entirely independently, such parameters as fuel composition, drop size, fuel-air ratio, combustion intensity, and turbulence intensity, and thus control and time-temperature history of a fuel droplet. Because the initial evaporation, pyrolysis, and combustion occur under well-stirred conditions, the distribution of molecular and radical species, unburned fuel droplets, and char particles leaving the region are the same as the steady-state distribution within the region. Therefore sampling at the exit of the well-stirred region defines the distribution of species in the well-stirred region without penetrating the region with a probe which could destroy the well-stirred character.

A perfectly stirred reactor is an ideal concept that can only be approached in practical applications, because perfectly stirred implies instantaneous mixing whereas real mixing processes occur at a finite rate. Also, perfectly mixed conditions require that the reactor volume be perfectly mixed on both a macro- and a micro-scale. In the practical sense the best approximation to a perfectly stirred condition that one can hope to attain occurs when the mixing time is a small fraction of the residence time in the reactor and that the scale of the turbulent eddies is small enough to insure adequate micro-scale, as well as macro-scale mixing. These conditions are attained by insuring that high velocity air jets are used along with air and fuel jets aimed to cross each other's paths to induce shear.

The combustor design shown in Figures 1 and 2 meets these criteria. The combustor itself is a cylindrical chamber with length equal to diameter, an exit port located axially at one end, and with four air jets and four fuel jets located at each end. Figure 1 shows the location and alignment of the air jets while Figure 2 shows the location and alignment of the fuel jets.

AIR JET CONSTRUCTION

The air jets are constructed from 3/4-inch nominal pipe, internally threaded to accept screw-in orifices. Currently two orifice sizes are available, 8 mm or 13 mm diameter. At any given air mass flow rate, switching between these orifices allows us to change the air jet momentum and kinetic energy. Thus, we can control and evaluate the effect of the air jet velocity on the mixing in the reactor independently of the other inlet parameters.

FUEL JETS

The fuel jets chosen for atomizing the fuel oil are Sonicore^R "H" series nozzles, Model No. 052H-A. These are air (or steam) atomizing nozzles which atomize the fuel using a standing sonic shock wave which is maintained between the tip of the nozzle and a resonator cup.

Variations in the atomizing air pressure can be used to control the mean droplet diameter and the bandwidth of the spray size distribution emitted from the nozzle. Measurements of the droplet size distribution performed by the

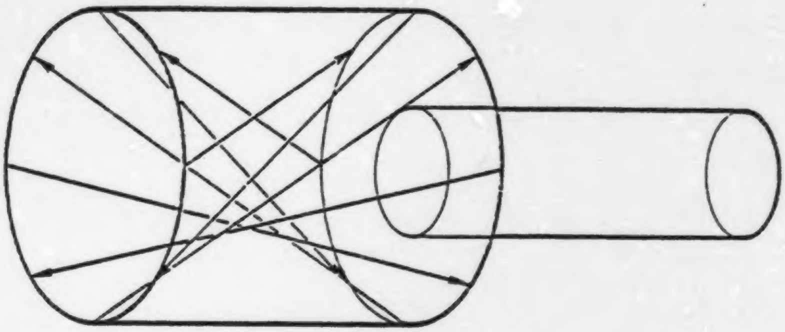

FIGURE 1. SKETCH OF AIR JETS IN WELL-STIRRED REACTOR

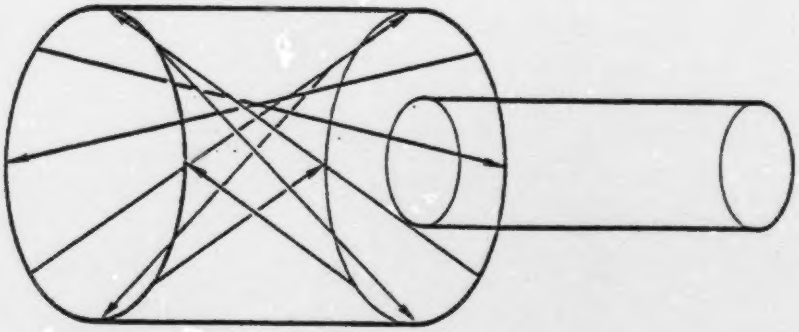

FIGURE 2. SKETCH OF 8 LIQUID FUEL JETS IN WELL-STIRRED REACTOR

International Flame Research Foundation(3) have sown that when using an oil with a viscosity of 19 centistokes (equivalent to a residual fuel oil at roughly 50 C) a 35 kPa atomizing air pressure produces a spray of droplets with diameters between 20 and 400 micrometers, with a mean diameter of approximately 100 micrometers. A 145 kPa atomizing air pressure produces a spray with droplet diameters between 12 and 28 micrometers, with a mean diameter of approximately 21 micrometers. These distributions are only minimally affected by changes in the oil feed rate.

Therefore, by using the Sonicore nozzles we can alter the fuel spray droplet mean diameter and distribution independently of the other fuel and air inlet parameters. Variations in the atomizing air pressure will alter the air flow rate through the fuel nozzles, but variations in the total air flow rate through all eight nozzles amounts to less than 10 percent of the combustion air required at a fuel flow rate of 1 g/s.

EVALUATION OF REACTOR MIXING

Since combustion in the reactor will be heterogeneous when firing with a residual fuel, it is necessary to determine if mixing in the reactor is of the idealized well-stirred type with respect to both the gaseous phase and the droplets. Consequently, evaluation of mixing was carried out with just air and a tracer gas to determine the gas phase mixing behavior, then with air and a liquid spray to determine droplet spray mixing behavior. Discussions of these separate evaluations follow.

GAS-PHASE MIXING

Cold Flow Model

A full-scale cold flow model of the proposed combustor was built to establish basic flow and mixing parameters. It was based on a requirement that the combustor be able to fire residual fuel oil at up to 25 g/s and that residence times in the well-stirred combustor range between 50 and 200 milliseconds. The cold flow model dimensions were set at 305 mm for the diameter by 305 mm long. Such a cylindrical reactor would yield a residence time of approximately 6.5 milliseconds when firing 25 g/s of residual fuel (requiring 353 g/s of combustion air) at an expansion ratio of four.

The cold flow model was constructed as a Lucite cylinder capped with wooden end plates. A 125 mm diameter hole was bored in an end-plate, and the edges of the hole rounded to create a smooth exit port. A 175 mm length of conduit was mounted to this end-plate, hereafter called the outface, for the purpose of smoothing the flow through the exit port and preventing the formation of recirculation eddies at the exit port. Four air jets were mounted in each end-plate with provisions for changing their angles of injection.

Droplet Lifetimes During Combustion

Since these experiments are intended to study the spray burning of fuel, it is important that the droplet lifetime in the combustor be reasonably long in comparison with the combustor residence time.

Hottel, Williams, and Simpson(4) experimentally studied the combustion of single residual fuel oil droplets in a furnace at temperatures between 900 and

1100 C using droplet diameters between 350 and 610 micrometers. Using their data on rates of burnout (meaning burnout of the liquid phase, with a carbonaceous particulate remaining) and extrapolating to droplet diameters of interest to us using the "d^2 law" ($\tau = d^2/\lambda$ where τ is the burnout time for a droplet of initial diameter d and λ is the burning rate constant), it was expected that 100 micrometers droplets would require 103 milliseconds for burnout, and 20 micrometer droplets would require 28 milliseconds for burnout.

It should also be noted that not all droplets remain in a backmix reactor for the same amount of time. The distribution of residence times is exponential. Therefore, there will always be at least a fraction of droplets, both large and small, that pass through the reactor in essentially zero time.

It was therefore expected that the combustion space would be full of droplets when oil was being burned. This was indeed the case. When the plug in the observation port was removed, a luminous flame with many visible burning oil drops issued from the observation port. (The combustor was under positive pressure at the higher firing rate). The burning oil drops were readily identified by their characteristic white smoke trails.

NO_2 Tracer Tests

The degree of backmixing in the cold flow model was evaluated using standard step change tracer techniques. NO_2 was used as the tracer and was injected simultaneously with the air into the model. NO_2 tracer was then shut off via a solenoid valve while the NO_2 concentration decay was measured at the reactor exit port. NO_2 exhibits a pronounced absorption of light with a wavelength of 441 nanometers, the wavelength of light emitted from a HeCd laser. Therefore, the concentration of NO_2 at the reactor exit port was measured by passing a beam of light from a HeCd laser through the reactor perpendicular to the axis, reflecting the beam from a mirror back through the reactor and to a detector. Thus double passage of the laser beam through the reactor volume yields values of NO_2 concentration averaged over the reactor volume rather than measuring concentration at a point.

Tracer Decay Theory. The ideal backmix reactor is a reactor in which the contents are well-stirred and uniform in composition throughout. The inlet stream to such a reactor is instantaneously mixed with the contents of the reactor, and the exit stream is of the same composition as the fluid within the reactor.

Analysis of the concentration of a tracer species in the ideal backmix reactor during a step change in tracer input from concentration C_0 to complete shutoff yields the following relationship

$$C = C_0 e^{-Qt/V} \tag{1}$$

where C = NO_2 concentration in the reactor volume and exit stream, molecules/cm^3

C_0 = NO_2 concentration at $t = 0$, molecules/cm^3

Q = air flow rate, m^3/sec

t = time, sec (NO_2 feed is shut off at $t = 0$)

V = reactor volume, m^3.

Since the laser beam intensity is being measured instead of the NO_2 concentration, the relationship between beam intensity and NO_2 concentration can be obtained from

$$I = I_0 e^{-C \sigma L} \tag{2}$$

where I = laser beam intensity, relative units

I_0 = laser beam intensity with no absorption (zero NO_2) concentration), relative units

σ = NO_2 spectral absorption coefficient at 441 nanometers, = 3.5×10^{-19} cm^2/molecule

L = absorption path length, 60.32 cm .

Combining the above equations yields

$$\ln \left\{ \ln \left(\frac{I_0}{I} \right) \right\} = \ln \left\{ \ln \left(\frac{I_0}{I(0)} \right) \right\} - \frac{Q}{V} t \tag{3}$$

which is a convenient form for analysis of our decay test data. In Equation (3), $I(0)$ represents the laser beam intensity at time zero ($t = 0$). A semilog plot of ln (I_o/I) on the log axis versus time for an ideal backmix reactor should yield a straight line with an intercept of ln $[I_c/I(0)]$ and a slope of $-Q/2.303V)$, where 2.303 is the result of converting from ln to $\log_{10}$. Therefore, a semilog plot of ln (I_o/I) versus time will give us an experimental reactor time constant which can be compared with the theoretical time constant, V/Q ($\equiv \tau$). The degree of agreement between these two gives us a measure of the ideality of the mixing in our backmix reactor.

Tracer Decay Test Results. Tracer decay tests were performed using step changes in the NO_2 input to evaluate the effects of 1) point of NO_2 injection, 2) velocity of the injected air, and 3) angle of the air jet injection, on the degree of mixing in the cold flow model. NO_2 was injected through nozzles both in the outface and the backface to determine the effect of NO_2 injection location. The air jet velocity at a given total air mass rate of input was varied by using either the 8 mm or 13 mm diameter orifices in the air jet tubes. The air jets were designed to inject air aimed at a point 45 degrees clockwise from the diagonally opposite point of injection, of Figure 1. The effect of different alignment angles was evaluated by measuring the NO_2 concentration decay with the air jets aligned at five different angles. The air jets were mounted in the end plates such that they could be aimed along the path line shown in Figure 4 for one of the air jets mounted in the backface. This line extends from the point diagonally opposite from the air jet to a point 67.5 degrees around the cylinder. Station numbers identified in the data represent the target points of the jets in inches along the 170 mm long line (see Fig. 3).

A typical recorder trace of the laser beam intensity during a decay test is shown in Figure 4. The laser beam intensity is a minimum at time zero then the NO_2 concentration is a maximum. The maximum laser beam intensity, I_o, occurs when the NO_2 concentration drops to zero. Time zero was established in these runs by the presence of a blip on the trace which was due to a noise signal from the NO_2 solenoid when closing.

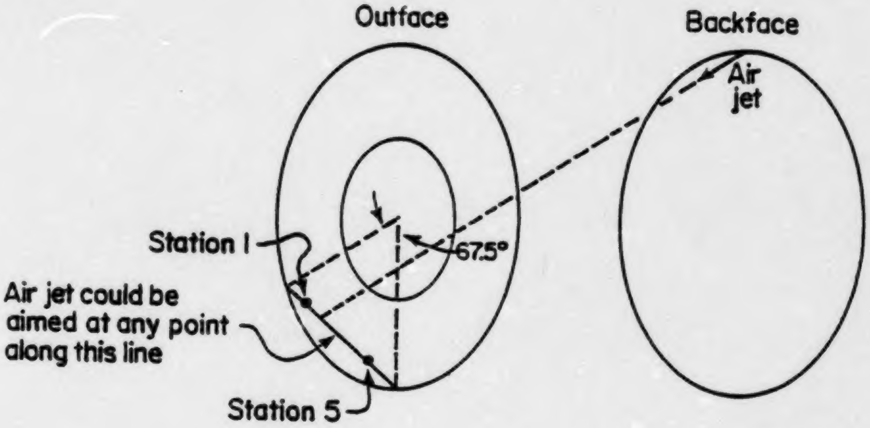
Outface
Backface
Air jet
Station 1
67.5°
Air jet could be aimed at any point along this line
Station 5

FIGURE 3. AIR JET ALIGNMENT PATH

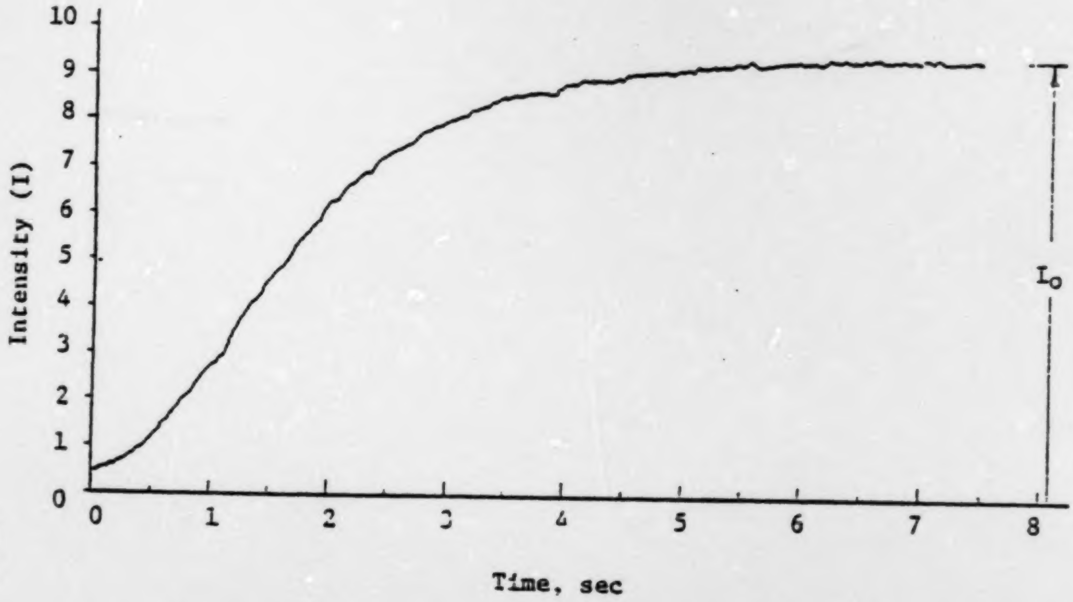

FIGURE 4. DECAY OF NO_2 ABSORPTION FOR COLD FLOW MODEL REACTOR FOR 8-mm NOZZLES AT STATION NO. 2 WITH NOMINAL FLOW RATE OF 28 g/s. (NO_2 INJECTED THROUGH NOZZLE IN BACKFACE.)

Table 1 indicates the various test conditions used with respect to NO_2 injection location, air jet orifice size, and aim point of the air jets. The air flow rates are approximately equal to those that will be used when firing oil at 2.5 g/s, but the time constants in these cold flow tests are larger by a factor of around four since there is no gas expansion in the cold flow tests. Figures 5 and 6 show the plots for three experimental runs. The plotted points were read from the recorded decay curves at 0.5 second intervals. The data points yielded good linear semilog plots with the worst discrepancy between the theoretical and experimental time constants being approximately eight percent. In the case of Figure 6, the theoretical time constant for a nominal flow rate of 28 g/s is 0.94 second, with observed values running between 0.87 and 0.98 seconds. Results from Figure 6 indicate an experimental time constant of 0.72 second which agrees very well with the theoretical value of 0.76 second.

In general, no significant differences in absorption decay were observed between either backface or outface injection of the NO_2 tracer. Well-stirred behavior also seemed to be present for all nozzle stations with the exception of Station No. 5 where for decay times beyond about 3 seconds there was a consistent decrease in decay rate from run to run which resulted in a nonlinearity on the semilog plot of ln (I_o/I) versus t. Station No. 2, which was closest to our desired air jet aim point of 45 degrees from the point diagonally opposite the jet, produced mixing behavior that can safely be characterized as being well-stirred. Furthermore, mixing with the air jets aimed at Stations 1 or 3 (reference Figure 6) also indicated well-stirred behavior, meaning that air jet alignment within several degrees of the 45 degree aim point is satisfactory.

The above tests actually only evaluated mixing on a macro-scale. A more comprehensive test covering microscale mixing would require a detailed mapping of the gas-flow pattern using point-type measurements. However, the extra effort to conduct the more comprehensive measurements was not considered necessary because of the relative simplicity of the reactor flow system. The fact that good mixing occurred when NO_2 was injected at different points and under a variety of flow conditions and air jet alignments gives strong support to the conclusion that the reactor design produces well-stirred flow.

TABLE 1. SUMMARY OF NO_2 MIXING MEASUREMENTS IN COLD FLOW MODEL

Diameter of Jet:	12.7 mm				8 mm			
Nominal Volume Flow Rate:	28 g/s		35 g/s		28 g/s		35 g/s	
Face:	Out	Back	Out	Back	Out	Back	Out	Back
Station No.								
1	DA	DA	DA	N	DA	DA	D	D
2	D	DA	DA	N	DA	DA	D	D
3	DA	DA	DA	N	DA	DA	D	D
4	D	D	D	N	D	D	D	D
5	DA	DA	DA	N	DA	DA	D	D

D = Duplicate measurements.

N = No measurements made.

A = Data Analyzed.

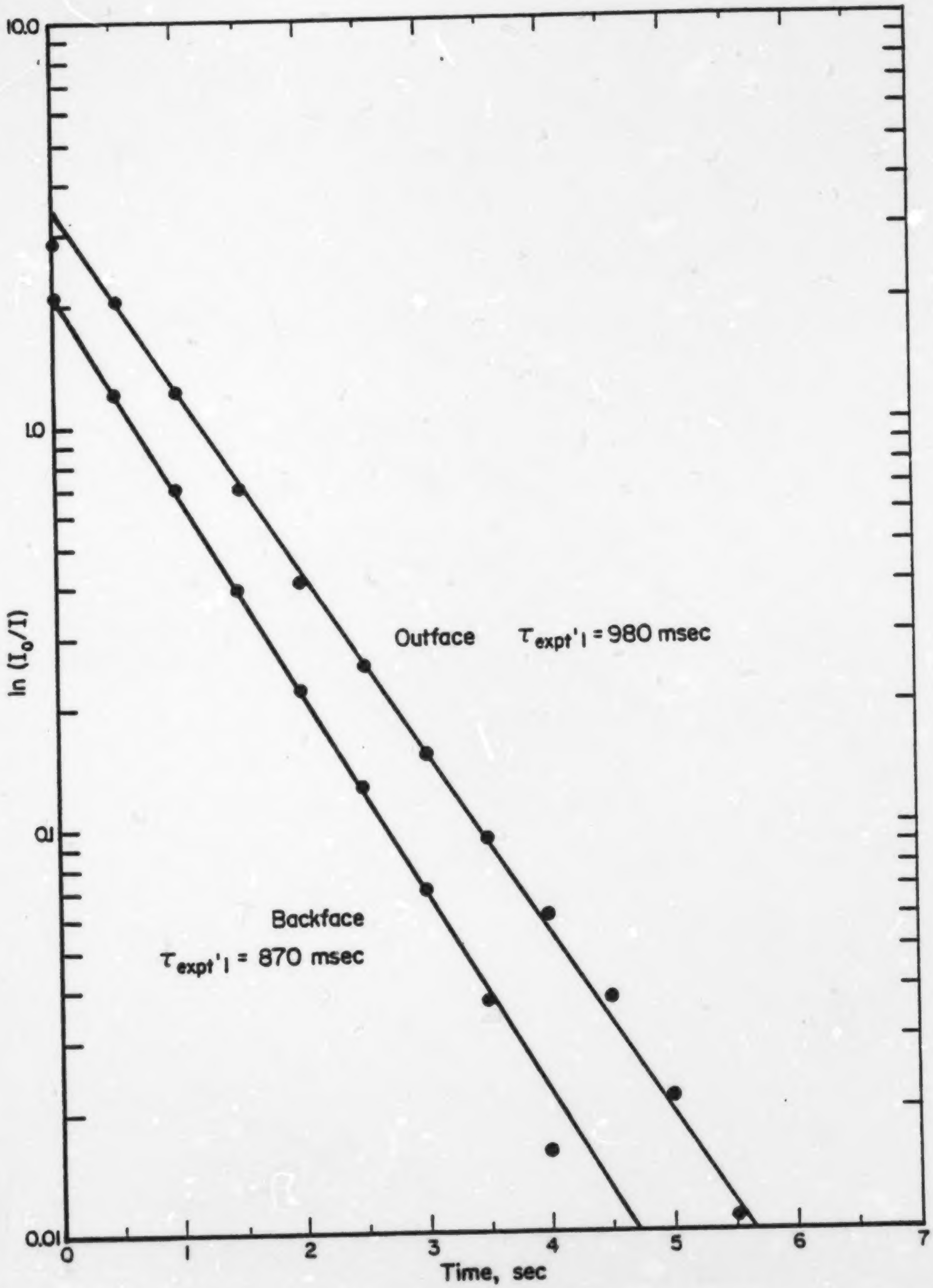

FIGURE 5. PLOT OF ABSORPTION DECAY FOR 8 mm NOZZLES AT STATION NO. 2 WITH NOMINAL FLOW RATE OF 28 g/s

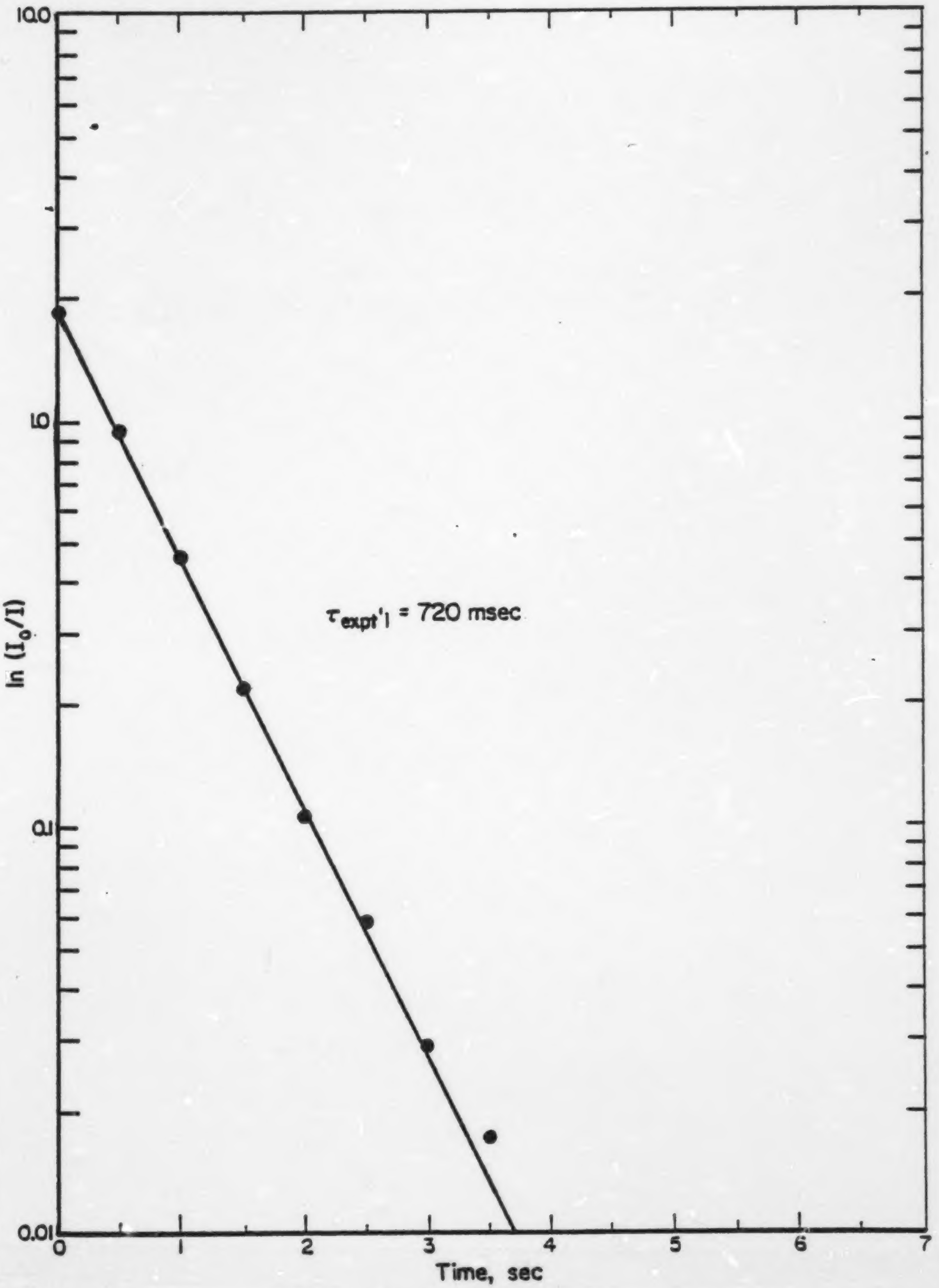

FIGURE 6. PLOT OF ABSORPTION DECAY FOR 12 mm NOZZLES AT STATION NO. 3 WITH FLOW RATE OF 35 g/s

DROPLET MIXING

Experimental Setup

Measurement of liquid droplet concentrations during the transient period of the step change decay tests was not as easy with droplets as with a purely gas phase system. Laser absorption cannot be used because the number density of droplets is orders of magnitude less than the number density of tracer gas molecules. Probes present a problem in that droplets coat their inner walls causing inaccurate concentration readings. The technique which best overcomes these objections is the Mie scattering procedure.

Mie scattering is the reflection and refraction of a light beam by droplets or particulates in a stream. The intensity of the reflected/refracted light at any given angle is a function of the droplet number density and the droplet-size distribution. Measurement of the beam intensity at three different angles allows calculation of both the drop-size distribution and concentration, although the iterative calculation procedure is time consuming and somewhat dependent upon the ability of the operator to make good initial guesses as to the solution. The procedure amounts to guessing at the drop-size distribution and density, then using the computer routine to calculate an intensity versus scattering angle curve and comparing computed with observed values.

A simpler approach, still using Mie scattering, is to utilize a liquid spray whose drop-size distribution remains constant during the transient tests. Such conditions produce a scattered beam whose intensity is proportional to the droplet density, therefore measurement of beam intensity at only one scattering angle is required and the need for the computer routine is eliminated. The experimental setup for this approach is shown in Figure 7.

Water would be the easiest fluid to use for the droplet mixing tests except for the fact that water evaporates quite readily at room temperature. As a consequence, the drop-size distribution would be changing during the concentration decay tests, necessitating the measurement of beam intensity at several scattering angles. To overcome this problem and to allow us to make scattering measurements at only one scattering angle, we used dioctyl phthalate (DOP) to simulate residual fuel oil. Dioctyl phthalate is a commercial plasticizer with a boiling point at 5 mm Hg of 231 C, a viscosity of 826

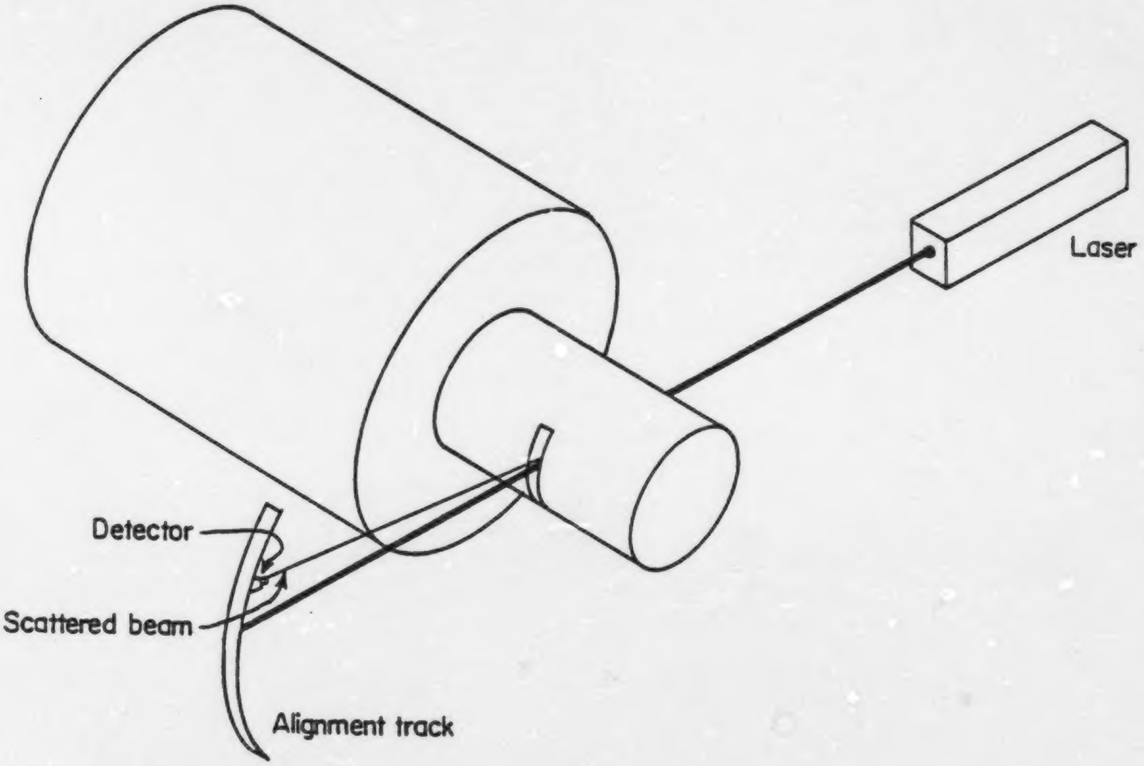
Laser
Detector
Scattered beam
Alignment track

FIGURE 7. MIE SCATTERING EXPERIMENTAL SETUP

centistokes (equivalent to a No. 6 fuel oil at roughly 38 C), and a specific gravity at 20/20 C of 0.986.

Experimental Results - Time Constants Greater than 500 msec

The first spray tests using dioctyl phthalate were conducted with atomizing air and DOP being injected through a Sonicore 052HA nozzle set in the backface of the model while air was being injected through all eight air jets. The atomizing air and DOP were then shut off using solenoid valves, and the decay in the DOP concentration in the reactor exit stream was measured via a detector picking up scattered laser light at scattering angles of 0.5 to 1.5 degrees.

Figure 8 shows a strip chart trace of the detector output as a function of time for a typical run. The upper trace shows the energizing current to the solenoid. The solenoid shut-off point was considered to be midway between where the current just started to die out and where it finally reached a null value. The detector output signal appears quite noisy during the solenoid on state because of some pickup of the 60-cycle hum. Also note that the time indicated as the start of the decay (t = 0), and the solenoid shutoff time are displaced by about 40 milliseconds. This is because the laser beam was measuring the concentration of particles in a conduit section at a point 120 mm from the reactor exit port. The 40 milliseconds represents the transportation lag between the exit port and the laser beam for air flowing at 39 l/s (the test condition) through a 128 mm diameter conduit section (velocity of 3.03 m/s per second).

The detector output decay curve is somewhat noisy because the detector was measuring the light scattered from approximately a one mm^3 volume in the exit stream. At the flow rates involved in these tests, the particle concentrations ranges from a few to less than one droplet per mm^3, hence the irregularity as particles moved into and out of the scattering region.

For an ideal well-stirred reactor, the exit stream concentration during a step change decay is, as described earlier,

$$C = C_0 e^{-t/\tau} \qquad (4)$$

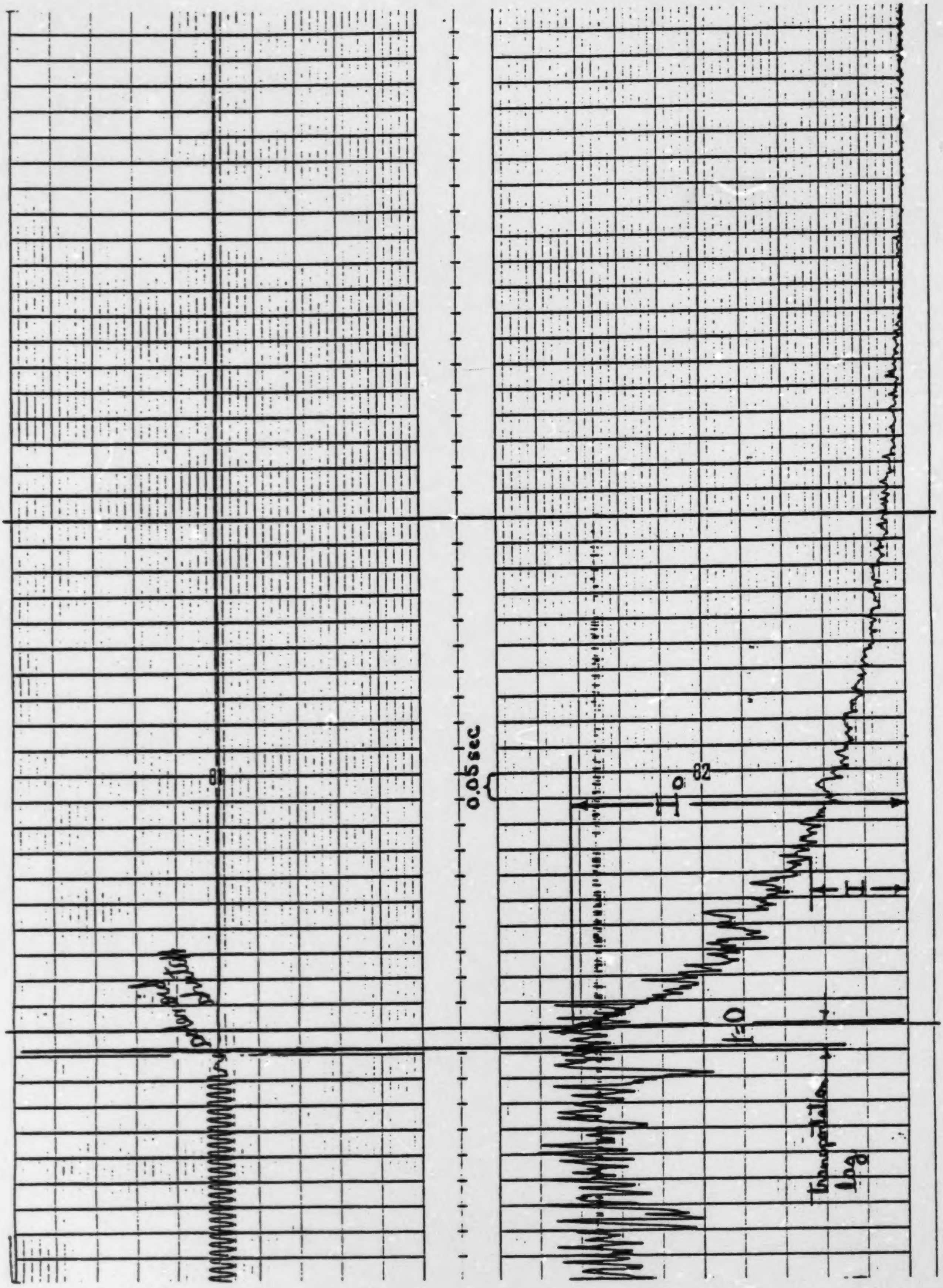

FIGURE 8. SOLENOID CURRENT AND SCATTERED LIGHT DETECTOR TRACES FOR A TYPICAL DECAY TEST

where, for the droplet tests, C is the droplet concentration (droplets of DOP/volume of air) in the exit stream (and in the reactor), C_o is the concentration at time $t = 0$, and τ is the reactor time constant (= V/Q; V = reactor volume, Q = volumetric air flow rate). Since the Mie scattering procedure uields a scattered laser beam whose intensity (I) is proportional to the droplet concentration, then

$$\frac{I}{I_o} = e^{-t/\tau} \tag{5}$$

or, converting to logarithms to the base 10,

$$\log_{10}\left(\frac{I}{I_o}\right) = \frac{1}{(2.3026\tau)}\, t \quad . \tag{6}$$

Therefore, by plotting I/I_o versus t on semilog paper, τ can be determined from the slope of the resultant line (slope $\equiv$ m) using the equation

$$\tau = -\,(2.3026\ m)^{-1}\ . \tag{7}$$

Five runs were made injecting DOP through a Sonicore nozzle in the backface and air through all eight air jets. Table 2 gives the test conditions for the five runs, along with the experimental and calculated reactor time constants. Run No. 1 was performed at an air flow rate comparable to that used for the gas phase mixing tests, while Runs 2 through 5 used an air flow rate of 39 l/s or 47 g/s (for a smaller time constant) with different DOP flow rates and aspirating air pressures to alter the droplet concentrations and sizes.

Figure 9 through 13 show the plots of log (I/I_o) versus t for the five runs along with the experimental values calculated from the slopes. When fitting straight lines to these data, only the points in the range $0.1 < (I/I_o) < 1.0$ were used. For I/I_o values less than 0.1, an error in reading I of only 0.1 chart division meant an error of approximately 0.03 in I/I_o, hence the scatter in the data below $I/I_o = 0.1$.

Figure 14 gives some idea of the relative droplet sizes for Runs 2 through 5. These are photographs of droplets deposited on microscope slides which were

TABLE 2. REACTOR TIME CONSTANTS

Run No.	Air Flow Rate, L/s	DOP Flow Rate, cm^3/min	Sonicore Nozzle Atomizing Air Pressure, kPa, gage	$\tau_{expt'l}$ (msec)	τ_{calc} (msec)
1	26	2.66	180	740	860
2	39	9.9	180	460	570
3	39	28.5	180	460	570
4	39	28.5	41	360	570
5	39	180	180	300	570

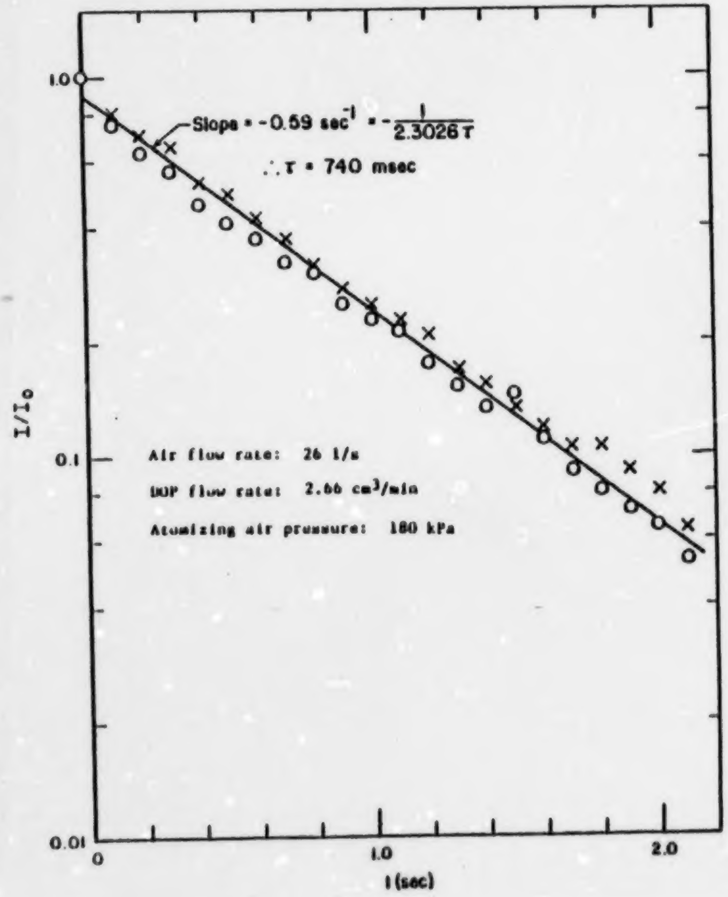

FIGURE 9. I/I$_0$ VERSUS TIME FOR RUN NO. 1

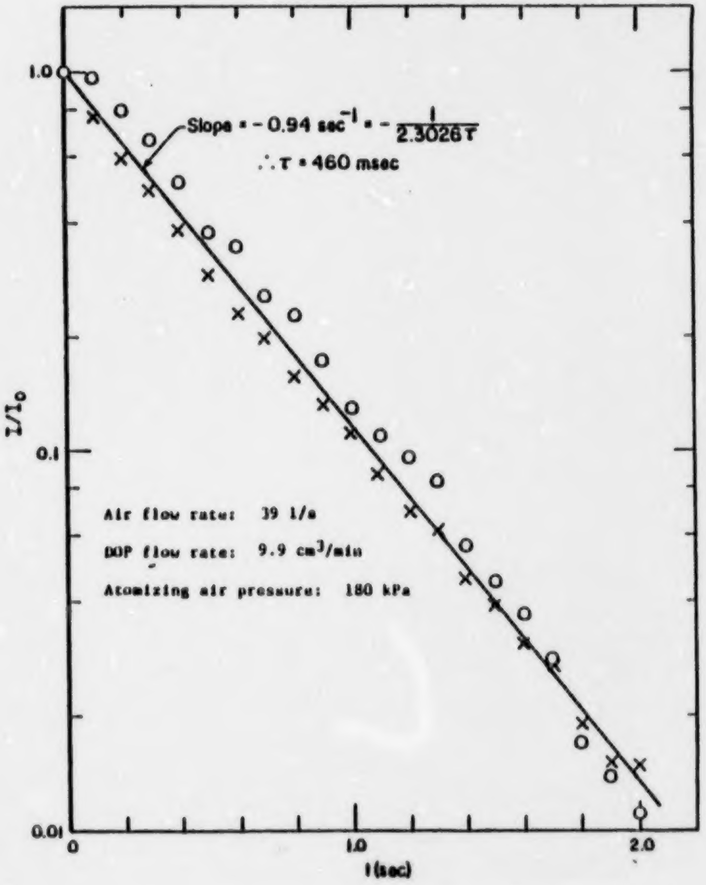

FIGURE 10. I/I$_0$ VERSUS TIME FOR RUN NO. 2

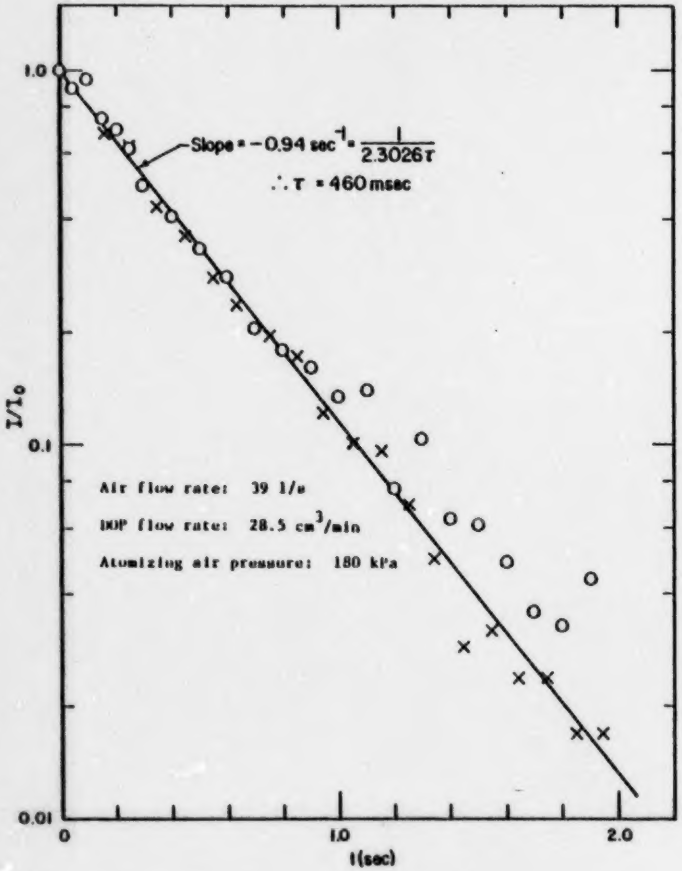

FIGURE 11. I/I_0 VERSUS TIME FOR RUN NO. 3

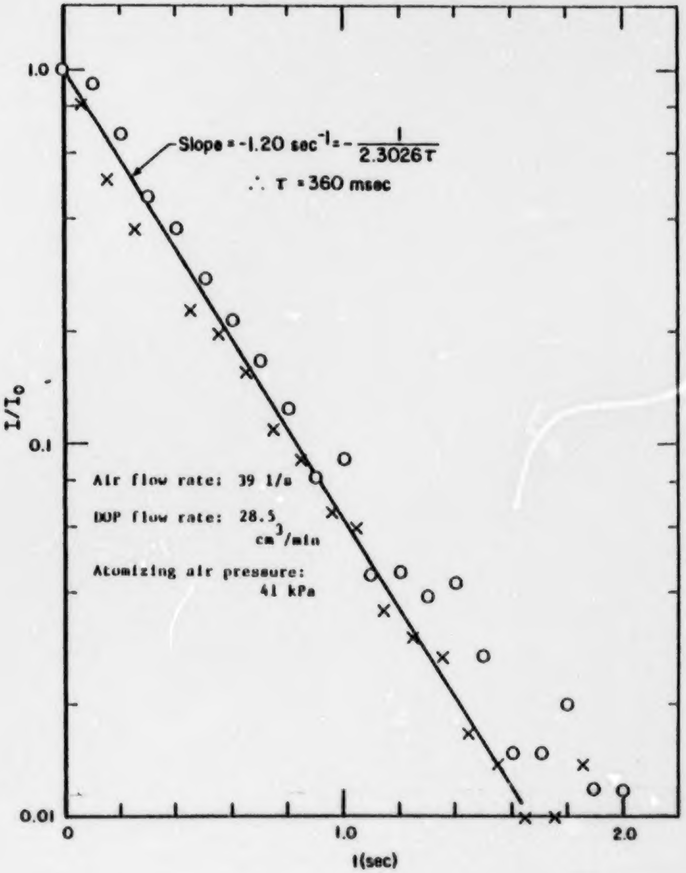

FIGURE 12. I/I_0 VERSUS TIME FOR RUN NO. 4

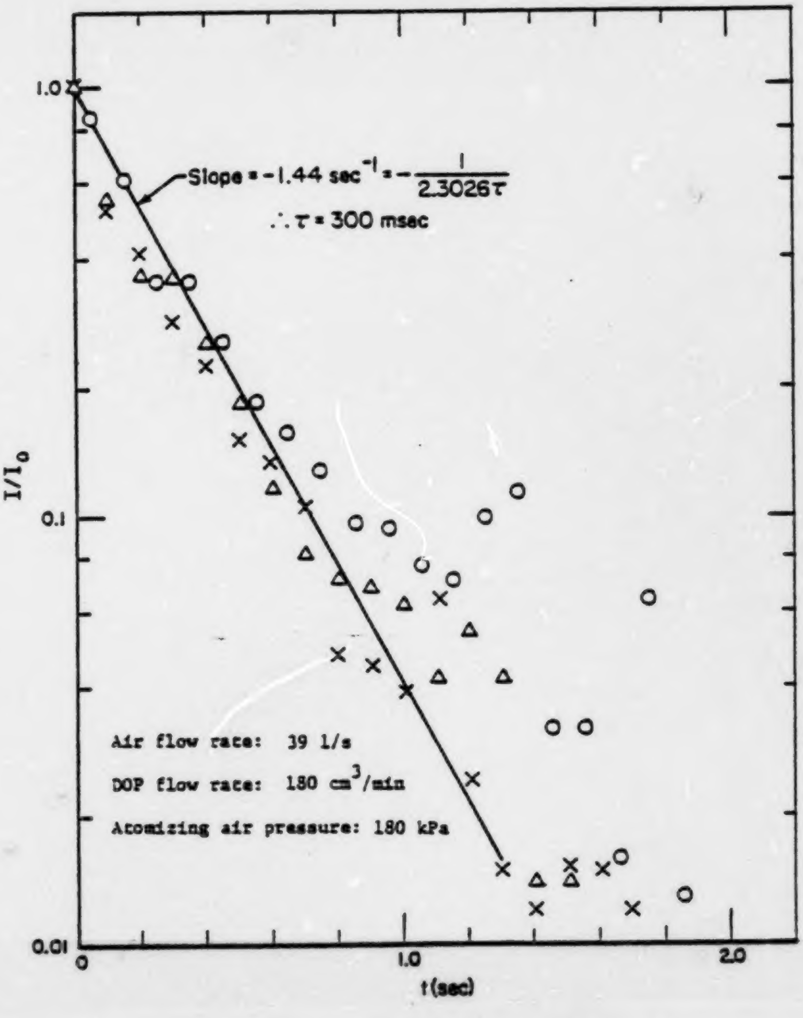

FIGURE 13. I/I$_0$ VERSUS TIME FOR RUN NO. 5

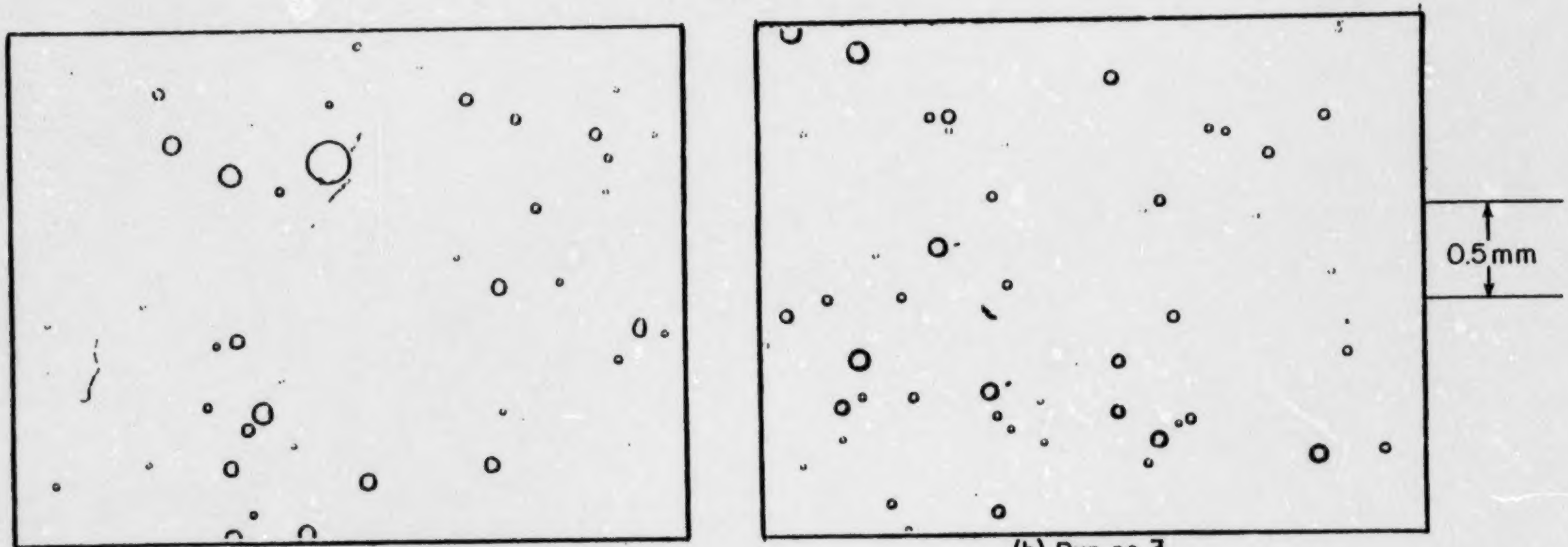

(a) Run no. 2

(b) Run no. 3

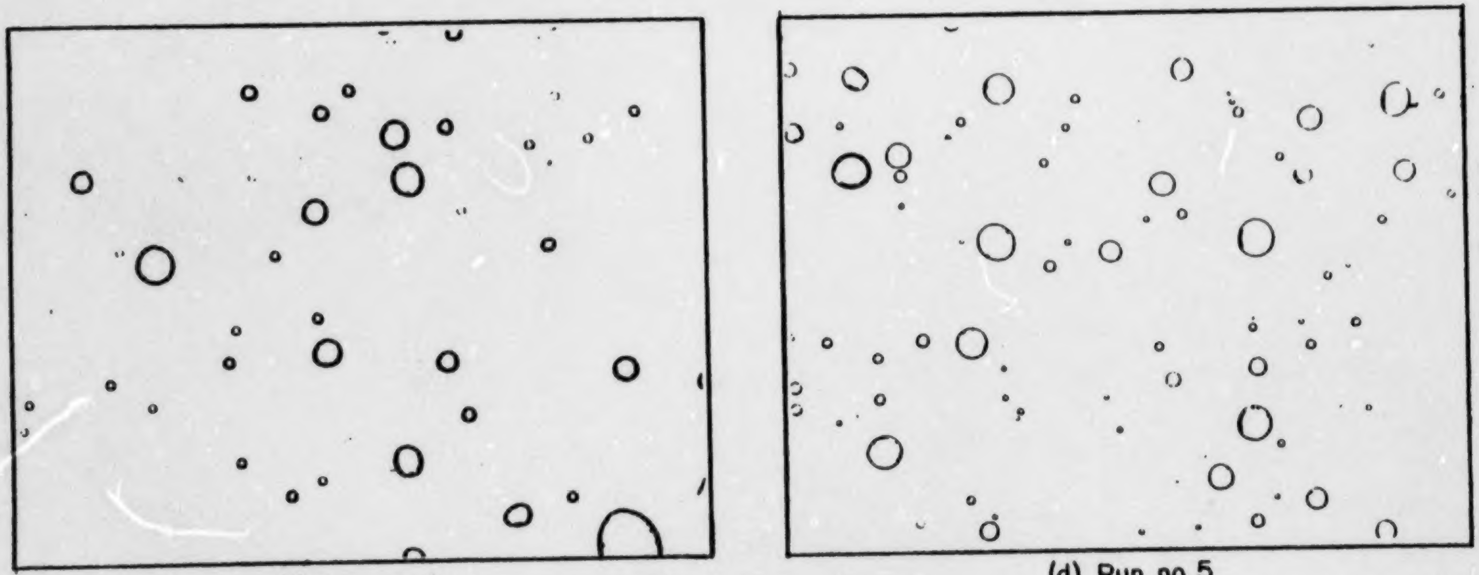

(c) Run no. 4

(d) Run no. 5

FIGURE 14. PHOTOGRAPHS OF DOP DROPLETS FOR RUNS 2, 3, 4, and 5.

quickly passed through the reactor exit stream while the Sonicore nozzle was injecting DOP into the reactor. Note that since the spherical droplets have adhered to and wetted the slide that the particle diameters shown are some three to five times greater than the actual droplet diameters. Also note that the largest particle diameters are for Runs 4 (lowest atomizing air pressure) and 5 (largest DOP flow rate).

Discussion of Results. Figures 9 through 13 indicate that the particle concentration decay is indeed exponential as would be expected from a backmix reactor. Also, all of the experimental time constants are within a factor of 1.9 of the theoretically predicted values. It can furthermore be noted that all of the experimental time constants are less than the theoretically predicted values, and especially so for Runs 4 and 5 which had the largest droplet sizes. Therefore, it appears that the cold flow model behaves as in ideal backmix reactor, but with some additional means of removing particles from the reactor volume besides blowing them out through the exit port.

Droplet Deposition of Reactor Walls. This additional means of droplet removal appears to be deposition of a substantial portion of the DOP on the reactor walls. Steady state flow tests run at the same air flow rates, DOP flow rates, and atomizing air pressures as for the decay tests have indicated that between 42 and 77 percent of the DOP injected into the reactor volume via the Sonicor nozzle deposited on the walls and collected as a puddle of fluid in the bottom of the reactor. As a result, it can be safely assumed taht during the reactor decay tests the droplets were being removed from the reactor volume both by transport through the exit port and by deposition on the reactor walls. The equation describing the change of droplet concentration during a decay test can then be written as

$$V\frac{dC}{dt} = -kC - cC \qquad (8)$$

where C is the concentration of droplets in the reactor (and the exit stream) and kC is the term which accounts for droplet removal via deposition on the reactor walls. The symbol k represents a deposition constant which is assumed to be independent of droplet concentraiton but may depend upon droplet size. This possible droplet size effect on k is of no consequence during a given run where the droplet-size distribution remains essentially constant.

Solving Equation (8) for $\log_{10}$ (C/C_o), and equating this with $\log_{10}$ yields

$$\log \frac{I}{I_o} = - \frac{1}{2.3026} \left[\frac{1}{\tau} + \frac{k}{V} \right] t \qquad (9)$$

Therefore, plotting log I/I_o versus time would uield a line of slope m where

$$m = \frac{-1}{2.3026} \left[\frac{1}{\tau} + \frac{k}{V} \right] \qquad (10)$$

The deposition constant, k, was determined by flowing a given volume of DOP through the SOnicore nozzle, then draining the reactor to determine the volume of DOP trapped by the walls. The volume of DOP that passed through the exit port was determined by difference. The equation describing this is

DOP input through Sonicore = DOP output by flow through the exist port + DOP output by deposition on the reactor walls (11)

or

$$F = QC_o t_1 + kC_o t_1 \qquad (12)$$

where F is the total volume of DOP injected through the nozzle and t_1 is the time required to inject volume F. Dividing both sides of Equation 12 by F yields

$$1 = \frac{QC_o t_1}{F} + \frac{kC_o t_1}{F} \qquad (13)$$

where $QC_o t_1/F$ represents the fraction of injected DOP which exited through the port and $kC_o t_1/F$ represents the fraction of DOP which was deposited on the walls. If $kC_o t_1/F$ is defined as b, then $QC_o t_1/F$ equals (1-b). Therefore

$$\frac{kC_o t_1/F}{QC_o t_1/F} = \frac{b}{1-b} \tag{14}$$

or

$$\frac{k}{Q} = \frac{b}{1-b} \; . \tag{15}$$

Multiplying the k/V term in Equation 10 by Q/Q and rearranging yields

$$m = - \frac{1}{2.3026} \left(\frac{1}{\tau} + \frac{k}{Q} \frac{Q}{V} \right) \tag{16}$$

Substituting $Q/V = 1/\tau$ and Equation 15 into the above yields

$$m = - \frac{1}{2.3026} \quad \frac{1}{\tau} + \frac{b}{L-b} \frac{1}{\tau} \tag{17}$$

then solving for τ yields

$$\tau = - \frac{1}{2.3026m} \quad \frac{1}{1-b} \tag{18}$$

The fraction of DOP collected on the walls, b, was determined by injecting between 180 and 300 ml of DOP through the SOnicore nozzle, then collecting the deposited DOP via a drain port in the bottom of the reactor. The DOP was allowed to drain for 45 minutes. The value of b was also evaluated one for each set of flow conditions by scraping the model walls with a rubber-edged scraper, injecting 300 ml of DOP at the rated flow conditions, then again scraping the reactor surfaces and collecting the material.

Table 3 shows the mean values of b determined from several experimental trials, the values of $\tau_{expt'l}$ calculated from Equation 18, and the theoretical time constant, τ_{calc}, based upon the particular flow conditions. Because of the large surface area of the cold flow model (300 mm diameter, 300 mm long) and the various cutouts in the model walls for the air and fuel jets, it was difficult to collect all of the DOP that deposited on the walls. This accounts for the large variation in the b values.

The $\tau_{expt'l}$ values shown in Table 3 are all greater than the theoretical time constants. This is somewhat due to the sensitivity of Equation 18 to the value of b. Since $\tau_{expt'l}$ is a function of m and b, that is, $\tau = f(m,b)$, and m and b are both subject to experimental error, the error band in τ can be calculated from

$$\Delta\tau = \frac{\partial f}{\partial m} \Delta m + \frac{\partial f}{\partial b} \Delta b \qquad (19)$$

TABLE 3. REACTOR TIME CONSTANTS TAKING DEPOSITION OF DOP ON THE WALLS INTO ACCOUNT

Run[a] No.	b (Percent of Total Feed Collected from the Reactor Walls	$\tau_{expt'l}$[b] (msec)	$\Delta\tau$[c] (msec)	τ_{calc} (msec)
1	.38 ± .18	1190	405	860
2	.58 ± .06	1190	210	570
3	.56 ± .14	1050	390	570
4	.68 ± .10	1130	410	570
5	.51 ± .05	620	95	570

(a) Refers to the run number and corresponding flow conditions shown in Table 2.

(b) Calculated using Equation 18.

(c) Calculated using Equation 20.

Performing the above operation on Equation 18 yields

$$\tau_{expt'l} = \frac{2.3026}{[2.3026m(1-b)]^2}\left((1-b)\,\Delta m - m\Delta b\right) \qquad (20)$$

The values given in Table 2 were calculated using a five percent tolerance on m and the maximum error for b as shown in Table 2.

Conclusions. The experimental flow time constants shown in Table 3 are all within a factor of two of the theoretical values of the time constant for an ideal well-stirred reactor. This amount off error is probably due to the wide variation in the amount of DOP which collected on the reactor walls. The preceding analysis assumed that the rate of droplet deposition on the walls was solely a function of the droplet concentration in the droplet/air mixture at a given droplet concentration in the droplet/air mixture at a given droplet-size distribution. It is quite conceivable, however, that the collection efficiency of droplets on the walls is also a function of the film thickness of DOP on the walls. That is during a decay test or steady state evaluation of b, the film thickness is thinnest initially so that droplets adhere to or are absorbed into this film at a particular efficiency (percentage of droplets striking the film which remain on the walls). At a later time, when the film thickness has increased, it is possible that the film collection efficiency increases or decreases. Hence, the value of b obtained during steady state tests could be an average value instead of a constant. Since the calculation of via Equation 18 is fairly sensitive to b (a variation in b of 0.01 changes the values of in Table 2 by between 12 and 36 milliseconds), then the discrepancy between the experimental and theoretical values could easily be caused by changes in the droplet collection efficiency of the film as determined by the film thickness.

Regardless of the above behavior, the decay test results with droplet injection have shown that the decay of the droplet concentration during a step change is exponential, as would be expected of an ideal backmix reactor. Also, the model of DOP deposition on the walls explains why the droplet concentration in the exit stream decays faster than that for an ideal well-stirred reactor with no deposition. Furthermore, a comparison between the decay test flow conditions, which produced a wide variation in droplet size and distribution, nd the corresponding values of b indicates that there is no definite correlation between droplet size and value of b. In other words, the reactor behavior does not indicate that droplets of a particular size are being preferentially removed from the reactor volume by deposition on the wall. This result further enhances the idea that the reactor operates as a well-stirred unit.

The test results just described, however, covered time constants of 570 milliseconds or greater. Although the air velocities from the air jets were equal to those which will occur in the hot combustor when firing, the residence times are greater than will occur in the hot combustor, since there is no expansion of the gases in the cold model. Therefore, to insure that the above behavior could be extrapolated to time constants around 200 milliseconds, a few droplet decay tests at the smaller time constant were run as described in the following section.

Experimental Results - Time Constants of 200 msec

Evaluation of the cold flow model behavior at a time constant of 200 milliseconds requires increasing the air and DOP flow rates by roughly a factor of three over the 570 millisecond test values in order to maintain the same droplet concentration. However, such an approach would have overloaded the single Sonicore nozzle that was used in the previous tests. The cold flow model was therefore altered by mounting a total of three Sonicore nozzles, whose locations and injection aim points are shown in Figure 15.

Using three Sonicore nozzles with an atomizing air pressure of 180 kPa, a total DOP injection rate of 147 cm^3/min., and a 111 l/s air flow rate, resulted in the scattered laser beam decay trace shown in Figure 16.

The Figure 16 data are plotted in Figure 17, and using just the relatively smooth data points from time equals zero to 0.4 second, yields an experimental time constant of 205 milliseconds, in excellent agreement with the calculated time constant of 200 milliseconds. Unfortunately, this agreement is probably more a matter of circumstance than being truly representative of reactor flow behavior.

The Figure 16 scattering signal is much more erratic than was the case with earlier tests at an 39 l/s air flow rate. The DOP deposition on the model walls during the 39 l/s flow tests resulted in a uniform film thickness on the

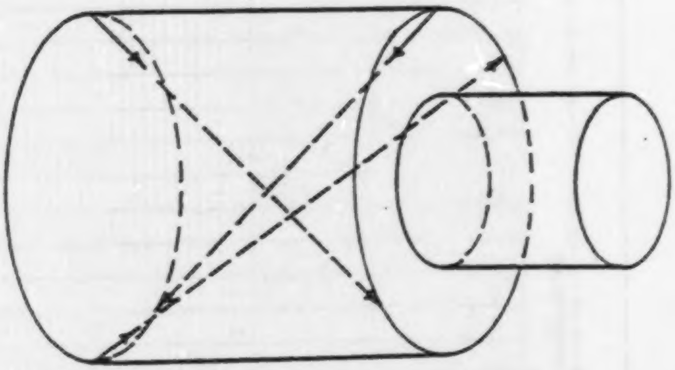

FIGURE 15. LOCATION AND ALIGNMENT OF THE SONICORE NOZZLES

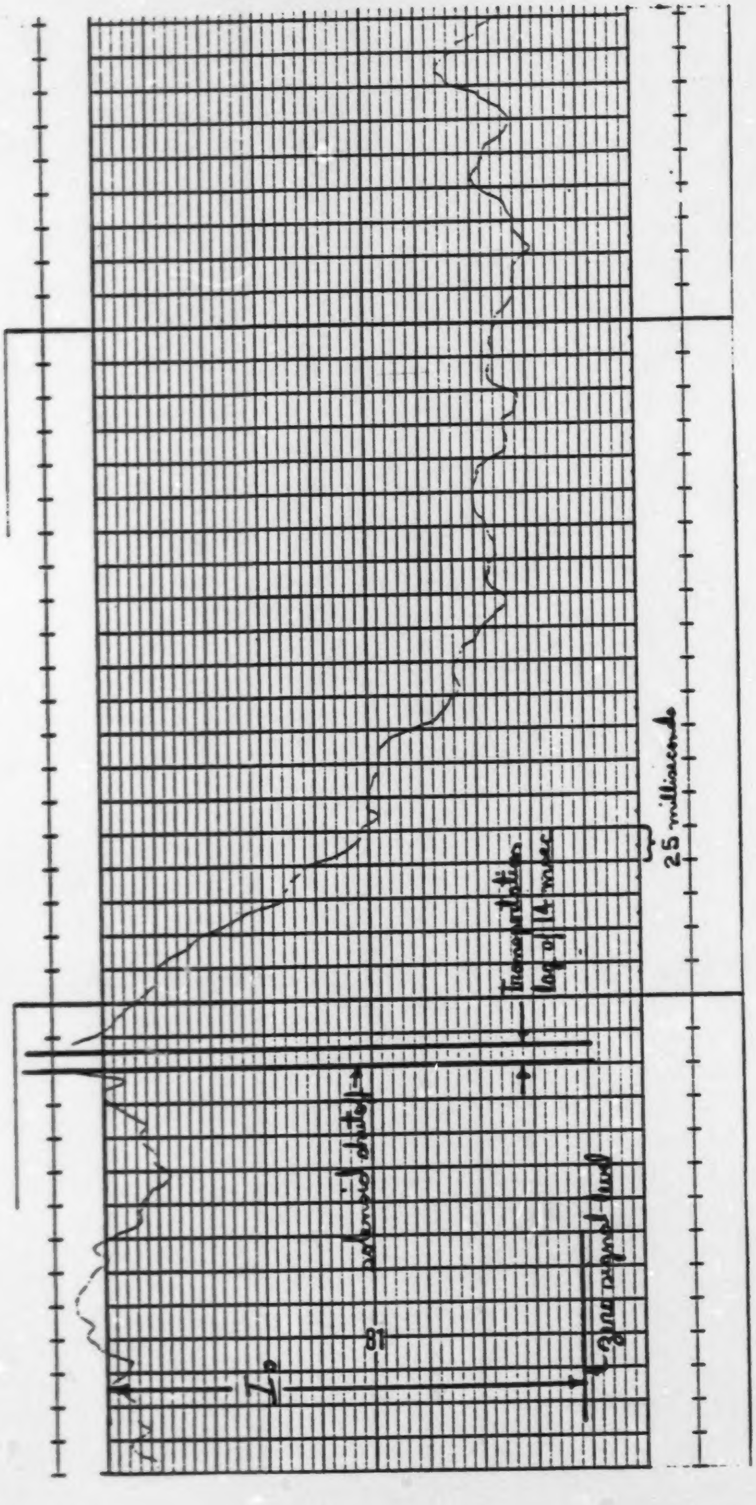

FIGURE 16. SCATTERED BEAM DETECTOR OUTPUT TRACE DURING A DECAY TEST (111 l/s air, 147 cm^3/min DOP, 180 kPa

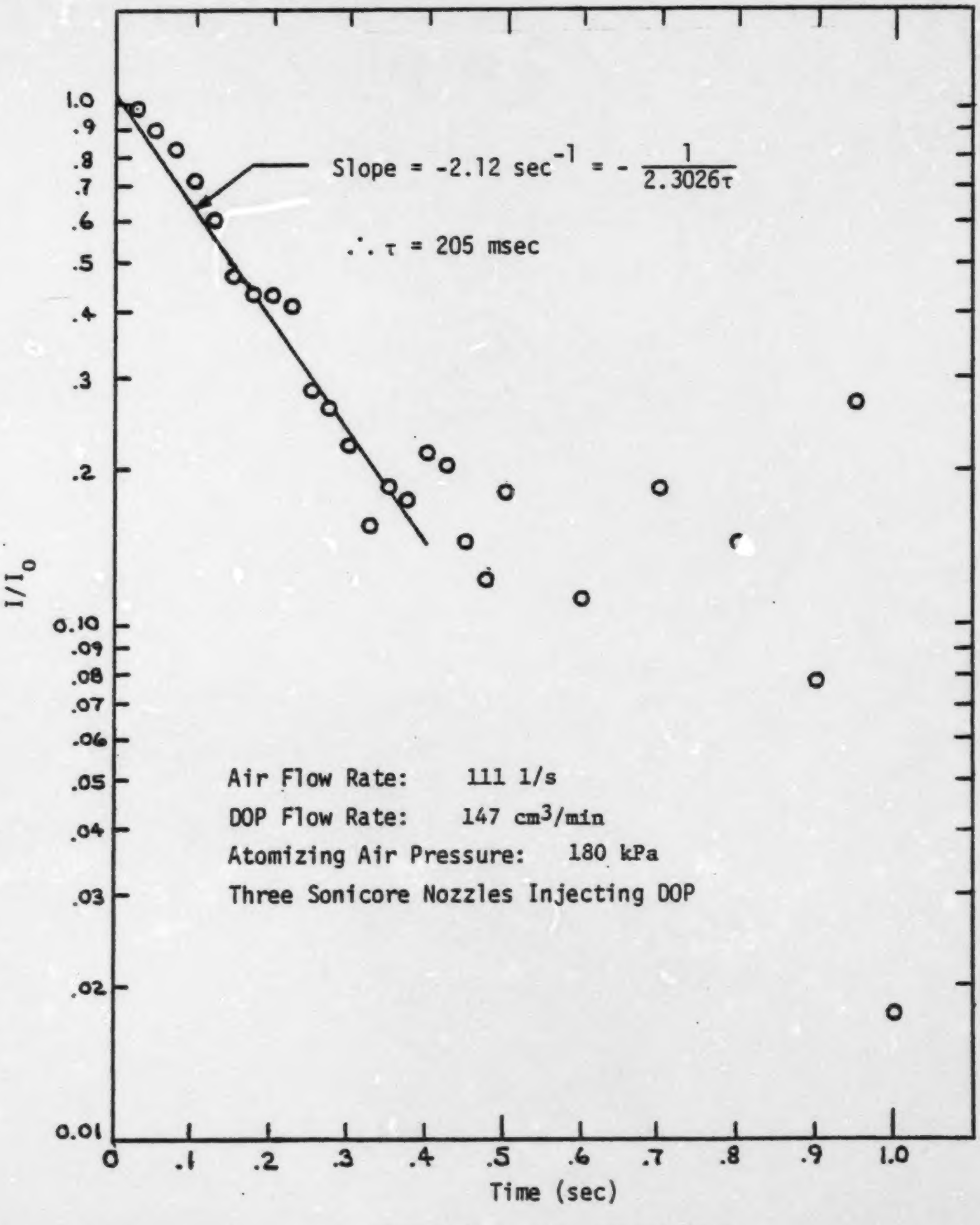

FIGURE 17. I/I$_0$ VERSUS TIME
(111 l/s air flow rate)

walls and a puddling of DOP at the bottom of the model. This puddle of DOP was gently blown around by the turbulent air flow but not to the extent that DOP was picked up and entrained in the air stream. The turbulence generated at an air flow rate of 111 l/s, however, was sufficiently intense to remove DOP from the liquid film on the reactor walls and to pick up large DOP droplets from the puddle at the bottom of the reactor. These large droplets, estimated to be up to two millimeters in diameter, were entrained in the air stream and carried out through the exit port. The effect of the large droplets passing through the laser beam scattering volume is shown as the large amplitude variations in the scattering signal trace of Figure 16. These fluctuations are not noise signals, but are representative of what is happening in the exit stream, where the scattering signal mean amplitude decays due to a drop in the concentration of the fine mist when the nozzles are shut off. The signal does not decay to a zero value, however, because large droplets continue to be picked up and blown out of the reactor for up to a half minute after the nozzles are shut off.

The presence of large droplets complicates the analysis of the scattering data not only because of the irregularities in the scattering signal, but also because of the effect of droplet size on the intensity of scattered light. When the droplet-size distribution remains constant, the intensity of scattered light at a given scattering angle is proportional to the droplet number density. If the droplet-size distribution changes, however, data taken simultaneously at three or more scattering angles are needed to resolve both the drop-size distribution and the droplet number density.

The exit stream at the instant of nozzle shutoff consists of a major portion of fine droplets and a minor fraction of the larger droplets extracted from the reactor walls and the puddled DOP. However, as the concentration of fine droplets decays, the concentration of coarse droplets decreases only slightly, thus the drop-size distribution of the total exit stream changes significantly during the decay test. Therefore, to obtain the necessary information on the spray decay in the exit stream it would be necessary to include additional detectors, choppers, and lock-in amplifiers in our present setup. Even if this were done, the next problem would be one of developing a mathematical model which would not only describe droplet deposition on the walls as derived earlier, but would also have to describe the removal of droplets from the walls and their entrainment in the air stream.

If the more complex experimental apparatus were constructed, data collected, and a model describing droplet deposition and removal developed, we would end up with a description of flow behavior in a reactor which extensively wets the walls with fuel. The hot combustor which is going to be used for firing residual fuel oil will not have the cold walls of the reactor model, and most likely would not exhibit the extensive droplet deposition phenomenon. Therefore, further analysis of the cold flow model appeared to be an unnecessary analytical exercise which would not improve our understanding of the hot combustor behavior.

It was then decided to construct the hot combustor to evaluate the extent of droplet deposition and to determine any other operating and/or design problems which might complicate the fuel NO_x experiments.

EXPERIMENTAL APPARATUS

COMBUSTOR CONSTRUCTION

Casting

The first combustor was cast in three pieces, as shown in Figure 18. This design was not very satisfactory because the joint length was excessive and extensive leakage of combustion gases out of the combustor occurred after only a short period of operation. Also, thermocouple wells cast into the wall were poorly placed, causing the refractory to fail at that point.

Therefore a second combustor was built using the design shown in Figure 19. Greencast 97-L castable refractory was used. A stepped seal was incorporated between the two halves of the combustor. This joint is tapered to unsure a snug fit. Layers of zirconia felt are used as a gasket where the surfaces meet. The combustion space is 250 mm in diameter and 242 mm long. The exit section is 127 mm in diameter. A 40 mm diameter port is located 75 mm from the front surface of the combustor. This two-piece design has worked out well. The tapered, stepped joint is snug; no leakage was noticeable during many hours of operation.

Wall Temperature Measurement

Holes for three thermocouples were cast into the combustor wall so that wall temperatures and wall heat fluxes could be calculated. These were equally spaced 35 mm apart in the 140 mm thick combustor wall. The holes were staggered over one quadrant of the cylinder to minimize stress on the wall. Type S thermocouples were inserted into these holes.

Combustor Insulation

The ends and circumference of the refractory casting have been insulated with approximately 25 mm of Cerafelt fibrous insulation. This insulation kept the stainless steel jacket from overheating. Also, it served as a plug to help contain any leakage from the combustor.

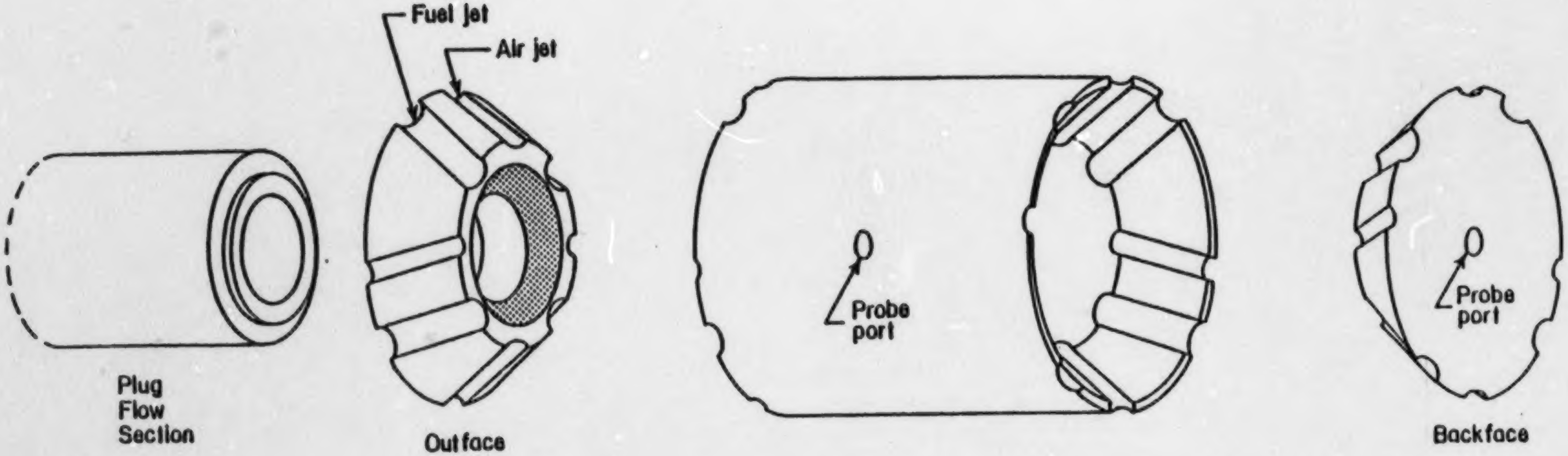
Fuel jet
Air jet
Plug
Flow
Section
Outface
Probe
port
Probe
port
Backface

FIGURE 18. EXPLODED VIEW OF COMBUSTOR I

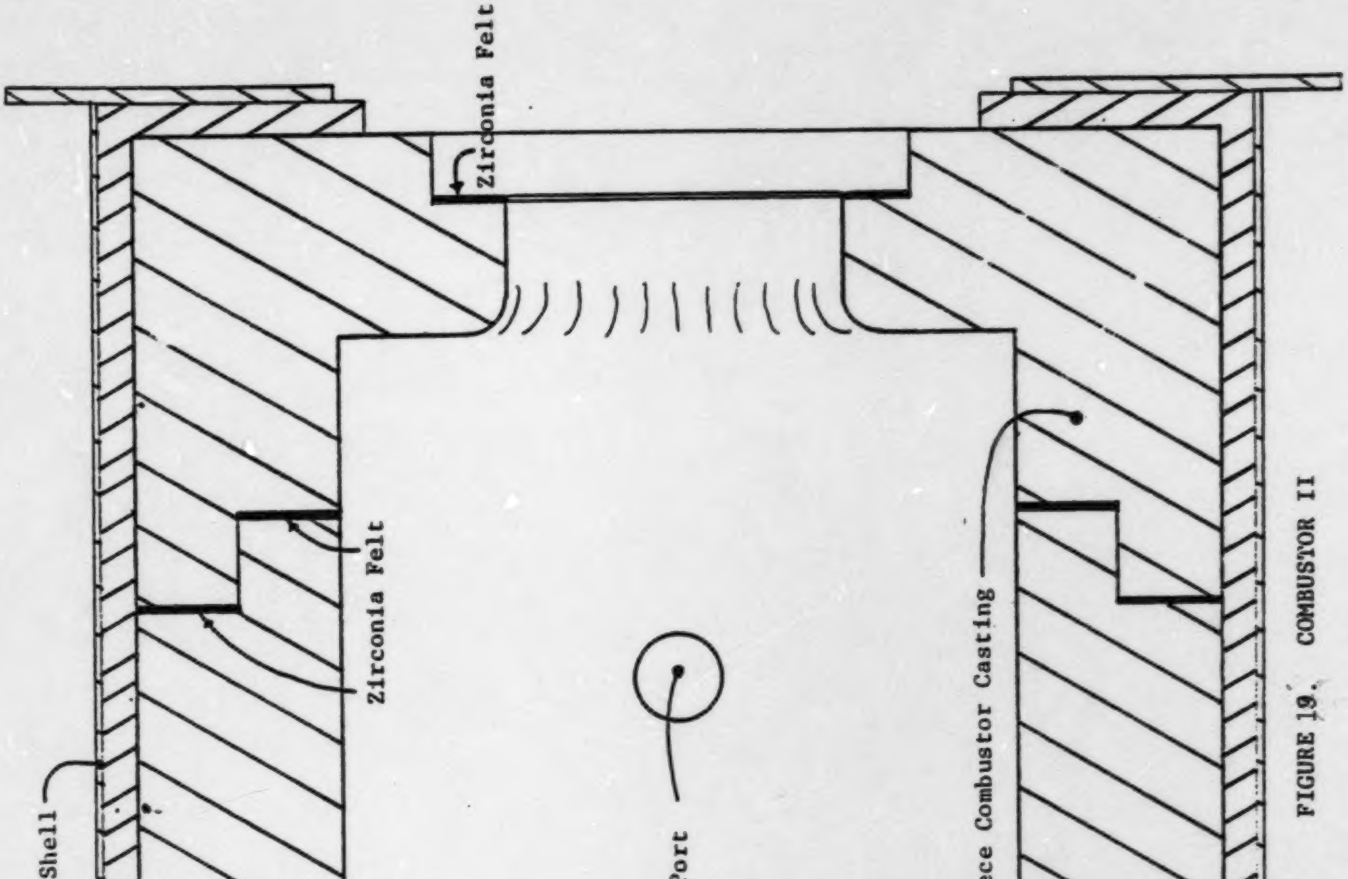
Zirconia Felt
Zirconia Felt
Zirconia Felt
Steel Containment Shell
Probe Port
Two-Piece Combustor Casting
Steel End Plate
CERA-Felt Insulation

FIGURE 19. COMBUSTOR II

Combustor Jacket

A stainless steel jacket was fabricated to fit the well-stirred combustor. This jacket also helped to contain any gas leakage from the combustion volume.

Air Jet Mounting

Figure 20 shows the mounting of the air jets. The air jets are the ones used in the cold flow model and are constructed from 3/4 in. nominal black pipe, internally threaded at one end to accept screw-in orifices. The orifice can be changed to allow control of the air velocity from the jet. The black pipe was mounted in a 25 mm ID, mullite tube cast into the refractory.

Fuel Nozzle Mounting

Model 052M-1 Sonicore nozzles were used in the hot combustor as opposed to the Model 052H-A used in the cold flow model. The Model 052M-B-1 nozzles are constructed entirely of stainless steel. This construction permits operation at higher temperatures than the Model 052H-A which has Viton or Teflon O-rings.

Figure 21 shows the mounting for the Sonicore nozzles. The nozzles were mounted in a water-cooled stainless steel chamber which was fitted into a 50-mm OD, 38-mm ID mullite tube. This mullite tube was also cast directly into the refractory.

A thermocouple was mounted in a hole bored in the wall of the tapered tip of one nozzle to measure the fuel oil temperature.

FLOW MEASUREMENT SYSTEM

All flows were monitored by the flow measurement system shown in Figure 22. This flow measurement system uses a thin-plate orifice and manometer combination to measure the combustion air. Rotometers are used in the atomizing air, natural gas and No. 2 oil lines. The latter was calibrated by time and mass measurements at different flow rates. The No. 5 oil is metered by a rotometer calibrated by time and mass measurements also. The fuel supply system allows either No. 2 or No. 5 oil to be taken from drums, filtered and

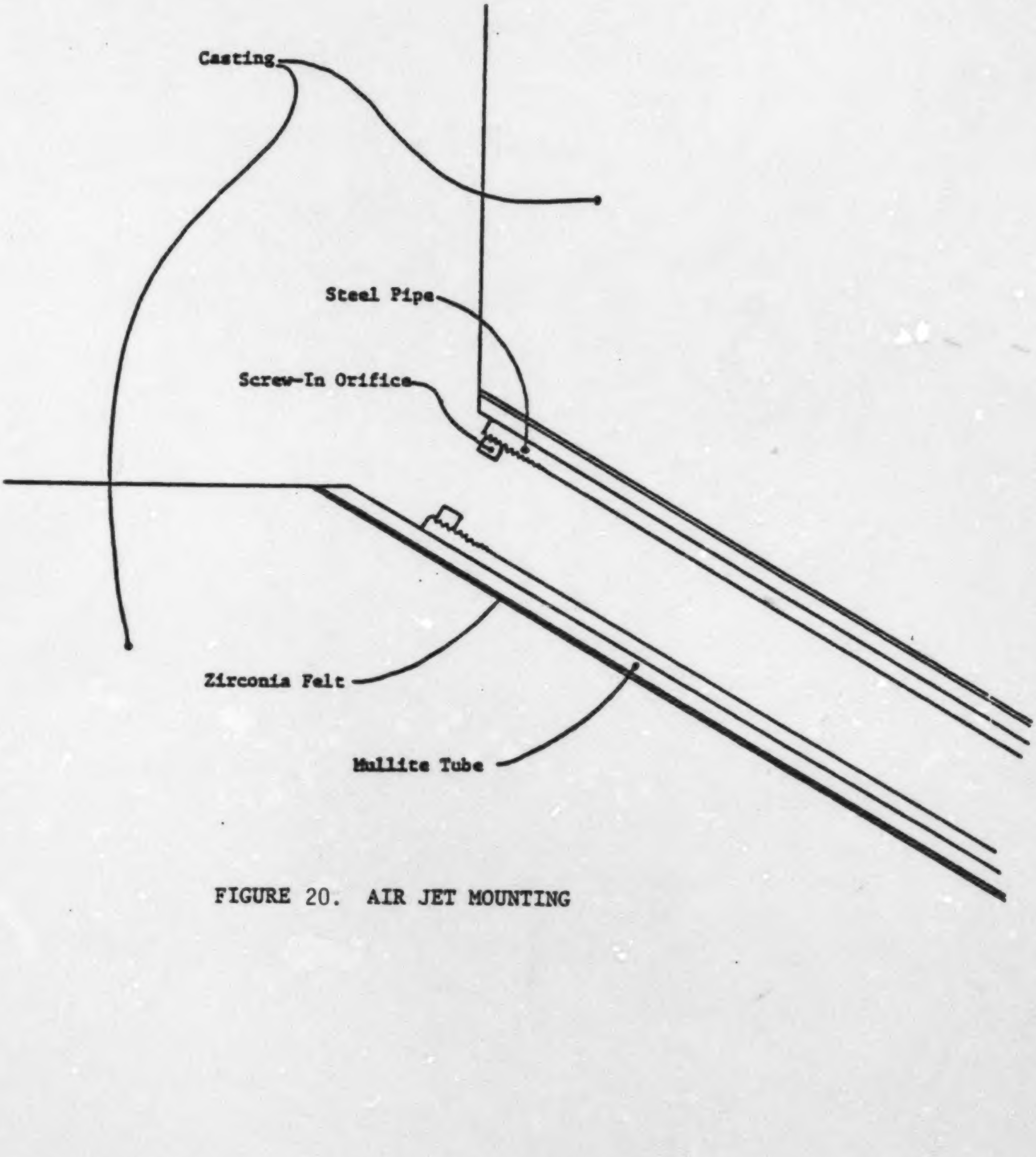
Casting
Steel Pipe
Screw-In Orifice
Zirconia Felt
Mullite Tube

FIGURE 20. AIR JET MOUNTING

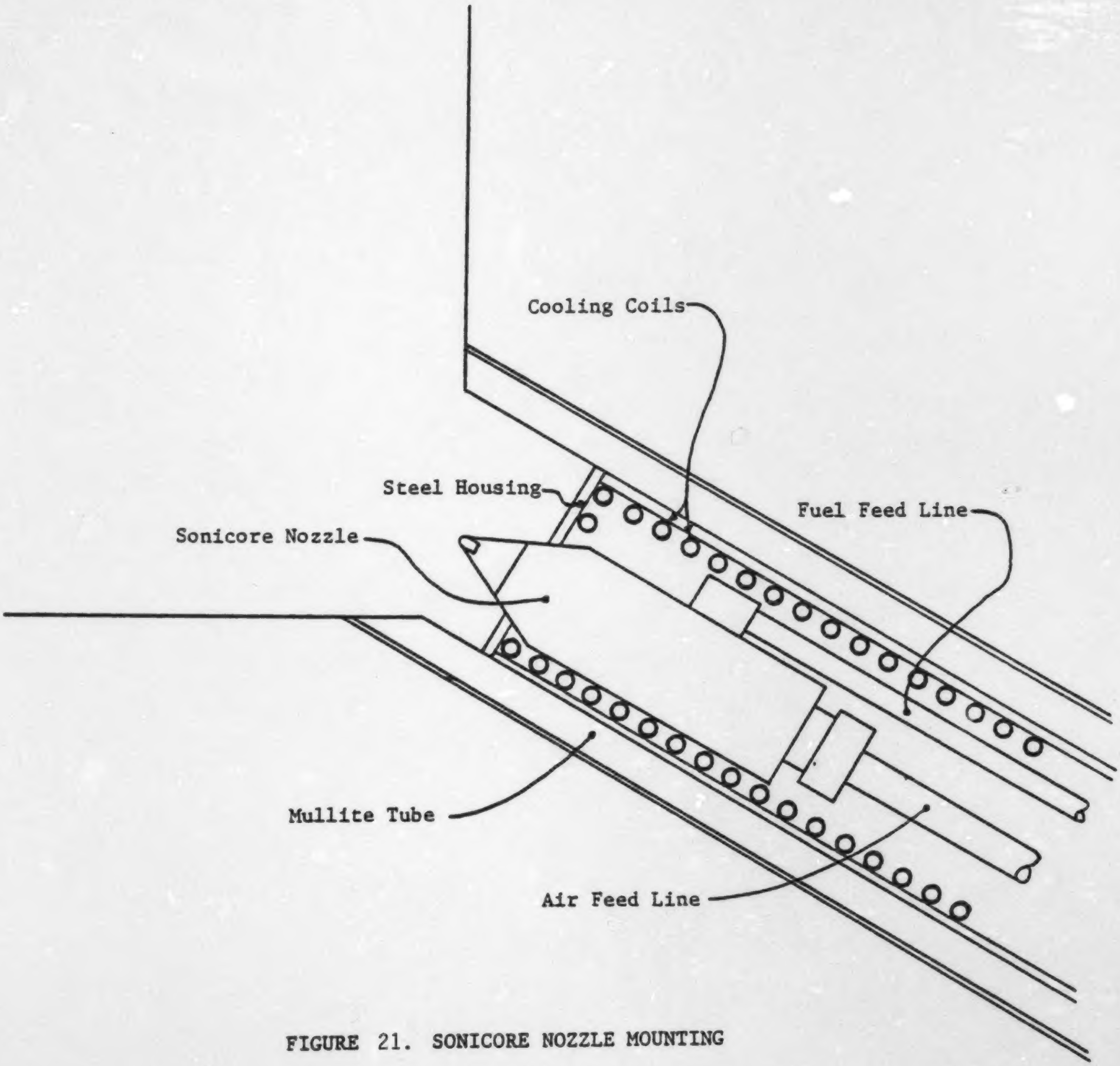
Cooling Coils
Steel Housing
Fuel Feed Line
Sonicore Nozzle
Mullite Tube
Air Feed Line

FIGURE 21. SONICORE NOZZLE MOUNTING

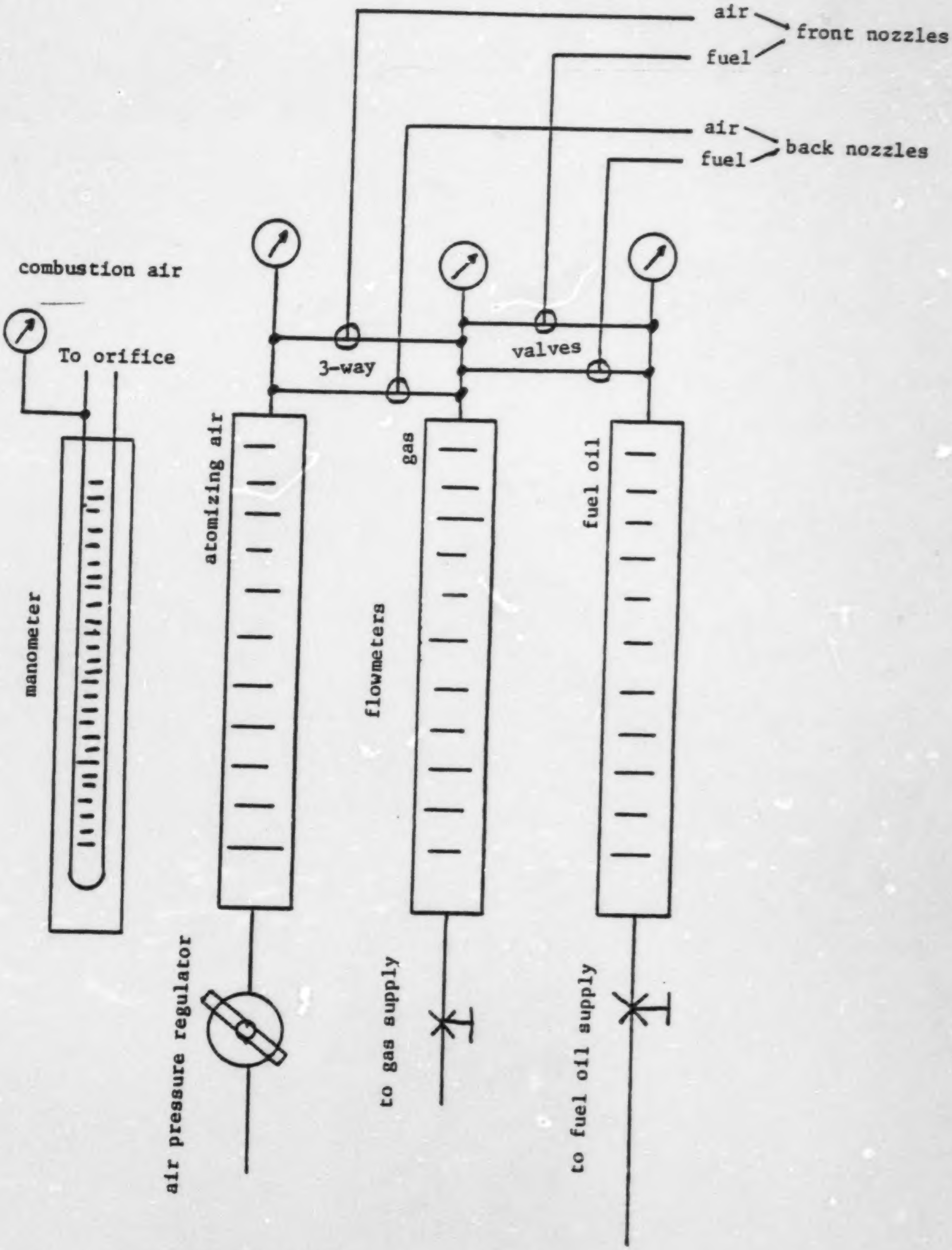
air
fuel
front nozzles
air
fuel
back nozzles
combustion air
To orifice
3-way
valves
manometer
atomizing air
gas
fuel oil
flowmeters
air pressure regulator
to gas supply
to fuel oil supply

FIGURE 22. FLOWS TO WELL-STIRRED COMBUSTOR

pumped to the rotometer for flow measurement. The oils can be preheated as necessary. The oil lines were heat traced and insulated to maintain proper oil temperature.

AFTERBURNER

In order to prevent large amounts of a flammable mixture from accumulating near the combustor exhaust and to help reduce the CO concentration an afterburner system was constructed. This system consists of a secondary air blower, gas pilot, flame failure monitor and mixing chamber. An 11-m stack helps to disperse the combustion gases. The blower is sized to provide the necessary oxygen to complete the burning of the fuel as well as that required by the gas pilot. Since the operation of the afterburner is largely unattended, a flame rectification-type flame failure safety control was used.

PREDICTION OF COMBUSTION PRODUCTS

Knowledge of the composition of the products of combustion is important in the design of the emissions measurement system, and also in the subsequent handling of those products. This was felt to be particularly important for high fuel-air equivalence ratios where the products composition was much different from the usual stack gas. A simple thermodynamic model was used to calculate the properties of equilibrium combustion products for various equivalence ratios and temperatures at which the combustion products equilibrium was assumed to be frozen. The computer code used for this purpose considered the gas phase products of combustion of hydrocarbon fuels containing C, H, O, and N atoms, and air. A more complete description of the computer code and algorithm is given in Reference 5.

These calculations predict CO concentrations of about 9 percent and hydrogen concentrations of about 11 percent for a of 1.6. Other concentrations are shown in Table 4. These results were used in the selection of emissions measuring equipment. They also showed that when the combustor is running rich the products are both flammable and toxic, necessitating an afterburner.

TABLE 4. PREDICTED PRODUCT MOLE FRACTIONS FOR $CH_{1.72}$ FUEL, T = 873 K, P = 101 kPa, ϕ = 1.6

```
    1.000 1.720 0.000 0.000    873.0000     101.0000        1.6000
0 0 0 0
           1    .1586E-10
           2    .9160E-24
           3    .5704E-25
           4    .1155E+00
           5    .4733E-14
           6    .8952E-01
           7    .6894E-17
           8    .2354E-24
           9    .4890E-01
          10    .1016E+00
          11    .6368E+00
          12    .7586E-02
```

NUMBERING CODE FOR PRODUCT SPECIES -

Subscript	Species
1	H
2	O
3	N
4	H_2
5	OH
6	CO
7	NO
8	O_2
9	H_2O
10	CO_2
11	N_2
12	Ar

DATA ACQUISITION SYSTEM

In order to efficiently carry out a series of combustor runs at different residence times, the instantaneous residence time should be known. This means having the exit temperature, pressure and composition data readily available for determination of the residence time. A data acquisition system was installed that both collects the necessary data and derives the desired calculated parameters.

FUEL

The well-stirred combustor was designed to operate using natural gas, Number 2 distillate oil or Number 5 residual oil as the fuel. When the combustor is fueled by natural gas, the result is very well-mixed homogeneous combustion that can form a baseline to which the fuel oil can be compared. The Number 2 oil provides a situation in which fuel droplets are present in the combustor. The Number 2 oil has a very low fuel nitrogen content. This fuel provides a situation where droplet burning is occurring in the combustor, and additional NO_x emissions can be ascribed to the type of burning. The residual oil contains a moderate amount of fuel nitrogen. This fuel formed the basis for the study of apparent fuel nitrogen conversion.

NATURAL GAS

The natural gas was supplied by Columbia Gas of Ohio. This gas is reported to be 96 percent methane, 2.5 percent ethane, 1 percent carbon dioxide, and 0.5 percent miscellaneous hydrocarbons. The density compared to air is 0.584. The heating value of this fuel, dry, is 38.3 MJ/m^3, or 56 MJ/kg.

NUMBER 2 OIL

The Number 2 oil used in this study was standard residential heating oil as sold by local distributors. Table 5 gives the analysis of the Number 2 fuel oil used.

TABLE 5. ANALYSIS OF NO. 2 OIL

Carbon	86.94%
Hydrogen	12.97%
Nitrogen	0.01%
Sulfur	0.19%
Ash	< 0.05%
Oxygen	< 0.5%
Carbon hydrogen ratio	$CH_{1.79}$

RESIDUAL OIL

The residual oil was a Number 5 oil of Indonesian-Malaysian origin supplied by EER. This oil is considered "light" and "sweet"; that is the viscosity is fairly low and the sulfur content low for oils of this type. Table 6 gives a complete analysis of this fuel oil.

FUEL NITROGEN ANALYSIS

The residual fuel oil was analyzed by two different laboratories; the results were 0.24 percent and 0.26 percent. The close agreement between the two analyses indicates that there is no problem with the nitrogen determination for this fuel.

TABLE 6. ANALYSIS OF RESIDUAL FUEL OIL(a)

Ultimate Analysis:	
Carbon, percent	86.53
Hydrogen, percent	11.93
Nitrogen, percent	0.24
Sulfur, percent	0.22
Ash, percent	0.036
Oxygen, percent (by difference)	1.04
Conradson carbon residue, percent	3.98
Asphaltene, percent	0.74
Flash point, °C	99
Pour point, °C	16
Density, jg/m^3	922
Viscosity, cst at 60 C	43
at 100 C	10
Heat of Combustion:	
Gross, kJ/kg	44,320
Net, kG/kg	41,780
Calcium, ppm	14
Iron, ppm	16
Manganese, ppm	0.13
Magnesium, ppm	3.6
Nickel, ppm	17
Sodium, ppm	57
Vanadium, ppm	2.3

Vacuum Distillation

	mm HG	°C	Boiling Point Corrected to 760 mm Hg, C	Nitrogen
Initial B.P.	2.4	68	230	--
10%	2.0	112	295	--
20% cut	1.7	146	343	0.009
30%	1.4	177	388	--
40% cut	1.2	197	422	0.045
50%	1.0	218	457	--
60% cut	1.0	249	497	0.096
70%	1.1	266	516	--
74%	1.8	322	580	0.21
Residue			Pyrolysis	0.66

(a) Analysis done by Truesdail Laboratories, Inc., Los Angeles, CA

EMISSIONS MEASUREMENT

SAMPLE SYSTEM

Figure 23 shows the overall layout of the sample system. Samples for analysis are withdrawn through a 2.8 mm ID high-purity alumina probe. A short, heated stainless steel tube connects the sample probe to a pair of filters. The probe has an integral heat exchanger to reduce the sample temperature rapidly. This heat exchanger provides sufficient cooling to reduce the sample temperature at the probe exit to about 150 C. The residence time of the sample in the hot (>150 C) portion of the sample probe is estimated to be 0.8 millisecond. The filter oven is maintained at a temperature of 150 C and contains a course glass wool filter and a 120-mm diameter Pallflex T60A20 Teflon-impregnated glass fiber filter.

A heated (150 C) stainless steel sample line takes the sample to a heated pump and then to the various monitoring instruments. The product gas for THC, NO, HCN, and NH_3 analysis is always heated. Product gas to the CO_2, CO, and O_2 instruments is cooled to condense out water vapor before being fed into these instruments.

HCN AND NH_3 ANALYSIS

Two parallel gas washing bottles are used for HCN and NH_3 absorption. The first, for HCN absorption, contains 0.1 M NaOH plus 5 g/l $CdCO_3$. The second, for NH_3 absorption contains 0.05 M H_2SO_4. Orion ion-selective electrodes are used for measuring both species and Orion procedures are followed for calibrating the meter and handling the sample solutions.

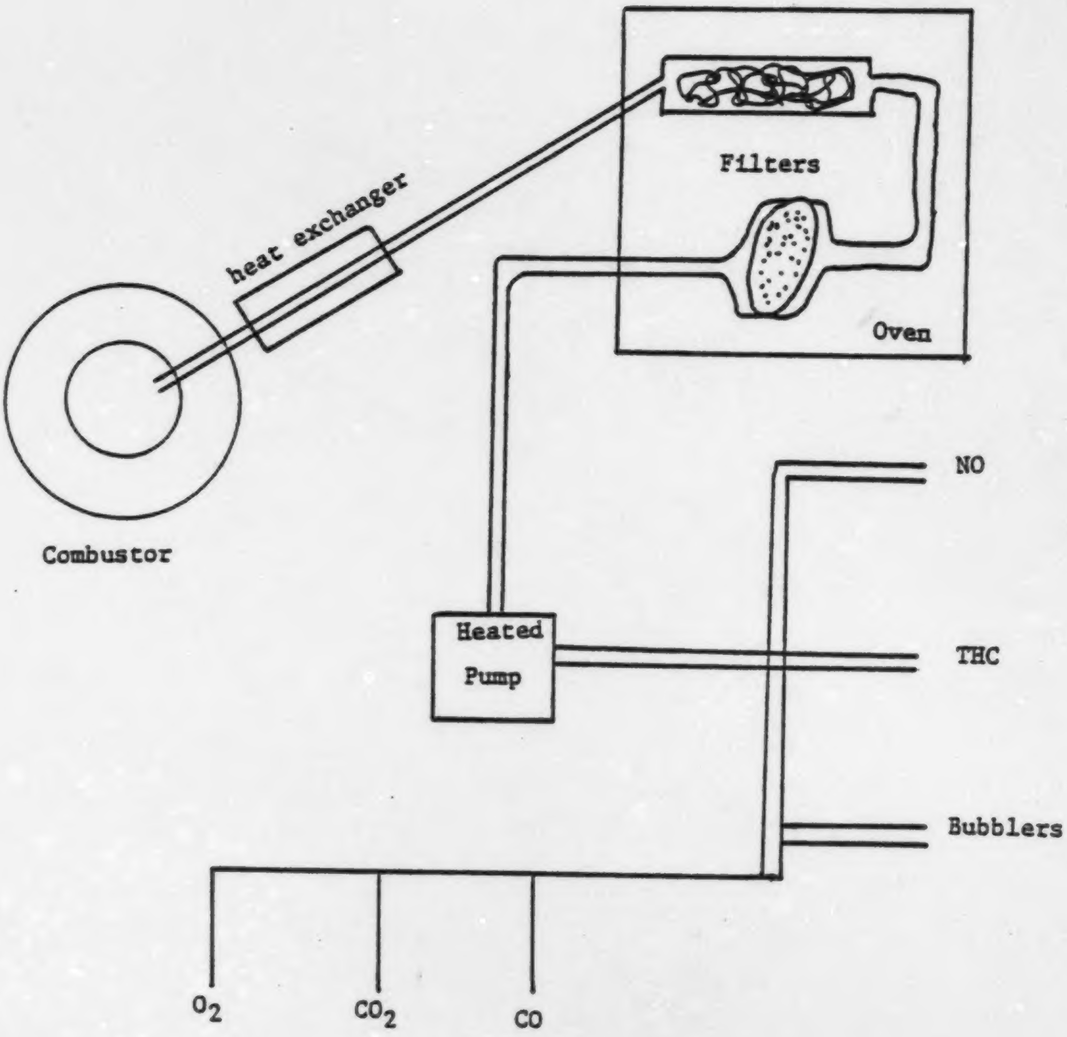
Filters
heat exchanger
Oven
Combustor
NO
Heated
Pump
THC
Bubblers
O_2
CO_2
CO

Figure 23 Sample System

RESULTS

INITIAL TEST FIRINGS

During the first year's effort, a number of "shakedown" tests were made of the well-stirred combustor. The purpose of these test firings was not so much to delve into the NO problem as to determine some of the operating characteristics of the combustor. Due to the short life of the first casting, these firings were not extensive. The results are summarized below.

Natural Gas

The combustor was initially fired on natural gas to heat the combustor walls so that the liquid fuels would fire in a stable manner. The natural gas was fed through the fuel lines of the Sonicore nozzles and was mixed with the atomizing air before before injected into the combustor (for these early tests). The natural gas/air mixture in the combustor was easily ignited using a propane torch, and the resultant burning was stable and easily maintained, even when starting with a cold combustor. Observation of the burning, as viewed through the exit port, showed the natural gas to be burning as jet flames extending from the Sonicore nozzles, a distance of 100-150 mm. A firing rate of 3 g/s was attained.

Number 2 Fuel Oil

The initial tests with Number 2 oil showed that this oil burned steadily once the wall temperatures had been brought up to 650 C. The combustor's inner walls stayed clean during these tests.

Residual Fuel Oil

Early tests with a residual oil preheated to 50-60 C were hampered by poor combustion of the fuel and rapid plugging of the fuel nozzles. Changes in the fuel and fuel supply system were made subsequent to these tests which resolved these problems.

NO_x TEST FIRINGS

Natural Gas Data

The well-stirred combustor was operated with natural gas both rich and lean. Figures 24-30 show the results of these tests. All HCN and NH_3 measurements were zero in these experiments. The NO levels appear reasonable for a high intensity gas burner(6); however, the peak value occurs at a richer condition than would have been expected on the basis of tests with other types of gas burners. The location of the peak NO seems to reflect the combustor temperature; the temperature peaks coincide with the NO peaks (of Figures 29 and 30).

Emission Index for NO

Because combustion is basically a process of chemical reaction, it is desirable to relate the products of the reaction to the reactant--the fuel. Owing to the uncertain composition of the fuel, its quantity is best measured on a mass basis. In order to allow the addition or comparison of the various nitrogen species, an emission index, moles of specie per gram of fuel burned, was used. In order to scale the resulting index, the quotient is multiplied by 10^6. This emission index differs from a mass/mass index merely by the molecular weight of the specie in question. Thus, EI_{NO} is defined as

$$EI_{NO} = \frac{\frac{gN}{14} \times 10^6}{g\ fuel}$$

The practice of reducing measured emissions values to a certain percent oxygen is often used with lean combustion. But this method becomes very awkward for rich mixtures and was therefore not used in this study.

Example

For an equivalence ratio of 1.2, 112 ppm of NO is measured.

$$EI_{NO} = \frac{(ppm\ NO)\ [\phi + (A/F)_{st}]}{(MW_{prod})\ (\phi)}$$

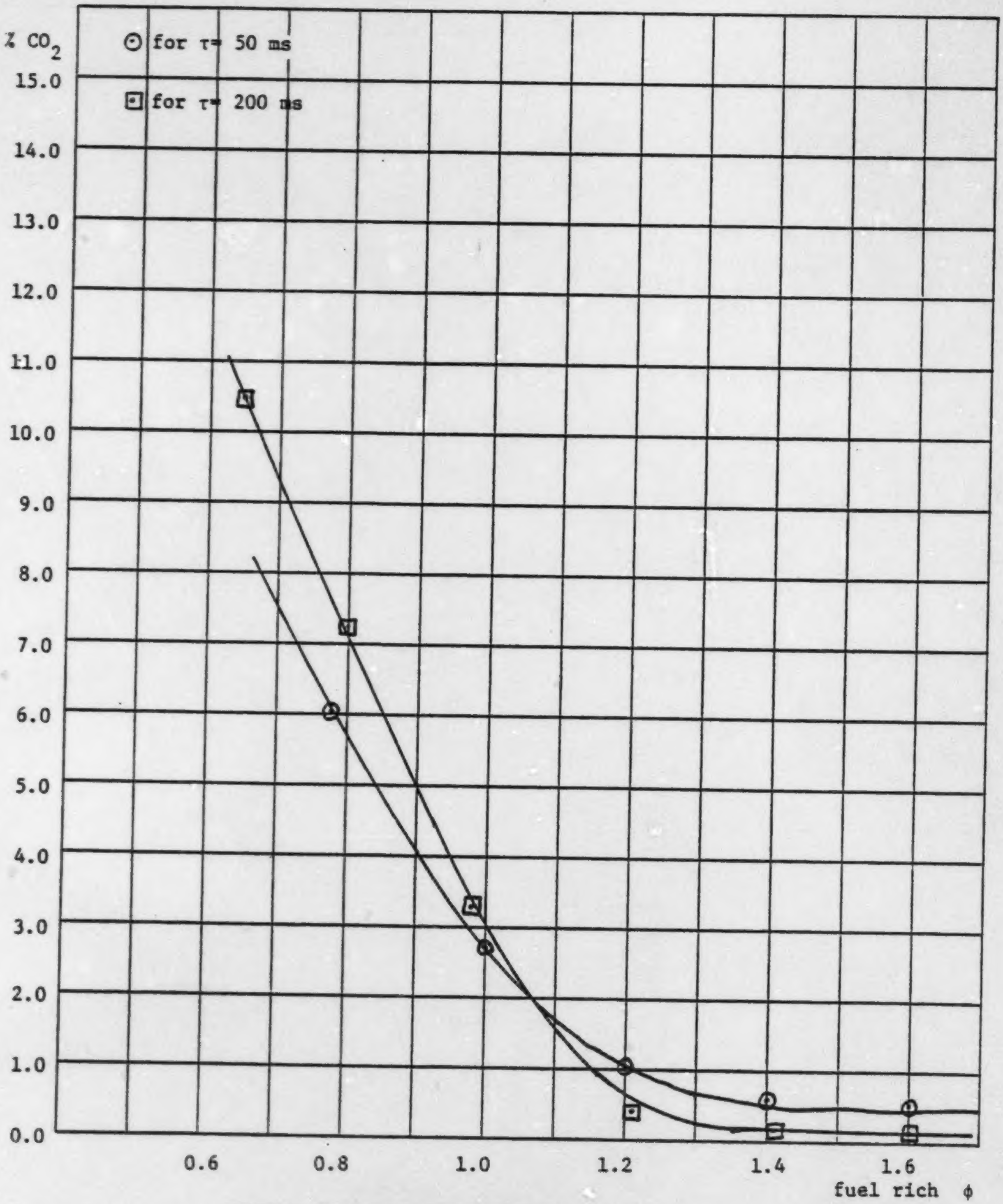

FIGURE 24 OXYGEN VS EQUIVALENCE RATIO

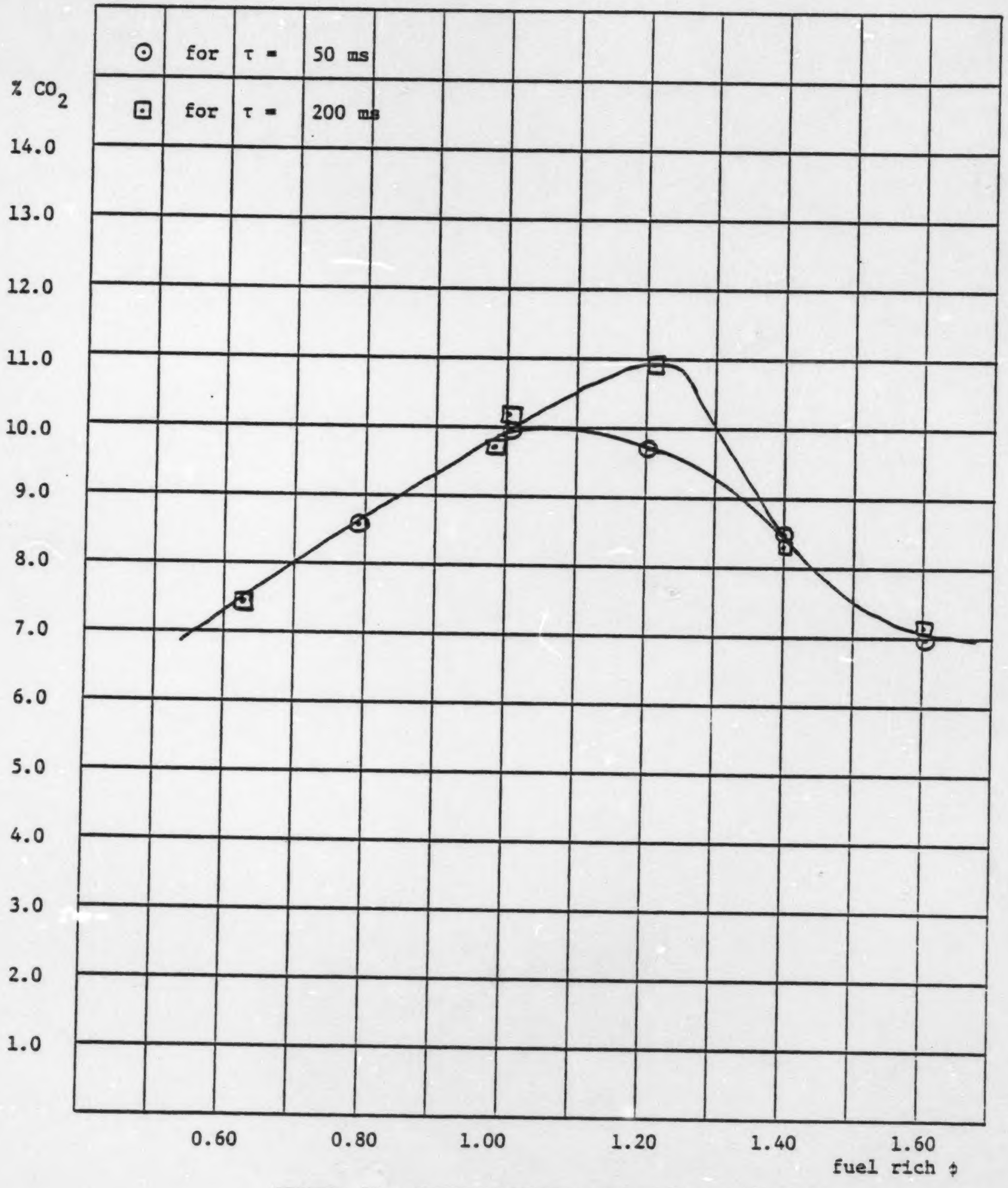

FIGURE 25 CARBON DIOXIDE VS EQUIVALENCE RATIO

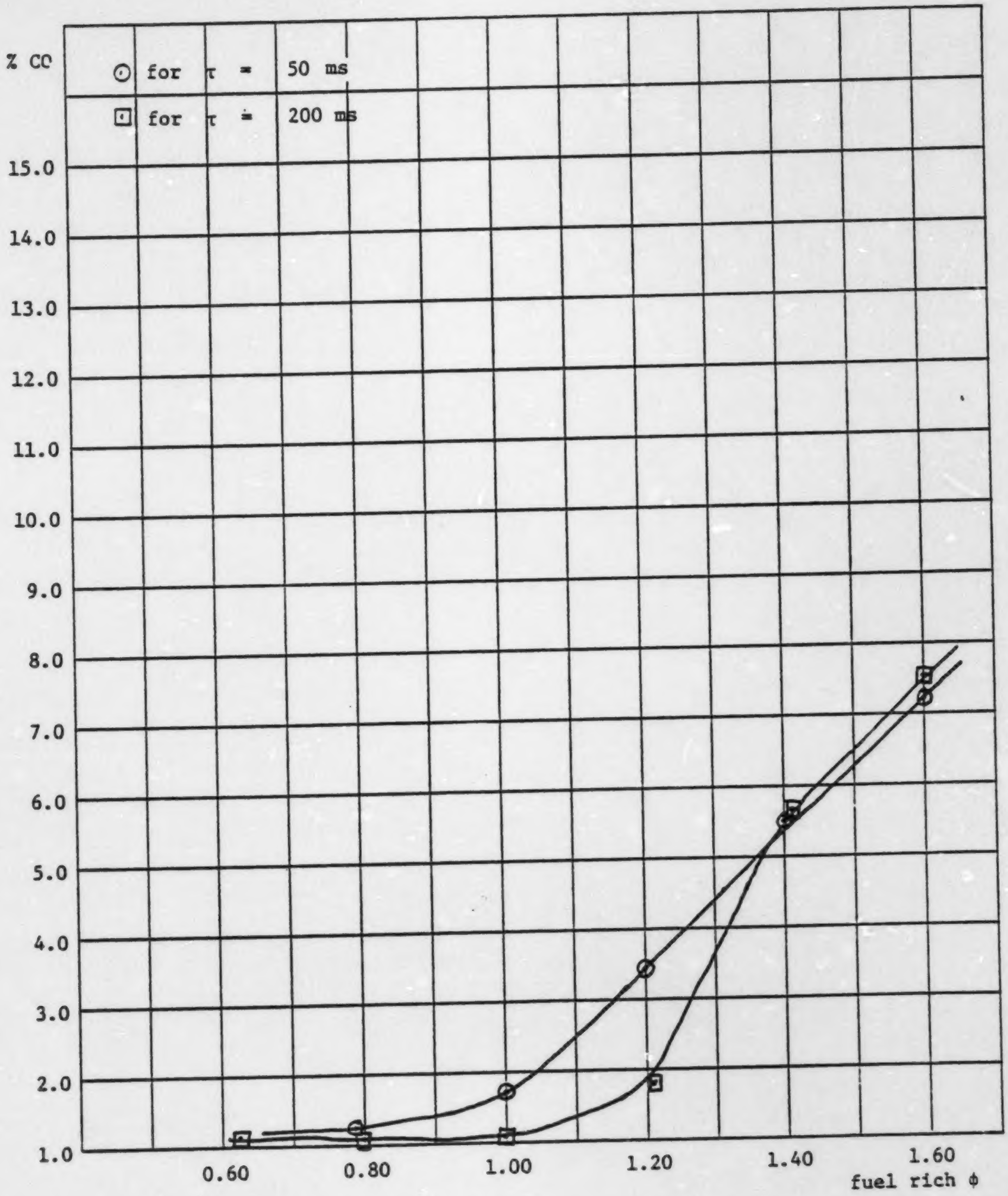

FIGURE 26 CARBON MONOXIDE VS EQUIVALENCE RATIO

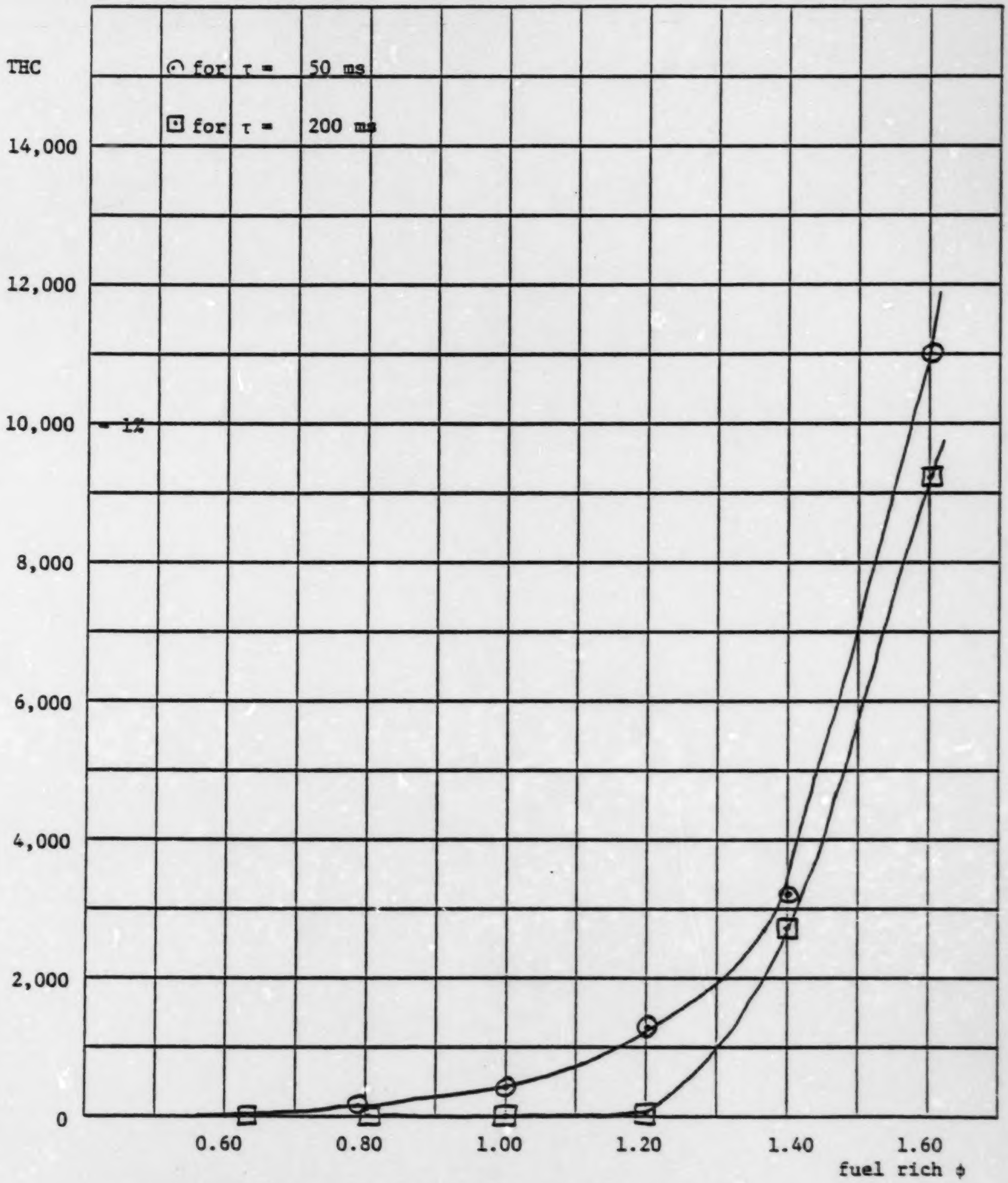

FIGURE 27 TOTAL HYDROCARBON VS EQUIVALENCE RATIO

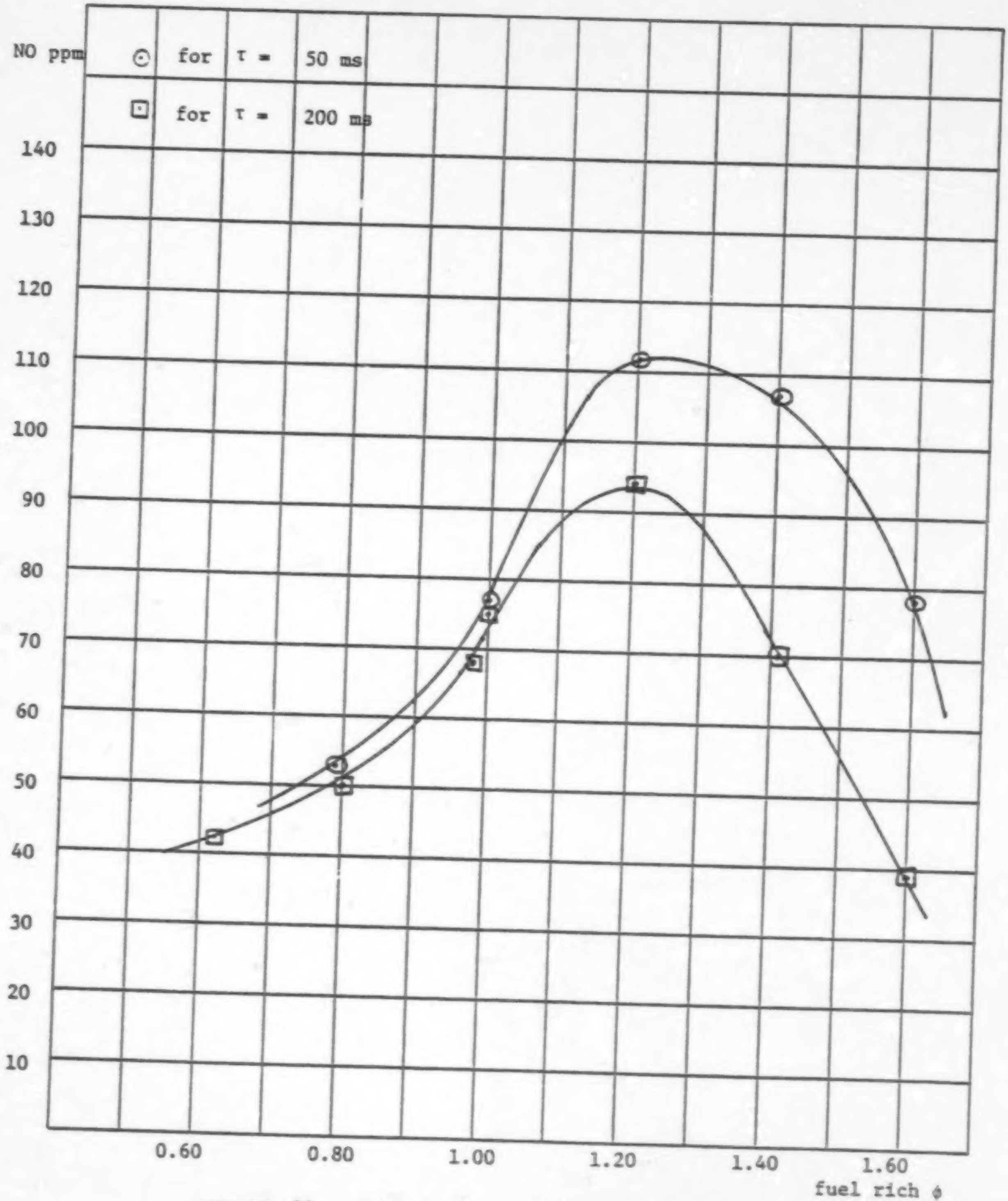

FIGURE 28 NITRIC OXIDE VS EQUIVALENCE RATIO

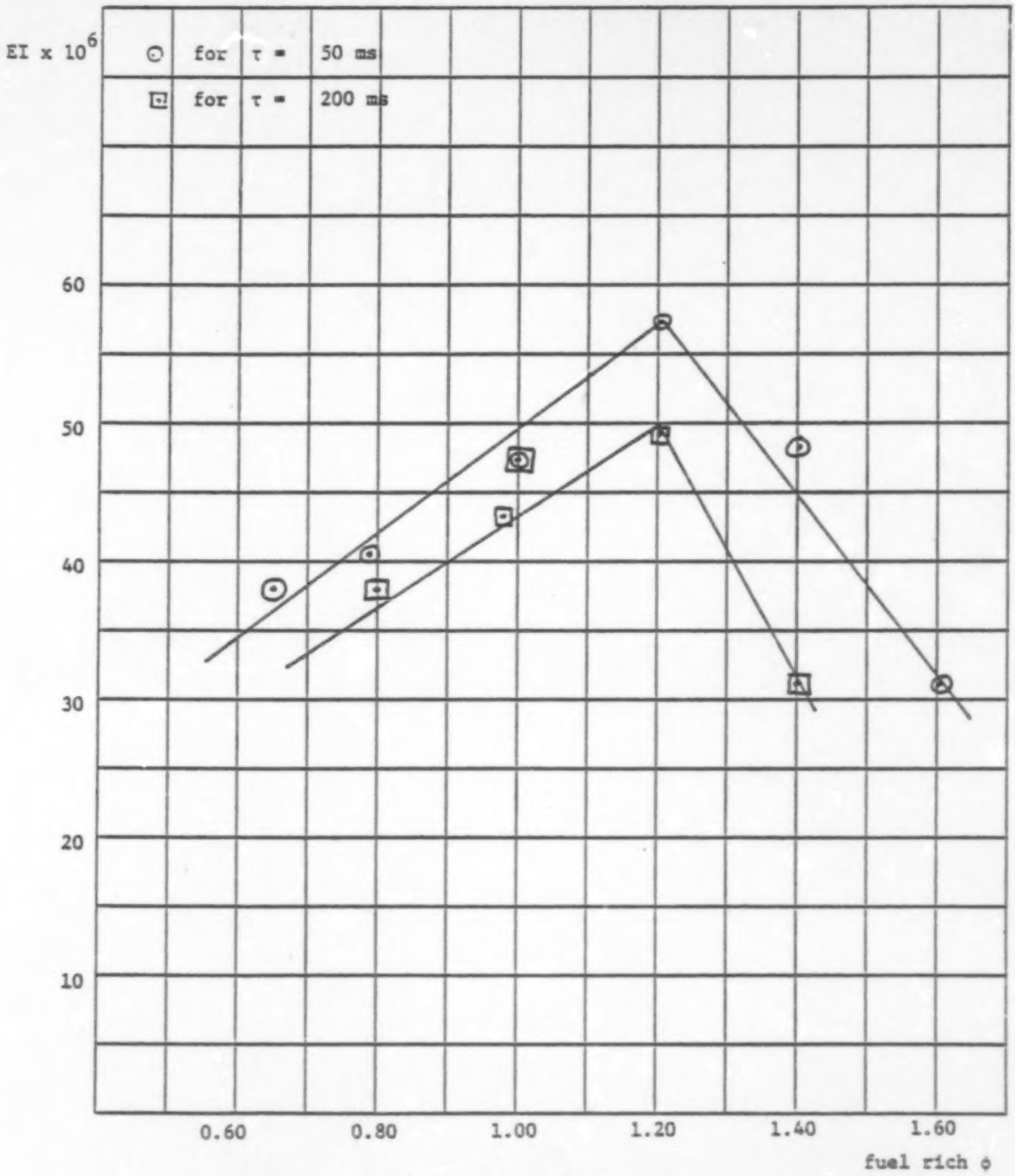

FIGURE 29 EI_{NO}, $\frac{\text{g mol NO}}{\text{g fuel}}$ VS EQUIVALENCE RATIO

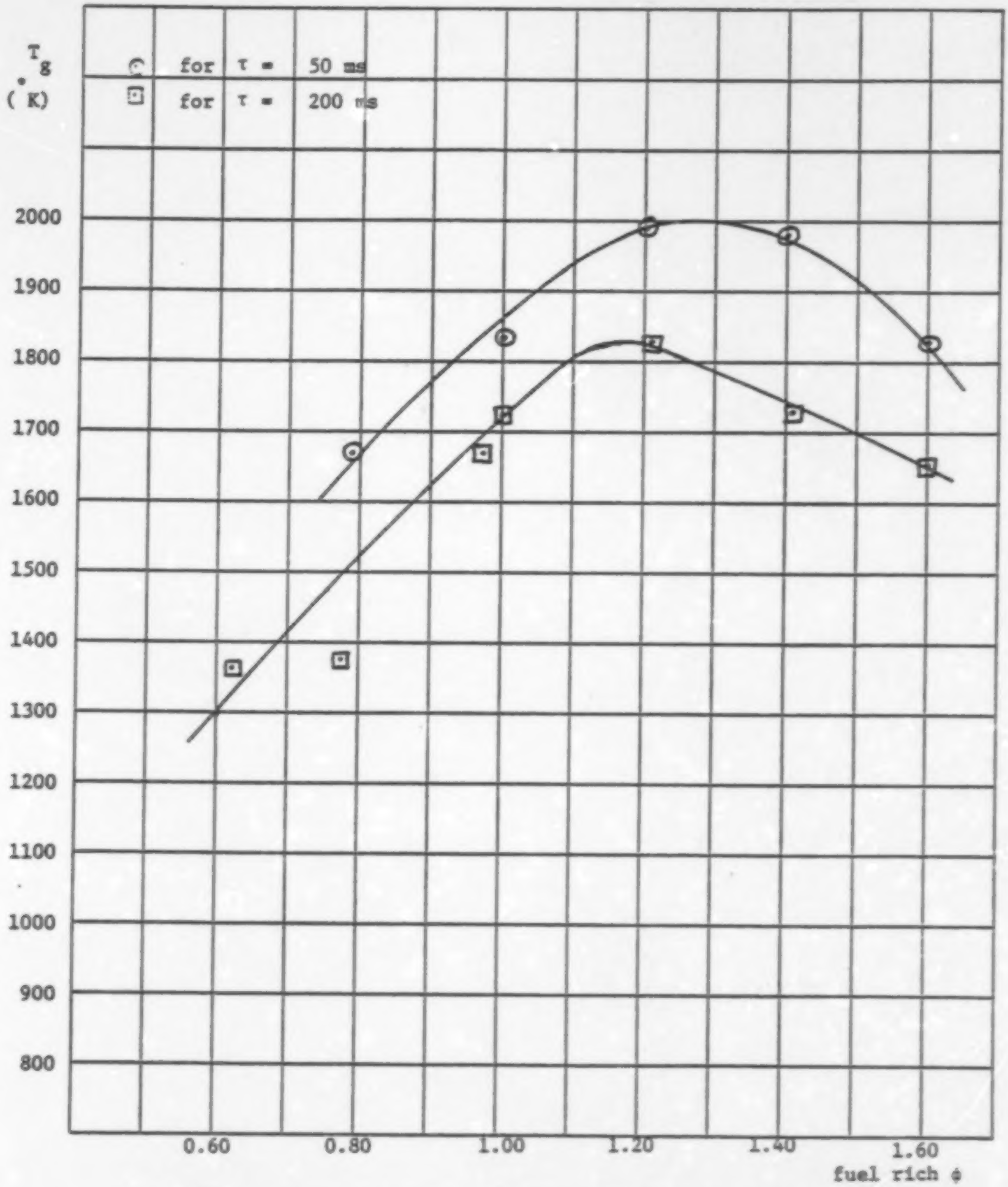

FIGURE 30 COMBUSTOR TEMPERATURE VS EQUIVALENCE RATIO

where

ppm NO = measured ppm NO

= equivalence ratio (>1, if rich)

$(A/F)_{st}$ = Stoichiometric air fuel ratio

MW_{prod} = average molecular weight of products

= taken as 28.5 (accurate to ± 5%)

EI_{NO} = 58

Operation with Number 2 Oil

Number 2 oil was burned both rich and lean in the combustor. The data are summarized in Table 7.

TABLE 7. EMISSIONS DATA FOR NUMBER 2 OIL

		T	O_2	CO	CD_2	NO	EI_{NO}
1.25	49 ms	1782 K	0.8%	1.3%	14.6%	273 ppm	118
0.65	50	(a)	10.2	0.0	8.4	104	81

(a) Thermocouple burned out.

No HCN or NH_3 was measured for the combustion of Number 2 oil. The flame was, of course, much more luminous than the natural gas flames. Although data is limited, the 273 ppm NO produced by the rich flame is much higher than a comparable value for natural gas where 110 ppm was measured, even though the natural gas flame was 200 K hotter than the oil flame. Likewise for the lean case, the Number 2 oil produced over twice as much NO as the natural gas. The higher level of NO may be an indication of a more prompt NO. The droplet burning that occurs in the oil flames will provide zones of rich burning that may be particularly conducive to prompt NO formation(7). No NH_3 or HCN was measured for the Number 2 oil. This is consistent with the lack of fuel nitrogen in this grade of oil, but not with the prompt NO.

Operation with Number 5 Oil

The Number 5 oil burned smoothly in the well-stirred combustor. No difficulties with ignition were noted. A slight coke buildup was noted when burning rich, but the volume was negligible in comparison with the combustor volume. Also, it should be noted that the residual oil was burned for up to 5 hours at a time, thus, providing ample time for any possible buildup to occur. This coke is probably related to the fact that the small cups were burned off several of the Sonicore nozzles. Although overall performance seemed good, the spray pattern may have been affected.

Toward the end of the series of tests with the residual oil, several nozzles were disabled. This occurred not because of clogging or coking in the nozzle, but because the heat from the flame was so intense that the nozzle and/or nozzle housing melted. This was apparently caused by the clogging of the small cooling tubes in the nozzle assemblies. A redesign of the nozzle cooling arrangement would cure this problem.

Overall, the performance of the fuel spray system was good and when the plug in the observation part was removed, a luminous flame with many burning oil drops were visible coming out of the port. (The combustor was under positive pressure at the higher firing rates.) The burning oil drops could be identified by their characteristic white smoke trails.

Although the amount of data for this fuel is less than for the natural gas, this reflects chiefly the limited time for experimentation rather than any real equipment limitation. Further work is necessary to verify the data that has been taken and complete the range of observations.

Emissions Data for Number 5 Oil

Results for combustor operation with Number 5 oil are given in Figures 31-37. Figure 38 shows a typical printout from the data monitoring and acquisition system identifying the system parameter values.

The emission index results for residual oil are particularly interesting. Both the long and short residence time data form curves with a definite peak and which appear linear on either side of the peak. The peak for a 50 ms residence time occurs at ϕ = 0.85 and the peak for the 150 ms residence time occurs at ϕ = 0.70.

Operation of the hydrocarbon analyzer was erratic and the data incomplete, so no graphical presentation is made. Oxygen and carbon dioxide levels are consistent with the fuel composition and combustion conditions. The carbon monoxide curve emphasizes that combustion was not as complete for the lower firing rate--longer residence time conditions.

HCN and NH_3 Measurement

With the exception of the data point taken at an equivalence ratio of 2.28 where 14 ppm of HCN was measured, no HCN or NH_3 was found. This lack of HCN or NH_3 is disturbing based on published observations of others(8,9) where considerable (> 100 ppm) amounts of HCN are observed in rich hydrocarbon flames to which pyridine has been added. We have taken special pains to find HCN and NH_3 in these experiments however; hence we feel that the observations are real, although we remained disturbed because of our expectations. All sample lines and filters were heated to 150 C and a heated pump was used. Both the gas absorbing solutions and the gas analyzers (including O_2) were downstream of the pump and thus under positive pressure. Small leaks here would not affect the result. Any leaks in the section of the sample system would yield an abnormally high O_2 reading; this would be particularly noticeable when burning rich and the O_2 concentration would be expected to be low or zero. A small amount of distilled water was used to wash any condensate in the glass tubes of the gas washing bottles down into the absorbing solution. After the NH_3 or CN determination was made using the ion-specific electrode, the sample solutions were spiked with a small amount of standard solution to be sure that the ion-specific and meter were responding properly, which they were.

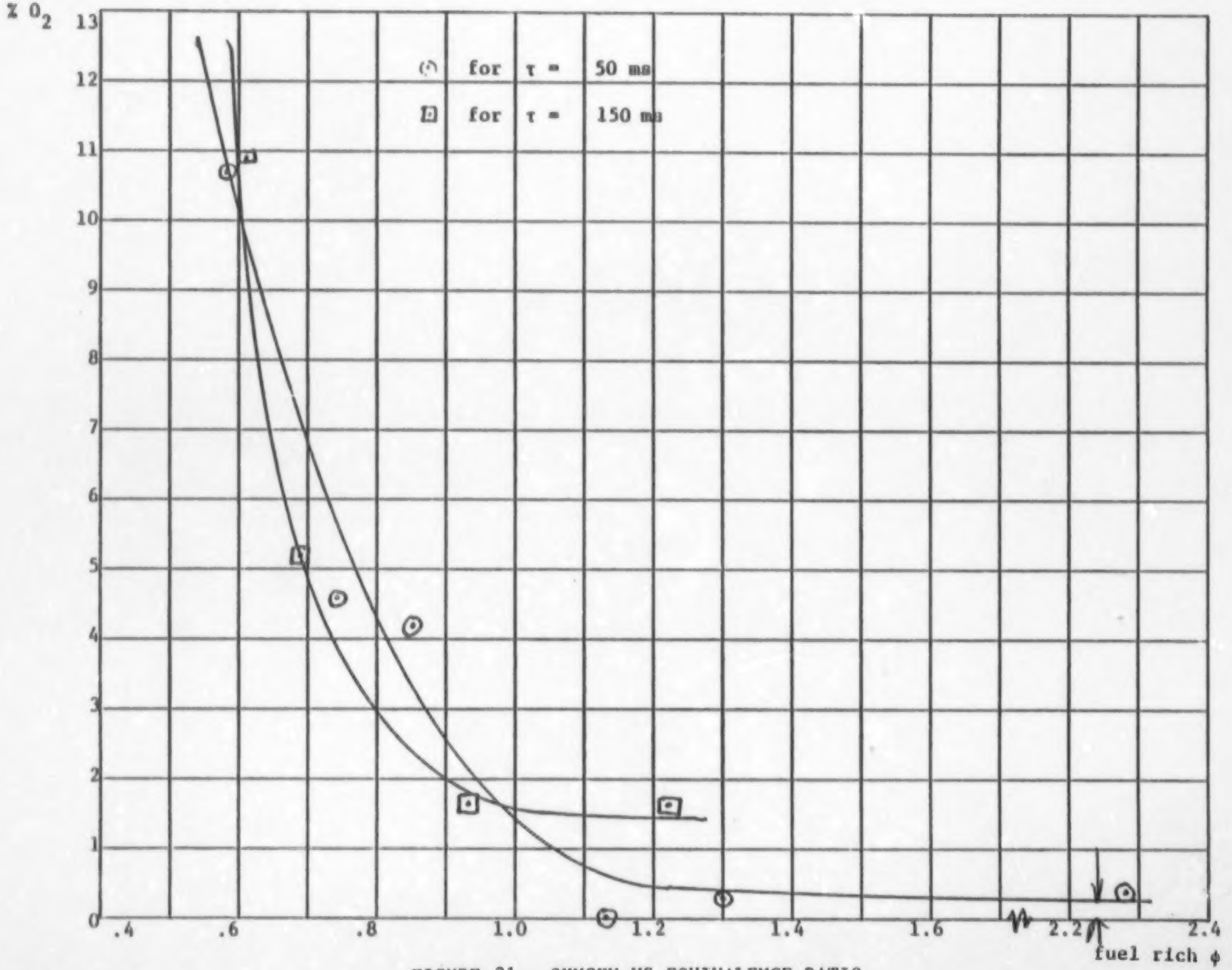

FIGURE 31 OXYGEN VS EQUIVALENCE RATIO

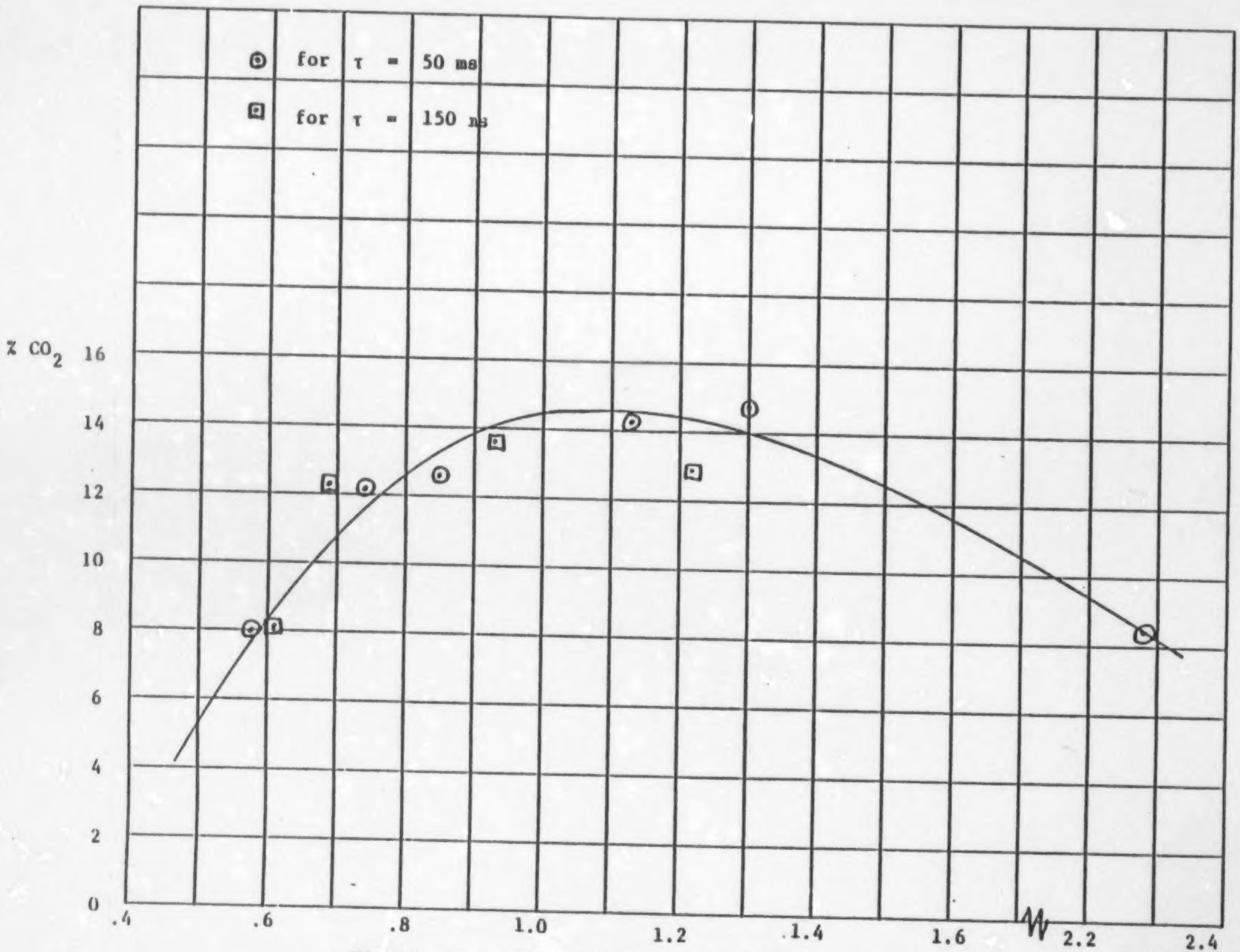

FIGURE 32 CARBON DIOXIDE VS EQUIVALENCE RATIO

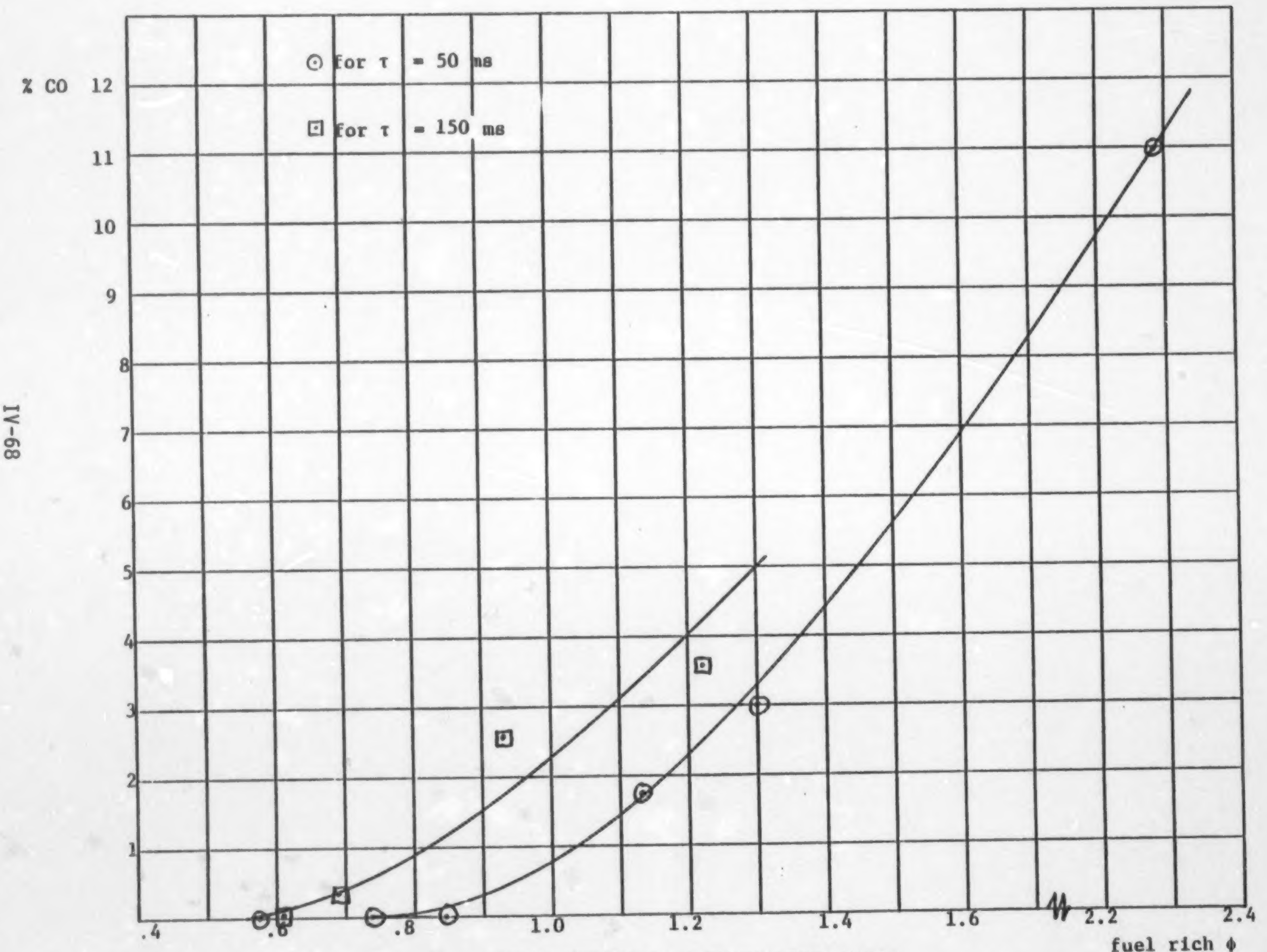

FIGURE 33 CARBON MONOXIDE VS EQUIVALENCE RATIO

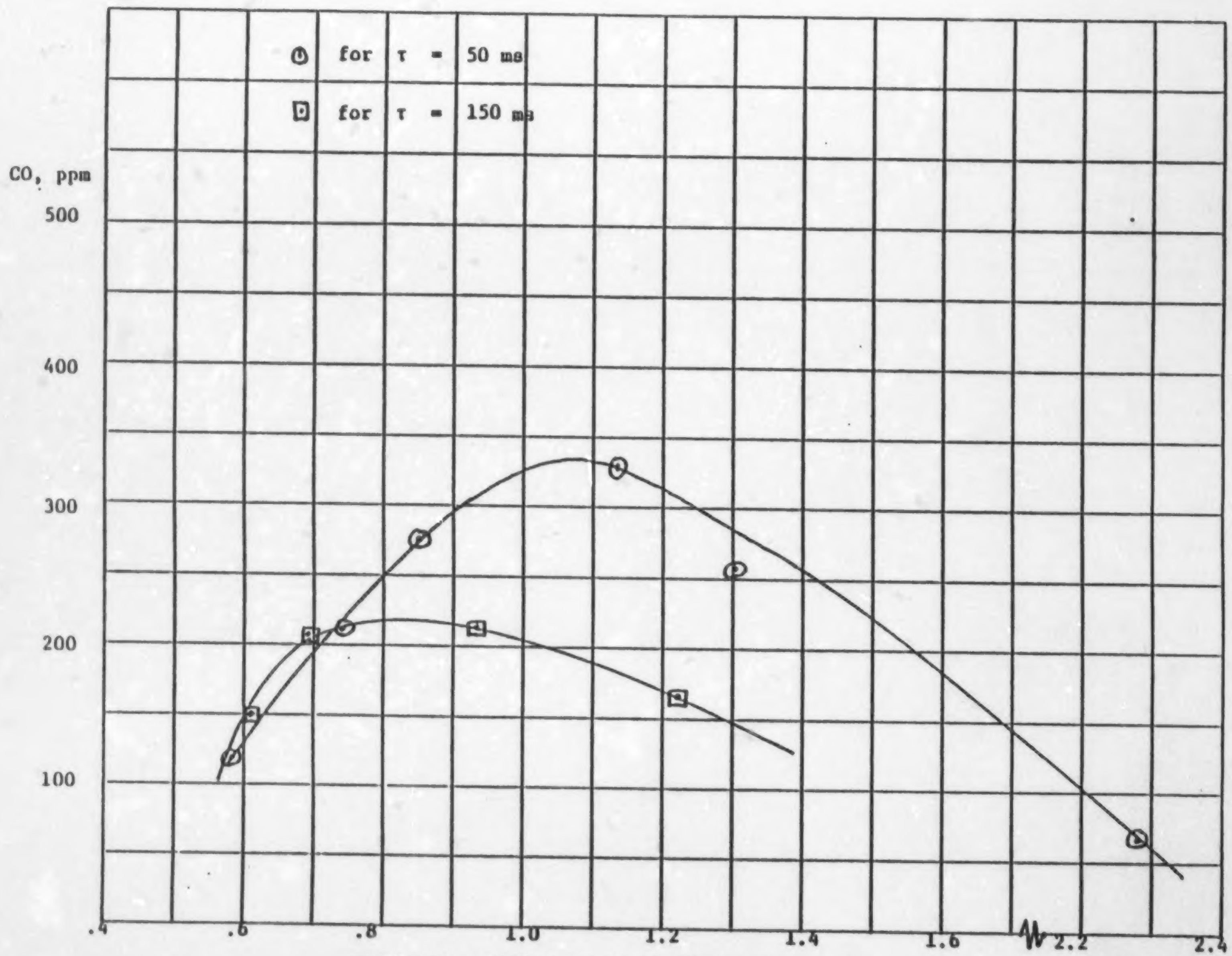

FIGURE 34. NITRIC OXIDE VS EQUIVALENCE RATIO

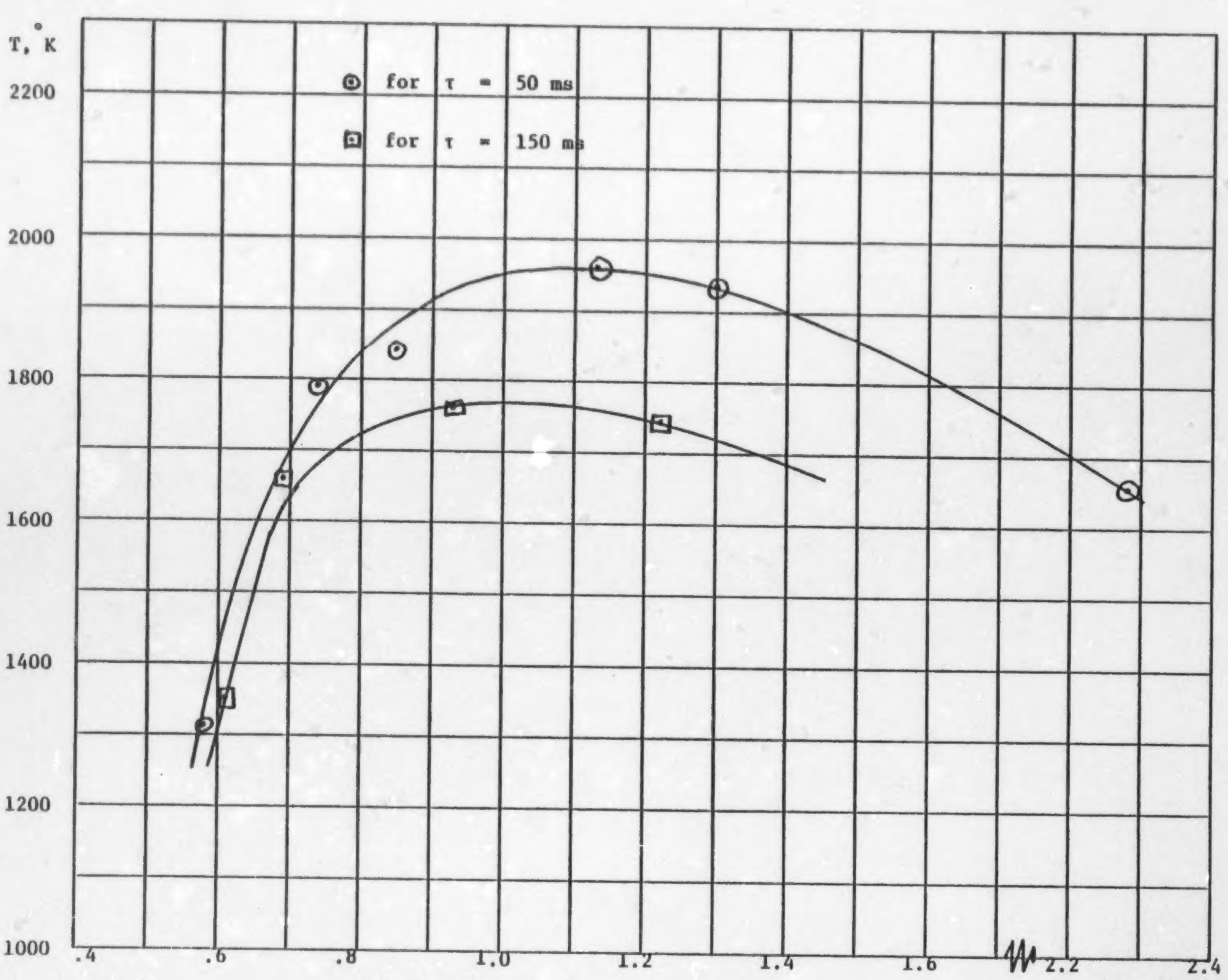

FIGURE 35. TEMPERATURE VS EQUIVALENCE RATIO

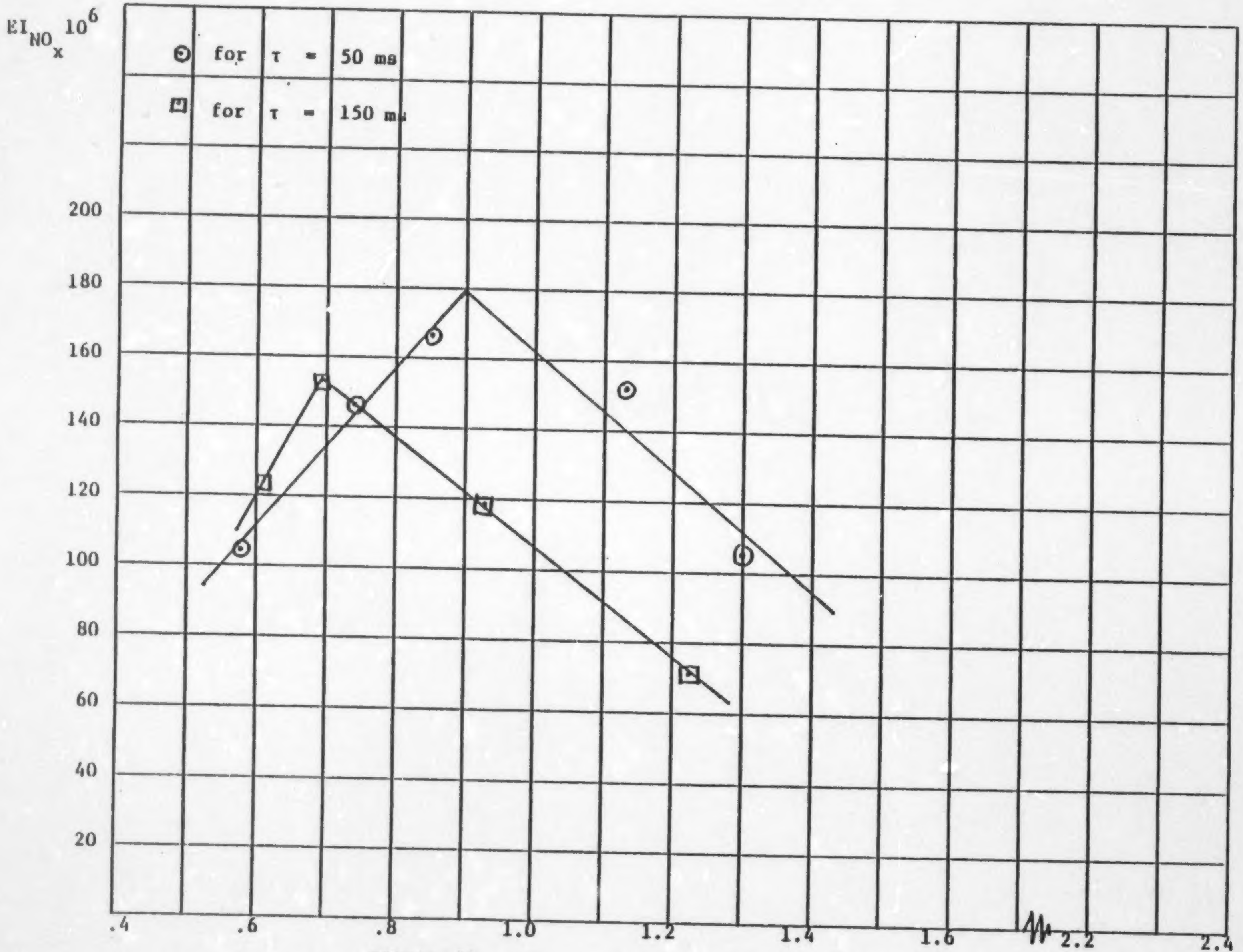

FIGURE 36 EI_{NO_x}, $\frac{\text{g mol NO}}{\text{g fuel}}$ VS EQUIVALENCE RATIO

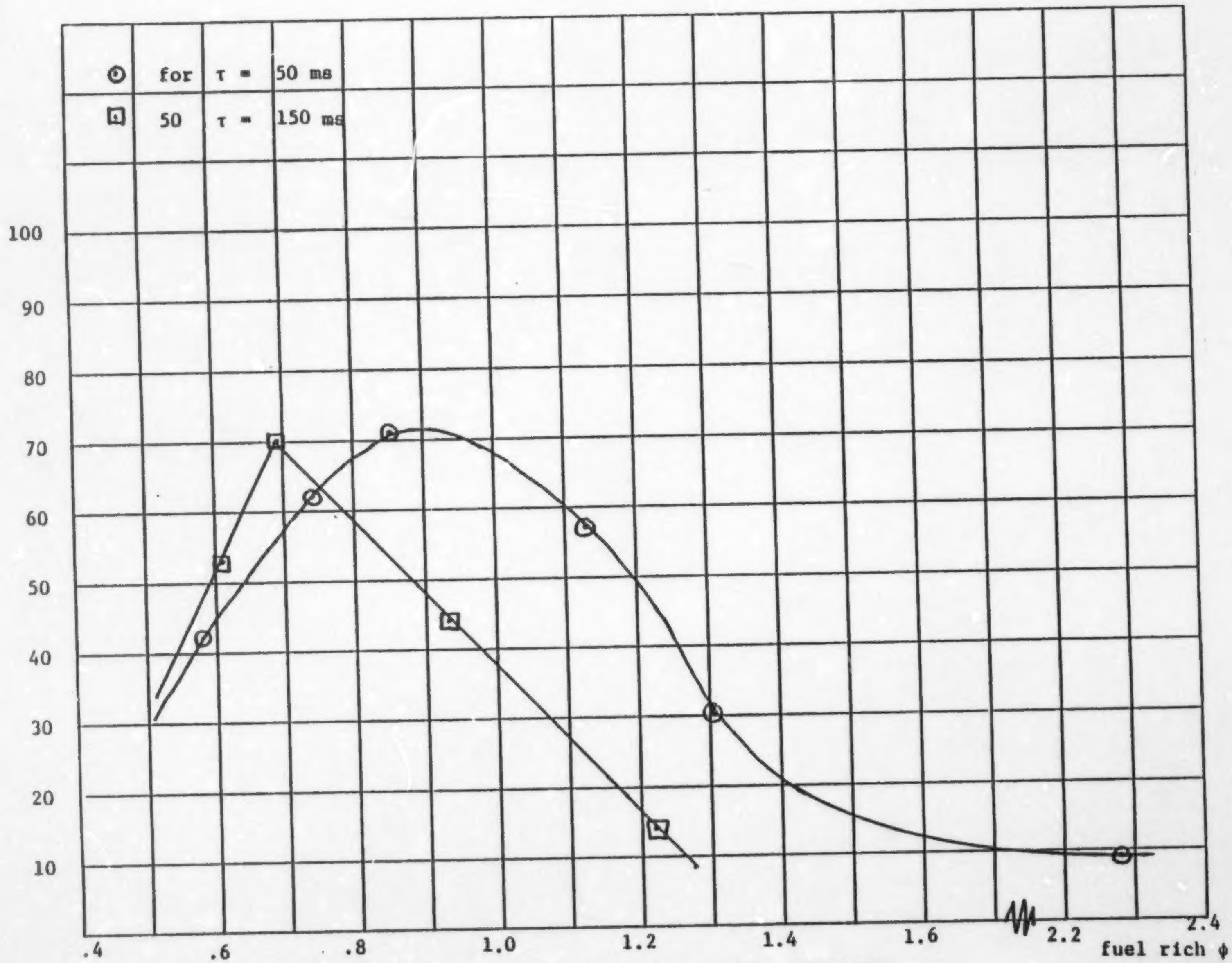

FIGURE 37 APPARENT PERCENT CONVERSION OF FUEL NITROGEN

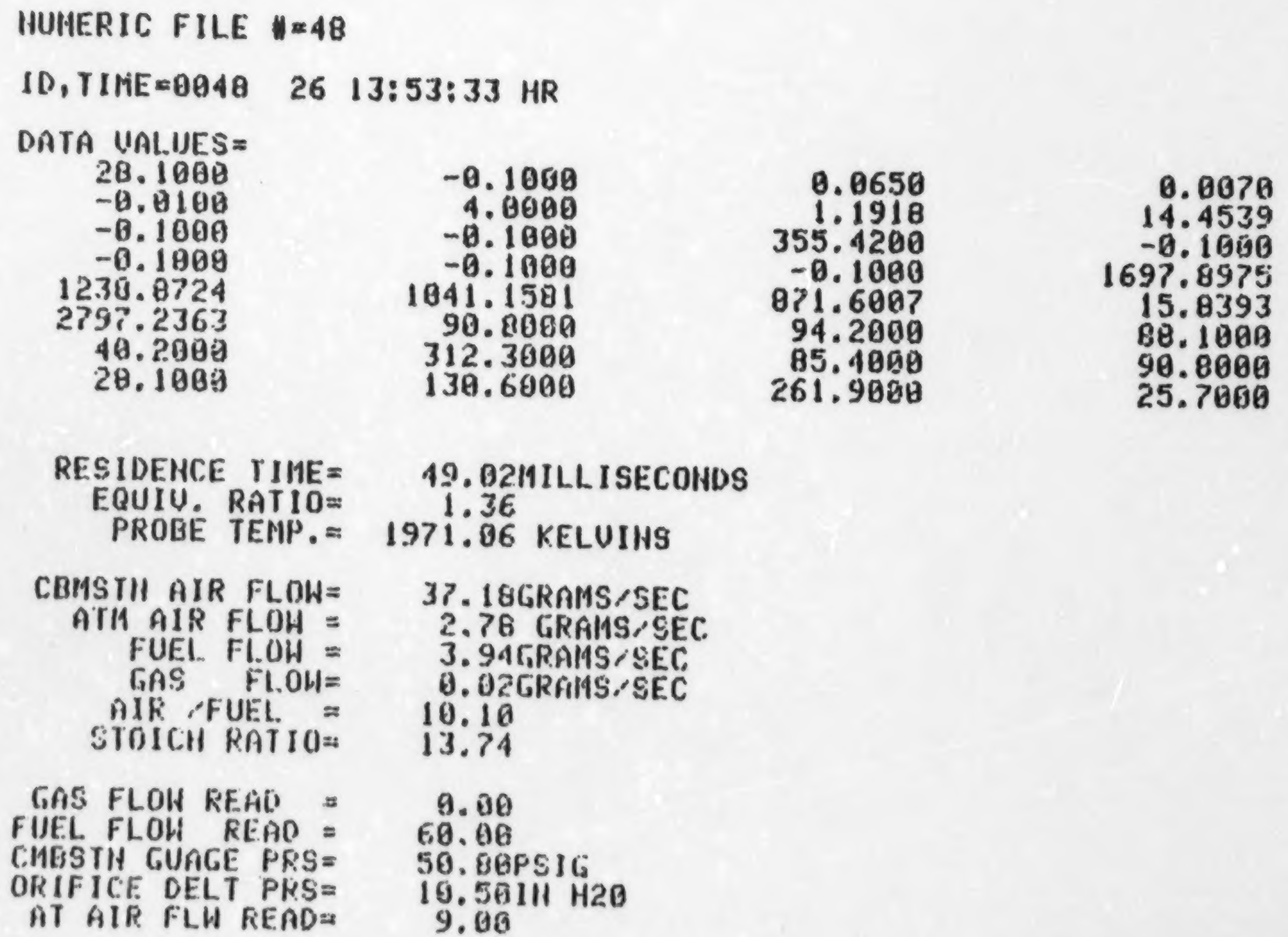

```
NUMERIC FILE #=48

ID,TIME=0048  26 13:53:33 HR

DATA VALUES=
     28.1000            -0.1000             0.0650             0.0070
     -0.0100             4.0000             1.1918            14.4539
     -0.1000            -0.1000           355.4200            -0.1000
     -0.1000            -0.1000            -0.1000          1697.8975
   1230.8724          1041.1581           871.6007            15.8393
   2797.2363            90.0000            94.2000            88.1000
     40.2000           312.3000            85.4000            90.8000
     20.1000           130.6000           261.9000            25.7000


  RESIDENCE TIME=    49.02MILLISECONDS
    EQUIV. RATIO=     1.36
     PROBE TEMP.=  1971.06 KELVINS

 CBMSTN AIR FLOW=    37.18GRAMS/SEC
   ATM AIR FLOW =     2.78 GRAMS/SEC
      FUEL FLOW =     3.94GRAMS/SEC
      GAS   FLOW=     0.02GRAMS/SEC
      AIR /FUEL  =   10.10
   STOICH RATIO=     13.74

 GAS FLOW READ   =    0.00
FUEL FLOW  READ =    60.00
CMBSTN GUAGE PRS=    50.00PSIG
ORIFICE DELT PRS=    10.50IN H20
 AT AIR FLW READ=     9.00
```

FIGURE 38 TYPICAL DATA RESULTS

The data of Foster and Keck(10) show that for a cylindrical burner with an air atomizing nozzle the HCN concentration at the exit (residence time 50 ms) decreased from 300 ppm to 18 ppm as the atomizing air pressure was increased from 274 to 446 kPa. The NH_3 concentration fell from 55 ppm to 20 ppm over this range. If this increased pressure is taken as a measure of mixing, then the conclusion is that better mixing reduces HCN formation substantially. (NO is reported to be relatively unchanged.) If this is so, then the HCN levels in the well-stirred combustor which is designed to give a very high degree of mixing would be expected to be so low as to be below the limit of detection for the standard gas absorption method used with the ion-selective electrodes. Thus if the increased mixing does cause a large decrease in HCN and NH_3 levels, then the results of this investigation and those of Foster and Keck are consistent.

Conversion of Fuel Nitrogen

Figure 35 shows the apparent conversion of fuel nitrogen. This graph was obtained by subtracting from the EI_{NO} for the residual oil the measured thermal EI_{NO} for natural gas at the same equivalence ratio and residence time, then dividing the remainder, the portion attributed to fuel nitrogen rather than thermal NO, by the expected EI_{NO} based on the amount of nitrogen in the fuel. Since the fuel is 0.24 percent N, then 1 gram of fuel has 0.0024 g of N, giving a ratio of

$$\frac{0.0024 \text{ g N}}{1 \text{ g fuel}}$$

or

$$\frac{\dfrac{0.0024 \times 10^6}{14} \text{ mol N}}{\text{g fuel}} = EI_{NO} = 171$$

This gives an EI_{NO}, fuel of 171. As an example, for an equivalence ratio of 0.58 and a residence time of 50 ms, the natural gas gave an expected EI of 33. The measured EI was 104 with the residual oil. Thus, 104 - 33 = 71 was attributed to the fuel nitrogen. Since an EI_{NO} of 171 was expected from the nitrogen in the fuel, the apparent conversion was (71/171) 100 or 42 percent.

Soot Formation

Although soot levels were not measured in this series of experiments, visual observation of the flame and experience with the sample probe filters gave a semi-quantitative measure of soot formation. Even with the residual oil, the soot was at a very low level until the flame was very rich in fuel. Appreciable sooting was not observed until the equivalence ratio was around 2. This is in contrast to typical heavy oil, burners that begin to look smoky as soon as the excess air approaches zero. It appears that the well-stirred design of the combustor tends to reduce soot formation.

CONCLUSIONS

This research program has shown that a combustor can be constructed that is reasonable described as "well-stirred" and that this combustor can be fired with natural gas, distillate oil, or residual oil. The emission levels of NO were comparable to commercial boilers for natural gas fuel and lower for the residual oil fuel. The peak EI_{NO} occurred at = 0.7 and = 0.9 burning residual oil at the long and short residence times, respectively. Soot formation was low until the combustion conditions became very fuel rich. The apparent conversion of the nitrogen in the residual fuel ranged from 70 percent for lean burning to 10 percent for rich burning. The apparent conversion of fuel nitrogen formed well-defined curves when plotted against equivalence ratio with the peak occurring leaner for the longer residence time. No HCN or NH_3 emissions were measured except for one very rich condition.

Of course, all these observations pertain to combustion on the macroscale. In the case of oil combustion, especially, it is obvious that the actual burning conditions must be related to the structure of the flame around the fuel drops. Increased mixing of the well-stirred combustor compared to other burners must alter this condition by bringing the fuel and oxidizer closer to each other, even though micromixing and molecular diffusion must still control at the flame front. The higher NO_x levels from oil flames may well be the result of oxidation of HCN and NH_3 formed in the rich parts of the flame zone. With vigorous mixing, these rich zones decrease and the rich flame NO mechanisms become less important. This decrease in the extent of rich burning would be consistent with the relatively lean peak in the EI_{NO} versus curve. Thus, it is the conditions at the drop that are controlling and the overall conditions are important to the degree that they influence these. Increasing the firing rate (and reducing the residence time) would increase velocities in the combustor and presumably lead to increased mixing. The shift in the peak of the EI_{NO} curve shows that the curve for the short residence time is shifted towards a more fuel-rich condition. Better mixing at the drop may make this equivalent to a leaner condition with poorer mixing. For the natural gas, where there is no droplet burning, the peaks for the two residence times occur at the same equivalence ratio and the higher firing rate gives more NO simply because the temperatures are hotter.

IMPLICATIONS FOR NO_x CONTROL

If the results shown in Figure 36 are confirmed, the desirability of staged combustion with a very rich first stage is clear. Also clear is the desirability of a very high level of mixing which reduces the soot level at the fuel rich conditions.

FUTURE WORK

The question of mixing could have been studied further by using different inlet velocities if more time had been available. Likewise, the effects of atomizer air pressure and drop-size distribution need clarification.

The nature of the nitrogen compounds in the fuel may be important. Even though the fuel contains nitrogen, doping with nitrogen-containing compounds would be valuable. It would particularly be interesting to use pyridine, since many results have been reported for this material. The measurement of nitrogen levels in the soot will be necessary for a complete accounting of the nitrogen in the system.

In addition to these very specific concerns, the well-stirred combustor work poses many fundamental questions. The mechanism of NO formation needs more elucidation before real predictions of combustor performance can be made. A more complete knowledge of the effects of various "macro" variables in the burning process will help to suggest which microvariables are the controlling ones.

Finally, the overall, absolute levels of NO_x emission achieved with this combustor should not be overlooked. Levels of NO_x emission much lower than those associated with current burner designs were achieved in a combustor that had a heat release rate of 12 MW/m^3. The low NO_x and high heat release rate certainly suggest the profitable development of a technology based on this design.

ACKNOWLEDGEMENTS

Appreciation is extended to J. F. Kircher, R. H. Barnes, E. L. Merryman, and D. R. Grieser for their assistance in designing the combustor and the experimental procedures for evaluating its mixing characteristics. Thanks are also extended to E. Cox, T. Lyons, D. Hupp, and J. Faught for their work in constructing the cold flow model and hot combustor, and in performing the experiments. W. Ivancic and P. Webb were most helpful in constructing and operating the emissions measurement system. Helpful discussions and program guidance were given by Randy Seeker of the Energy and Environmental Research Corporation and by Steve Lanier, initial Project Officer of the U.S. Environmental Protection Agency's "Fundamental Combustion Research Applied to Pollution Control".

REFERENCES

1. Beer, J. M., Sarofim, A. F., Hanson, S. P., and Gupta, A. K., "High Temperature Pyrolysis of Oil Droplet and Coal Particle Streams", In: Proceedings of the Fifth Fundamental Combustion Research Contractors Workshop, EPA-600/9-83-001 (NTIS PB83-164483), p. 277, January 1983.

2. Seeker, W. R., and Samuelsen, G. S., "Spray Characterization", In: Proceedings of the Fifth Fundamental Combustion Research Contractors Workshop, EPA-600/9-83-001 (NTIS PB83-164483), p. 495, January 1983.

3. "Sonicore Atomizers--Measurement of Droplet-Size Distribution", International Flame Research Foundation, IJmuiden, June 2, 1978, Doc. Nr. 3131/1.

4. Hottel, H. C., Williams, G. C., and Simpson, H. C., "Combustion of Droplets of Heavy Liquid Fuels", Fifth Symposium (Int'l) on Combustion, Reinhold Publishing Corp., New York, 101-129 (1955).

5. Olikara, C. and Borman, G., SAE Paper 750468.

6. Lim, K. J., et al., "Technology Assessment Report for Industrial Boiler Applications: NO_x Combustion Modification", EPA-600/7-79-178f (NTIS PB80-177215), December 1979.

7. Hayhurst, A. N. and Vince, I. M., Prog. Energy Combustion Sci., 6, 35 (1980).

8. Takagi, T., Tatsumi, T., and Ogasawara, M., "Nitric Oxide Formation from Fuel Nitrogen in Staged Combustion: Roles of HCN and NHi", Combustion and Flame, 35, 17 (1979).

9. Haynes, B. S., Iverach, D., and Kirov, N. Y., "The Behavior of Nitrogen Species in Fuel Rich Hydrocarbon Flames", Fifteenth Symposium (International) on Combustion, The Combustion Institute, Pittsburgh, PA, p. 1093.